DNA Nanostructures as Platforms for Chemical Transformations

by

Tuan Trinh

A thesis submitted to McGill University in partial fulfillment of the requirements for the degree of Doctor of Philosophy

Department of Chemistry, McGill University
Montréal, Quebec, Canada
April 2019

I dedicated this thesis to my family: my father Thang, my mother Huong, my younger sister and my grandparents; and to my girlfriend Tram, for your constant love and support.

Abstract

DNA is an exceptional material for bottom-up assembly of nanostructures with arbitrary shapes and high level of complexity due to its programmability, predictability and biocompatibility. Variety of well-defined DNA nanostructures ranging from a few nanometers to microns can be constructed with unparalleled precision and control. Beyond the self-assembly perspective, chemists have discovered that DNA can provide an excellent template for chemical reactions with high selectivity because it can significantly increase the local concentration of appended reactants. This thesis aims to explore the possibility of using minimalist DNA nanostructures as templates for chemical transformations to generate unique DNA-hybrid materials. First, the use of DNA micelle as a new reaction platform to enable DNA functionalization with highly hydrophobic molecules in aqueous media is investigated. The hydrophobic core of the DNA micelle can act as a reaction auxiliary that facilitates the conjugation of complementary DNA strands to hydrophobic units. Due to the sequence-controlled properties of each component used for DNA micelles assembly, reactivity can be easily tuned and studied. Second, the use of DNA nanostructures for templating reactions is expanded further to two-dimensional (2D) chemical transfer of DNA strand patterns, from a multi-arm DNA junction to a small molecule. This "printing" approach is highly modular, and it allows the resulting branched DNA-small molecule can be controlled precisely in terms of DNA sequences, valency and directionalities (5'-3'). Finally, a three-dimensional (3D) DNA "printing" method using minimal DNA cages to well-defined polymeric materials is presented. The organization of DNA strands on these scaffolds creates DNA strand patterns that can be efficiently transferred to a crosslinked polymer core inside the cage with precise control over the number, directionality, geometry and sequence anisotropy of DNA strands. The resulting DNA-imprinted polymer nanoparticles can be programmed to assemble into asymmetric higher order structures using DNA hybridization. These unique DNA-hybrid molecules can find numerous potential applications. The work presented in chapter 2 opens an opportunity to synthesize a variety of DNA hybrid materials with hydrophobic molecules, which are useful in DNA and small molecule therapeutic delivery, diagnostics, nanopore formation and self-assembly. Branched DNA-imprinted small molecules demonstrated in chapter 3 can be useful in the field of DNA nanotechnology as building blocks for wireframe DNA nanostructures, branching staple strands in DNA origami and tunable templates for material organization. The DNA-imprinted

polymeric particles in chapter 4 can serve as precisely-defined "multi-arm junctions" to create highly complex structures in a predictable manner. They can also be useful in applications such as drug delivery, barcoded diagnostic or building blocks for non-centrosymmetric polymer patterning. Overall, the approaches introduced in this thesis can be used to make functional DNA-hybrid structures, with an emphasis on simplifying synthetic efforts while retaining structural complexity.

Résumé

L'ADN est un matériau exceptionnel pour l'assemblage par approche ascendante de nanostructures de formes arbitraires comportant un haut niveau de complexité grâce à sa nature programmable, prévisible et biocompatible. Une grande variété de structures d'ADN bien définies s'étalant de quelques nanomètres à plusieurs micromètres peut être construite avec un niveau de précision et de contrôle inégalé. Au-delà des perspectives qu'offre l'ADN en auto-assemblage, les chimistes ont découvert que les nanostructures en ADN offrent une excellente plateforme pour créer des réactions chimiques avec un haut niveau de sélectivité parce qu'il permet d'augmenter significativement la concentration locale des réactifs qui y sont annexés. Cette thèse a pour but d'explorer la possibilité d'utiliser des nanostructures d'ADN minimalistes en tant que plateformes afin d'exécuter des transformations chimiques qui génèrent des matériaux hybrides uniques à base d'ADN. Premièrement, l'usage de micelles d'ADN en tant que nanoréacteurs permettant la fonctionnalisation de l'ADN avec des molécules hautement hydrophobes en milieu aqueux est investigué. Le cœur hydrophobe des micelles d'ADN peut agir en tant qu'auxiliaire de réaction, ce qui facilite la conjugaison des brins d'ADN complémentaires aux unités hydrophobes. Grâce aux propriétés acquises par le contrôle de la séquence de chaque composante utilisée dans l'assemblage des micelles d'ADN, la réactivité peut être facilement ajustée et étudiée. Deuxièmement, l'utilisation de nanostructures d'ADN afin de guider des réactions est étendue au transfert chimique de séquences d'ADN en deux dimensions (2D), à partir de jonctions d'ADN à plusieurs branches vers de petites molécules. Cette approche « d'impression » est hautement modulaire et permet aux conjugués ramifiés d'ADN et de petites molécules d'être contrôlés précisément en fonction de leurs séquences d'ADN, valence et direction (5'-3'). Finalement, une méthode « d'impression » d'ADN en trois dimensions utilisant des cages d'ADN minimalistes afin de produire des matériaux polymériques bien définis est présentée. L'organisation de l'ADN sur ces nanostructures crée des motifs de séquences d'ADN qui peuvent être transférés efficacement à un cœur polymérique réticulé situé à l'intérieur de ces cages d'ADN et ce, avec un contrôle sur le nombre, la direction, la géométrie et l'anisotropie des séquences des brins d'ADN. Les particules polymériques d'ADN imprimées de cette façon peuvent ensuite être programmées pour s'assembler en structures asymétriques de plus haute complexité à l'aide de l'appariement des bases de l'ADN. Ces structure hybrides à base d'ADN présentent de nombreuses applications

potentielles. Les travaux présentés dans le chapitre 2 ouvrent la porte vers la synthèse d'une variété de matériaux d'ADN hybrides qui seront utiles dans les domaines de la livraison thérapeutique d'ADN et de petites molécules, le diagnostic et la formation et auto-assemblage de nanopores. Les petites molécules réticulées avec de l'ADN décrites dans le chapitre 3 peuvent être utiles dans le domaine de la nanotechnologie en ADN en tant que matériau de construction pour les nanostructures en ADN, brins « agrafe » pour l'ADN origami et patrons adressables pour l'organisation de matériaux. Les particules polymériques imprimées avec de l'ADN présentées dans le chapitre 4 peuvent servir en tant que « jonctions multi-bras » bien définies afin de créer des structures de haute complexité de manière prévisible. Elles peuvent aussi être utiles dans des applications telles que la livraison ciblée de médicaments, le design programmé à partir de code-barres ou matériau de construction pour la création de polymères non-centrosymétriques à motifs. En somme, les approches introduites dans cette thèse peuvent être utilisées afin de créer des structures d'ADN hybrides fonctionnelles, avec une emphase sur la simplification des efforts synthétiques requis tout en retenant la complexité structurelle des molécules résultantes.

Translated by Katherine Bujold

Acknowledgments

Although this thesis has only my name on the cover, the work presented within it would not be possible without the support of many people and I am grateful to them who helped me throughout my Ph.D at McGill.

Firstly, I would like to thank my Ph.D supervisor Professor Hanadi Sleiman for being a fantastic supervisor for the past five years – thank you for your patience, guidance and for continuously challenging me. Your creativity, enthusiasm, support and constructive criticism have always inspired and encouraged me. Thank you for giving me a great opportunity to carry out my Ph.D research in an excellent research group with fascinating chemistry. Not only being a great mentor, Dr. Sleiman is also an excellent teacher with her famous Supramolecular Chemistry class. Also, I would like to thank Professor Gonzalo Cosa and Professor Nicolas Moitessier for being my review committee members over the years. I appreciated all the comments and suggestions.

I am grateful to Dr. Pongphak Chidchob, who have trained me since the first day in the Sleiman Lab. I would not join the lab without Dr. Chidchob, who was making an effort to change my mind in a winter day at Tim Hortons on Sherbrooke Street. It was amazing and thank you for that, Pongphak! I also owed Pongphak for his devoted training on essential lab and research skills and insightful discussions for my projects, especially for the work presented in chapter 2. Also, thanks for always going to have Pho with me. Mohini Ramkaran for training me on AFM and TEM. Violeta Toader for showing me some synthesis skills – you are one of the sweetest persons in the Sleiman lab.

To the people I have had chance to work with: Tom Edwardson for always answering my questions when I first joint the lab. Danny Bousmail, thanks for always writing the best poem at Christmas dinner and asking me for tuna steaks from Costco (:P). Justin Conway for all your lab jokes. Donatien and Aurelie – keep up the French front in lab with raclette, foie gras, wine and cheese. Alex Prinzen for all the mess and smell you have made me suffer throughout the years and for all the molecules you have synthesized for me. Johans (a big fan of Android and Windows) for your arguments and debates over lunch time – sorry Johans but I do love Apple! Michael for your

help in the lab and for bringing me the chocolate cake at Cheskie's in the morning whenever I want them – they are truly delicious. Nicole – I admire your talent in art and music. Xin for always being kind and showing us amazing Chinese dishes. Katherine for all your advice and help in the lab, and of course, the early morning coffee at Tim Hortons. Hassan for all the Rap-hip hop music in the lab, although they make me headache. Kai for going with me to French classes at YMCA for almost 6 months – it was a great time. Empar for your kindness and great Spanish wine! Dani Saliba for all the McDonald frites, pitas with garlic sauce that I stole from you and for being a good collaborator. Chris Lachance for always bring Chartreuse whenever we have raclette at my place! Felix for telling me your ideas and making fun of me. Casey for organizing group meetings for us and baking great cakes for my birthday! Pierre Picchetti for the Saturday morning coffee and the homemade Carbonara. Dr. Chenyi Liao and Professor Jianing Li from the University of Vermont for all the simulations for the projects presented in chapter 3 and 4.

I am grateful to all other Sleiman group members, past and present, colleagues and friends - Albert Daubry, Alexa Carla Bobica, Alexander Rousina-Webb, Amani Hariri (special hug to Amani!), Amine Garci, Farhad Khan, Hammond Sun, Irene Ponzo, Jathavan Asohan, John Hsu, Kamila Mustafina, Keith Husted, Kimberly Metera, Kitty Chen, Klaudia Englert, Maciej Barlog, Mohammad Askari, Sally Xiao, Sanchit Gupta, Sean Laxton, Sonia Romero, Tolulope Ifabiyi (alphabetical, first name). It has been an absolute pleasure!

I would like to also thank Ms. Chantal Marotte and the McGill Chemistry administration team, who have been very helpful from before I ever arrived in Montreal right to the end. I would like to thank Dr. Alexander Wahba and Dr. Nadim Sadee for the help in mass spectrometry. I would also like to thank CSACS, NSERC, McGill University and Dr. and Mrs. Milton Leong for the financial support and funding during my doctoral studies.

Finally, I would like to thank my whole family, Thang Trinh, Mai Huong Ha, Phuong Anh and my grandparents, and to my girlfriend Tram Dang, for your unconditionally love and support over the past years.

Table of Contents

List of figures

List of tables

List of abbreviations

1D	One dimensional
2D	Two dimensional
3D	Three dimensional
3WJ	Three-way junction
4WJ	Four-way junction
A	Adenine
Å	Angstrom
ACN	Acetonitrile
AFM	Atomic force microscopy
AGE	Agarose gel electrophoresis
Alk	Alkyne
bp	Base-pair
C	Cytosine
Cb	cube
C12	Hexaethylene
$CDCl_3$	Deuterated chloroform
CPG	Controlled-pore glass
Cryo-EM	Cryogenic electron microscopy
DCC	N,N'-Dicyclohexylcarbodiimide
DLS	Dynamic light scattering
DMSO	Dimethyl sulfoxide
DMF	Dimethylformamide
DMT	Dimethoxytrityl
DNA	Deoxyribonucleic acid
DTS	DNA-templated synthesis
DX	Double crossover
ds	Double-stranded
EDC	1-Ethyl-3-(3-dimethylaminopropyl)carbodiimide

EDTA	Ethylenediaminetetraacetic acid
ESI-MS	Electrospray ionization mass spectrometry
Fmoc	Fluorenylmethyloxycarbonyl chloride
G	Guanine
HE	Hexaethylene
HEG	Hexaethylene glycol
HEPES	(4-(2-hydroxyethyl)-1-piperazineethanesulfonic acid)
LC-MS	Liquid chromatography- mass spectrometry
MD	Molecular dynamics
MMT	Monomethoxytrityl
MW	Molecular weight
NH_2	amino
NHS	N-hydroxysuccinimide
NMR	Nuclear magnetic resonance
nt	nucleotide
PAGE	Polyacrylamide gel electrophoresis
PBS	Phosphate buffered saline
PCR	Polymerase chain reaction
R_h	Hydrodynamic radius
RNA	Ribonucleic acid
RP-HPLC	Reversed-phase high-performance liquid chromatography
RT	Room temperature
T	Thymine
TAMg	Tris/acetate/magnesium
TBE	Tris/borate/EDTA
TEAA	Triethylammonium acetate
TEM	Transmission electron microscopy
TFA	Trifluoroacetic acid
TLC	Thin-layer chromatography
T_m	Melting temperature
Tris	Tris(hydroxymethyl)aminomethane

THF	Tetrahydrofuran
ss	Single-stranded
SSTs	Single-stranded tiles

Contribution of authors

Chapter 2, **Tuan Trinh** helped design and develop the project, primarily contributed to the production of experimental data from DNA synthesis, HPLC purification, mass spectrometry, electrophoresis, dynamic light scattering and wrote the paper. **Pongphak Chidchob** helped design the project, synthesized some DNA strands, aided data interpretation and AFM imaging. **Hassan S. Bazzi** provided some funding for the work. **Hanadi F. Sleiman** designed the project, guided interpretation of data, result discussion, co-wrote the paper and provided funding for the project.

Chapter 3, **Tuan Trinh** helped design the project, developed the concept, primarily contributed to production of experimental data from DNA synthesis, HPLC, gel electrophoresis, AFM imaging and mass spectroscopy and wrote the paper. **Daniel Saliba** helped to synthesize several DNA strands, generated temporal growth backbones and carried out all PCR amplification experiments. **Chenyi Liao** and **Jianing Li** carried out molecular modelling of the junction. **Donatien de Rochambeau** synthesized alkyne modification for DNA synthesis. **Alexander Lee Prinzen** synthesized tetra-azido functionalized small molecule. **Hanadi F. Sleiman** designed the project, guided interpretation of data, result discussion, co-wrote the paper and provided funding for the project.

Chapter 4, **Tuan Trinh** helped design the project, developed the concept, primarily contributed to production of experimental data from DNA synthesis, HPLC, gel electrophoresis, AFM imaging, dynamic light scattering and mass spectroscopy and wrote the paper. **Chenyi Liao** and **Jianing Li** carried out modelling for the cube with DNA amphiphiles. **Violeta Toader, Maciej Barlog** and **Hassan S. Bazzi** synthesized hexaethylene phosphoramidite for DNA synthesis. **Hanadi F. Sleiman** designed the project, guided interpretation of data, result discussion, co-wrote the paper and provided funding for the project.

| 1 |

Introduction

1.1. Preface

This thesis seeks to explore the use of DNA nanostructures as platforms for chemical transformations, more specifically in the context of DNA functionalization with hydrophobic molecules and DNA pattern transfer onto other materials. Over the last three decades, DNA has emerged as an exceptional material in nanotechnology, due to its biocompatibility, monodispersity and predictable and programmable molecular recognition, generating a large number of nanostructures for applications in drug delivery, diagnostics and material science. This chapter gives a brief overview of DNA structural features and synthesis. Key contributions in the field of structural DNA nanotechnology and supramolecular DNA assembly are then discussed. Finally, recent advances in the field of DNA-templated synthesis are summarized, which provide context for upcoming chapters in this thesis.

1.2. DNA and Structural Properties

Deoxyribonucleic acid (DNA) is widely known as the molecule of life for its role in preserving and carrying human genetic code. The discovery of the double helical structure of DNA in 1953 by Watson, Crick[1] and Franklin[2] has transformed modern bioscience. Particularly, it has had a tremendous impact on molecular biology and paved the way to significant contributions such as the polymerase chain reaction (PCR) and DNA sequencing. Moreover, the predictable and programmable molecular recognition of DNA has also revealed it as an excellent building block for constructing nanostructures and greatly inspired the fields of nanotechnology and supramolecular chemistry.

DNA is a relatively simple biopolymer composed of four nucleoside monomers. These consist of nitrogen-containing bases (nucleobases) attached to five-membered deoxyribose units, which are then connected by phosphodiester bonds. Adenine (A) and guanine (G) can form specific hydrogen bonds to thymine (T) and cytosine (C), respectively **(Figure 1.1).** These A:T and G:C hydrogen bonding motifs are called Watson-Crick base pairing. In aqueous solution, free energies of the A:T and G:C bonds are calculated as -4.3 and -5.8 kcal/mol, respectively.[3]

Two DNA single strands having complementary sequences can come together to form double-stranded DNA. The relative stability of DNA duplexes can be roughly determined by the percentage of G/C bases (known as GC-content) since G:C base pairing is stronger than A:T base pairing. In Nature, DNA is mostly found in a double-stranded form. DNA strands are hybridized in an antiparallel fashion, meaning that the 3'-end of one strand is on the same side of the 5'-end of another strands. Importantly, DNA hybridization is highly cooperative and driven by a combination of multiple non-covalent interactions including hydrogen bonding, π-π stacking between bases, Van der Waals forces, and hydrophobic effect.[4]

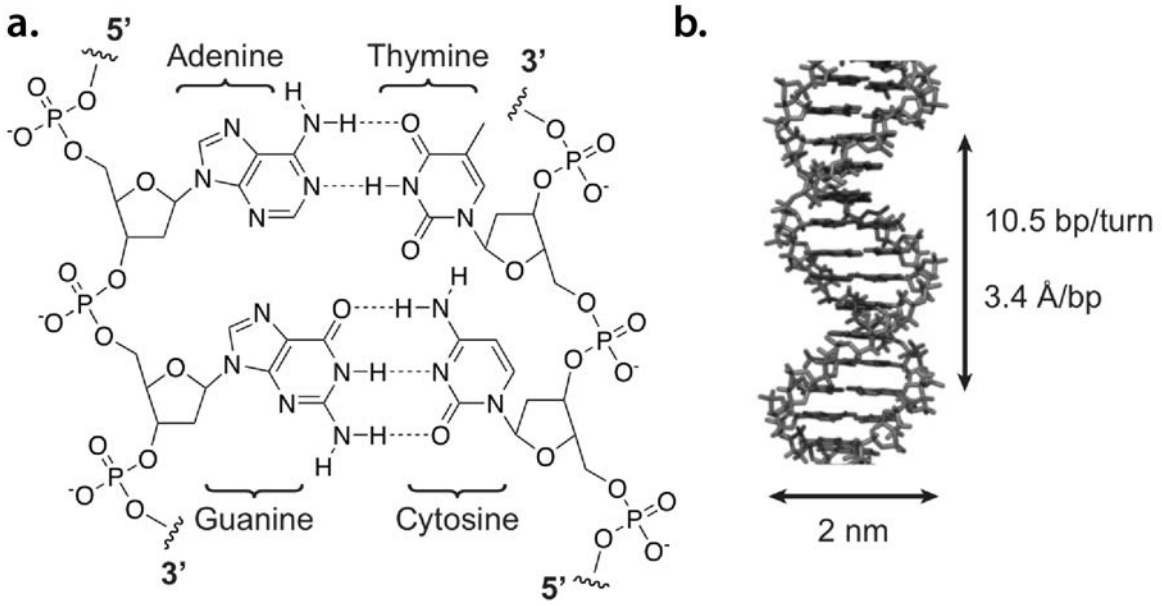

Figure 1.1 | DNA and structural features. **a.** Watson-Crick base pairing motifs. **b.** Structural parameters of B-form DNA double helix.

There are at least three DNA forms were found in nature, A-DNA, B-DNA and Z-DNA. The most common double helical structure is B-form double-stranded DNA (B-DNA). In terms of structural parameters, this right-handed duplex has very well-defined dimension with a diameter of 2 nm and ~10.5 bases per helical turn, with a pitch length of 3.4 nm **(Figure 1.1**).[5] The DNA double helix appears as a linear and stiff molecule with the persistence length of about 50 nm or ~150 base pairs, although this can vary significantly depending on external condition.[6] The formation of DNA double helix is a highly cooperative process that requires cations to balance the electrostatic repulsions. Moreover, rather than Watson-Crick base

pairing, there are many examples showing that modified base pairing such as Hoogsteen base pairing can lead to unique structures such as i-motif [7] or G-quadruplex.[8] The well-defined 3D structure of B-DNA constitutes the fundamental design element for DNA materials, which is one of the most iconic examples of self-assembling materials.

1.2.1. DNA synthesis

The development of DNA synthesis has significantly advanced not only the field of DNA assembly but also biotechnology as a whole. In term of synthesis, the main challenge with DNA lies in the perfect control in DNA sequence. Over the past few decades, there have been many different approaches and coupling chemistries have been developed by many groups such as Khorana, Letsinger, Caruthers, Beaucage and Ogilvie.[9-13] An important aspect of the synthesis is that it is carried out on a solid-support such as controlled-pore glass (CPG) or polystyrene (PS) beads. CPGs is more widely used compared to PS beads. Solid-phase synthesis has made the process amenable to automation. CPG normally has 500-1000 Å pores. Although smaller pores are known to be more mechanically robust, synthetic efficiency decreases significantly when oligonucleotides have more than 40 bases in length. With longer oligonucleotide (about 100 bases in length), 1000 Å solid support has proved satisfactory for the synthesis. Regarding the coupling chemistry, the most widely used method is based on phosphoramidite chemistry, initially developed by Letsinger and then Caruthers and Beaucage in 1981, and still in use now **(Figure 1.2**).[14] Phosphoramidite moieties are highly reactive electrophiles, thus allowing each coupling step to occur rapidly in high yield. With current technology, DNA of up to 200 bases in length can be practically synthesized using an automated DNA synthesizer in the laboratory.

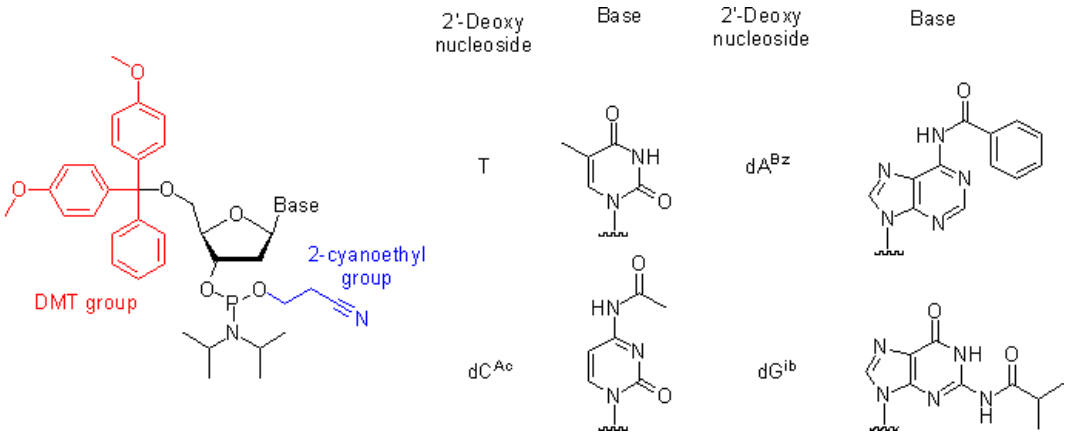

Figure 1.2 | **Chemical structure of phosphoramidites used in solid-phase DNA synthesis**.

In contrast to DNA biosynthesis happening in nature, oligonucleotide synthesis proceeds in the 3'- to 5'-direction. The synthetic cycle contains four major steps: deblocking, coupling, capping and oxidation (**Figure 1.3**). In more detail, **1)** the synthetic cycle starts with deblocking step, where the nucleotide is deprotected at the 5'-end using tricholoroacetic acid to remove the dimethoxytrityl (DMT) protecting group and expose reactive hydroxyl group.

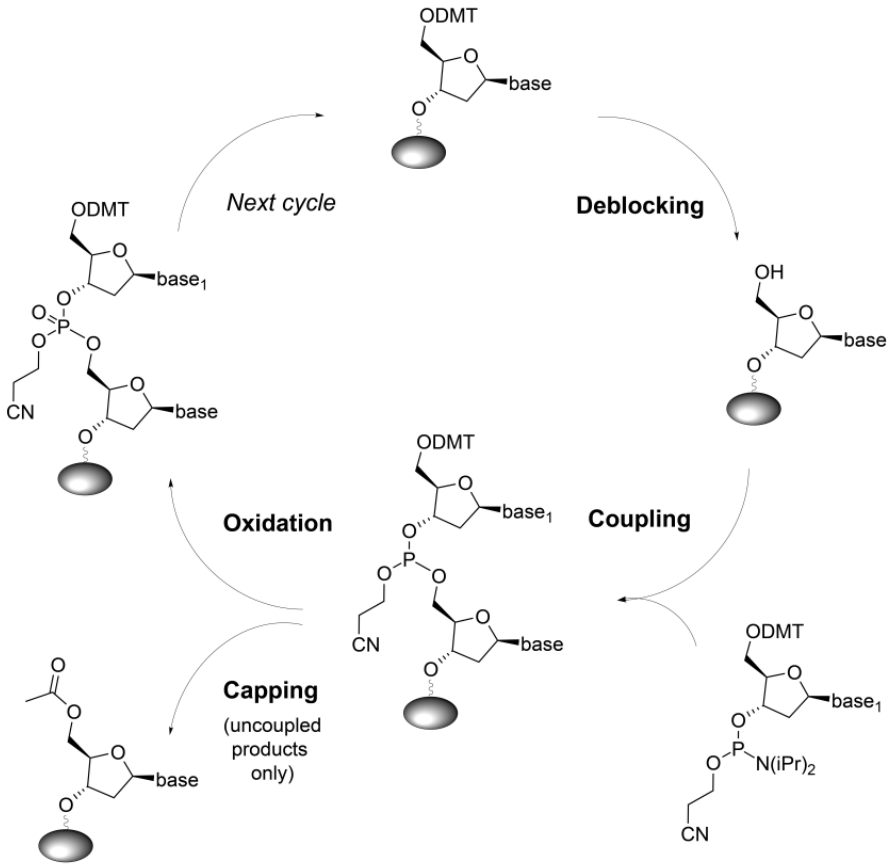

Figure 1.3 | DNA synthesis cycle based on phosphoramidite chemistry. It has 4 main steps: Deblocking, coupling, oxidation and capping.

Cleaved DMT carbocation exhibits strong absorbance at 498 nm (typically strong orange color), which can be a useful indicator for coupling yield of the previous nucleoside. Next, **2)** A new monomer as 5'-DMT protected deoxynucleoside (2-cyanoethyl,N,N-diisopropyl) phosphoramidite is introduced. This step is carried out under acidic conditions using tetrazole derivative as an activator. Then, **3)** nucleosides that have failed to react are capped using acetic anhydride before the next coupling. The capping step is particularly important as it reduces side products caused by unreacted 5'-hydroxyl groups, which potentially can complicate purification steps. Lastly, **4)** the phosphorus (P) is oxidized from the P(III) to P(V) using iodine solution. The cycle then begins again with the deblocking step and an introduction of the next monomer until the desired product is fully grown on the bead. Once the oligonucleotide is synthesized, it is cleaved from the solid support with aqueous solution of ammonia at elevated

temperature (normally at 65ºC) to remove all protecting groups and yield the desired product. With the advent of this technology, the cost of synthetic oligonucleotides has been significantly decreasing over the past few years, and this has enabled their use in the fields of nanotechnology, biomedicine and supramolecular chemistry.

1.3. Structural DNA nanotechnology

1.3.1. Early approaches

The use of DNA for building nanostructures has become well-established since its inception in the beginning of 1982 pioneered by Nadrian Seeman.[15-16] Inspired by the six-finned fish in an Escher painting, Seeman hoped to create three-dimensional crystalline lattices out of interconnected rigid rods of DNA duplexes, in which proteins could be encapsulated and subsequently crystalized **(Figure 1.4)**. His revolutionary vision set the foundation of DNA nanotechnology and the field has delivered a great number of advances in the control of matter at nanoscale level.

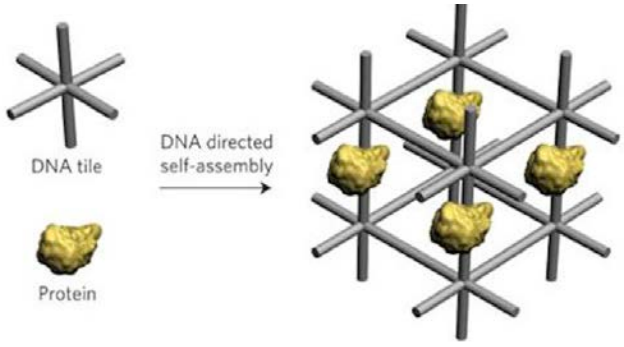

Figure 1.4 | Original proposal. Seeman's original idea of using DNA junctions to build 3D scaffolds that could be used for protein crystallization. Adapted with permission from reference 16 (Nature Publishing Group, 2011).

DNA has a one-dimensional structure; therefore, to build more complex structures, it is necessary to go beyond its linearity. Initially, Seeman designed three- and four-way junctions which could be connected periodically to form networks via short single-stranded DNA (ssDNA) overhangs (i.e. single-stranding portions) bearing complementary sequences were positioned at the end of each arm (called "sticky ends") **(Figure 1.5a)**.[15, 17-18] This was the first example showing how DNA could be used to build extended

networks and nanostructures. However, the sequences in these junctions are self-complementary and the branching point can readily migrate, thus rapidly destroying the junction. To address this limitation, in 1983, Seeman introduced sequence asymmetry to create immobile junction and hence lacking the two-fold symmetry.[19] This important idea was further expanded with the design of 5-, 6-, 8- and 12-way junctions **(Figure 1.5c)**.[20-22] Remarkably, multi-armed junctions were also used to form the first discrete 3D DNA cube in 1991, although the yield was relatively low (**Figure 1.5b**).[23] However, it was quickly realized that these structures have high degree of flexibility. It was therefore not suitable for building higher order structures and a new way of making more rigid networks was highly sought at that time.

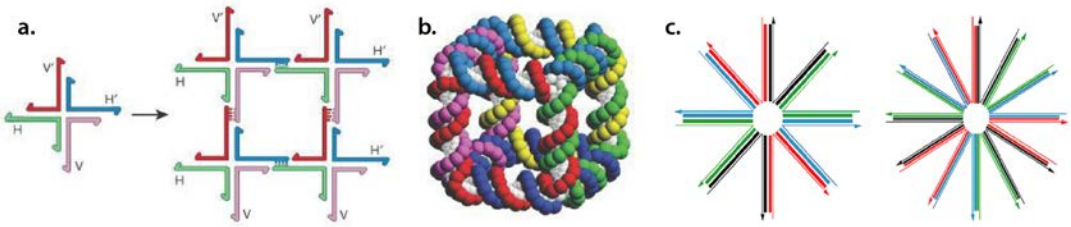

Figure 1.5 | Holliday junction approach. a and b. Holiday Junction for building 2D extended network and DNA cube. Adapted with permission from reference 18 (Nature Publishing group, 2003) **c.** Design of multi-arm DNA junction. Adapted with permission from reference 22 (American Chemical Society, 2007)

1.3.2. Tile-based assembly

To overcome the flexibility issue of Holliday-type branched junctions presented in the early work, the use of double-crossover (DX) junctions as building blocks was proposed, in which the number of branched points (crossovers) was increased. Crossovers are defined as strands that start on one DNA helix and switch over to a neighboring helix, thus connecting them. DX motifs consist of two Holliday junctions which are connected by helical domains. The helical domains can be parallel (DP) or anti-parallel (DA); anti-parallel versions are more stable and therefore more commonly used. DX molecules offer geometric rigidity and stability.[24] In fact, DX structures are estimated to be twice as stiff

as normal duplexes.[25-26] These DX tile motifs were quickly adopted for assembly into extended 2D lattices via complementary "sticky-ends", similar to Holliday-type junctions, and characterized by atomic force microscopy (AFM) **(Figure 1.6a)**.[27] This approach has led to the creation of a number of DNA tile motifs featuring crossovers designed to implement rigidity and promote assembly of higher-order arrays.[28-29] More complex structures such as DNA nanoribbons, nanotubes and complex helix bundles were also realized using this approach.[30-33] The idea has been expanded to even more rigid triple crossover motifs or tensegrity triangles as well **(Figure 1.6b and 1.6c).**[34-35]

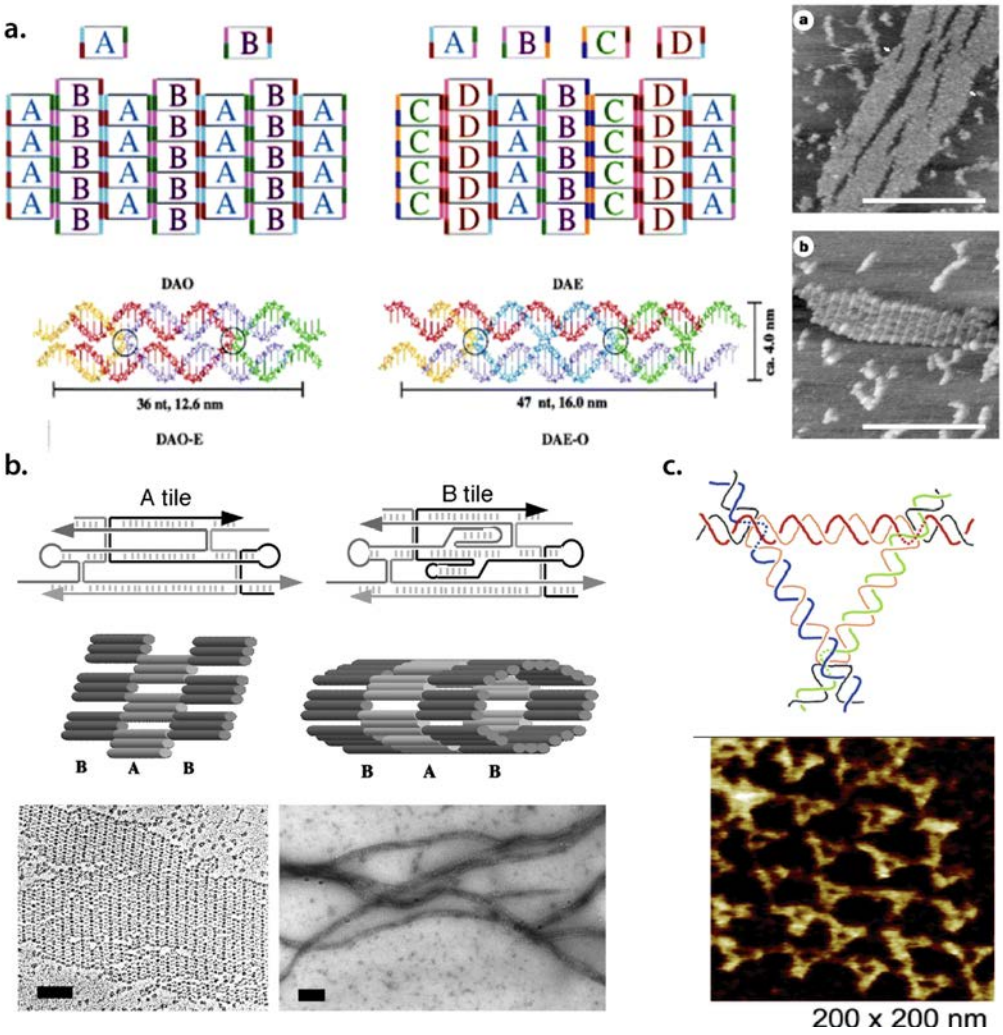

Figure 1.6 | Crossover motifs. a. Double-crossover motifs and their assemblies into 2D crystals. Adapted with permission from reference 27 (Nature Publishing Group, 1998**). b.** Triple-crossover

motifs and their assemblies into flat lattice and tubes. Adapted with permission from reference 34 (PNAS, 2004). **c.** Design of tensegrity triangles. Adapted with permission from reference 35 (American Chemical Society, 2006)

It was then realized that sequence symmetry, in which the number of unique sequences are minimized, plays a key role in enabling the formation of large DNA structures, as it simplifies sequence design, reduces the number of required DNA strands and minimizes unpredictable distortions in the assemblies.[36] Drawing on this success, tile-based assembly has been expanded to multidirectional junctions that use several crossover points to introduce rigidity, thus allowing access to unique structures such as capsular geometries and sheets **(Figure 1.7a)**.[35, 37-40] Moreover, the construction of an aperiodic patterned DNA barcode lattice (e.g. 01101 or 10010) by direct nucleation assembly with an information-carrying input strand was also reported.[41] Interestingly, Winfree *et al.* showed that algorithmic tile (Wang tiles) which are squares in different colors can grow into non-periodic 2D crystal (**Figure 1.7b)**.[42-43] Finally, long range 3D tile-based assembly was reported in the work by Seeman and Mao, who showed the a design of 3D macroscopic DNA crystal self-assembled based on the DNA tensegrity triangle. The crystal structure was resolved to allow structural characterization of this nanostructured DNA-based material at high resolution, opening the way to design crystals and well-ordered DNA nanostructures **(Figure 1.7c)**.[44]

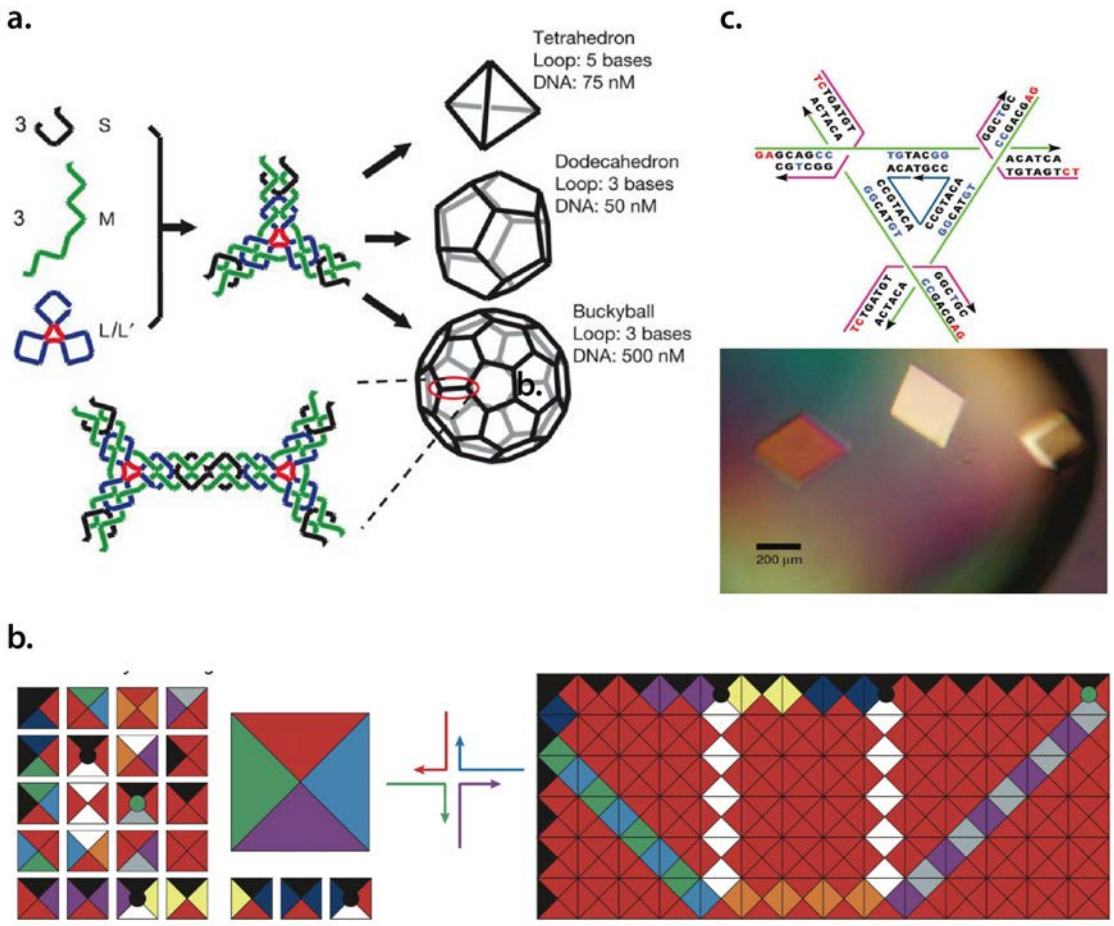

Figure 1.7 | Tile-based assembly a. Three-point star motifs in assembly of DNA polyhedron. Reproduced with permission from reference 40 (Nature Publishing Group, 2008). **b.** Tensegrity motifs used to create 3D DNA crystal. Reproduced with permission from reference 44 (Nature Publishing Group, 2009). **c.** Wang tiles assembly. Each Wang tile color can only assembly with their neighbors having the same colors. Reproduced with permission from reference 222 (Nature Publishing Group 2018).

Overall, structural DNA nanotechnology has been used to create a number of well-defined self-assembled nanostructures. It offers an opportunity to organize nanomaterials such as proteins, nanoparticles or aptamers;[38, 45-47] with the possibility to be used in many applications ranging from DNA computing to drug delivery.

1.4. DNA origami and brick assembly

Tile-based assembly can produce various well-defined large structures, but they are mostly periodic and symmetrical. It also offers poor size control of assembled structures as the assembly proceeds via a step-growth polymerization mechanism. To overcome this challenge, Paul Rothemund in 2006 introduced a completely new approach to create robust, asymmetric nanostructures called "DNA origami",[48] which significantly increased the complexity of DNA nanostructures. In this breakthrough, Rothemund used a long genomic, single-stranded DNA, isolated from a bacteriophage (commonly used ~7429 nucleotides long M13mp18) folded into pre-determined shape using hundreds short DNA strands (16-20 nts) called "staple" strands **(Figure 1.8).** An attractive feature of DNA origami is that staple strands interacting with the scaffold are usually not purified and can be used large stoichiometric excess, thereby greatly simplifying the assembly process. Due to its simplicity and structural versatility, this approach has rapidly transformed the landscape of DNA nanotechnology. In terms of structural design, using a long strand of DNA and computer interface (e.g. Cadnano), a user can vary the arrangement of staple strands to manipulate the backbone into virtually any shapes in the laboratory.[49-51] The scaffold could be folded into variety of arbitrary designs such smiley faces, rectangular, stars and many other complex patterns.[48, 52]

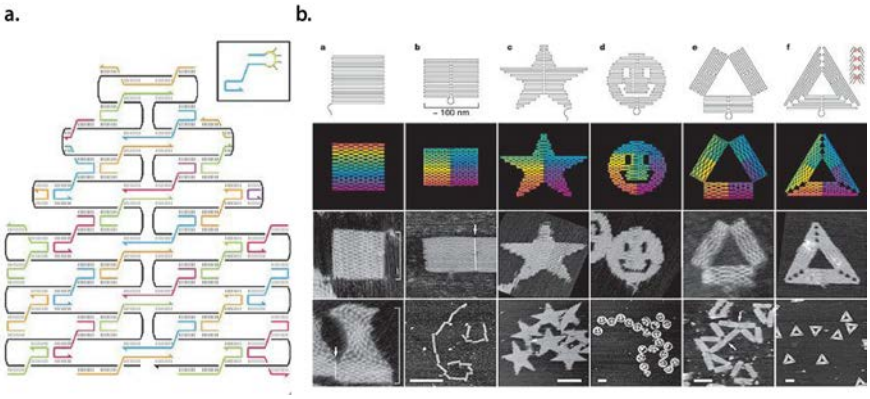

Figure 1.8 | Two-dimensional DNA origami. **a** and **b**. The long viral scaffold strand is folded into different 2D shapes by hundreds of colored staple strands. Reproduced with permission from reference 48 (Nature Publishing Group, 2006).

However, DNA origami was limited to 2D structures until 2009, when major approaches were developed to push it to the third dimension. In one method, hollow 3D objects such

as a DNA tetrahedron and DNA box were created by folding flat DNA origami sheets with the use of linking strands (**Figure 1.9a** and **1.9b)**.[53-54] Subsequently, a stacking strategy of multiple layers of DNA helices into honeycomb and square lattices was shown to efficiently generate complex and rigid 3D DNA origami **(Figure 1.9c).**[55-56] Interestingly, by inserting/deleting base pairs, which altered the distances between crossovers points, twist and curvature in 3D DNA origami could be introduced **(Figure 1.9d)**.[57] The assembly of highly curved surfaces, reconfigurable Mobius bands and catenanes and complex quasi-crystalline wireframe structures with curvilinear patterns, was also achieved by Hao Yan and co-workers **(Figure 1.9e)**.[58-60]

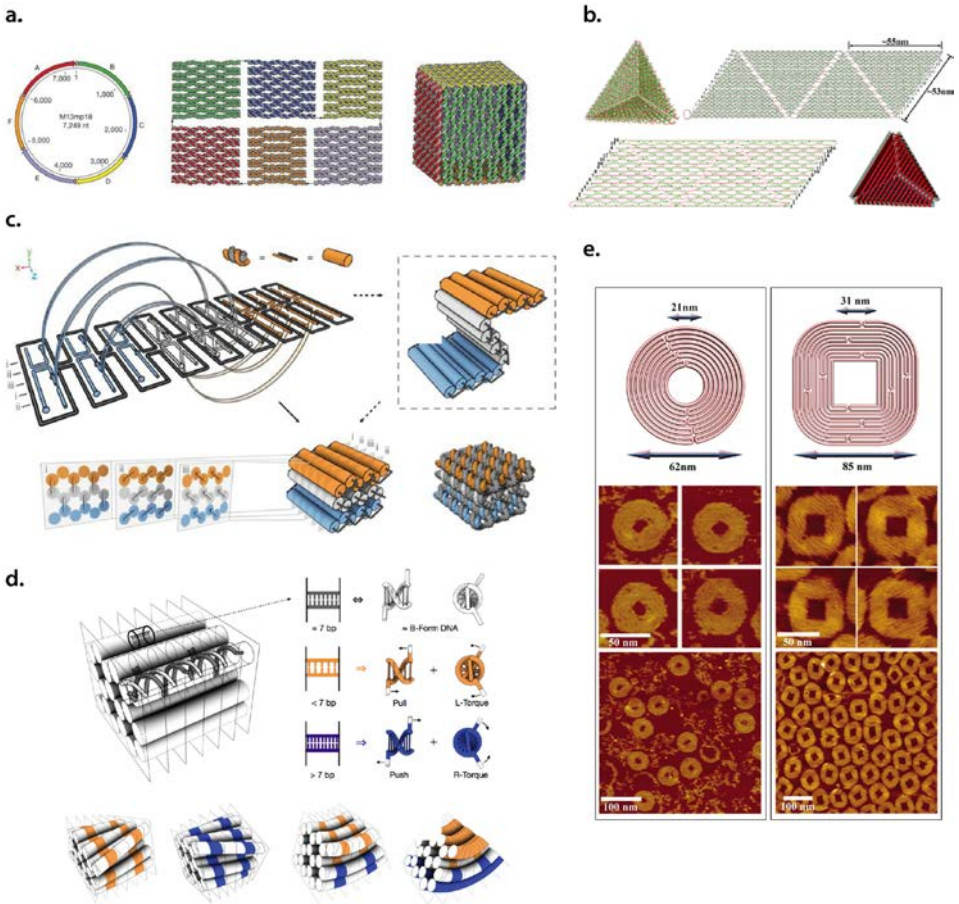

Figure 1.9 | Three-dimensional DNA origami. **a** and **b**. Folding flat 2D origami sheets into hollow 3D structures. Reproduced with permission from reference 53 and 54 (American Chemical Society, 2009 and Nature Publishing Group, 2009). **c.** Layering of origami sheet to generate 3D DNA origami structure. Reproduced with permission from reference 55 (Nature Publishing Group, 2009)

d. Inserting/deleting bases results in twisted and curvature structures. Adapted with permission from reference 57 (AAAS, 2009) **e.** Introduction of curvature to create complex 3D DNA origami. Adapted with permission from reference 58 (AAAS, 2011).

More recently, the concept of tile-based DNA assembly has been simplified in terms of structural design by Yin *et al.* where they considered a single-stranded DNA as a tile, termed single-stranded tiles (SSTs) or brick assembly. The method allows the generation of complex nanostructures like DNA origami but without the need of a long viral scaffold (M13 scaffold). The group has developed extended 2D arrays and expanded the approach to assembly of 3D structures **(Figure 1.10a and 1.10b).**[61-62] Remarkably, the group also reported a strategy to create prescribe 3D shapes in only one annealing step using hundreds of 32-nucleotide (32-nt) single DNA strands **(Figure 1.10c)**.[63]

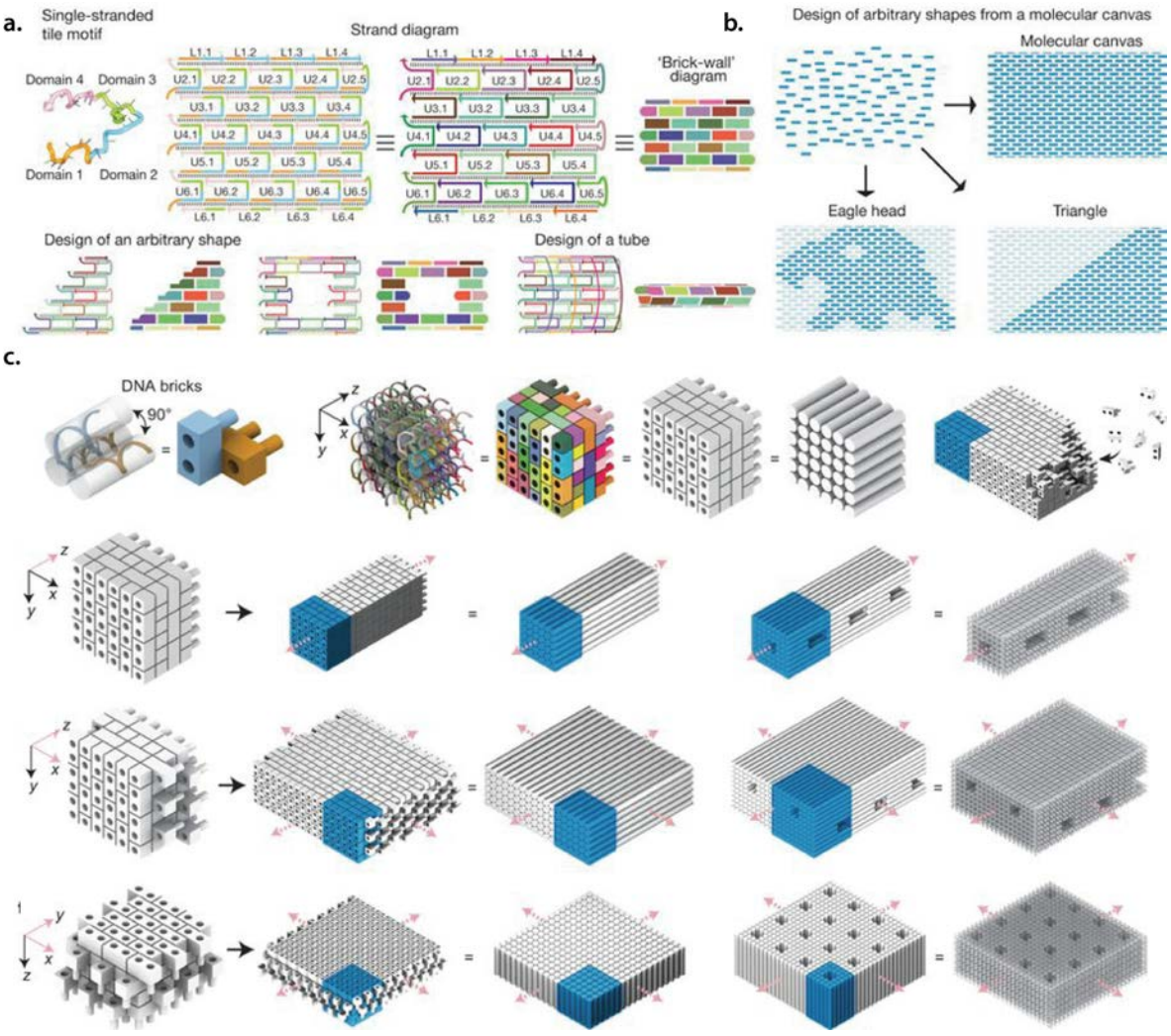

Figure 1.10 | Single-stranded tiles approach. a and **b.** Design of single-stranded tiles motif used in the assembly of arbitrary shapes. Reproduced with permission in reference 61 (Nature Publishing Group, 2012). **c.** Design and assembly of DNA bricks consisting of 32-nucleotide with four 8-nt binding domains. Reproduce with permission in reference 63 (Nature Publishing Group, 2014).

Importantly, origami scaffolds of folded DNA are packed with known sequences (200 sites) that could be used to position DNA-binding cargo just a few nanometers apart. Patterning on DNA origami object can be easily achieved since individual staple strands are unique and could be modified with synthetic groups or overhang sequences, allowing site-specific placement of cargo molecules (e.g. proteins, peptides, virus capsids or nanoparticles) on the origami scaffold. For example, it has been used in organizing enzyme

cascades, drug delivery, nanofabrication with synthetic nanomaterials, studying protein-protein interaction or as lipid membrane nanopores **(Figure 1.11)**. [64-75]

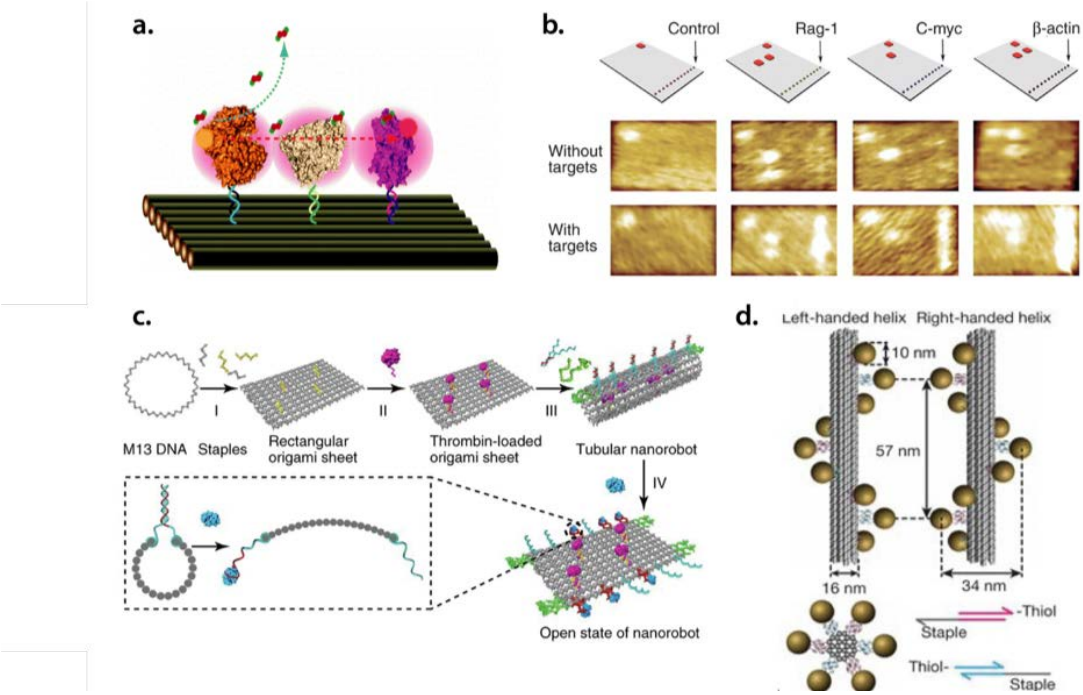

Figure 1.11 | Patterning on DNA origami. a. Assembly of glucose oxidase (GOx)/ Horseadish peroxidase (HRP) protein pair with a protein bridge for enzyme cascades. Reproduced with permission from reference 69 (American Chemical Society, 2012) **b.** Detection of mRNA after hybridization to a DNA origami template. Reproduced with permission from reference 74 (AAAS, 2008) **c.** DNA nanorobot delivers a cancer therapeutic in the presence of a molecular trigger in vivo. Adapted with permission from reference 70 (Nature Publishing Group, 2018) **d**. Chiral nanoparticles assembled on DNA origami. Reproduced with permission from reference 72 (Nature Publishing Group, 2012).

More recently, several breakthroughs in the field of DNA origami, both in terms of complexity and scalability were reported. Although DNA origami enables creating and patterning DNA nanostructures in great precision, it presents a few key drawbacks. First, the scale of such structures has been restricted to dimension provided by the long scaffold strand. Moreover, it seems unlikely that the M13 scaffold can encode the optimal sequence for efficient folding of all possible structures. To address this issue, Qian and co-workers

were able to produce DNA origami arrays with sizes up to 0.5 square micrometers allowing to render images such as Mona Lisa using multistage assembly process termed "fractal assembly" **(Figure 1.12a)**.[76] An online tool called FracTile Compiler was also created which allows users to select a canvas size up to 8 x 8 tiles and upload an image. The software then automatically converts the image into pixels and shows each stage of the fractal assembly process, thus making the approach more accessible to the community. Dietz *et al.*, in the same journal issue, also reported a strategy to create large-scale DNA assemblies with sizes up to 1.2 gigadaltons and 450 nanometers in diameter with up to 90% yield, revealed by TEM measurements **(Figure 1.12b)**.[77] The approach was based on 3D shape complementary programmed by changing salt concentration and annealing temperature.

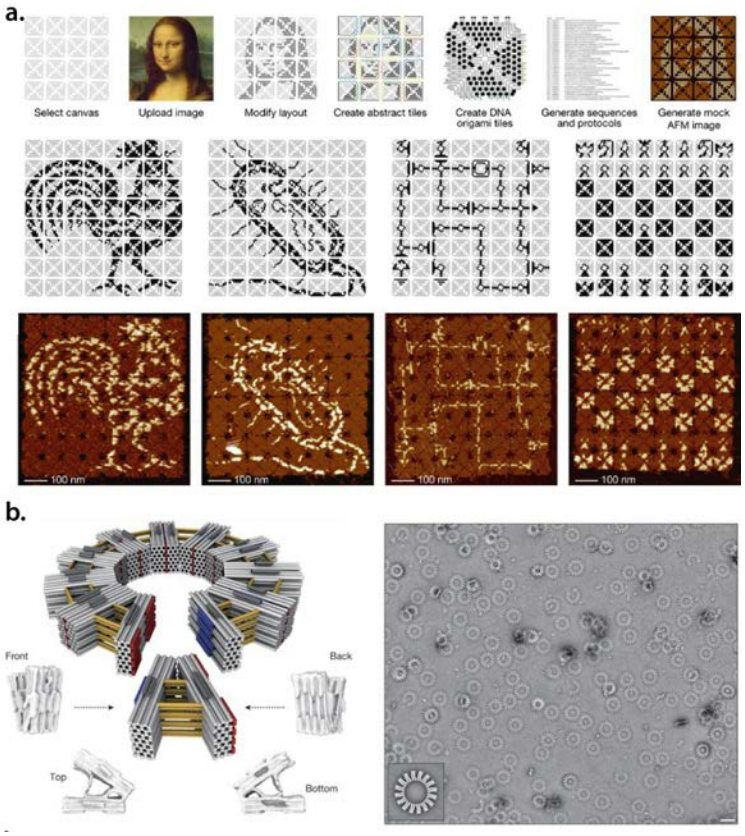

Figure 1.12 | Super DNA origami. **a.** "Fractal assembly" of complex DNA origami pattern. Reproduced with permission from reference 76 (Nature Publishing Group, 2017) **b.** Gigadalton-

scale DNA assembly produced from multiple multi-layer DNA origami object (a V brick). Reproduced with permission from reference 77 (Nature Publishing Group, 2017).

Another main difficulty is that the use of these structures obtained by DNA origami method has been limited to applications that require only a small amount of materials. To address this issue, the Dietz group demonstrated that the production of single staple strands can be scaled up in a cost-efficient manner by using bacteriophages. These single strands of DNA contain both a scaffold and staples separated by built-in "scissors" called DNAzymes, which can be activated by the introduction of zinc ions. Using this approach, the group was able to produce up to 163 mg of 70-nm-long nanorod **(Figure 1.13a)**.[78] The term "single-stranded DNA/RNA origami" was also introduced in the same year, where Yin *et al.* described a single DNA or RNA strand that can self-fold into complex and unknotted structures. They successfully constructed variety of multi-kilobases single-stranded DNA and RNA structures that could be replicated *in vitro* and in living cells **(Figure 1.13d** and **e).**[79]

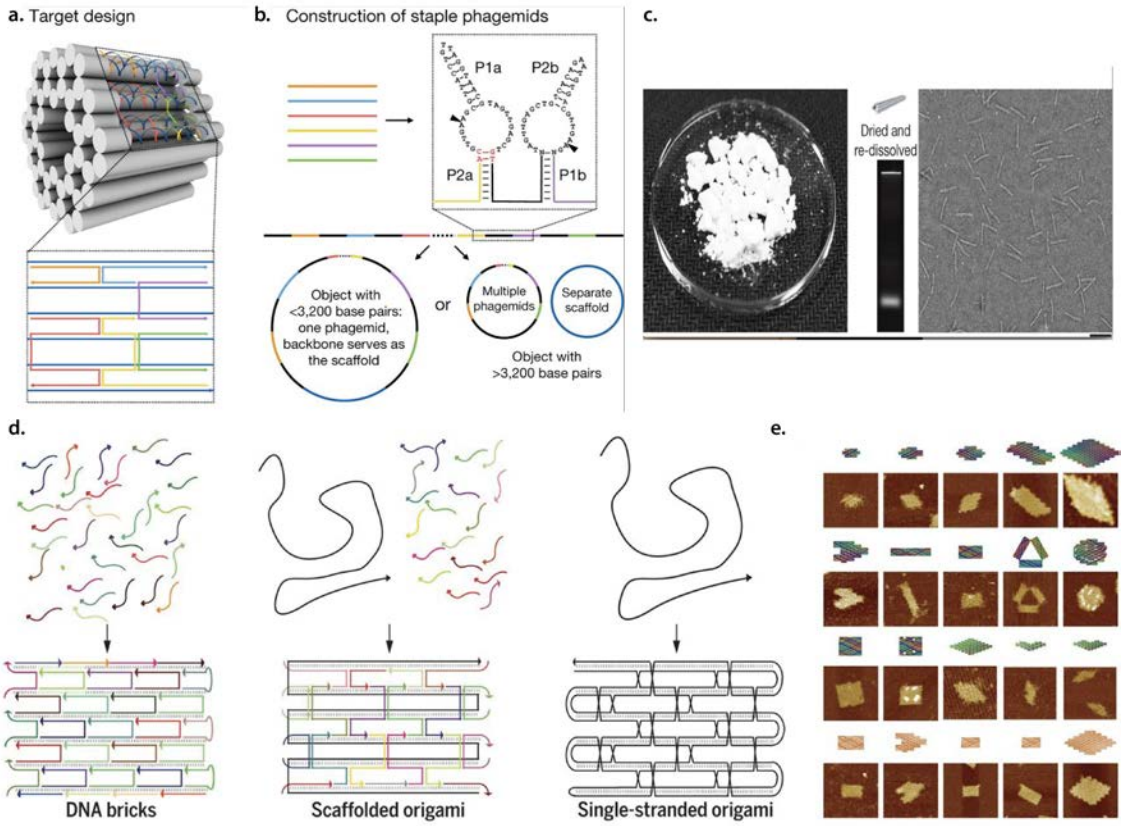

Figure 1.13 | a and **b. Biotechnological method to scale up DNA origami both in quantity and size.** Scale-up DNA origami using bacteriophages to produce ssDNA containing hundreds of staple-strand sequences **c.** Photo of 267 mg of dried powder containing 163 mg of a DNA origami nanorod. Reproduced with permission from reference 78 (Nature Publishing Group, 2017) **d. Single-stranded DNA origami**. Folding of single-stranded DNA or RNA into an unknotted compact ssOrigami structure. Reproduced with permission from reference 79 (AAAS, 2017).

Since its introduction, DNA origami has quickly gained the attention of scientists from many fields as a versatile construction method used in DNA nanotechnology due to the accessibility of the approach. While size and quantity of DNA origami have been scaled up, a large number of strands is still required to fold a single structure and the need to use an excess of the staples, producing waste, may hinder the use of DNA origami in some future applications. This is where a sub-field called "supramolecular DNA assembly" becomes highly attractive, as it combines diverse interactions with conventional Watson-

Crick base pairing to achieve new assembly motifs, while simplifying design rules and minimizing sequence space.

1.5. Supramolecular DNA assembly

As discussed in the earlier sections, DNA is a fascinating example of the power of biomolecules as it is one of the most predictable and programmable self-assembling materials. While the field of DNA nanotechnology has seen many breakthroughs in both structural DNA nanotechnology and DNA origami over the past few decades, the scaffold designs are strictly limited to DNA base pairing. Many great advances in other fields such as organic, polymer and supramolecular chemistry may hold a great opportunity to revolutionize the field. Supramolecular chemistry over the last 50 years has developed in-depth understanding of non-covalent interactions and molecular recognition to program the self-assembly. Supramolecular DNA assembly specifically aims to combine DNA self-assembly with synthetic molecules, in order to generate new materials and structures through variety of non-covalent interactions. The introduction of diverse interactions beyond Watson-Crick base pairing may be a way to increase control over self-assembly, open opportunities to new structures which were not previously attainable.

1.5.1. DNA with organic vertices

Rather than using crossover motifs (e.g. DX tiles) to introduce branched junctions, synthetic vertices can be incorporated to DNA in order to break its linear mode of assembly. An early example of this was demonstrated by the work of Bergstrom *et al.*, where these two-arm vertex molecules can direct the angles and assembly motifs, resulting in a set of cyclic DNA nanostructures **(Figure 1.14a)**.[80] To achieve well-defined assembly structures, Sleiman group developed DNA-m-terphenyl-based vertices having two different DNA sequences and generated a supramolecular DNA hexagon, which was then used as a scaffold for organization of gold nanoparticles **(Figure 1.14b)**.[81] This strategy has been expanded further to construct 2D DNA polygons as precursors for 3D assembly. For

example, cyclic ssDNA triangle was also constructed and could then be used to organize materials by simple hybridization to its single-stranded regions **(Figure 1.14c)**.[82]

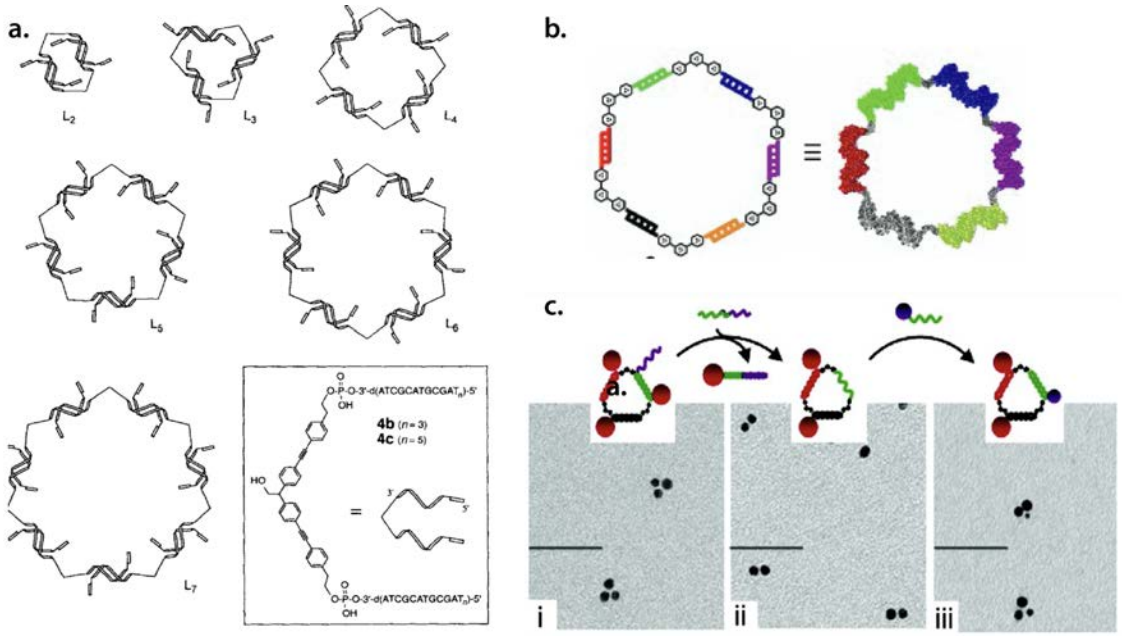

Figure 1.14 | Insertion of organic vertices. a. Assembly of self-complementary branched DNA motifs to produce discrete macrocycles. Adapted with permission from reference 80 (Wiley, 1997) **b**. Hexagonal structure was generated by asymmetric DNA-rigid organic vertices. Adapted with permission from reference 81 (Wiley, 2006) **c.** DNA triangle with three gold nanoparticles was generated with dynamic structural switching. Adapted with permission from reference 82 (American Chemical Society, 2007).

Beyond providing simple structural definition, synthetic molecules can also expand the valency of the attached DNA. The von Kiedrowski group is one of the first who have pushed further the approach from conventional 2-arm to 3-arm molecules. The method involves a 3'-trisoligonucleotidyl template with three individual defined sequences, followed by hybridization of three complementary DNAs bearing 5'-hydrazide modifications. Then, a molecule bearing three aldehyde functional groups can be added to generate a branched molecule containing three different DNA strands **(Figure 1.15a)**.[83] Higher branching units were also made by the Shchepinov, Richert and Nguyen group. Nguyen *et al.* presented an efficient, solid-phase synthesis of a rigid tetravalent molecule-

DNA conjugate. High effective molarity when doing the coupling on bead led to the formation of small molecule-DNA hybrids having four identical DNA strands ($SMDH_4$) as a major product **(Figure 1.15b)**.[84] In the context of self-assembly, two complementary $SMDH_4$ building blocks can aggregate into DNA polymeric particles whose sizes are highly dependent on the assembly time and concentration **(Figure 1.15c).**[85] Shchepinov *et al.* adapted the conventional DNA synthesis to make dendritic oligonucleotides (up to 27 DNA arms).[86-87] Richert *et al.* synthesized four-arm hybrid containing only 2 bases (G and C) each arm and interestingly, the linker rigidity favors crystallization and induces formation of solid at 95°C **(Figure 1.15d)**.[88-89]

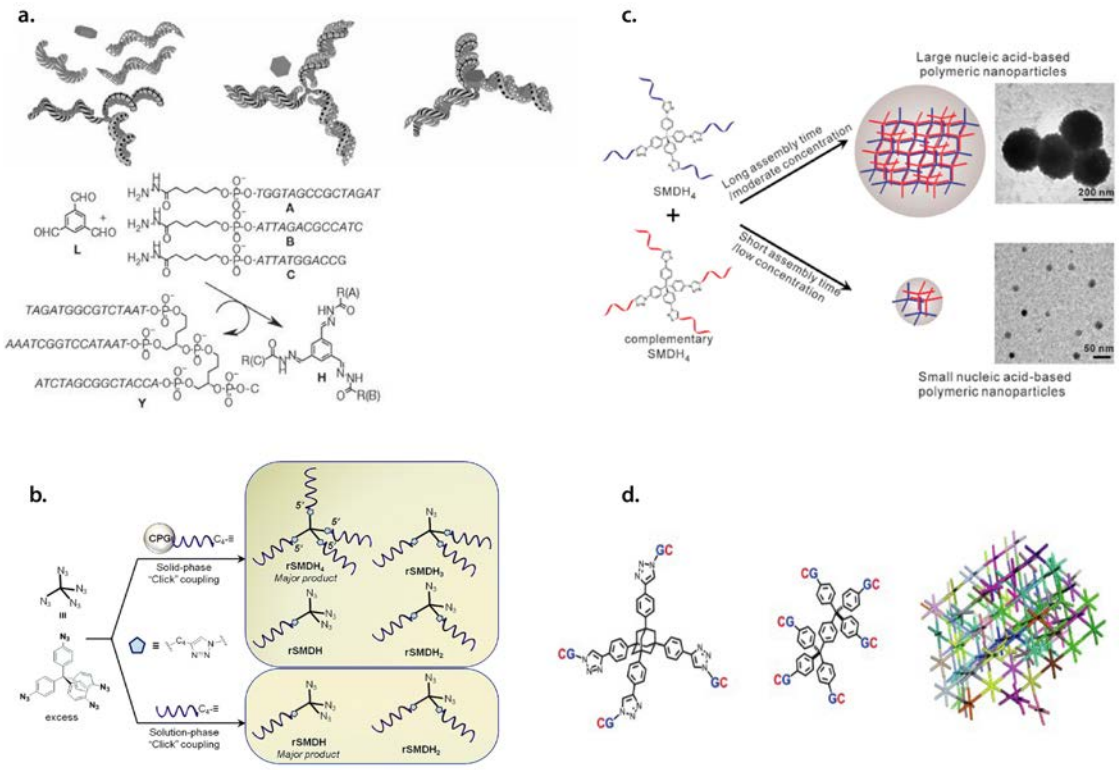

Figure 1.15 | Multi-arm branched small molecules. a. Chemical copying of connectivity using 3-arm template. Adapted with permission from reference 83 (Nature Publishing Group, 2002) **b.** Solid-phase synthesis of $SMDH_4$ using copper-catalyzed "click" chemistry. Reproduced with permission from reference 84 (Royal Society of Chemistry, 2014) **c.** Self-assembly behavior of two $SMDH_4$ depending on concentration and assembly time. Adapted with permission from reference

85 (American Chemical Society, 2015) **d.** 4-arm small molecule core containing GC bases can form solid at 95°C. Reproduced with permission from reference 88 (Wiley, 2011).

A great deal of research has been made over the past years to use these DNA-synthetic molecule precursors for building 3D nanostructures. As one of the first examples, Sleiman *et al*. presented a modular approach to construct 3D polyhedral using a set of single-stranded and cyclic DNA building blocks that contain rigid organic molecules as their vertices. Various cage geometries or even DNA nanotubes can be realized **(Figure 1.16a** and **b)**.[90-94] Later, Kiedrowski and co-workers reported the assembly of DNA dodecahedron from 20 trisoligonucleotides with C_{3h} linkers.[95] The influence of linker flexibility on the assembly outcome was also investigated by the team.[96]

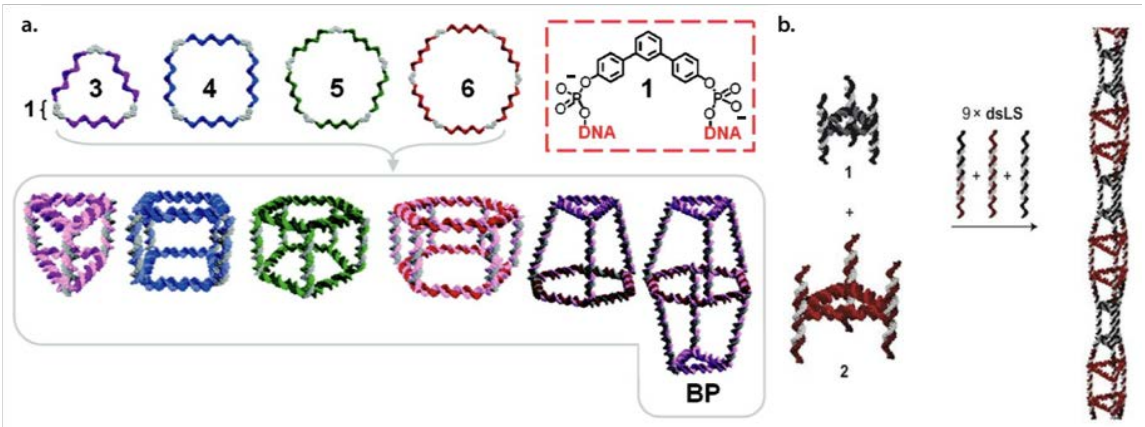

Figure 1.16 | Modular 3D DNA architectures. **a.** 3D prisms with different geometries can be realized using 2D cyclic structures having organic vertices. Adapted with permission from reference 91 (American Chemical Society, 2007) **b.** Expansion of the approach to build DNA nanotube structure. Adapted with permission from reference 90 (Nature Publishing Group, 2010).

Importantly, the incorporation of synthetic units into DNA was found to have a great impact on the assembly outcome, as it significantly enhances DNA hybridization stability and cooperativity, promotes highly ordered long-range assembly and directs the assembled product distribution.[97-102] Greschner *et al.* found that the introduction of a short triphenylene linker can increase the stability of DNA duplex by 10°C in melting temperature (T_m).[101] Melting temperature is the temperature at which 50% of double-

stranded DNA is converted to its single-stranded form. They also showed that a small DNA-intercalating molecule can equilibrate DNA structures into a single product.[102] However, despite their significant promise, these branching units have not been extensively examined because they are difficult to synthesize with the need of multiple orthogonal protecting groups and the resulting branched structures are mostly symmetrical with identical DNA strands.[103-105] Therefore, a facile method to generate asymmetric branching units is highly needed in order to push forward this promising area of research.

1.5.2. Metal-DNA complexes

The synthetic insertions discussed so far have primarily been used for structural purposes: directing angles and defining geometry of DNA assembly. However, those DNA-organic hybrids usually do not possess any active function. Supramolecular chemistry has been exploring metal coordinating ligands in self-assembly for a long time as they provide access to a rich diversity of coordination geometries and functionalities.[106-107] Replacing "passive" organic vertices with metal coordinating ligands, such as bipyridine (bpy), can introduce another supramolecular aspect to DNA assembly. Early examples of metal-complex insertions into DNA were shown by the Sleiman and McLaughlin group.[108-110] Sleiman *et al.* inserted a bpy ligand in the middle of DNA strand using solid-phase synthesis and they presented the first cyclic metal-DNA nanostructures bearing DNA-branched ruthenium (II) complexes. Without the metal, these flexible bpy vertices resulted in a larger cyclic product distribution.[109] Also, some other groups reported the synthesis of a two-, four- and six-arm branched DNA motifs using a metal coordinated geometry, [110-113] which are able to self-assemble into networks.

In addition, DNA can be used to template metal binding into ligand pockets. Different site-specific ligands (e.g. terpyridine and phenanthroline) have been inserted into DNA strands and they are highly selective for four-, five- and six-coordinate metal ions. Combining two different ligands terpyridine (tpy) and diphenyl phenanthroline (dpp) with DNA strands, three unique ligand environments are realized that provide three distinct binding sites for Fe(II), Co(II) and Cu(I) **(Figure 1.17a)**. These metal-DNA duplexes exhibit significantly

higher T_m than a normal DNA duplex and are able to adjust redox state when placed in the incorrect ligand environment.[114]A DNA triangle containing three Cu(I) ions at three corners has been reported by Yang *et al*. and the distance between metal ions could be reversibly modified by DNA hybridization.[115] The approach was further expanded to create 3D metal-nucleic acid cages **(Figure 1.17b)**.[116] Interestingly, the authors also described a DNA-templated method for the formation of a chiral metal-DNA junction containing a single copper (I) unit at the center and four different single-stranded DNA arms. This metal-DNA junction can serve as a unique building block for the assembly of a metal-DNA nanotubular structure **(Figure 1.17c)**.[117]

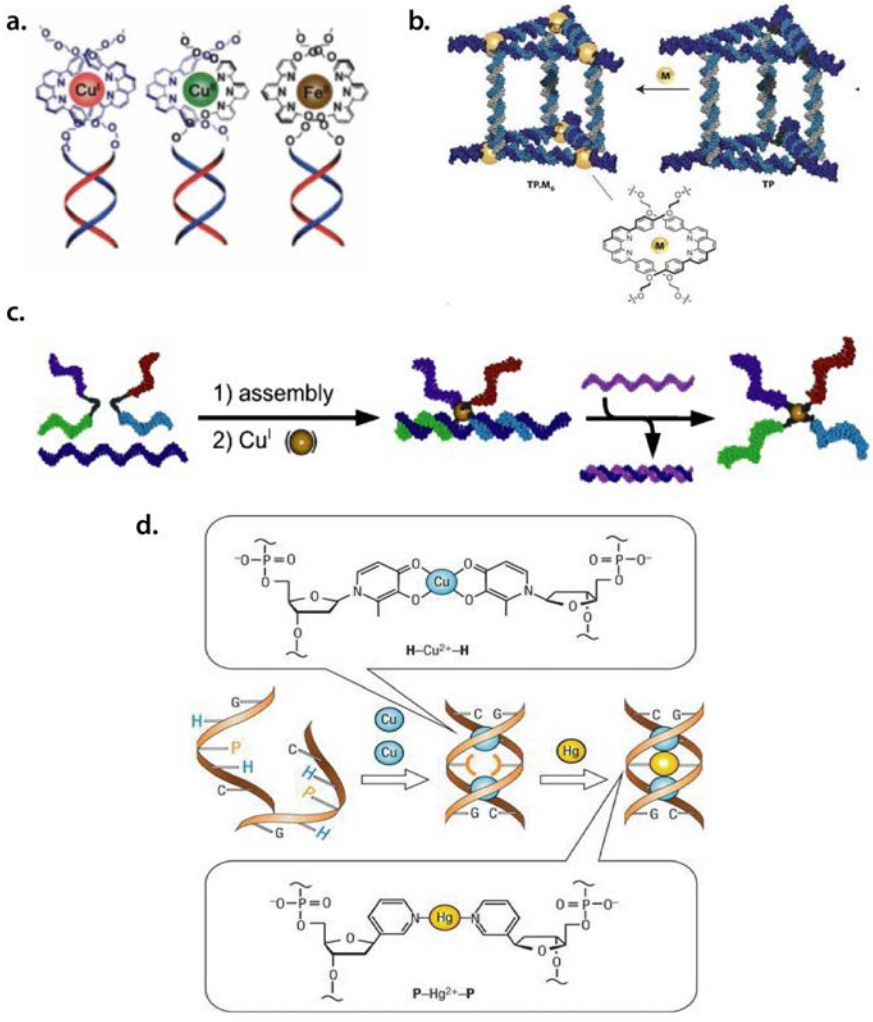

Figure 1.17 | Metal-DNA assembly. **a.** DNA-templated creation of ligand environment for metal coordination. Adapted with permission from reference 114 (Wiley, 2009) **b.** Metal-nucleic cage.

Adapted with permission from reference 116 (Nature Publishing Group, 2009) **c.** Assembly of chiral metal 4-way junction. Adapted with permission from reference 117 (Wiley, 2011) **d.** Stacking of multiple metal ions in artificial DNA duplex. Reproduced with permission from reference 118 (Nature Publishing Group, 2006)

Another commonly used approach is to incorporate metal ions into DNA involves the modification of DNA bases with metal binding ligands, which was pioneered by the Shionoya group, where they replaced natural nucleobases with hydroxypyridone nucleobases. Different metal ions could be stacked on top of one another inside the duplexes by various types of modifications on nucleobases, thereby opening the door to the preparation of well-defined molecular wires **(Figure 1.17d)**.[118] In summary, the incorporation of metal ions into DNA provides unique functionalities that could potentially be applied to many areas such as catalysis, nanoelectronics and sensing.[119-121]

1.5.3. DNA-amphiphilic molecules

Block copolymer self-assembly is an important research area and it has been being used in various applications such as drug delivery, self-assembly and catalysis.[122-124] Amphiphilic block copolymer contains both hydrophilic and hydrophobic components in the same structure. Amphiphiles typically undergo microphase separation with strong aggregation of hydrophobic parts in aqueous solution mainly driven by hydrophobic effect. By carefully controlling the ratio between hydrophobic and hydrophilic part, wide range of predictable morphologies can be obtained such as spherical micelles, cylindrical micelles, vesicles and lamellae.[124] To increase the long-range order of self-assembled DNA structures, chemists are working to covalently attach DNA to hydrophobic molecules. As such, by combining DNA, which is hydrophilic, and hydrophobic molecules/polymers, it can take advantage of the long-range assembly properties of amphiphiles, while retaining the addressability and programmability of DNA. There are two main classes of DNA amphiphiles: **1)** DNA-lipid and **2)** DNA-polymer conjugate. In this section, the synthetic approach and self-assembly aspect of this class of material will be discussed.

1.5.3.1.Synthetic methodology

A number of approaches to synthesize DNA amphiphiles have been reported but can be divided into two main methods: pre-synthetic and post-synthetic.[125] Pre-synthetic approaches involve the use of solid-phase coupling chemistry in DNA synthesis to incorporate hydrophobic molecules. Hydrophobic molecules are normally modified with reactive handles, which can react with functionalized DNA strands on solid support. Very often, hydrophobes are modified to have phosphoramidite moiety to make use of the high yielding phosphoramidite chemistry in DNA synthesis. Several different coupling mechanisms (e.g. "click" chemistry) also were developed and carried out directly on bead **(Figure 1.18).**[105, 126] Generally, pre-synthetic approaches generally have higher yield and are faster due to high local concentration of reactive functionalities on the solid support.

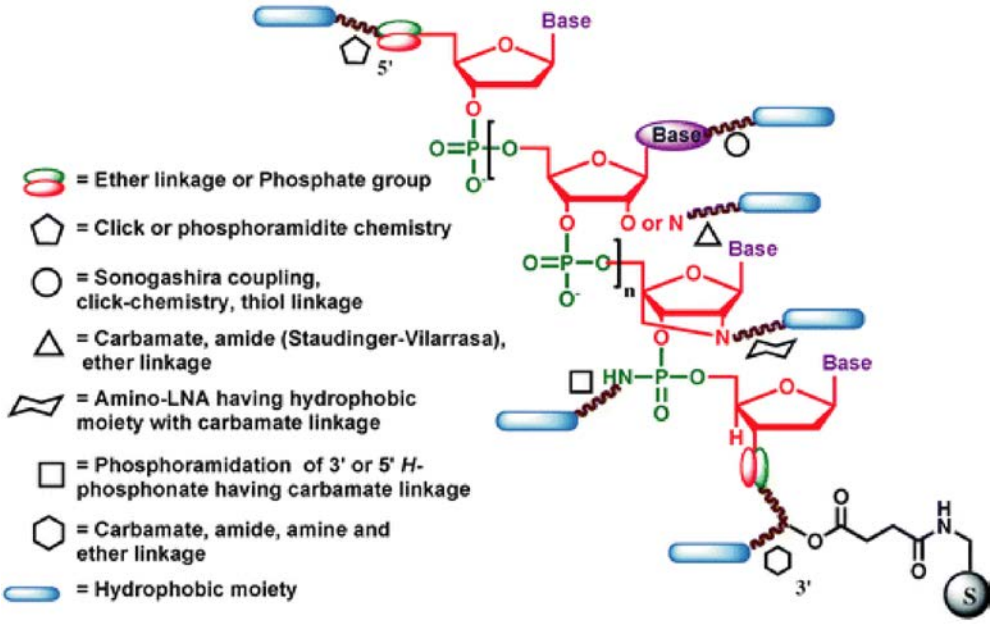

Figure 1.18 | Synthesis of DNA amphiphiles. Possibilities to modify DNA backbone are presented. Reproduced with permission from reference 125 (Royal Society of Chemistry, 2011)

One major pitfall of the pre-synthetic approach is that while it typically works very well with small molecules, it is not well-suited with long hydrophobic polymers due to small solid support pore size (500-2000 Å).[127-128] More importantly, the linkage chemistry between DNA and hydrophobic molecules needs to be robust enough to survive harsh conditions during solid-phase synthesis. On the other hand, post-synthetic strategies can potentially address this issue which involve the attachment of hydrophobic molecules to DNA strands after being deprotected in a selected solvent. These approaches are known to happen under milder conditions. Hydrophilic molecules and polymers can be efficiently attached to DNA in aqueous media.[129-131] Post-synthetic approach, however, is normally limited by the incompatible solubility between the hydrophobic moieties and hydrophilic DNA.

1.5.3.2. DNA-amphiphiles self-assembly

The covalent modifications of DNA strands with hydrophobic molecules has led to the creation of new self-assembled DNA nanostructures over different length scales. In the context of self-assembly, DNA-lipid and DNA block copolymer conjugates have been made and can self-assemble in a number of interesting morphologies. For example, DNA block copolymers were induced to switch between different morphologies with externally added DNA strands or enzymes **(Figure 1.19b)**.[132-133] Herrmann *et al.* was able to switch morphology reversibly from a spherical core/shell structure to elongated DNA-polymeric fiber with DNA-b-poly(propylene oxide) block copolymer **(Figure 1.19a)**.[133] Sleiman and co-workers synthesized a short DNA duplex-oligo (ethylene glycol) conjugate which can assemble into long fibers and 2D networks in selective solvents.[134]. More recently, a high-yielding method to append multiple long alkyl chains in a row to DNA with controlled sequence was reported and more importantly, the resulting DNA-polymeric molecule can further self-assemble in aqueous media to yield highly monodisperse spherical micelles. The self-assembly behavior is highly dependent on the polymer sequence added to DNA.[135] In addition to exploiting hydrophobic properties of lipids and polymers, other interactions such as π-π stacking were also applied by Haner *et al.* to generate DNA-grafted supramolecular

polymers in 1D and 2D using DNA-oligo pyrene conjugates **(Figure 1.19d)**.[136-138] Sleiman *et al.* recently discovered that adding a single cyanine dye to the DNA-b-oligohexaethylene chains described earlier[135] can induce a drastic change in morphology from spherical micelles to long DNA nanofibers with controlled dimensionality, due to π stacking between cyanine dye molecules **(Figure 1.19d)**.[139]

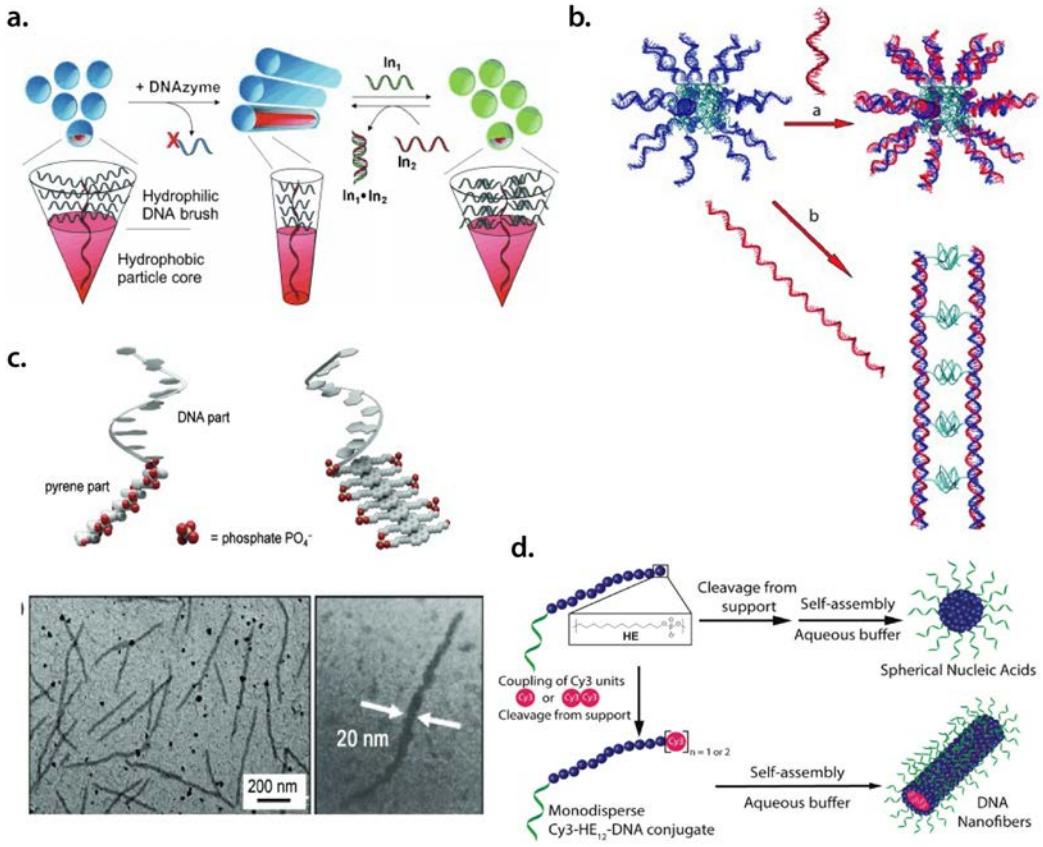

Figure 1.19 | Self-assembly and dynamic behavior of DNA amphiphiles. a. Programmable shape-shifting micelles using two stimuli. Adapted with permission from reference 132 (Wiley, 2010) **b.** DNA-poly (propylene oxide) undergoes morphological change in the presence of external DNA stimuli. Reproduced with permission from reference 133 (Wiley, 2007) **c.** Fiber formation of DNA-oligo pyrene conjugate. Adapted with permission from reference 137 (Wiley, 2015) **d.** Morphological change from spherical nucleic acids to DNA nanofibers with an addition of a cyanine dye molecule. Reproduced with permission from reference 139 (American Chemical Society, 2018)

Decorating DNA-lipid/polymers conjugate onto DNA scaffolds is also interesting as it is possible manipulate their assembly behavior. A temperature responsive polymer, poly(n-isopropylacrylamide) (poly (NIPAM)), was successfully conjugated to a DNA tetrahedron via copper catalyzed "click" reaction. The conjugated structure undergoes a morphological change from a single tetrahedron to a giant, well-defined aggregate with temperature change, as confirmed by AFM, DLS and cryogenic electron microscopy (cryoEM) **(Figure 1.20a)**.[140] DNA cages were hybridized to sequence-controlled amphiphilic DNA-polymers to yield different assembly modes. Specifically, when four DNA-polymer conjugates at specific length are decorated on one side of DNA cubes, they aggerate in aqueous media into dimer, trimer and etc. With a relatively long polymer on both sides of the DNA cube, monodisperse spherical micelles with hydrophobic cores and DNA scaffolds on their exterior are observed. The internal hydrophobic core is able to capture and release small molecule drugs **(Figure 1.20c, d and 1.20e).**[141-143] Very recently, using the same strategy with DNA-cholesterol conjugate, the Sleiman group was able to induce similar assembly modes and interestingly, the DNA-cholesterol cubes acted as lipid membrane nanopores, constituting the first open-walled DNA nanopores and reproducing functions of membrane proteins **(Figure 1.20e)**.[144] Furthermore, larger structures such as DNA origami can be manipulated in terms of self-assembly through the incorporation of hydrophobic molecules. Cholesterol-modified, single-layered DNA origami can be folded into sandwich-like structures, reported by Simmel *et al*. Interestingly, in the presence of lipid bilayers or surfactants, the double-layered DNA origami can be unfolded.[145] Recently, Shih and Lin *et al.* used 3D DNA origamis as scaffolds to produce homogenous liposomes with different sizes, which were molded in the shape of the origamis.[146] Liu and co-workers developed an approach called "framed-guided" assembly in which the inside frame dictates assembly structures rather than intrinsic properties of amphiphilic molecules. The method was applied to guide the assembly of DNA amphiphiles using DNA origami or gold nanoparticles **(Figure 1.20b & 1.20f)**.[147-149]

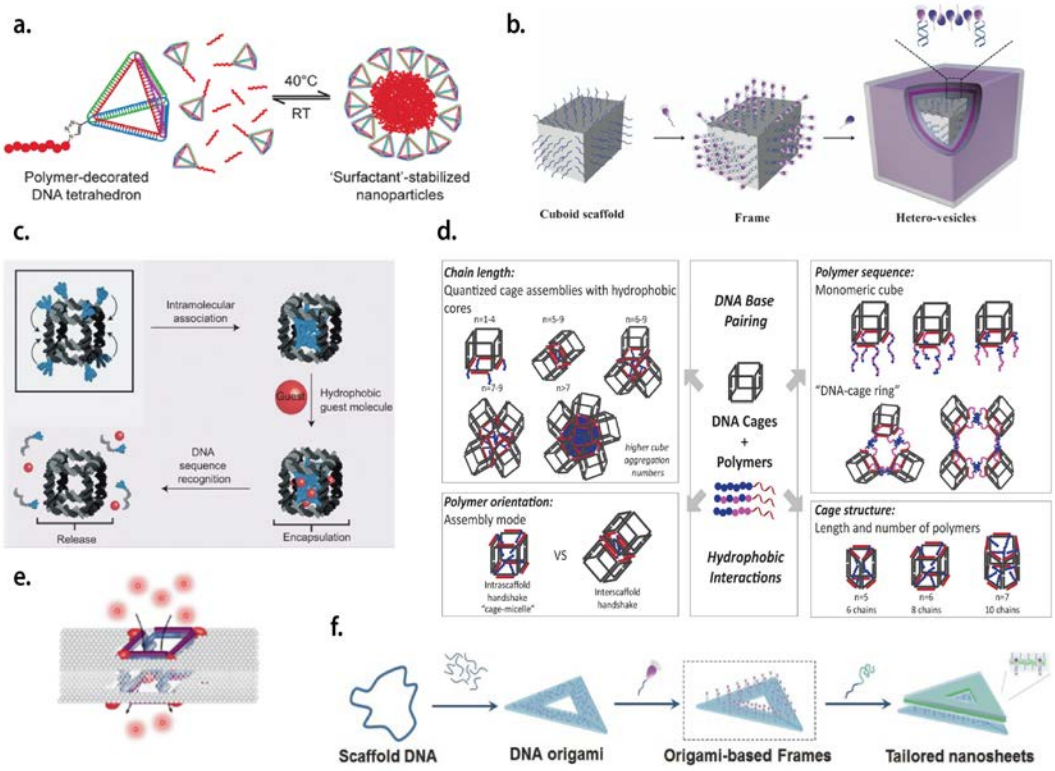

Figure 1.20 | Integration of DNA amphiphiles on DNA nanostructures. **a.** Temperature-responsive aggregation of poly (N-isopropylacrylamide) functionalized-DNA tetrahedron. Adapted with permission from reference 140 (American Chemical Society, 2013) **b.** Frame-guided assembly process with a DNA origami cube scaffold. Adapted with permission from reference 146 (Wiley, 2016) **c.** Decoration of dendritic DNA-polymer conjugate on DNA cube. Adapted with permission from reference 143 (Nature Publishing Group, 2013) **d.** Quantized assembly of DNA cube decorated with DNA-oligo hexaethylene conjugates. Reproduced with permission from reference 142 (American Chemical Society, 2015) **e.** DNA-cholesterol cube can act as nanopore on lipid membrane. Adapted with permission from reference 144 (American Chemical Society, 2018) **f**. Controlling 2D nanosheets of amphiphilic molecules through frame-guided assembly. Reproduced with permission from reference 148 (Wiley, 2016).

It is clear that the incorporation of hydrophobic entities to DNA is highly advantageous, especially in the context of self-assembly. Simple modification of DNA strands can induce different unique assembly modes that have never been achieved before with Watson-Crick base pairing. Beyond this, DNA amphiphiles also show great promise in

many other applications such as drug delivery, lipid bilayer anchoring or signal transduction.[150-157]

1.6. DNA-templated synthesis (DTS)

So far in this chapter, we have seen that using nucleic acids as building block has truly transformed nanoscience, as it is an excellent material for constructing structures at nanoscale. However, beyond the self-assembly perspective, chemists have discovered that DNA constitutes a wonderful scaffold for manipulating chemical reactivity. We, as chemists, normally manipulate and control reactivity of chemical substances in a solution at high concentration (typically millimolar to molar range) to ensure random collisions between functional groups participating in a reaction. On the other hand, nature controls reactivities of substrates at significantly lower concentration (nano- to micromolar range (nM- μM)). At this concentration range, random collision probability is low. Nature uses high effective concentration, governed by a macromolecular template, to enable chemical reactivity of biological reactions, that then take place at much more diluted concentration than those performed in chemical laboratory. Particularly, DNA-templated synthesis plays an important role in replication, transcription and translation of genetic information. At suitably low concentration (nM), reaction rates between building blocks are enhanced in the presence of DNA-DNA and DNA-protein interactions. DNA-templated synthesis has proven useful in many fields such as diagnostics, polymer formation and drug and reaction discovery.[158-159] In this section, we will mainly focus on recent advances of DTS in the context of templated ligation, DNA duplex crosslinking and small molecule/oligomer synthesis mediated by DTS.

1.6.1. Early day of DTS and applications of DTS in templated ligation and crosslinking

Early examples mostly explored nucleic acid-templated synthesis to facilitate the formation of DNA oligomers, where single-stranded DNA (or RNA) served as a template

to catalyze the formation of phosphodiester bond, which was of great interest in many groups at that time, such as Gilham, Orgel and many others, before the advent of automated DNA synthesis.[160-164] For example, Letsinger and co-workers reported a fast ligation between a phosphorothioate and an α-halo acyl functional group with up to 90% conversion in only 20 minutes.[165] Kool *et al.* have demonstrated chemical auto-ligation processes, involving the reaction of a phosphothioate or -selenoate anion on one strand with a 5'-carbon atom bearing an iodine leaving group on the other strand **(Figure 1.21a)**.[166-169]

The idea of using DNA-templated reaction was expanded further beyond analogues of the phosphoribose backbone to other chemistries, which were then applied to the development of a number of strategies in two main topics: templated crosslinking and templated ligation. In the context of templated inter-strand crosslinking, Fujimoto *et al.* reported one of the first examples of irreversible photo-crosslinking between DNA strands using [2+2] cycloaddition between a *p*-carbamoylvinyl phenol nucleoside and an adenosine on the complementary strand **(Figure 1.21b)**.[170] RNA complements can also be linked together using reversible photo-crosslinking reaction demonstrated by the same group **(Figure 1.21c)**.[171] A number of strategies for crosslinking DNA strands have been developed to achieve greater selectivity when joining two complementary strands **(Figure 1.21d)**.[171-175]

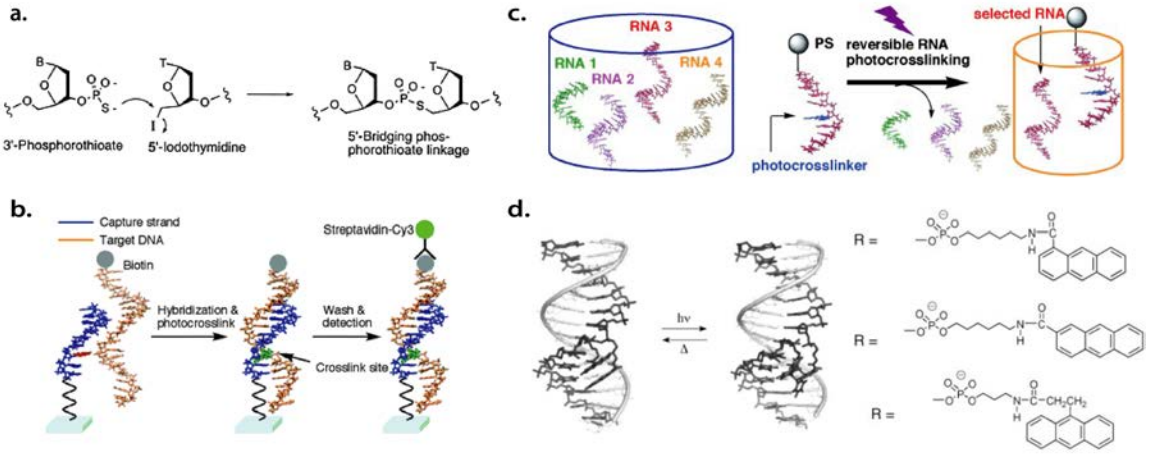

Figure 1.21 | Early example and templated DNA crosslinking. **a.** Formation of phosphorothioate bond using 3'-phosphorothioate and 5'-iodothymidine. Adapted with permission from reference 168 (Elsevier, 1997) **b.** Interstrand photo crosslinking between RNA strands with high specificity.

Reproduced with permission from reference 171 (Wiley, 2009) **c.** Photo crosslinking via p-carbamoylvinyl phenol nucleosides. Reproduced with permission from reference 170 (Royal Society of Chemistry, 2007) **d.** Photo crosslinking using anthracene dimerization. Reproduced with permission from reference 173 (Oxford, 2007).

The topic of templated strand ligation has been active for a number of years where numerous reactions with different levels of selectivity and efficiency have been shown to serve the purpose. This part summarizes only some key findings in this topic. [2+2] cycloaddition was used to form a thymine dimer or reversible ligation of DNAs as reported by Saito and co-workers **(Figure 1.22a)**.[176] Jyo *et al*. proposed an alternative way of using anthracene photodimerization for DNA photo-ligation. The method achieves high rate of conversion within several minutes and was shown to be useful for single nucleotide polymorphism detection.[173] In modern chemistry, copper-catalyzed alkyne-azide coupling ("click") chemistry has become a powerful approach that is widely used in various fields including chemical biology and drug discovery; due to its selectivity, biocompatibility and versatility.[177-178] It has inspired many groups to evaluate this reaction in the context of DNA-templated reactions. For instance, peptide nucleic acid (PNA) fragments could be joint together by copper-catalyzed reaction using a DNA template.[179] The Brown group explored the use of templated "click" reaction in producing a covalently closed single-stranded DNA circle and a double-stranded DNA pseudohexagon,[180] as characterized by MS, HPLC and enzyme digestion **(Figure 1.22b)**. Surprisingly, very recently, the group discovered that multiple triazole linkers in ligation product, resulted from copper-catalyzed "click" reaction, are fully compatible in living systems as they can be replicated and transcribed both *in vitro* and *in vivo* **(Figure 1.22c)**.[181] This finding can conceivably help to overcome the challenge of synthesizing epigenetically modified genes and genomes. Gothelf *et al.* reported an efficient and reliable method to dimerize, trimerize and polymerize generation-4 polyamidoamine (PAMAM) dendrimers using templated "click" reaction. The approach can be useful with other types of macromolecules or nanoparticles **(Figure 1.22d)**.[182] A number of reactions, including nucleophilic substitution, condensation and cross-coupling, have been also developed (see below in the next section).[183] Another interesting strategy in DNA-templated synthesis was described by

Sheppard and Czlapinski involving coordination chemistry between Ni^{2+} or Mn^{2+} in the presence of 2-salicylaldehydes and ethylenediamine **(Figure 1.22e)**.[184] The approach is highly efficient and has been subsequently used to synthesize conjugated structures (will be discussed below in section **1.6.6**).

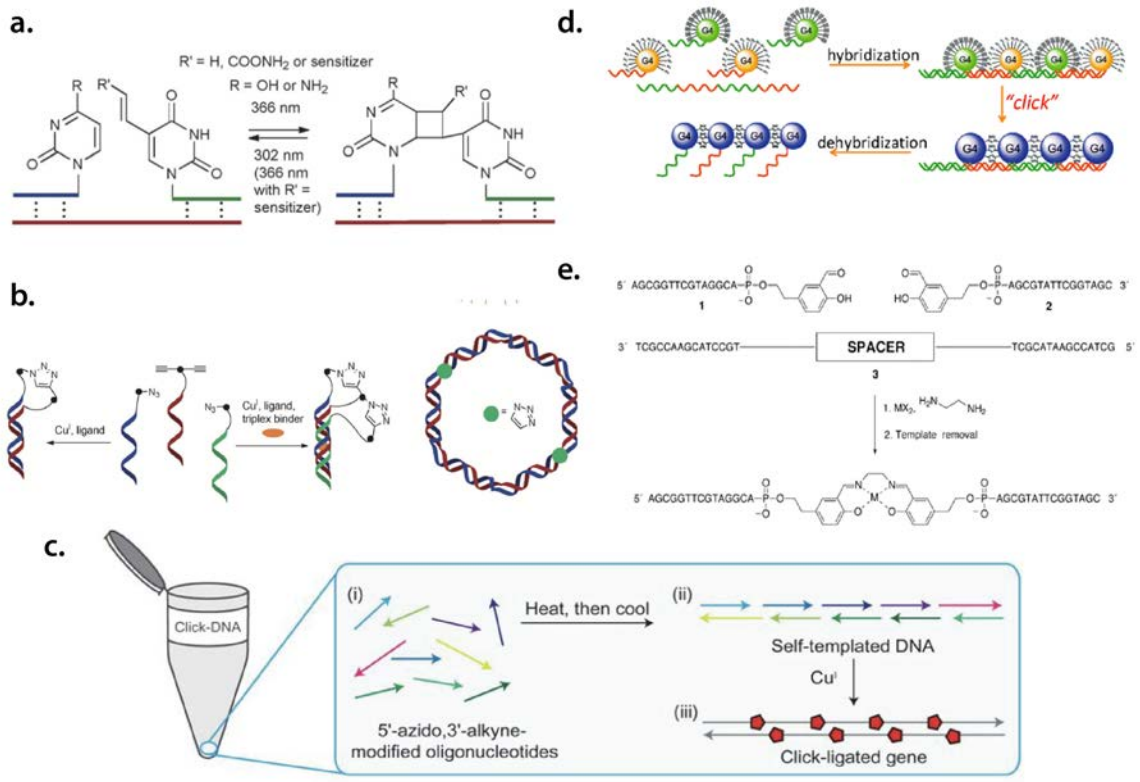

Figure 1.22 | Templated DNA strands ligation. a. Reversible templated [2+2] photoligation of DNA strands. Adapted with permission from reference 176 (American Chemical Society, 2000) **b.** A double-stranded DNA pseudohexagon formation using templated "click" chemistry. Reproduced with permission from reference 180 (American Chemical Society, 2007) **c.** Templated-ligation of PAMAM dendrimers. Reproduced with permission from reference 182 (American Chemistry Society, 2010) **d.** Templated "click" ligation of DNA backbone which can be transcribed both *in vitro* and *in vivo*. Adapted with permission from reference 181 (Nature Publishing Group, 2017). **e.** Templated ligation using Mn^{2+} salt. Adapted with permission from reference 184 (American Chemical Society, 2001)

The integrity of DNA-based architectures is highly dependent on the salt concentration, temperature or nucleases.[185-187] As such, improving stability of DNA structures is of great significance to many applications. The development of efficient strategies to crosslink and ligate DNA strands opened an opportunity to stabilize DNA nanostructures, thus improving the robustness of structures with the depletion of salt, at high temperature, and *in vivo.* A DX tile can be stabilized by reversible covalent disulfide bond.[188] Majima *et al.* reported a way to crosslink a micrometer-scale DNA rod structure using bismaleimide linkers, as characterized by gel electrophoresis and AFM **(Figure 1.23a)**.[189] In another example, DNA catenanes, assembled by single-stranded tiles, can be covalently "locked" using copper-catalyzed "click" chemistry in nearly quantitative yield, resulting in structures that have higher resistance to low cation concentrations, elevated temperatures and nucleases **(Figure 1.23b)**.[190] Many other examples were shown to efficiently stabilize DNA structures via crosslinking.[191-193] Very recently, Dietz *et al.* explored the use of thymidine covalent dimerization under 310 nm light in stabilizing DNA origami structures. The structures were found to be more stable in physiological conditions and cation-depleted environment, confirmed by gel electrophoresis and cryoEM studies **(Figure 1.23c)**.[194] The group then modified one blunt end with 3-cyanovinylcarbazole and placed a thymidine (T) at the other end. Upon irradiating 365 nm light, a covalent bond between two these moieties can be formed. Interestingly, the same bond can be efficiently cleaved with an exposure to 310 nm light in just few seconds, resulting in a new reversible way to crosslink DNA assemblies.[195]

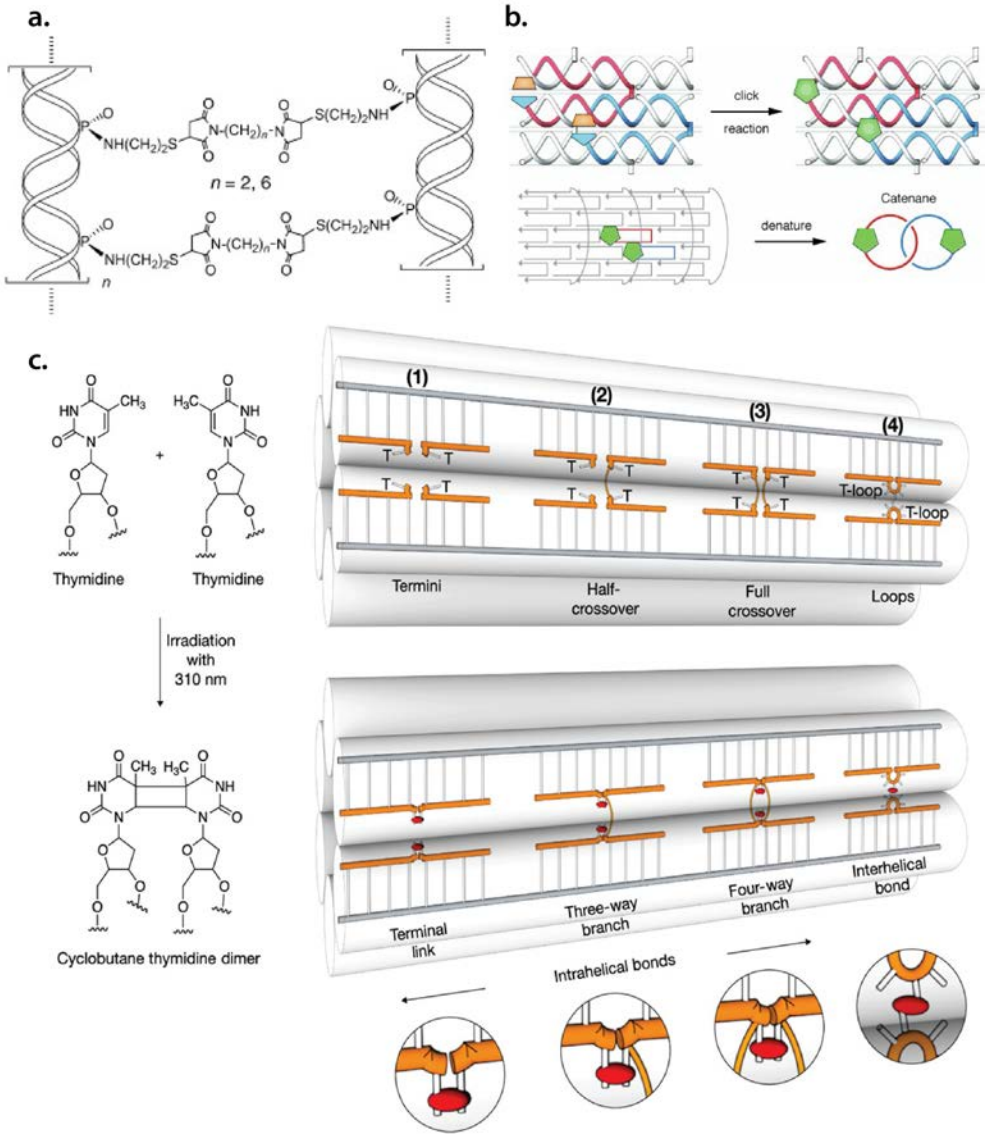

Figure 1.23 | Stabilization of DNA nanostructures. **a.** Crosslinking a micrometer-scale DNA rod structure using bismaleimide linkers. Adapted with permission from reference 189 (Wiley, 2003) **b.** Locking DNA catenanes by templated "click" chemistry. Reproduced with permission from reference 190 (Wiley, 2015) **c.** Stabilizing DNA origami using thymidine dimerization. Reproduced with permission from reference 194 (AAAS, 2018).

1.6.2. Multistep reactions using DNA-templated synthesis

DTS can be used for complex small molecule synthesis and the Liu group at Harvard University is a pioneer in this area. In the early days, the main effort mostly

focused on the development of many different reactions for DNA-templated synthesis (DTS). A and B reactive moieties are brought in close proximity by DNA hybridization, thus facilitating the bond formation due to high local concentration **(Figure 1.24)**. With this arrangement, DTS has been explored with variety of chemistries such as Wittig olefination, Heck coupling, reductive amination and Huisgen cycloaddition to broaden reaction scope of templated strands ligation. [183, 196-200] A list of possible chemistries are summarized below in **Figure 1.24**.

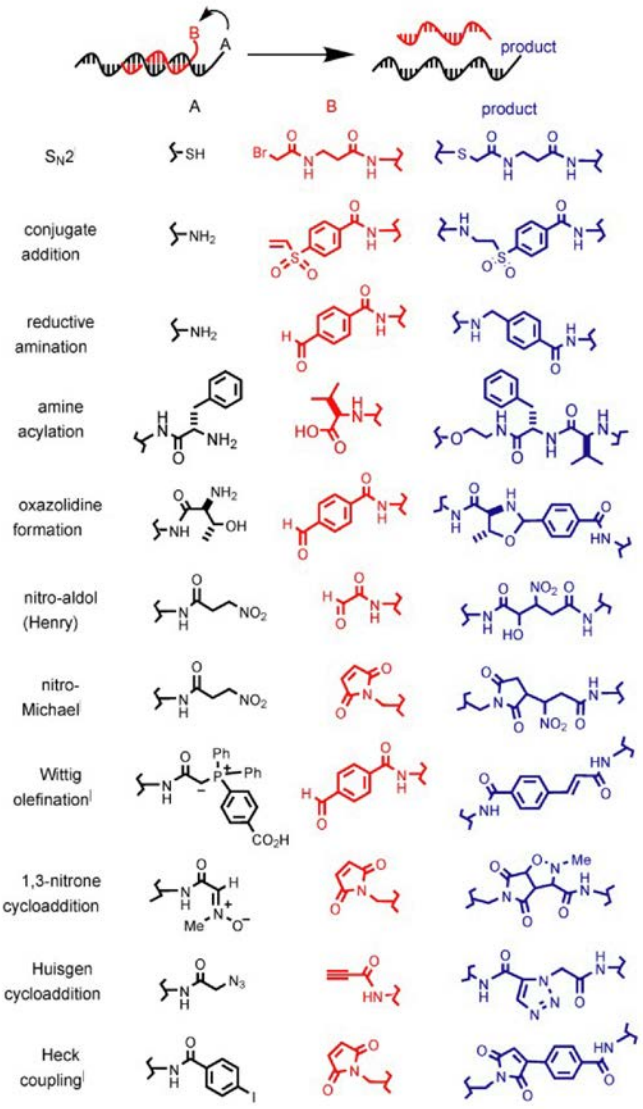

Figure 1.24 | Reaction scope of DTS. DTS can be performed using variety of chemistries. Reproduced with permission from reference 183 (Wiley, 2004).

Moreover, the Liu group early on realized that functional group close proximity might not be necessary in many DNA-templated reactions such as amine acylation and Wittig cycloaddition **(Figure 1.25)**.[196-197] The discovery of distance-independent DTS sets the foundation to many discoveries, as it allows a single template to be translated into complex molecules in a progressive manner. The finding can be explained in a simple way that the bond formation occurs at a faster rate than DNA hybridization which is mostly driven by high dilution and aqueous solvent. High dilution eliminates the formation of undesired dimers and oligomers since the reaction was performed at very low concentration (typically nM- μM). In addition, aqueous solvent proves to be better solvent than non-aqueous alternatives as the rate-determining transition states of many reactions above are more polar than starting materials.

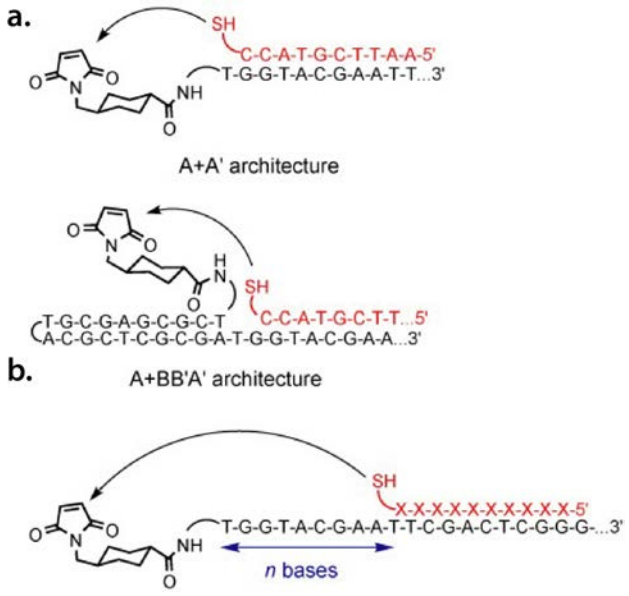

Figure 1.25 | Distance-independent DTS. DTS can be performed using variety of chemistries. Reproduce with permission from reference 183 (Wiley, 2004).

The synthesis of complex molecules using DTS requires multiple succeeding steps. Following the discovery of distance-independent DTS, the group first developed a number of linker (i.e. scarless, 'useful scar' and autocleaving linkers) and purification strategies (e.g. using biotin-streptavidin interaction) that allow the product of DNA-templated

reaction to proceed subsequent steps **(Figure 1.26)**.[201] For instance, first, an amino-modified DNA template **(3)** is hybridized to a DNA reagent strand incorporated with the "scarless linker" **(1)**, thus allowing efficient ligation of two strands via amide bond formation **(2)** due to elevated local concentration. In order to enable the next steps, the template strand needs to be cleaved from the reagent-template product **(2)**, regenerating an available amino functionality. To do that, an increase in pH to 11.8 cleaved the sulfone linker at the carbamate functionality, thereby liberating an amine group on the template strand. After the process, a new amino acid was transferred successfully from the reagent strand to the template strand. These linkers are particularly attractive because the template strand can be cleaved without the introduction of additional chemical wastes.

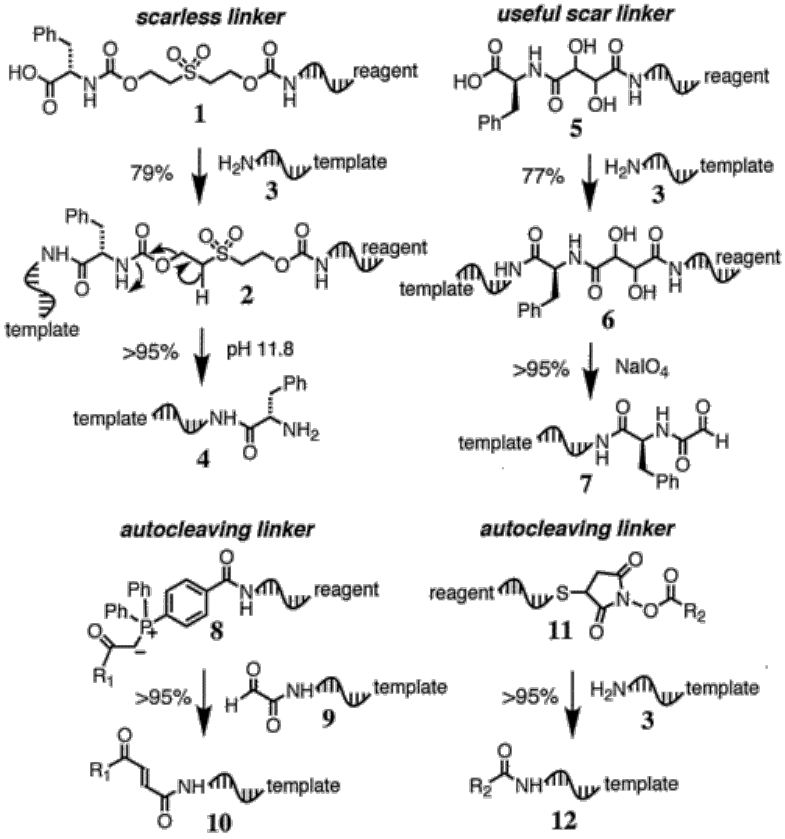

Figure 1.26 | Different linkers for multi-step DNA-templated synthesis. Reproduced with permission from reference 201 (American Chemical Society, 2002).

They were then successfully integrated into DNA templates, which underwent three successive templated reaction yielding tripeptide. This is the first example of multistep synthesis by DTS (**Figure 1.27**).

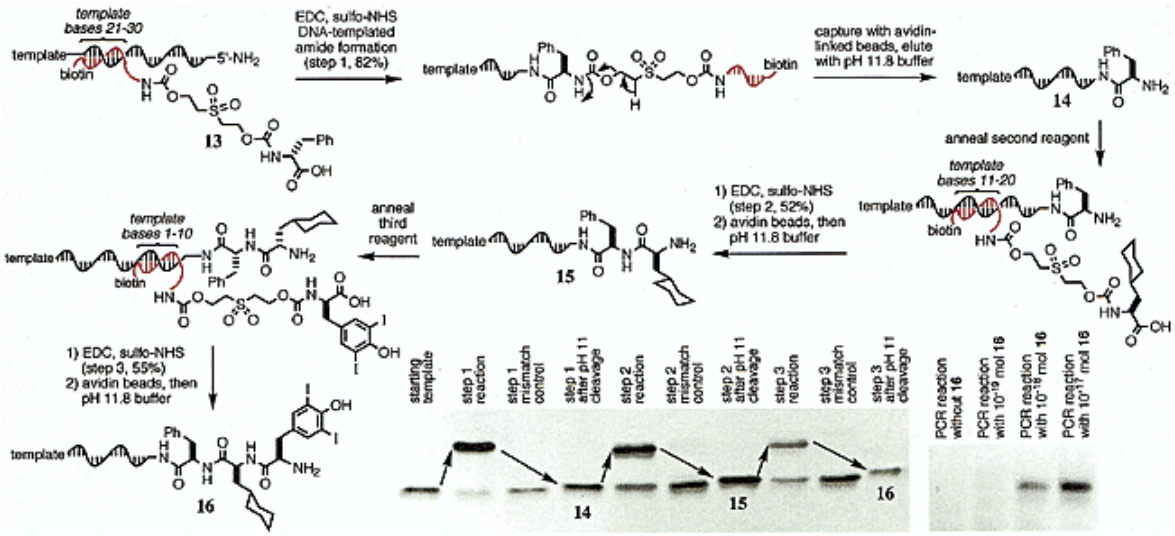

Figure 1.27 | First example of multistep synthesis by DTS using "scarless linker".
Reproduced with permission from reference 201 (American Chemical Society, 2002).

Drawing on this success, a number of strategies and template architectures (e.g. T, omega (Ω) and Y) were developed that greatly expanded the scope of multistep DTS. The Ω template is particularly useful in some *distance-dependent* DNA-templated reactions such as reductive amination **(Figure 1.28a)**.[198] The T architecture enables two DNA-templated reactions to take place on a single template in one step **(Figure 1.28b)**. As an example, the Ω and T architectures have been implemented together successfully to achieve the efficient DNA-templated synthesis of N-acyloxazolidine targets (up to 51% yield), which are prominent examples of heterocycles found in biologically active natural products **(Figure 1.28c)**.[202] In the same year, the group applied multistep DTS to generate a library of macrocycles. They subjected each 48-base starting template having three "codons" to three successive DNA-templated amine acylation reactions with building blocks conjugated to DNA 10- or 12-mer DNA reagents, similar to tRNAs. Although macrocycles are quite challenging to synthesize with conventional organic synthesis, DNA-templated synthesis

significantly simplifies the process and also allows the generation of a large libraries that were used for screening target protein binding **(Figure 1.28d)**.[203-204]

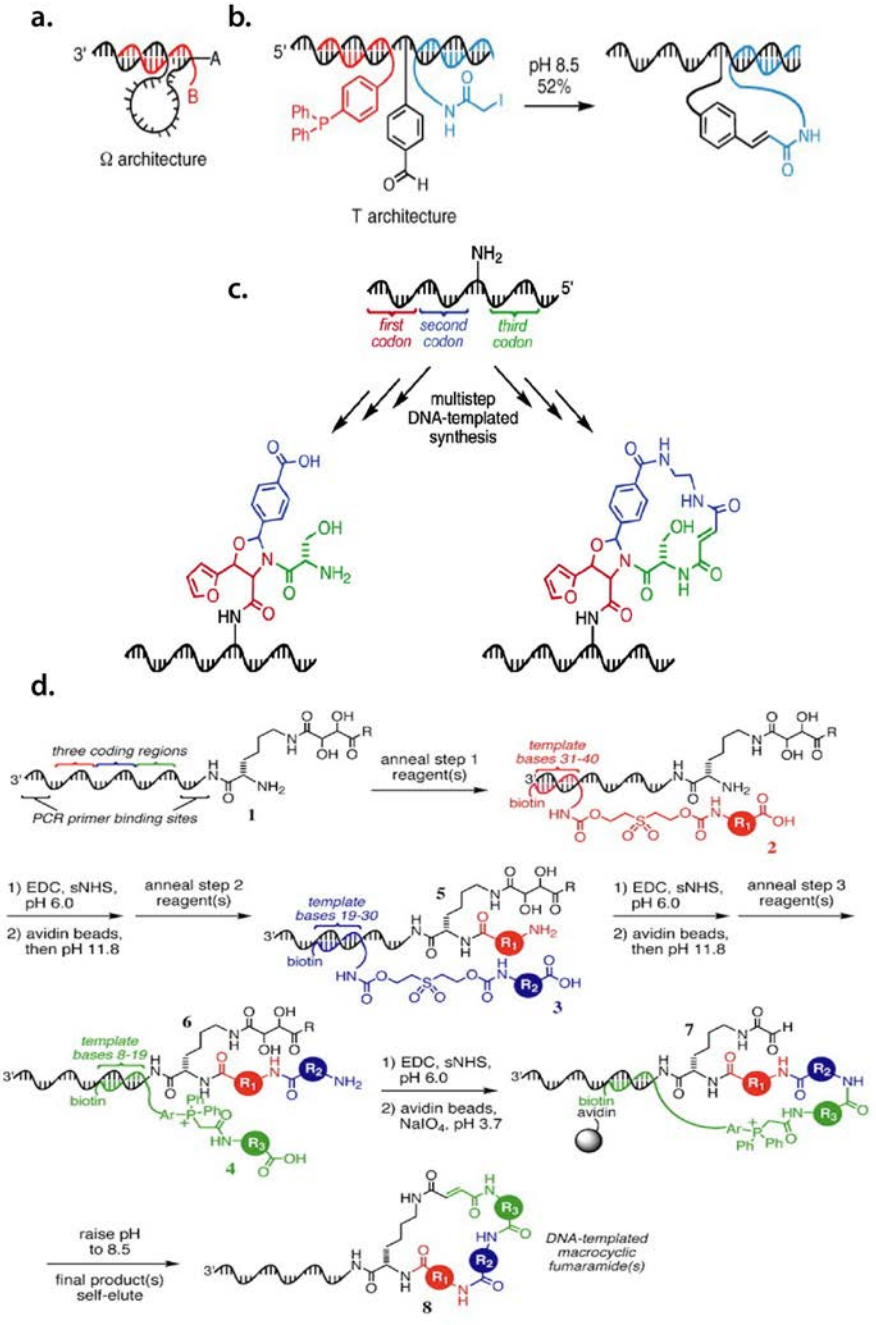

Figure 1.28 | Different DTS motifs. a. Ω architecture for DTS. Adapted with permission from reference 198 (Wiley, 2003) **b**. T architecture for two DNA-templated happen at the same time. Adapted with permission from reference 198 (Wiley, 2003) **c.** Application of Ω and T architectures

in the synthesis of N-acyloxazolidine. Adapted with permission from reference 202 (American Chemical Society, 2004) **d.** Multistep DTS for the generation of library of macrocycles. Reproduced with permission from reference 203 (AAAS, 2004).

1.6.3. Sequence-controlled synthesis using DTS

Nature achieves complex synthesis in a single operation by enzyme mediated increase of the effective molarity of reagents. In the absence of enzymes, this task has proven to be a big challenge. The Liu group demonstrated a method to perform ordered multistep synthesis of a triolefin and a tripeptide using temperature-controlled DTS in one-pot, where all reagents are present simultaneously.[205] The group engineered a DNA template in such a way that, by changing temperature, it undergoes stepwise sequence-programmed changes in the DNA secondary structure. These changes expose hybridization sites for DTS, thus enabling reactivities between functional groups to be modulated. The order of the building blocks in the final product was confirmed using Matrix Assisted Laser Desorption/Ionization mass spectroscopy (MALDI-TOF MS). The method, however, is limited by the requirement for a different arrangement of substrates for each step and temperature **(Figure 1.29a)**. A pharmaceutical company Vipergen Aps together with the Gothelf group presented a unique architecture to generate a combinatorial library of peptides via multistep DTS, where they employed a three-way yoctoliter reactor built up from three DNA strands **(Figure 1.29b)**.[206] While it provides a constant reaction environment with high effective molarity at the center of the junction, doing multiple steps synthesis (more than 5 steps) can be challenging.

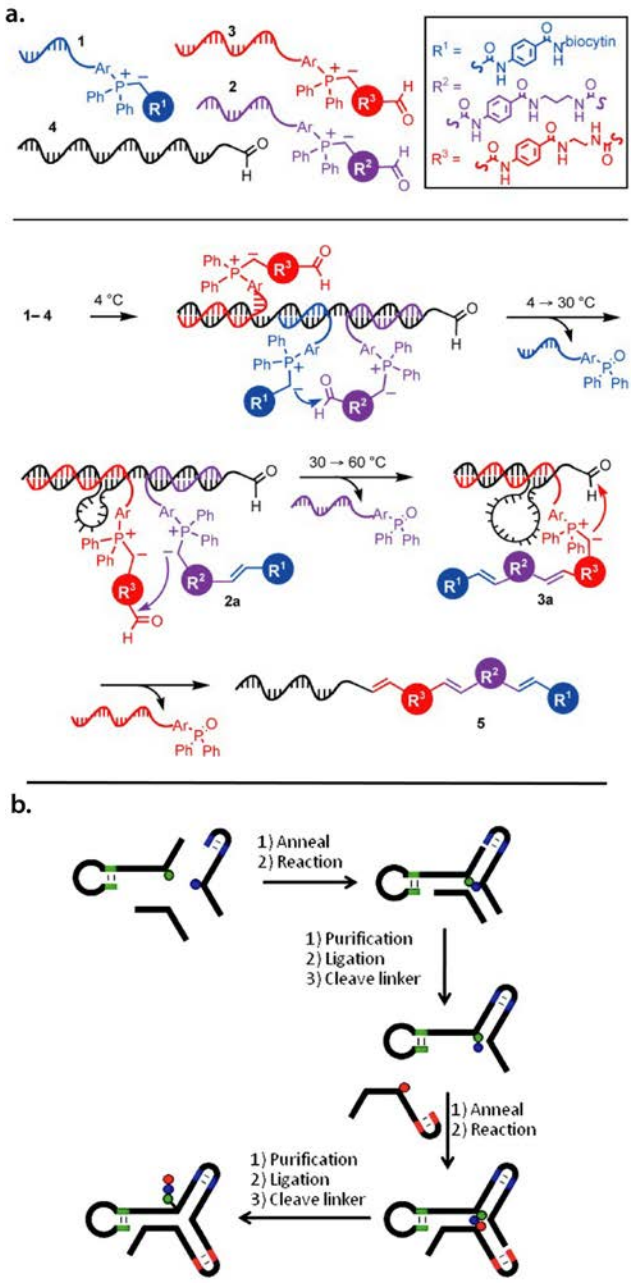

Figure 1.29 | Ordered synthesis in single solution. a. Sequence-controlled tripeptide and triolefin are synthesized by DTS using temperature control. Adapted with permission from reference 205 (Wiley, 2005) **b.** Yoctoliter reactor for the synthesis of combinatorial library of peptides. Reproduced with permission from reference 206 (American Chemical Society, 2009).

Recent advances in dynamic DNA nanotechnology give rise to a variety of new reaction platforms in DTS. Various DNA-based devices have been designed to use DNA strand-

displacement reactions, in which a partial hybridized DNA strand is displaced by a fully complementary strand initiated at a single-stranded domain (called "toehold").[207] Based on this, two strategies were developed individually by both the O'Reilly and Liu group. Specifically, McKee *et al.* achieved the synthesis of sequence-controlled oligo-olefin 4-mer using DNA-templated Wittig chemistry in which products swapped between new and old DNA strands with the help of a "remover strand" that displaces expended reagent DNA as a waste product **(Figure 1.30a)**.[208] This could provide a way to generate long sequence-controlled oligomer using DTS. Separately, the Liu group reported an efficient six-step DTS with the overall yield of 35%, equivalent to about 83% yield each step, characterized by gel electrophoresis and MS. Longer DNA templates could potentially generate products having more than six monomers in this case **(Figure 1.30b)**.[209] Another template mechanism was also reported later on, where the synthesis is controlled by the sequential additions of instruction strands bringing two reactants into close proximity, followed by the strand exchange of growing monomers. Up to 6-mer sequence-controlled peptide was produced using this approach **(Figure 1.30c)**.[210]

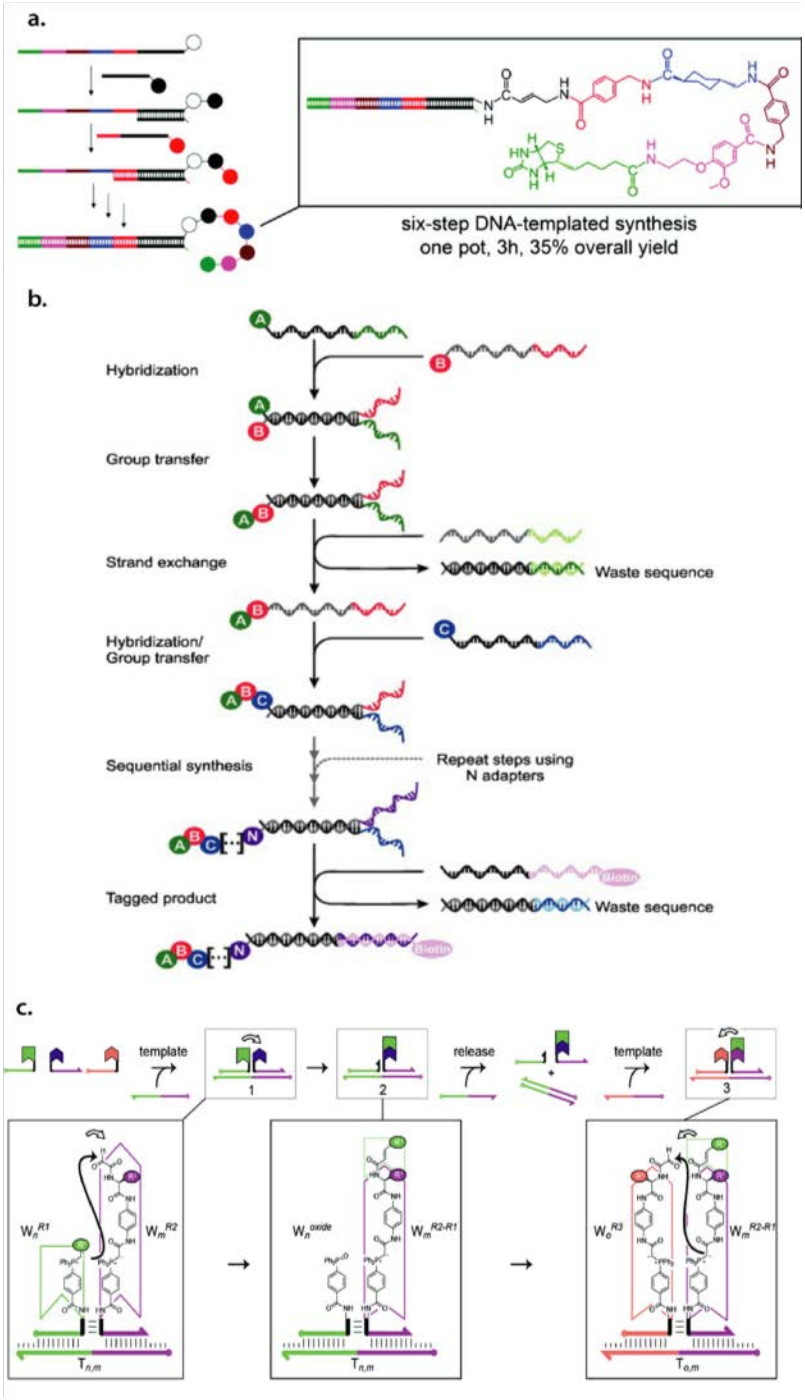

Figure 1.30 | Strand displacement strategy in multistep DTS. a. Six-step DTS to generate oligopeptide. Reproduced with permission from reference 209 (American Chemical Society, 2011) **b.** Sequence-controlled synthesis of 4-mer oligo olefin using DTS. Reproduced with permission from reference 208 (Wiley, 2010) **c.** 6-mer sequence-controlled peptide generated by the addition of instruction strands followed by the strand exchange. Adapted with permission from reference 210 (American Chemical Society, 2012)

Interestingly, inspired by a DNA "nanowalker" reported by Mao *et al.*,[211] that autonomously and processively moves along a DNA track in unidirectional manner, the first autonomous DNA walker performing a series of DNA-templated amine acylation reactions as it moves from station to station along the track was developed in 2010, where oligoamides were generated with a sequence-programmed, autonomous manner in one-pot, which was primarily characterized by mass spectroscopy. This system presents several appealing features: it does not require any external intervention and produces desired products more quickly and more efficiently (~ 45% overall yield) **(Figure 1.31a)**.[212] More recently, Turberfield and co-workers demonstrated a programmable and autonomous DNA-based system based on DNA hybridization chain reaction (HCR), resulting in sequence-controlled polyolefin and polypeptide chains attached to DNA chain as final products. The products can be then amplified, read and used for *in vitro* selection experiments **(Figure 1.31b)**.[213]

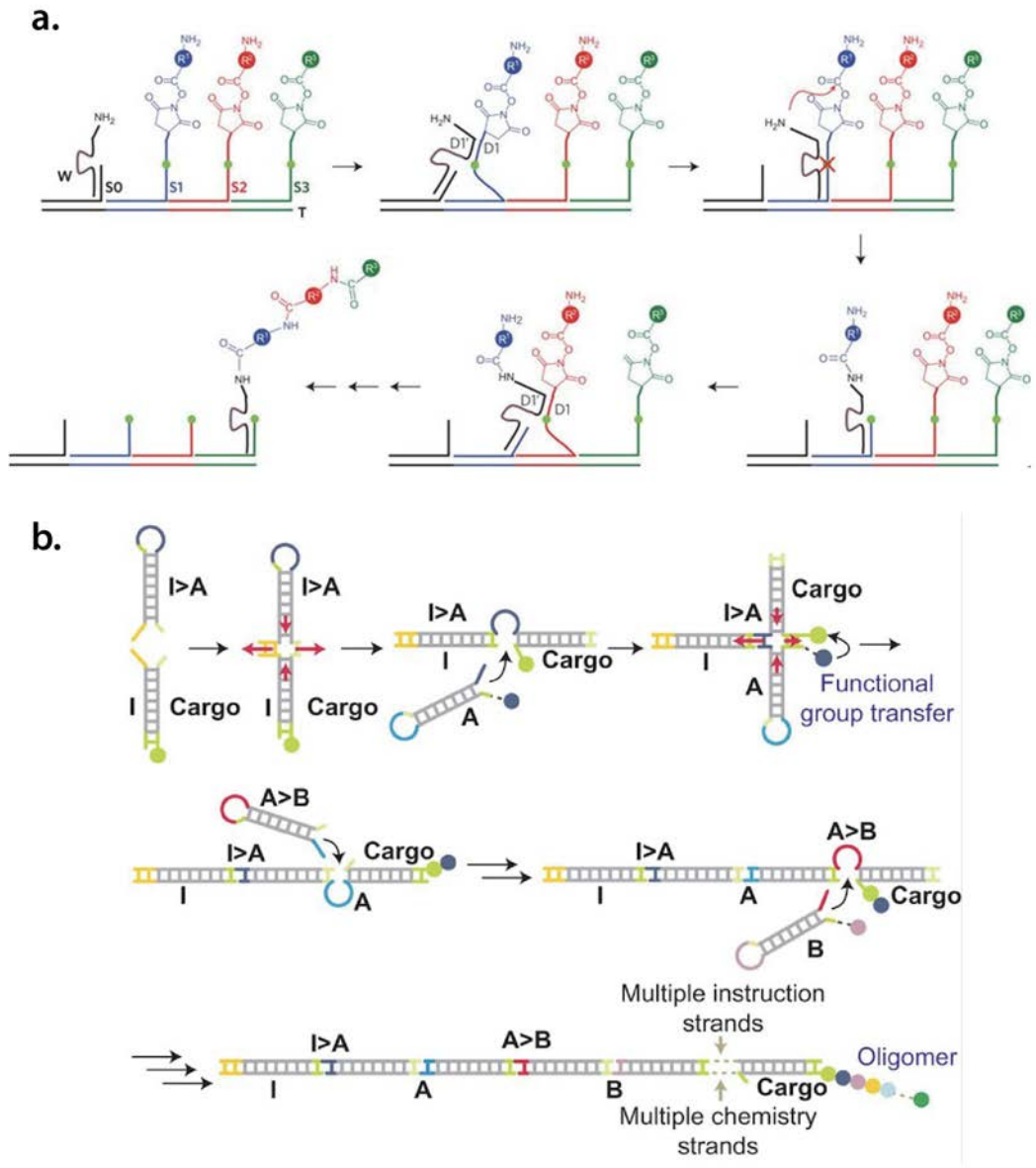

Figure 1.31 | Autonomous DTS. **a.** Generation of oligoamides by DNA "walker". Reproduced with permission from reference 212 (Nature Publishing Group, 2010) **b.** DNA hybridization chain reaction in sequence-controlled synthesis of polyolefin and polypeptide. Adapted with permission from reference 213 (Nature Publishing Group, 2016).

1.6.4. Functional group transformation using DTS

Another interesting research direction that is worth mentioning is to use DTS for functional group transformations, which can greatly expand the capabilities of DTS. For instance, using the Staudinger reaction between a tertiary phosphine and an organic azide, the Liu group successfully transformed azides into primary amines, carboxylic acids and thiols. They then employed the method to generate four sequence-programmed sulfonamide, carbamate, urea and thiourea products in a single solution **(Figure 1.32)**.[214] The method expands the synthetic capabilities of DTS by addressing the need for reagents to be tethered to DNA strands.

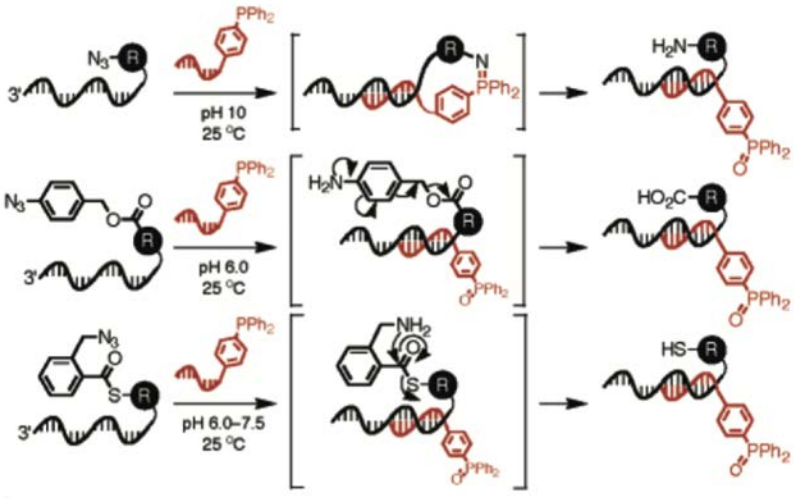

Figure 1.32 | Functional groups transformation using DTS. Adapted with permission from reference 214 (American Chemical Society, 2005).

1.6.5. New template motifs for DNA-templated synthesis

So far, we mainly examined the use of single-stranded templates to bind complementary DNA via Watson-Crick base pairing. Beside these single-stranded templates, double-stranded DNA can also catalyze chemical reactions. An early example was shown by Dervan and co-workers in 1989, where a DNA double helix can direct sequence-specific formation of a phosphodiester linkage directed by Hoogsteen base

pairing.[215] Later, they also explored that double-stranded DNA-templated reaction can accelerate the dimerization via "click chemistry" of two 6-ring hairpin polyamides containing N-methylpyrrole and N-methylimidazole, which bind minor groove **(Figure 1.33a)**.[216] These single-stranded and double-stranded templates represent one dimensional platforms for DTS. More recently, Herrmann *et al.* introduced a micellar scaffold for organic reactions, which allows DNA-templated reaction happened in three-dimensional DNA micelles formed by the self-assembly of amphiphilic DNA-b-polypropylene oxide copolymer in aqueous solution. The group reported that using DNA micelles as nanoreactors, dimerization of two DNA strands is efficient via different chemistries such as Michael addition and amide formation with up to 81% yield **(Figure 1.33b)**.[217]

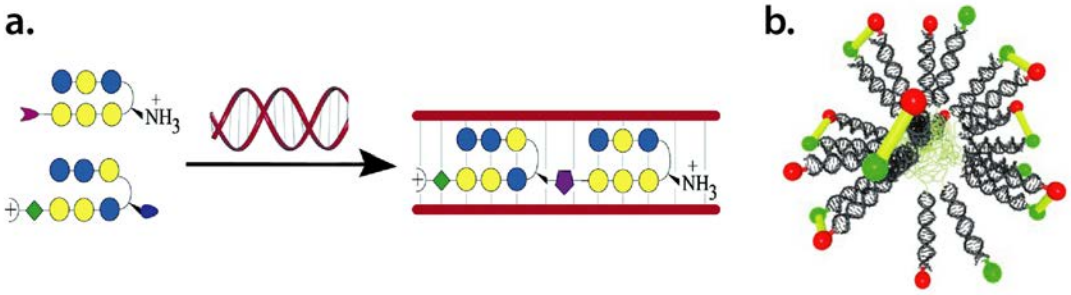

Figure 1.33 | Other motifs in DTS. a. Double-stranded DNA catalyzes the dimerization of two 6-ring hairpin polyamides. Reproduced with permission from reference 216 (American Chemical Society, 2003) **b.** DNA micelles as nanoreactor for dimerization of DNA strands. Adapted with permission from reference 217 (Wiley, 2006).

1.6.6. DNA-templated assembly of synthetic conjugated nanostructures

DNA-templated synthesis has proven to be a reliable method to produce complex organic molecules in a sequential manner. It also provides a new way to assemble synthetic conjugated nanostructures. Inspired by the earlier work of Sheppard *et al.*[184] presented in the section **1.6.1**, Gothelf and co-workers adapted this approach to report an interesting application of DNA-templated metallo-salen complex in building linear and branched conjugate structures. They synthesized linear DNA-functionalized oligo (phenylene ethynylene) modules (LOMs) and tripoidal DNA-functionalized modules (TOMs) using

conventional solid-phase phosphoramidite chemistry.[218] When annealed together, the salicylaldehyde of two modules are brought in close proximity and then linked together by ethylenediamine and a manganese (II) carbonate salt. LOMs and TOMs can come together in different ways to yield discrete self-assembled salen-linked structures (e.g. linear, angled branch points and multiway junctions). These structures are found to be significantly more stable with an increase in melting temperature (T_m) of 17-26°C **(Figure 1.34a)**.[219] Inserting a disulfide (S-S) bond between DNA and monomer side chain allows DNAs to be cleaved from the assembled structures, thus further extending the design possibilities of the approach. However, these salen-based complexes were found to be unstable in the presence of reducing reagents. Several studies were performed to address this issue.[220] For example, alumininum-salen-coupled LOM dimers were reported with remarkable stability in tris-(2-carboxyethyl) phosphine (TCEP), by which the DNAs template can be excluded in the self-assembled organic structures **(Figure 1.34b)**.[221] Based on these works, the same group expanded to template synthesis of monodisperse conjugated molecular wires with a length up to 8 nm by Glaser-Eglington reactions in water **(Figure 1.34c)**.[222]

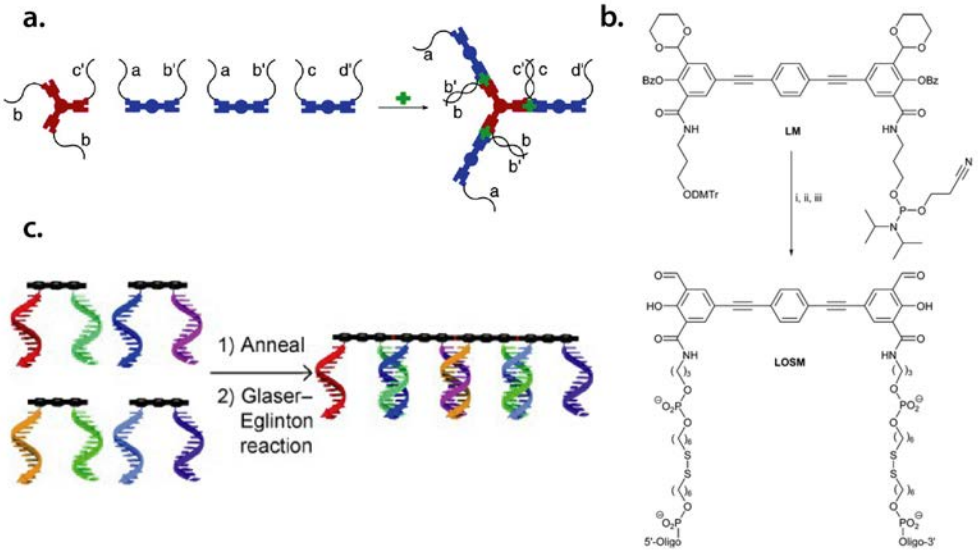

Figure 1.34 | DNA-templated assembly of synthetic conjugated nanostructures. a. A different self-assembled structures can be generated by LOMs and TOMs. Reproduced with permission from reference 219 (American Chemical Society, 2004) **b.** Incorporation of S-S bond into the assembled structures. Adapted with permission from reference 221 (Royal Society of Chemistry, 2004). **c.**

Synthesis of molecular wire using templated Glaser-Eglington reaction in water. Reproduced with permission from reference 222 (Wiley, 2011).

1.7. Context and scope of this thesis

The field of DNA nanotechnology has taken DNA out of its biological context and used this molecule as a building block for bottom-up assembly of nanostructures. Thanks to the predictable and programmable Watson-Crick base pairing, a wide range of DNA architectures in 1D, 2D and 3D with different shapes and levels of complexity can be realized.[223] However, these approaches often require a large number of DNA strands (in many cases can be up to hundreds of strands). In the Sleiman lab, we adopted a "DNA minimal" approach as an alternative strategy in which new functionalities and assembly motifs can be achieved through the addition of synthetic fragments. This approach is of great interest to many different applications from material science to drug delivery that are actively pursued in the laboratory.[141-143, 152, 224-225] While synthetic modifications can provide new ways to control DNA self-assembly, they introduce many challenges such as complicated synthesis of reaction precursors and tedious purification.

DNA-templated synthesis has evolved considerably since the early 2000 as a powerful approach to control and enable chemical reactivity. We envisioned that the DNA minimal structures previously built in the laboratory can be explored as attractive platforms for performing chemical transformations with high specificity and selectivity, thereby generating unique DNA-hybrid structures in a simple way while retaining complexity. Within this context, the research presented in this thesis is specifically focused on the synthesis and development of new DNA-hybrid materials using DNA nanostructures as reaction templates, by which reactive functionalities are brought into close proximity, resulting in efficient chemical reactions.

Chapter 2 describes a facile method to directly functionalize DNA strands with highly hydrophobic molecules in aqueous environment. This method efficiently addresses

the difficulty in solvent incompatibility between DNA and organic molecules. Inspired by the earlier work of Edwardson *et al.* from our lab,[135] we explore the use of highly monodispersed DNA-oligohexaethylene based micelles as nanoreactors for the purpose of direct DNA functionalization. We demonstrate that a library of highly hydrophobic molecules can be conjugated efficiently to DNA or DNA amphiphiles using the DNA micelles in aqueous media, whereas low reactivities are observed in the absence of the DNA template. The sequence-controlled nature of the method allows us to modulate and study the reactivities by deliberately changing number of monomers and positions of functional groups.

Chapter 3 focuses on the development of synthetic methodology to functionalize multi-arm branched molecules with different DNA strands in a site-specific manner. Historically, the Sleiman lab reported an efficient method to integrate two different DNA strands on an organic vertex using solid-phase synthesis.[93] Using the same approach, the attachment of three or more different DNA strands can be laborious and inefficient, as it requires multiple protecting groups and tedious purification steps. Moreover, in solution, it is almost impossible to generate DNA-small molecule structures having specific DNA strand patterns, mainly due to the random collisions of reactants. To address this challenge, the work in this chapter seeks to answer a fundamental synthetic question: *can we simplify the synthetic process of these DNA-branched molecules and can we make it to happen in solution?* Inspired by the yoctoliter reactor as described earlier in this chapter,[206] we employ a simple three-way DNA junction to "print" DNA strand patterns on a small molecule having multiple functionalities in only one-step. This class of DNA-imprinted small molecules can bring a new flavor to DNA self-assembly as they can dictate structural definition and greatly influence assembly outcome. Moreover, they can provide a unique platform to chemically replicate to make daughter generations and to organize nanomaterials (e.g. protein) in a controlled manner in 2D, as being presented at the end of this chapter.

Finally, chapter 4 seeks to explore the possibility of using 3D DNA nanostructures as scaffolds to generate unique DNA-imprinted polymeric particles. Previous works by

Chidchob *et al*. and Serpell *et al*. showed that DNA cube-micelle structures can be formed with the decoration of a specific number of DNA amphiphiles.[141-142] An appealing feature of this structure is that eight sides of the DNA cube are totally addressable and can be completely unique. Hence, developing from our findings in chapter 2 and 3, we crosslink the micellar core inside the cube and transfer (or "print") DNA patterns from the cube to the crosslinked polymeric core. The number of monomers making up the core and exterior DNA strands can be varied using different DNA cage structures. Importantly, the resulting particles are highly stable and can self-assemble in a directional manner, which is of significant interest to many applications.

1.8. References

1. Watson, J. D.; Crick, F. H. C., Molecular Structure of Nucleic Acids: A Structure for Deoxyribose Nucleic Acid. *Nature* **1953,** *171* (4356), 737-738.

2. Franklin, R. E.; Gosling, R. G., Evidence for 2-Chain Helix in Crystalline Structure of Sodium Deoxyribonucleate. *Nature* **1953,** *172* (4369), 156-157.

3. Stofer, E.; Chipot, C.; Lavery, R., Free Energy Calculations of Watson−Crick Base Pairing in Aqueous Solution. *J. Am. Chem. Soc.* **1999,** *121* (41), 9503-9508.

4. Protozanova, E.; Frank-Kamenetskii, M. D.; Yakovchuk, P., Base-stacking and base-pairing contributions into thermal stability of the DNA double helix. *Nucleic Acids Research* **2006,** *34* (2), 564-574.

5. Wang, J. C., Helical repeat of DNA in solution. *Proceedings of the National Academy of Sciences* **1979,** *76* (1), 200-203.

6. Brinkers, S.; Dietrich, H. R. C.; de Groote, F. H.; Young, I. T.; Rieger, B., The persistence length of double stranded DNA determined using dark field tethered particle motion. *The Journal of Chemical Physics* **2009,** *130* (21), 215105.

7. Zeraati, M.; Langley, D. B.; Schofield, P.; Moye, A. L.; Rouet, R.; Hughes, W. E.; Bryan, T. M.; Dinger, M. E.; Christ, D., I-motif DNA structures are formed in the nuclei of human cells. *Nature Chemistry* **2018,** *10* (6), 631-637.

8. Henderson, E.; Hardin, C. C.; Walk, S. K.; Tinoco, I.; Blackburn, E. H., Telomeric DNA oligonucleotides form novel intramolecular structures containing guanine·guanine base pairs. *Cell* **1987,** *51* (6), 899-908.

9. Tener, G. M.; Khorana, H. G.; Markham, R.; Pol, E. H., Studies on Polynucleotides. II.1 The Synthesis and Characterization of Linear and Cyclic Thymidine Oligonucleotides2. *Journal of the American Chemical Society* **1958,** *80* (23), 6223-6230.

10. Letsinger, R. L.; Kornet, M. J., Popcorn Polymer as a Support in Multistep Syntheses. *J. Am. Chem. Soc.* **1963,** *85* (19), 3045-3046.

11. Letsinger, R. L.; Mahadevan, V., Oligonucleotide Synthesis on a Polymer Support1,2. *J. Am. Chem. Soc.* **1965,** *87* (15), 3526-3527.

12. Letsinger, R. L.; Mahadevan, V., Stepwise Synthesis of Oligodeoxyribonucleotides on an Insoluble Polymer Support1,2. *J. Am. Chem. Soc.* **1966,** *88* (22), 5319-5324.

13. Alvarado-Urbina, G.; Sathe, G.; Liu, W.; Gillen, M.; Duck, P.; Bender, R.; Ogilvie, K., Automated synthesis of gene fragments. *Science* **1981,** *214* (4518), 270-274.

14. Beaucage, S. L.; Caruthers, M. H., Deoxynucleoside phosphoramidites—A new class of key intermediates for deoxypolynucleotide synthesis. *Tetrahedron Lett.* **1981,** *22* (20), 1859-1862.

15. Seeman, N. C., Nucleic acid junctions and lattices. *Journal of Theoretical Biology* **1982,** *99* (2), 237-247.

16. Pinheiro, A. V.; Han, D.; Shih, W. M.; Yan, H., Challenges and opportunities for structural DNA nanotechnology. *Nat. Nanotech.* **2011,** *6*, 763.

17. Broker, T. R.; Lehman, I. R., Branched DNA molecules: Intermediates in T4 recombination. *Journal of Molecular Biology* **1971,** *60* (1), 131-149.

18. Seeman, N. C., DNA in a material world. *Nature* **2003,** *421*, 427.

19. Kallenbach, N. R.; Ma, R.-I.; Seeman, N. C., An immobile nucleic acid junction constructed from oligonucleotides. *Nature* **1983,** *305* (5937), 829-831.

20. Ma, R. I.; Kallenbach, N. R.; Sheardy, R. D.; Petrillo, M. L.; Seeman, N. C., Three-arm nucleic acid junctions are flexible. *Nucleic acids research* **1986,** *14* (24), 9745-9753.

21. Wang, Y.; Mueller, J. E.; Kemper, B.; Seeman, N. C., Assembly and characterization of five-arm and six-arm DNA branched junctions. *Biochemistry* **1991,** *30* (23), 5667-5674.

22. Wang, X.; Seeman, N. C., Assembly and Characterization of 8-Arm and 12-Arm DNA Branched Junctions. *J. Am. Chem. Soc.* **2007,** *129* (26), 8169-8176.

23. Chen, J.; Seeman, N. C., Synthesis from DNA of a molecule with the connectivity of a cube. *Nature* **1991,** *350* (6319), 631-633.

24. Li, X.; Yang, X.; Qi, J.; Seeman, N. C., Antiparallel DNA Double Crossover Molecules As Components for Nanoconstruction. *J. Am. Chem. Soc.* **1996,** *118* (26), 6131-6140.

25. Fu, T. J.; Seeman, N. C., DNA double-crossover molecules. *Biochemistry* **1993,** *32* (13), 3211-3220.

26. Sa-Ardyen, P.; Vologodskii, A. V.; Seeman, N. C., The Flexibility of DNA Double Crossover Molecules. *Biophysical Journal* **2003,** *84* (6), 3829-3837.

27. Winfree, E.; Liu, F.; Wenzler, L. A.; Seeman, N. C., Design and self-assembly of two-dimensional DNA crystals. *Nature* **1998,** *394*, 539.

28. Lin, C.; Liu, Y.; Rinker, S.; Yan, H., DNA Tile Based Self-Assembly: Building Complex Nanoarchitectures. *ChemPhysChem* **2006,** *7* (8), 1641-1647.

29. Zhang, F.; Jiang, S.; Li, W.; Hunt, A.; Liu, Y.; Yan, H., Self-Assembly of Complex DNA Tessellations by Using Low-Symmetry Multi-arm DNA Tiles. *Angew. Chem. Int. Ed.* **2016,** *55* (31), 8860-8863.

30. Rothemund, P. W. K.; Ekani-Nkodo, A.; Papadakis, N.; Kumar, A.; Fygenson, D. K.; Winfree, E., Design and Characterization of Programmable DNA Nanotubes. *J. Am. Chem. Soc.* **2004,** *126* (50), 16344-16352.

31. Mitchell, J. C.; Harris, J. R.; Malo, J.; Bath, J.; Turberfield, A. J., Self-Assembly of Chiral DNA Nanotubes. *J. Am. Chem. Soc.* **2004,** *126* (50), 16342-16343.

32. Park, S. H.; Barish, R.; Li, H.; Reif, J. H.; Finkelstein, G.; Yan, H.; LaBean, T. H., Three-Helix Bundle DNA Tiles Self-Assemble into 2D Lattice or 1D Templates for Silver Nanowires. *Nano Lett.* **2005,** *5* (4), 693-696.

33. Mathieu, F.; Liao, S.; Kopatsch, J.; Wang, T.; Mao, C.; Seeman, N. C., Six-Helix Bundles Designed from DNA. *Nano Lett.* **2005,** *5* (4), 661-665.

34. Liu, D.; Park, S. H.; Reif, J. H.; LaBean, T. H., DNA nanotubes self-assembled from triple-crossover tiles as templates for conductive nanowires. *Proceedings of the National Academy of Sciences* **2004,** *101* (3), 717-722.

35. Liu, D.; Wang, M.; Deng, Z.; Walulu, R.; Mao, C., Tensegrity: Construction of Rigid DNA Triangles with Flexible Four-Arm DNA Junctions. *J. Am. Chem. Soc.* **2004,** *126* (8), 2324-2325.

36. He, Y.; Tian, Y.; Chen, Y.; Deng, Z.; Ribbe, A. E.; Mao, C., Sequence Symmetry as a Tool for Designing DNA Nanostructures. *Angewandte Chemie International Edition* **2005,** *44* (41), 6694-6696.

37. Zhang, C.; Ko, S. H.; Su, M.; Leng, Y.; Ribbe, A. E.; Jiang, W.; Mao, C., Symmetry Controls the Face Geometry of DNA Polyhedra. *J. Am. Chem. Soc.* **2009,** *131* (4), 1413-1415.

38. Zhang, C.; Tian, C.; Guo, F.; Liu, Z.; Jiang, W.; Mao, C., DNA-Directed Three-Dimensional Protein Organization. *Angew. Chem. Int. Ed.* **2012,** *51* (14), 3382-3385.

39. He, Y.; Chen, Y.; Liu, H.; Ribbe, A. E.; Mao, C., Self-Assembly of Hexagonal DNA Two-Dimensional (2D) Arrays. *J. Am. Chem. Soc.* **2005,** *127* (35), 12202-12203.

40. He, Y.; Ye, T.; Su, M.; Zhang, C.; Ribbe, A. E.; Jiang, W.; Mao, C., Hierarchical self-assembly of DNA into symmetric supramolecular polyhedra. *Nature* **2008,** *452*, 198.

41. Yan, H.; LaBean, T. H.; Feng, L.; Reif, J. H., Directed nucleation assembly of DNA tile complexes for barcode-patterned lattices. *Proceedings of the National Academy of Sciences* **2003,** *100* (14), 8103-8108.

42. Rothemund, P. W. K.; Papadakis, N.; Winfree, E., Algorithmic Self-Assembly of DNA Sierpinski Triangles. *PLOS Biology* **2004,** *2* (12), e424.

43. Algorithmic Self-Assembly of DNA: Theoretical Motivations and 2D Assembly Experiments AU - Winfree, Erik. *Journal of Biomolecular Structure and Dynamics* **2000,** *17* (sup1), 263-270.

44. Zheng, J.; Birktoft, J. J.; Chen, Y.; Wang, T.; Sha, R.; Constantinou, P. E.; Ginell, S. L.; Mao, C.; Seeman, N. C., From molecular to macroscopic via the rational design of a self-assembled 3D DNA crystal. *Nature* **2009,** *461*, 74.

45. Zhang, X.; Yadavalli, V. K., Functional self-assembled DNA nanostructures for molecular recognition. *Nanoscale* **2012,** *4* (7), 2439-2446.

46. Yan, H.; Park, S. H.; Finkelstein, G.; Reif, J. H.; LaBean, T. H., DNA-Templated Self-Assembly of Protein Arrays and Highly Conductive Nanowires. *Science* **2003,** *301* (5641), 1882-1884.

47. Li, H.; Park, S. H.; Reif, J. H.; LaBean, T. H.; Yan, H., DNA-Templated Self-Assembly of Protein and Nanoparticle Linear Arrays. *J. Am. Chem. Soc.* **2004,** *126* (2), 418-419.

48. Rothemund, P. W. K., Folding DNA to create nanoscale shapes and patterns. *Nature* **2006,** *440*, 297.

49. Marblestone, A. H.; Vazquez, A.; Church, G. M.; Douglas, S. M.; Teerapittayanon, S.; Shih, W. M., Rapid prototyping of 3D DNA-origami shapes with caDNAno. *Nucleic Acids Research* **2009,** *37* (15), 5001-5006.

50. Jabbari, H.; Aminpour, M.; Montemagno, C., Computational Approaches to Nucleic Acid Origami. *ACS Combinatorial Science* **2015,** *17* (10), 535-547.

51. Benson, E.; Mohammed, A.; Gardell, J.; Masich, S.; Czeizler, E.; Orponen, P.; Högberg, B., DNA rendering of polyhedral meshes at the nanoscale. *Nature* **2015,** *523*, 441.

52. Castro, C. E.; Kilchherr, F.; Kim, D.-N.; Shiao, E. L.; Wauer, T.; Wortmann, P.; Bathe, M.; Dietz, H., A primer to scaffolded DNA origami. *Nature Methods* **2011,** *8*, 221.

53. Ke, Y.; Sharma, J.; Liu, M.; Jahn, K.; Liu, Y.; Yan, H., Scaffolded DNA Origami of a DNA Tetrahedron Molecular Container. *Nano Lett.* **2009,** *9* (6), 2445-2447.

54. Andersen, E. S.; Dong, M.; Nielsen, M. M.; Jahn, K.; Subramani, R.; Mamdouh, W.; Golas, M. M.; Sander, B.; Stark, H.; Oliveira, C. L. P.; Pedersen, J. S.; Birkedal, V.; Besenbacher, F.; Gothelf, K. V.; Kjems, J., Self-assembly of a nanoscale DNA box with a controllable lid. *Nature* **2009,** *459*, 73.

55. Ke, Y.; Douglas, S. M.; Liu, M.; Sharma, J.; Cheng, A.; Leung, A.; Liu, Y.; Shih, W. M.; Yan, H., Multilayer DNA Origami Packed on a Square Lattice. *j. Am. Chem. Soc.* **2009,** *131* (43), 15903-15908.

56. Douglas, S. M.; Dietz, H.; Liedl, T.; Högberg, B.; Graf, F.; Shih, W. M., Self-assembly of DNA into nanoscale three-dimensional shapes. *Nature* **2009,** *459*, 414.

57. Dietz, H.; Douglas, S. M.; Shih, W. M., Folding DNA into Twisted and Curved Nanoscale Shapes. *Science* **2009,** *325* (5941), 725-730.

58. Han, D.; Pal, S.; Nangreave, J.; Deng, Z.; Liu, Y.; Yan, H., DNA Origami with Complex Curvatures in Three-Dimensional Space. *Science* **2011,** *332* (6027), 342-346.

59. Han, D.; Pal, S.; Liu, Y.; Yan, H., Folding and cutting DNA into reconfigurable topological nanostructures. *Nat. Nanotech.* **2010,** *5*, 712.

60. Zhang, F.; Jiang, S.; Wu, S.; Li, Y.; Mao, C.; Liu, Y.; Yan, H., Complex wireframe DNA origami nanostructures with multi-arm junction vertices. *Nat. Nanotech.* **2015,** *10*, 779.

61. Wei, B.; Dai, M.; Yin, P., Complex shapes self-assembled from single-stranded DNA tiles. *Nature* **2012,** *485*, 623.

62. Ke, Y.; Ong, L. L.; Shih, W. M.; Yin, P., Three-Dimensional Structures Self-Assembled from DNA Bricks. *Science* **2012,** *338* (6111), 1177-1183.

63. Ke, Y.; Ong, L. L.; Sun, W.; Song, J.; Dong, M.; Shih, W. M.; Yin, P., DNA brick crystals with prescribed depths. *Nat. Chem.* **2014,** *6*, 994.

64. Ding, B.; Deng, Z.; Yan, H.; Cabrini, S.; Zuckermann, R. N.; Bokor, J., Gold Nanoparticle Self-Similar Chain Structure Organized by DNA Origami. *J. Am. Chem. Soc.* **2010,** *132* (10), 3248-3249.

65. Pal, S.; Deng, Z.; Ding, B.; Yan, H.; Liu, Y., DNA-Origami-Directed Self-Assembly of Discrete Silver-Nanoparticle Architectures. *Angew. Chem. Int. Ed.* **2010,** *49* (15), 2700-2704.

66. Saccà, B.; Meyer, R.; Erkelenz, M.; Kiko, K.; Arndt, A.; Schroeder, H.; Rabe, K. S.; Niemeyer, C. M., Orthogonal Protein Decoration of DNA Origami. *Angew. Chem. Int. Ed.* **2010,** *49* (49), 9378-9383.

67. Rinker, S.; Ke, Y.; Liu, Y.; Chhabra, R.; Yan, H., Self-assembled DNA nanostructures for distance-dependent multivalent ligand–protein binding. *Nat. Nanotech.* **2008,** *3*, 418.

68. Endo, M.; Yang, Y.; Sugiyama, H., DNA origami technology for biomaterials applications. *Biomaterials Science* **2013,** *1* (4), 347-360.

69. Fu, J.; Liu, M.; Liu, Y.; Woodbury, N. W.; Yan, H., Interenzyme Substrate Diffusion for an Enzyme Cascade Organized on Spatially Addressable DNA Nanostructures. *Journal of the American Chemical Society* **2012,** *134* (12), 5516-5519.

70. Li, S.; Jiang, Q.; Liu, S.; Zhang, Y.; Tian, Y.; Song, C.; Wang, J.; Zou, Y.; Anderson, G. J.; Han, J.-Y.; Chang, Y.; Liu, Y.; Zhang, C.; Chen, L.; Zhou, G.; Nie, G.; Yan, H.; Ding, B.; Zhao, Y., A DNA nanorobot functions as a cancer therapeutic in response to a molecular trigger in vivo. *Nature Biotechnology* **2018,** *36*, 258.

71. Wang, P.; Meyer, T. A.; Pan, V.; Dutta, P. K.; Ke, Y., The Beauty and Utility of DNA Origami. *Chem* **2017,** *2* (3), 359-382.

72. Kuzyk, A.; Schreiber, R.; Fan, Z.; Pardatscher, G.; Roller, E.-M.; Högele, A.; Simmel, F. C.; Govorov, A. O.; Liedl, T., DNA-based self-assembly of chiral plasmonic nanostructures with tailored optical response. *Nature* **2012,** *483*, 311.

73. Samanta, A.; Zhou, Y.; Zou, S.; Yan, H.; Liu, Y., Fluorescence Quenching of Quantum Dots by Gold Nanoparticles: A Potential Long Range Spectroscopic Ruler. *Nano Lett.* **2014,** *14* (9), 5052-5057.

74. Ke, Y.; Lindsay, S.; Chang, Y.; Liu, Y.; Yan, H., Self-Assembled Water-Soluble Nucleic Acid Probe Tiles for Label-Free RNA Hybridization Assays. *Science* **2008,** *319* (5860), 180-183.

75. Williams, B. A. R.; Lund, K.; Liu, Y.; Yan, H.; Chaput, J. C., Self-Assembled Peptide Nanoarrays: An Approach to Studying Protein–Protein Interactions. *Angew. Chem. Int. Ed.* **2007,** *46* (17), 3051-3054.

76. Tikhomirov, G.; Petersen, P.; Qian, L., Fractal assembly of micrometre-scale DNA origami arrays with arbitrary patterns. *Nature* **2017,** *552*, 67.

77. Wagenbauer, K. F.; Sigl, C.; Dietz, H., Gigadalton-scale shape-programmable DNA assemblies. *Nature* **2017,** *552*, 78.

78. Praetorius, F.; Kick, B.; Behler, K. L.; Honemann, M. N.; Weuster-Botz, D.; Dietz, H., Biotechnological mass production of DNA origami. *Nature* **2017,** *552*, 84.

79. Han, D.; Qi, X.; Myhrvold, C.; Wang, B.; Dai, M.; Jiang, S.; Bates, M.; Liu, Y.; An, B.; Zhang, F.; Yan, H.; Yin, P., Single-stranded DNA and RNA origami. **2017,** *358* (6369), eaao2648.

80. Shi, J.; Bergstrom, D. E., Assembly of Novel DNA Cycles with Rigid Tetrahedral Linkers. *Angew. Chem. Int. Ed.* **1997,** *36* (1-2), 111-113.

81. Aldaye, F. A.; Sleiman, H. F., Sequential Self-Assembly of a DNA Hexagon as a Template for the Organization of Gold Nanoparticles. *Angew. Chem. Int. Ed.* **2006,** *45* (14), 2204-2209.

82. Aldaye, F. A.; Sleiman, H. F., Dynamic DNA Templates for Discrete Gold Nanoparticle Assemblies: Control of Geometry, Modularity, Write/Erase and Structural Switching. *J. Am. Chem. Soc.* **2007,** *129* (14), 4130-4131.

83. Eckardt, L. H.; Naumann, K.; Matthias Pankau, W.; Rein, M.; Schweitzer, M.; Windhab, N.; von Kiedrowski, G., Chemical copying of connectivity. *Nature* **2002,** *420*, 286.

84. Thaner, R. V.; Eryazici, I.; Farha, O. K.; Mirkin, C. A.; Nguyen, S. T., Facile one-step solid-phase synthesis of multitopic organic–DNA hybrids via “click” chemistry. *Chem. Sci.* **2014,** *5* (3), 1091-1096.

85. Hong, B. J.; Eryazici, I.; Bleher, R.; Thaner, R. V.; Mirkin, C. A.; Nguyen, S. T., Directed Assembly of Nucleic Acid-Based Polymeric Nanoparticles from Molecular Tetravalent Cores. *J. Am. Chem. Soc.* **2015,** *137* (25), 8184-8191.

86. Udalova, I. A.; Bridgman, A. J.; Southern, E. M.; Shchepinov, M. S., Oligonucleotide dendrimers: Synthesis and use as polylabelled DNA probes. *Nucleic Acids Research* **1997,** *25* (22), 4447-4454.

87. Southern, E. M.; Elder, J. K.; Mir, K. U.; Shchepinov, M. S.; Frank-Kamenetskii, M. D., Oligonucleotide dendrimers: stable nano-structures. *Nucleic Acids Research* **1999,** *27* (15), 3035-3041.

88. Singh, A.; Tolev, M.; Meng, M.; Klenin, K.; Plietzsch, O.; Schilling, C. I.; Muller, T.; Nieger, M.; Bräse, S.; Wenzel, W.; Richert, C., Branched DNA That Forms a Solid at 95 °C. *Angew. Chem. Int. Ed.* **2011,** *50* (14), 3227-3231.

89. Meng, M.; Ahlborn, C.; Bauer, M.; Plietzsch, O.; Soomro, S. A.; Singh, A.; Muller, T.; Wenzel, W.; Bräse, S.; Richert, C., Two Base Pair Duplexes Suffice to Build a Novel Material. *ChemBioChem* **2009,** *10* (8), 1335-1339.

90. Aldaye, F. A.; Lo, P. K.; Karam, P.; McLaughlin, C. K.; Cosa, G.; Sleiman, H. F., Modular construction of DNA nanotubes of tunable geometry and single- or double-stranded character. *Nat. Nanotech.* **2009,** *4*, 349.

91. Aldaye, F. A.; Sleiman, H. F., Modular Access to Structurally Switchable 3D Discrete DNA Assemblies. *J. Am. Chem. Soc* **2007,** *129* (44), 13376-13377.

92. Lo, P. K.; Karam, P.; Aldaye, F. A.; McLaughlin, C. K.; Hamblin, G. D.; Cosa, G.; Sleiman, H. F., Loading and selective release of cargo in DNA nanotubes with longitudinal variation. *Nat. Chem.* **2010,** *2*, 319.

93. McLaughlin, C. K.; Hamblin, G. D.; Sleiman, H. F., Supramolecular DNA assembly. *Chem. Soc. Rev.* **2011,** *40* (12), 5647-5656.

94. Hariri, A. A.; Hamblin, G. D.; Gidi, Y.; Sleiman, H. F.; Cosa, G., Stepwise growth of surface-grafted DNA nanotubes visualized at the single-molecule level. *Nat. Chem.* **2015,** *7*, 295.

95. Zimmermann, J.; Cebulla, M. P. J.; Mönninghoff, S.; von Kiedrowski, G., Self-Assembly of a DNA Dodecahedron from 20 Trisoligonucleotides with C3h Linkers. *Angew. Chem. Int. Ed.* **2008,** *47* (19), 3626-3630.

96. Panagiotidis, C.; Kath-Schorr, S.; von Kiedrowski, G., Flexibility of C3h-Symmetrical Linkers in Tris-oligonucleotide-Based Tetrahedral Scaffolds. *ChemBioChem* **2016,** *17* (3), 254-259.

97. Kuroda, T.; Sakurai, Y.; Suzuki, Y.; Nakamura, A. O.; Kuwahara, M.; Ozaki, H.; Sawai, H., Assembly of DNA Nanostructures with Branched Tris-DNA. *Chem. Asia J.* **2006,** *1* (4), 575-580.

98. Gothelf, K. V.; Thomsen, A.; Nielsen, M.; Cló, E.; Brown, R. S., Modular DNA-Programmed Assembly of Linear and Branched Conjugated Nanostructures. *J. Am. Chem. Soc* **2004,** *126* (4), 1044-1046.

99. Eryazici, I.; Yildirim, I.; Schatz, G. C.; Nguyen, S. T., Enhancing the Melting Properties of Small Molecule-DNA Hybrids through Designed Hydrophobic Interactions: An Experimental-Computational Study. *J. Am. Chem. Soc.* **2012,** *134* (17), 7450-7458.

100. Hong, B. J.; Cho, V. Y.; Bleher, R.; Schatz, G. C.; Nguyen, S. T., Enhancing DNA-Mediated Assemblies of Supramolecular Cage Dimers through Tuning Core Flexibility and DNA Length—A Combined Experimental–Modeling Study. *J. Am. Chem. Soc.* **2015,** *137* (41), 13381-13388.

101. Greschner, A. A.; Toader, V.; Sleiman, H. F., The Role of Organic Linkers in Directing DNA Self-Assembly and Significantly Stabilizing DNA Duplexes. *J. Am. Chem. Soc.* **2012,** *134* (35), 14382-14389.

102. Greschner, A. A.; Bujold, K. E.; Sleiman, H. F., Intercalators as Molecular Chaperones in DNA Self-Assembly. *J. Am. Chem. Soc.* **2013,** *135* (30), 11283-11288.

103. Gothelf, K. V.; Brown, R. S., A Modular Approach to DNA-Programmed Self-Assembly of Macromolecular Nanostructures. *Chem. Eur. J.* **2005,** *11* (4), 1062-1069.

104. Ponomarenko, A. I.; Brylev, V. A.; Sapozhnikova, K. A.; Ustinov, A. V.; Prokhorenko, I. A.; Zatsepin, T. S.; Korshun, V. A., Tetrahedral DNA conjugates from pentaerythritol-based polyazides. *Tetrahedron* **2016,** *72* (19), 2386-2391.

105. Okochi, K. D.; Monfregola, L.; Dickerson, S. M.; McCaffrey, R.; Domaille, D. W.; Yu, C.; Hafenstine, G. R.; Jin, Y.; Cha, J. N.; Kuchta, R. D.; Caruthers, M.; Zhang, W., Synthesis of Small-Molecule/DNA Hybrids through On-Bead Amide-Coupling Approach. *The Journal of Organic Chemistry* **2017,** *82* (20), 10803-10811.

106. Lehn, J.-M., Supramolecular Chemistry—Scope and Perspectives Molecules, Supermolecules, and Molecular Devices (Nobel Lecture). *Angew. Chem. Int. Ed. Eng.* **1988,** *27* (1), 89-112.

107. Sauvage, J.-P., From Chemical Topology to Molecular Machines (Nobel Lecture). *Angew. Chem. Int. Ed.* **2017,** *56* (37), 11080-11093.

108. Vargas-Baca, I.; Mitra, D.; Zulyniak, H. J.; Banerjee, J.; Sleiman, H. F., Solid-Phase Synthesis of Transition Metal Linked, Branched Oligonucleotides. *Angew. Chem. Int. Ed.* **2001,** *40* (24), 4629-4632.

109. Mitra, D.; Di Cesare, N.; Sleiman, H. F., Self-Assembly of Cyclic Metal–DNA Nanostructures using Ruthenium Tris(bipyridine)-Branched Oligonucleotides. *Angew. Chem. Int. Ed.* **2004,** *43* (43), 5804-5808.

110. Stewart, K. M.; McLaughlin, L. W., Four-Arm Oligonucleotide Ni(II)−Cyclam-Centered Complexes as Precursors for the Generation of Supramolecular Periodic Assemblies. *J. Am. Chem. Soc.* **2004,** *126* (7), 2050-2057.

111. Choi, J. S.; Kang, C. W.; Jung, K.; Yang, J. W.; Kim, Y.-G.; Han, H., Synthesis of DNA Triangles with Vertexes of Bis(terpyridine)iron(II) Complexes. *J. Am. Chem. Soc.* **2004,** *126* (28), 8606-8607.

112. Stewart, K. M.; Rojo, J.; McLaughlin, L. W., Ru(II) Tris(bipyridyl) Complexes with Six Oligonucleotide Arms as Precursors for the Generation of Supramolecular Assemblies. *Angew. Chem. Int. Ed.* **2004,** *43* (43), 5808-5811.

113. Sartor, V.; Irvoas, J.; Bordeau, G.; Chouini-Lalanne, N., Multivalent Azide-Functionalized Polypyridyl Ruthenium Complexes and Their DNA Conjugates through Click Chemistry. *Eur. J. Inorg. Chem.* **2017,** *2017* (20), 2661-2670.

114. Yang, H.; Rys, A. Z.; McLaughlin, C. K.; Sleiman, H. F., Templated Ligand Environments for the Selective Incorporation of Different Metals into DNA. *Angew. Chem. Int. Ed.* **2009,** *48* (52), 9919-9923.

115. Yang, H.; Sleiman, H. F., Templated Synthesis of Highly Stable, Electroactive, and Dynamic Metal–DNA Branched Junctions. *Angew. Chem. Int. Ed.* **2008,** *120* (13), 2477-2480.

116. Yang, H.; McLaughlin, C. K.; Aldaye, F. A.; Hamblin, G. D.; Rys, A. Z.; Rouiller, I.; Sleiman, H. F., Metal–nucleic acid cages. *Nat. Chem.* **2009,** *1*, 390.

117. Yang, H.; Altvater, F.; de Bruijn, A. D.; McLaughlin, C. K.; Lo, P. K.; Sleiman, H. F., Chiral Metal–DNA Four-Arm Junctions and Metalated Nanotubular Structures. *Angew. Chem. Int. Ed.* **2011,** *50* (20), 4620-4623.

118. Tanaka, K.; Clever, G. H.; Takezawa, Y.; Yamada, Y.; Kaul, C.; Shionoya, M.; Carell, T., Programmable self-assembly of metal ions inside artificial DNA duplexes. *Nat. Nanotech.* **2006,** *1*, 190.

119. Breaker, R. R.; Joyce, G. F., A DNA enzyme that cleaves RNA. *Chemistry & Biology* **1994,** *1* (4), 223-229.

120. Barton, J. K.; Olmon, E. D.; Sontz, P. A., Metal complexes for DNA-mediated charge transport. *Coordination Chemistry Reviews* **2011,** *255* (7), 619-634.

121. Morgan, J. R.; Nguyen, D. V. X.; Frohman, A. R.; Rybka, S. R.; Zebala, J. A., Reversible Metal-Dependent Destabilization and Stabilization of a Stem-Chelate-Loop Probe Binding to an Unmodified DNA Target. *Bioconjugate Chemistry* **2012,** *23* (10), 2020-2024.

122. Allen, C.; Maysinger, D.; Eisenberg, A., Nano-engineering block copolymer aggregates for drug delivery. *Colloids and Surfaces B: Biointerfaces* **1999,** *16* (1), 3-27.

123. Discher, D. E.; Eisenberg, A., Polymer Vesicles. *Science* **2002,** *297* (5583), 967-973.

124. Mai, Y.; Eisenberg, A., Self-assembly of block copolymers. *Chemical Society Reviews* **2012,** *41* (18), 5969-5985.

125. Patwa, A.; Gissot, A.; Bestel, I.; Barthélémy, P., Hybrid lipid oligonucleotide conjugates: synthesis, self-assemblies and biomedical applications. *Chem. Soc. Rev.* **2011,** *40* (12), 5844-5854.

126. Thaner, R. V.; Eryazici, I.; Farha, O. K.; Mirkin, C. A.; Nguyen, S. T., Facile one-step solid-phase synthesis of multitopic organic-DNA hybrids via "click" chemistry. *Chem. Sci.* **2014,** *5* (3), 1091-1096.

127. Pokholenko, O.; Gissot, A.; Vialet, B.; Bathany, K.; Thiéry, A.; Barthélémy, P., Lipid oligonucleotide conjugates as responsive nanomaterials for drug delivery. *Journal of Materials Chemistry B* **2013,** *1* (39), 5329-5334.

128. Carneiro, K. M. M.; Hamblin, G. D.; Hänni, K. D.; Fakhoury, J.; Nayak, M. K.; Rizis, G.; McLaughlin, C. K.; Bazzi, H. S.; Sleiman, H. F., Stimuli-responsive organization of block copolymers on DNA nanotubes. *Chem. Sci.* **2012,** *3* (6), 1980-1986.

129. Oishi, M.; Hayama, T.; Akiyama, Y.; Takae, S.; Harada, A.; Yamasaki, Y.; Nagatsugi, F.; Sasaki, S.; Nagasaki, Y.; Kataoka, K., Supramolecular Assemblies for the Cytoplasmic Delivery of Antisense Oligodeoxynucleotide: Polyion Complex (PIC) Micelles Based on Poly(ethylene glycol)-SS-Oligodeoxynucleotide Conjugate. *Biomacromolecules* **2005,** *6* (5), 2449-2454.

130. Oishi, M.; Nagasaki, Y.; Itaka, K.; Nishiyama, N.; Kataoka, K., Lactosylated Poly(ethylene glycol)-siRNA Conjugate through Acid-Labile β-Thiopropionate Linkage to Construct pH-Sensitive Polyion Complex Micelles Achieving Enhanced Gene Silencing in Hepatoma Cells. *J. Am. Chem. Soc.* **2005,** *127* (6), 1624-1625.

131. Fong, R. B.; Ding, Z.; Long, C. J.; Hoffman, A. S.; Stayton, P. S., Thermoprecipitation of Streptavidin via Oligonucleotide-Mediated Self-Assembly with Poly(N-isopropylacrylamide). *Bioconjugate Chemistry* **1999,** *10* (5), 720-725.

132. Chien, M.-P.; Rush, A. M.; Thompson, M. P.; Gianneschi, N. C., Programmable Shape-Shifting Micelles. *Angew. Chem. Int. Ed.* **2010,** *49* (30), 5076-5080.

133. Ding, K.; Alemdaroglu, F. E.; Börsch, M.; Berger, R.; Herrmann, A., Engineering the Structural Properties of DNA Block Copolymer Micelles by Molecular Recognition. *Angew. Chem. Int. Ed.* **2007,** *46* (7), 1172-1175.

134. Carneiro, K. M. M.; Aldaye, F. A.; Sleiman, H. F., Long-Range Assembly of DNA into Nanofibers and Highly Ordered Networks Using a Block Copolymer Approach. *J. Am. Chem. Soc.* **2010,** *132* (2), 679-685.

135. Edwardson, T. G. W.; Carneiro, K. M. M.; Serpell, C. J.; Sleiman, H. F., An Efficient and Modular Route to Sequence-Defined Polymers Appended to DNA. *Angew. Chem. Int. Ed.* **2014,** *53* (18), 4567-4571.

136. Vybornyi, M.; Rudnev, A. V.; Langenegger, S. M.; Wandlowski, T.; Calzaferri, G.; Häner, R., Formation of Two-Dimensional Supramolecular Polymers by Amphiphilic Pyrene Oligomers. *Angew. Chem. Int. Ed.* **2013,** *125* (44), 11702-11707.

137. Vyborna, Y.; Vybornyi, M.; Rudnev, A. V.; Häner, R., DNA-Grafted Supramolecular Polymers: Helical Ribbon Structures Formed by Self-Assembly of Pyrene–DNA Chimeric Oligomers. *Angew. Chem. Int. Ed.* **2015,** *54* (27), 7934-7938.

138. Vybornyi, M.; Bur-Cecilio Hechevarria, Y.; Glauser, M.; Rudnev, A. V.; Häner, R., Tubes or sheets: divergent aggregation pathways of an amphiphilic 2,7-substituted pyrene trimer. *Chem. Comm.* **2015,** *51* (90), 16191-16193.

139. Bousmail, D.; Chidchob, P.; Sleiman, H. F., Cyanine-Mediated DNA Nanofiber Growth with Controlled Dimensionality. *J. Am. Chem. Soc.* **2018,** *140* (30), 9518-9530.

140. Wilks, T. R.; Bath, J.; de Vries, J. W.; Raymond, J. E.; Herrmann, A.; Turberfield, A. J.; O'Reilly, R. K., "Giant Surfactants" Created by the Fast and Efficient Functionalization of a DNA Tetrahedron with a Temperature-Responsive Polymer. *ACS Nano* **2013,** *7* (10), 8561-8572.

141. Serpell, C. J.; Edwardson, T. G. W.; Chidchob, P.; Carneiro, K. M. M.; Sleiman, H. F., Precision Polymers and 3D DNA Nanostructures: Emergent Assemblies from New Parameter Space. *J. Am. Chem. Soc.* **2014,** *136* (44), 15767-15774.

142. Chidchob, P.; Edwardson, T. G. W.; Serpell, C. J.; Sleiman, H. F., Synergy of Two Assembly Languages in DNA Nanostructures: Self-Assembly of Sequence-Defined Polymers on DNA Cages. *J. Am. Chem. Soc.* **2016,** *138* (13), 4416-4425.

143. Edwardson, T. G. W.; Carneiro, K. M. M.; McLaughlin, C. K.; Serpell, C. J.; Sleiman, H. F., Site-specific positioning of dendritic alkyl chains on DNA cages enables their geometry-dependent self-assembly. *Nat. Chem.* **2013,** *5*, 868.

144. Chidchob, P.; Offenbartl-Stiegert, D.; McCarthy, D.; Luo, X.; Li, J.; Howorka, S.; Sleiman, H. F., Spatial Presentation of Cholesterol Units on a DNA Cube as a Determinant of Membrane Protein-Mimicking Functions. *J. Am. Chem. Soc.* **2019,** *141* (2), 1100-1108.

145. List, J.; Weber, M.; Simmel, F. C., Hydrophobic Actuation of a DNA Origami Bilayer Structure. *Angewandte Chemie International Edition* **2014,** *53* (16), 4236-4239.

146. Yang, Y.; Wang, J.; Shigematsu, H.; Xu, W.; Shih, W. M.; Rothman, J. E.; Lin, C., Self-assembly of size-controlled liposomes on DNA nanotemplates. *Nat. Chem.* **2016,** *8*, 476.

147. Dong, Y.; Yang, Y. R.; Zhang, Y.; Wang, D.; Wei, X.; Banerjee, S.; Liu, Y.; Yang, Z.; Yan, H.; Liu, D., Cuboid Vesicles Formed by Frame-Guided Assembly on DNA Origami Scaffolds. *Angew. Chem. Int. Ed.* **2017,** *56* (6), 1586-1589.

148. Zhao, Z.; Chen, C.; Dong, Y.; Yang, Z.; Fan, Q.-H.; Liu, D., Thermally Triggered Frame-Guided Assembly. *Angew. Chem. Int. Ed.* **2014,** *53* (49), 13468-13470.

149. Zhou, C.; Zhang, Y.; Dong, Y.; Wu, F.; Wang, D.; Xin, L.; Liu, D., Precisely Controlled 2D Free-Floating Nanosheets of Amphiphilic Molecules through Frame-Guided Assembly. *Adv. Mater.* **2016,** *28* (44), 9819-9823.

150. List, J.; Weber, M.; Simmel, F. C., Hydrophobic Actuation of a DNA Origami Bilayer Structure. *Angew. Chem. Int. Ed.* **2014,** *53* (16), 4236-4239.

151. Wu, Y.; Sefah, K.; Liu, H.; Wang, R.; Tan, W., DNA aptamer–micelle as an efficient detection/delivery vehicle toward cancer cells. *Proceedings of the National Academy of Sciences* **2010,** *107* (1), 5-10.

152. Lacroix, A.; Edwardson, T. G. W.; Hancock, M. A.; Dore, M. D.; Sleiman, H. F., Development of DNA Nanostructures for High-Affinity Binding to Human Serum Albumin. *J. Am. Chem. Soc.* **2017,** *139* (21), 7355-7362.

153. Bousmail, D.; Amrein, L.; Fakhoury, J. J.; Fakih, H. H.; Hsu, J. C. C.; Panasci, L.; Sleiman, H. F., Precision spherical nucleic acids for delivery of anticancer drugs. *Chem. Sci.* **2017,** *8* (9), 6218-6229.

154. Avakyan, N.; Conway, J. W.; Sleiman, H. F., Long-Range Ordering of Blunt-Ended DNA Tiles on Supported Lipid Bilayers. *j. Am. Chem. Soc.* **2017,** *139* (34), 12027-12034.

155. Alemdaroglu, F. E.; Alemdaroglu, N. C.; Langguth, P.; Herrmann, A., DNA Block Copolymer Micelles – A Combinatorial Tool for Cancer Nanotechnology. *Adv. Mater.* **2008,** *20* (5), 899-902.

156. Albinsson, B.; Hannestad, J. K.; Börjesson, K., Functionalized DNA nanostructures for light harvesting and charge separation. *Coordination Chemistry Reviews* **2012,** *256* (21), 2399-2413.

157. Zhou, C.; Zhang, Y.; Dong, Y.; Wu, F.; Wang, D.; Xin, L.; Liu, D., Precisely Controlled 2D Free-Floating Nanosheets of Amphiphilic Molecules through Frame-Guided Assembly. *Advanced Materials* **2016,** *28* (44), 9819-9823.

158. Silverman, A. P.; Kool, E. T., Detecting RNA and DNA with Templated Chemical Reactions. *Chem. Rev.* **2006,** *106* (9), 3775-3789.

159. O'Reilly, R. K.; Turberfield, A. J.; Wilks, T. R., The Evolution of DNA-Templated Synthesis as a Tool for Materials Discovery. *Acc. Chem. Res.* **2017,** *50* (10), 2496-2509.

160. Naylor, R.; Gilham, P. T., Studies on Some Interactions and Reactions of Oligonucleotides in Aqueous Solution*. *Biochemistry* **1966,** *5* (8), 2722-2728.

161. Orgel, L. E., Unnatural Selection in Chemical Systems. *Accounts of Chemical Research* **1995,** *28* (3), 109-118.

162. Wu, T.; Orgel, L. E., Nonenzymic template-directed synthesis on hairpin oligonucleotides. 2. Templates containing cytidine and guanosine residues. *J. Am. Chem. Soc* **1992,** *114* (14), 5496-5501.

163. Ye, J.; Gat, Y.; Lynn, D. G., Catalyst for DNA Ligation: Towards a Two-Stage Replication Cycle. *Angew. Chem.* **2000,** *112* (20), 3787-3789.

164. Bruick, R. K.; Dawson, P. E.; Kent, S. B. H.; Usman, N.; Joyce, G. F., Template-directed ligation of peptides to oligonucleotides. *Chemistry & Biology* **1996,** *3* (1), 49-56.

165. Gryaznov, S. M.; Letsinger, R. L., Chemical ligation of oligonucleotides in the presence and absence of a template. *J. Am. Chem. Soc* **1993,** *115* (9), 3808-3809.

166. Xu, Y.; Karalkar, N. B.; Kool, E. T., Nonenzymatic autoligation in direct three-color detection of RNA and DNA point mutations. *Nature Biotech.* **2001,** *19*, 148.

167. Xu, Y.; Kool, E. T., Rapid and Selective Selenium-Mediated Autoligation of DNA Strands. *J. Am. Chem. Soc* **2000,** *122* (37), 9040-9041.

168. Xu, Y.; Kool, E. T., A novel 5′-iodonucleoside allows efficient nonenzymatic ligation of single-stranded and duplex DNAs. *Tetrahedron Lett.* **1997,** *38* (32), 5595-5598.

169. Xu, Y.; Kool, E. T., Chemical and enzymatic properties of bridging 5′- S - phosphorothioester linkages in DNA. *Nucleic Acids Research* **1998,** *26* (13), 3159-3164.

170. Ami, T.; Ito, K.; Yoshimura, Y.; Fujimoto, K., Sequence specific interstrand photocrosslinking for effective SNP typing. *Organic & Biomolecular Chemistry* **2007,** *5* (16), 2583-2586.

171. Yoshimura, Y.; Ohtake, T.; Okada, H.; Fujimoto, K., A New Approach for Reversible RNA Photocrosslinking Reaction: Application to Sequence-Specific RNA Selection. *ChemBioChem* **2009,** *10* (9), 1473-1476.

172. Yoshimura, Y.; Ohtake, T.; Okada, H.; Fujimoto, K., Development of a rapid and reversible photocrosslinking of RNA. *Nucleic Acids Symposium Series* **2009,** *53* (1), 197-198.

173. Jyo, A.; Tabara, M.; Mukae, M.; Arslan, P.; Ihara, T., Detection of one base mismatch using photochemical ligation. *Nucleic Acids Symposium Series* **2007,** *51* (1), 287-288.

174. Yoshimura, Y.; Okada, H.; Ohtake, T.; Tsukaguchi, T.; Fujimoto, K., A selective and sensitive detection of SNP between rice cultivars by using DNA photoligation. *Nucleic Acids Symposium Series* **2009,** *53* (1), 199-200.

175. Peng, X.; Hong, I. S.; Li, H.; Seidman, M. M.; Greenberg, M. M., Interstrand Cross-Link Formation in Duplex and Triplex DNA by Modified Pyrimidines. *J. Am. Chem. Soc.* **2008,** *130* (31), 10299-10306.

176. Fujimoto, K.; Matsuda, S.; Takahashi, N.; Saito, I., Template-Directed Photoreversible Ligation of Deoxyoligonucleotides via 5-Vinyldeoxyuridine. *J. Am. Chem. Soc* **2000,** *122* (23), 5646-5647.

177. Rostovtsev, V. V.; Green, L. G.; Fokin, V. V.; Sharpless, K. B., A Stepwise Huisgen Cycloaddition Process: Copper(I)-Catalyzed Regioselective “Ligation” of Azides and Terminal Alkynes. *Angew. Chem. Int. Ed.* **2002,** *41* (14), 2596-2599.

178. Meldal, M.; Tornøe, C. W., Cu-Catalyzed Azide−Alkyne Cycloaddition. *Chem. Rev.* **2008,** *108* (8), 2952-3015.

179. Chouikhi, D.; Barluenga, S.; Winssinger, N., Clickable peptide nucleic acids (cPNA) with tunable affinity. *Chemical Communications* **2010,** *46* (30), 5476-5478.

180. Kumar, R.; El-Sagheer, A.; Tumpane, J.; Lincoln, P.; Wilhelmsson, L. M.; Brown, T., Template-Directed Oligonucleotide Strand Ligation, Covalent Intramolecular DNA Circularization and Catenation Using Click Chemistry. *J. Am. Chem. Soc* **2007,** *129* (21), 6859-6864.

181. Kukwikila, M.; Gale, N.; El-Sagheer, A. H.; Brown, T.; Tavassoli, A., Assembly of a biocompatible triazole-linked gene by one-pot click-DNA ligation. *Nat. Chem.* **2017,** *9*, 1089.

182. Liu, H.; Tørring, T.; Dong, M.; Rosen, C. B.; Besenbacher, F.; Gothelf, K. V., DNA-Templated Covalent Coupling of G4 PAMAM Dendrimers. *J. Am. Chem. Soc.* **2010,** *132* (51), 18054-18056.

183. Li, X.; Liu, D. R., DNA-Templated Organic Synthesis: Nature's Strategy for Controlling Chemical Reactivity Applied to Synthetic Molecules. *Angew. Chem. Int. Ed.* **2004,** *43* (37), 4848-4870.

184. Czlapinski, J. L.; Sheppard, T. L., Nucleic Acid Template-Directed Assembly of Metallosalen−DNA Conjugates. *J. Am. Chem. Soc* **2001,** *123* (35), 8618-8619.

185. Hahn, J.; Wickham, S. F. J.; Shih, W. M.; Perrault, S. D., Addressing the Instability of DNA Nanostructures in Tissue Culture. *ACS Nano* **2014,** *8* (9), 8765-8775.

186. Perrault, S. D.; Shih, W. M., Virus-Inspired Membrane Encapsulation of DNA Nanostructures To Achieve In Vivo Stability. *ACS Nano* **2014,** *8* (5), 5132-5140.

187. Kim, H.; Surwade, S. P.; Powell, A.; O'Donnell, C.; Liu, H., Stability of DNA Origami Nanostructure under Diverse Chemical Environments. *Chemistry of Materials* **2014,** *26* (18), 5265-5273.

188. De Stefano, M.; Vesterager Gothelf, K., Dynamic Chemistry of Disulfide Terminated Oligonucleotides in Duplexes and Double-Crossover Tiles. *ChemBioChem* **2016,** *17* (12), 1122-1126.

189. Endo, M.; Majima, T., Parallel, Double-Helix DNA Nanostructures Using Interstrand Cross-Linked Oligonucleotides with Bismaleimide Linkers. *Angew. Chem. Int. Ed.* **2003,** *42* (46), 5744-5747.

190. Cassinelli, V.; Oberleitner, B.; Sobotta, J.; Nickels, P.; Grossi, G.; Kempter, S.; Frischmuth, T.; Liedl, T.; Manetto, A., One-Step Formation of "Chain-Armor"-Stabilized DNA Nanostructures. *Angew. Chem. Int. Ed.* **2015,** *54* (27), 7795-7798.

191. Rajendran, A.; Endo, M.; Katsuda, Y.; Hidaka, K.; Sugiyama, H., Photo-Cross-Linking-Assisted Thermal Stability of DNA Origami Structures and Its Application for Higher-Temperature Self-Assembly. *J. Am. Chem. Soc.* **2011,** *133* (37), 14488-14491.

192. Kukwikila, M.; Gale, N.; El-Sagheer, A. H.; Brown, T.; Tavassoli, A., Assembly of a biocompatible triazole-linked gene by one-pot click-DNA ligation. *Nature Chemistry* **2017,** *9*, 1089.

193. Manuguerra, I.; Croce, S.; El-Sagheer, A. H.; Krissanaprasit, A.; Brown, T.; Gothelf, K. V.; Manetto, A., Gene assembly via one-pot chemical ligation of DNA promoted by DNA nanostructures. *Chem. Comm.* **2018,** *54* (36), 4529-4532.

194. Gerling, T.; Kube, M.; Kick, B.; Dietz, H., Sequence-programmable covalent bonding of designed DNA assemblies. *Sci. Adv.* **2018,** *4* (8), eaau1157.

195. Gerling, T.; Dietz, H., Reversible Covalent Stabilization of Stacking Contacts in DNA Assemblies. *Angew. Chem. Int. Ed.* **2019,** *0* (0).

196. Gartner, Z. J.; Kanan, M. W.; Liu, D. R., Expanding the Reaction Scope of DNA-Templated Synthesis. *Angew. Chem.* **2002,** *114* (10), 1874-1878.

197. Gartner, Z. J.; Liu, D. R., The Generality of DNA-Templated Synthesis as a Basis for Evolving Non-Natural Small Molecules. *J. Am. Chem. Soc* **2001,** *123* (28), 6961-6963.

198. Gartner, Z. J.; Grubina, R.; Calderone, C. T.; Liu, D. R., Two Enabling Architectures for DNA-Templated Organic Synthesis. *Angew. Chem. Int. Ed.* **2003,** *42* (12), 1370-1375.

199. Ficht, S.; Mattes, A.; Seitz, O., Single-Nucleotide-Specific PNA−Peptide Ligation on Synthetic and PCR DNA Templates. *J. Am. Chem. Soc.* **2004,** *126* (32), 9970-9981.

200. El-Sagheer, A. H.; Cheong, V. V.; Brown, T., Rapid chemical ligation of oligonucleotides by the Diels–Alder reaction. *Organic & Biomolecular Chemistry* **2011,** *9* (1), 232-235.

201. Gartner, Z. J.; Kanan, M. W.; Liu, D. R., Multistep Small-Molecule Synthesis Programmed by DNA Templates. *J. Am. Chem. Soc.* **2002,** *124* (35), 10304-10306.

202. Li, X.; Gartner, Z. J.; Tse, B. N.; Liu, D. R., Translation of DNA into Synthetic N-Acyloxazolidines. *J. Am. Chem. Soc.* **2004,** *126* (16), 5090-5092.

203. Gartner, Z. J.; Tse, B. N.; Grubina, R.; Doyon, J. B.; Snyder, T. M.; Liu, D. R., DNA-Templated Organic Synthesis and Selection of a Library of Macrocycles. *Science* **2004,** *305* (5690), 1601.

204. Tse, B. N.; Snyder, T. M.; Shen, Y.; Liu, D. R., Translation of DNA into a Library of 13 000 Synthetic Small-Molecule Macrocycles Suitable for in Vitro Selection. *J. Am. Chem. Soc.* **2008,** *130* (46), 15611-15626.

205. Snyder, T. M.; Liu, D. R., Ordered Multistep Synthesis in a Single Solution Directed by DNA Templates. *Angew. Chem. Int. Ed.* **2005,** *44* (45), 7379-7382.

206. Hansen, M. H.; Blakskjær, P.; Petersen, L. K.; Hansen, T. H.; Højfeldt, J. W.; Gothelf, K. V.; Hansen, N. J. V., A Yoctoliter-Scale DNA Reactor for Small-Molecule Evolution. *J. Am. Chem. Soc.* **2009,** *131* (3), 1322-1327.

207. Zhang, D. Y.; Seelig, G., Dynamic DNA nanotechnology using strand-displacement reactions. *Nat. Chem.* **2011,** *3*, 103.

208. McKee, M. L.; Milnes, P. J.; Bath, J.; Stulz, E.; Turberfield, A. J.; O'Reilly, R. K., Multistep DNA-Templated Reactions for the Synthesis of Functional Sequence Controlled Oligomers. *Angew. Chem. Int. Ed.* **2010,** *49* (43), 7948-7951.

209. He, Y.; Liu, D. R., A Sequential Strand-Displacement Strategy Enables Efficient Six-Step DNA-Templated Synthesis. *J. Am. Chem. Soc.* **2011,** *133* (26), 9972-9975.

210. McKee, M. L.; Milnes, P. J.; Bath, J.; Stulz, E.; O'Reilly, R. K.; Turberfield, A. J., Programmable One-Pot Multistep Organic Synthesis Using DNA Junctions. *J. Am. Chem. Soc.* **2012,** *134* (3), 1446-1449.

211. Tian, Y.; He, Y.; Chen, Y.; Yin, P.; Mao, C., A DNAzyme That Walks Processively and Autonomously along a One-Dimensional Track. *Angew. Chem.* **2005,** *117* (28), 4429-4432.

212. He, Y.; Liu, D. R., Autonomous multistep organic synthesis in a single isothermal solution mediated by a DNA walker. *Nat. Nanotech.* **2010,** *5*, 778.

213. Meng, W.; Muscat, R. A.; McKee, M. L.; Milnes, P. J.; El-Sagheer, A. H.; Bath, J.; Davis, B. G.; Brown, T.; O'Reilly, R. K.; Turberfield, A. J., An autonomous molecular assembler for programmable chemical synthesis. *Nat. Chem.* **2016,** *8*, 542.

214. Sakurai, K.; Snyder, T. M.; Liu, D. R., DNA-Templated Functional Group Transformations Enable Sequence-Programmed Synthesis Using Small-Molecule Reagents. *J. Am. Chem. Soc.* **2005,** *127* (6), 1660-1661.

215. Luebke, K. J.; Dervan, P. B., Nonenzymatic ligation of oligodeoxyribonucleotides on a duplex DNA template by triple-helix formation. *J. Am. Chem. Soc.* **1989,** *111* (23), 8733-8735.

216. Poulin-Kerstien, A. T.; Dervan, P. B., DNA-Templated Dimerization of Hairpin Polyamides. *j. Am. Chem. Soc.* **2003,** *125* (51), 15811-15821.

217. Alemdaroglu, F. E.; Ding, K.; Berger, R.; Herrmann, A., DNA-Templated Synthesis in Three Dimensions: Introducing a Micellar Scaffold for Organic Reactions. *Angew. Chem. Int. Ed.* **2006,** *45* (25), 4206-4210.

218. Nielsen, M.; Thomsen, A. H.; Cló, E.; Kirpekar, F.; Gothelf, K. V., Synthesis of Linear and Tripoidal Oligo(phenylene ethynylene)-Based Building Blocks for Application in Modular DNA-Programmed Assembly. *J. Org. Chem.* **2004,** *69* (7), 2240-2250.

219. Gothelf, K. V.; Thomsen, A.; Nielsen, M.; Cló, E.; Brown, R. S., Modular DNA-Programmed Assembly of Linear and Branched Conjugated Nanostructures. *J. Am. Chem. Soc.* **2004,** *126* (4), 1044-1046.

220. Nielsen, M.; Dauksaite, V.; Kjems, J.; Gothelf, K. V., DNA-Directed Coupling of Organic Modules by Multiple Parallel Reductive Aminations and Subsequent Cleavage of Selected DNA Sequences. *Bioconjugate Chem.* **2005,** *16* (4), 981-985.

221. Brown, R. S.; Nielsen, M.; Gothelf, K. V., Self-assembly of aluminium–salen coupled nanostructures from encoded modules with cleavable disulfide DNA-linkers. *Chem. Comm.* **2004,** (13), 1464-1465.

222. Ravnsbæk, J. B.; Jacobsen, M. F.; Rosen, C. B.; Voigt, N. V.; Gothelf, K. V., DNA-Programmed Glaser–Eglinton Reactions for the Synthesis of Conjugated Molecular Wires. *Angew. Chem. Int. Ed.* **2011,** *50* (46), 10851-10854.

223. Seeman, N. C.; Sleiman, H. F., DNA nanotechnology. *Nat. Rev. Mat.* **2017,** *3*, 17068.

224. Bujold, K. E.; Hsu, J. C. C.; Sleiman, H. F., Optimized DNA "Nanosuitcases" for Encapsulation and Conditional Release of siRNA. *J. Am. Chem. Soc.* **2016,** *138* (42), 14030-14038.

225. Bousmail, D.; Amrein, L.; Fakhoury, J. J.; Fakih, H. H.; Hsu, J. C. C.; Panasci, L.; Sleiman, H. F., Precision spherical nucleic acids for delivery of anticancer drugs. *Chemical Science* **2017,** *8* (9), 6218-6229.

| 2 |

Using DNA micelles as nanoreactors for DNA conjugation

This chapter is composed mainly of the work published as "DNA micelles as nanoreactors: efficient DNA functionalization with hydrophobic organic molecules" by Tuan Trinh, Pongphak Chidchob, Hassan S. Bazzi and Hanadi F. Sleiman in Chemical Communications, 2016, **52**, 10914-10917.

Author contributions:

Tuan Trinh helped design and develop the project, primarily contributed to the production of experimental data from DNA synthesis, HPLC purification, mass spectrometry (MS), electrophoresis, dynamic light scattering (DLS), AFM imaging and wrote the paper. **Pongphak Chidchob** helped design the project, synthesized some DNA strands, aided data interpretation and performed some AFM imaging. **Hassan S. Bazzi** provided funding for the work. **Hanadi F. Sleiman** designed the project, guided interpretation of data, result discussion, co-wrote the paper and provided funding for the project.

2.1. Preface

DNA is an excellent material to build structures at the nanoscale level. As can be seen in chapter 1, various structures with any arbitrary shapes and high complexity can be potentially assembled with the development of structural DNA nanotechnology, DNA origami and supramolecular DNA nanotechnology. In addition, DNA nanostructures can provide an appealing platform to carry out chemical transformations with a high degree of control. DNA-hydrophobic conjugates are an important class of materials, with numerous biological and materials applications. In this chapter, we demonstrate a simple method to attach highly hydrophobic moieties to DNA strands and amphiphiles via amide chemistry using spherical DNA micelles. Long lipid chains, chromophores and polymers can be conjugated in aqueous environment with high yield, under mild conditions and with short reaction times. This approach relies on using the hydrophobic core of DNA-amphiphile micelles as reaction auxiliaries that facilitate the conjugation of complementary DNA strands to hydrophobic units. The approach also allows efficient conjugation directly to DNA amphiphiles. It is possible to tune reactivity by precisely positioning the reactive units on the DNA-amphiphiles. This general method can be applied to

functionalize DNA for many useful applications ranging from oligonucleotide and small molecule delivery, nanopore mimetics, to DNA self-assembly and nanotechnology.

2.2. Introduction

The conjugation of nucleic acids (DNA) to hydrophobic molecules, polymers or drugs can generate an important class of bio-hybrid materials, which lend themselves to a broad range of biomedical applications such as gene therapy,[1-4] drug delivery [5-8] and biosensing [9-12] as well as material science.[13-18] To date, there are two main approaches to conjugate DNA to molecules, relying either on solid-phase or on solution-phase synthesis. While solid-phase approaches that incorporate non-natural moieties into DNA are versatile and powerful,[19-21] the molecules to be introduced need to be adequately modified for phosphoramidite synthesis, and importantly, they need to be stable to the relatively harsh deprotection conditions used. The yields for incorporation of long lipidic or polymeric chains using this method are also typically low due to the small pore size of the solid support.[22] Hydrophilic molecules and polymers can be efficiently attached to post-synthesized DNA strands in water.[23-26] However, attaching hydrophobic moieties to DNA in aqueous solution still remains a great challenge, in large part because of solvent incompatibility between DNA and hydrophobic molecules.[27-29] In order to address this issue, Herrmann *et al.* have recently reported a method to carry out reactions between DNA and hydrophobic molecules in organic solvents, by adding positively charged surfactants with long alkyl chains.[30] However, removing surfactants after the reaction can be an issue.

Micellar reactions constitute an important methodology for efficient and green synthetic organic transformations.[31] These rely on the use of surfactants to form micellar aggregates in aqueous solution, and take advantage of the hydrophobic effect to bring together reactants within the core of these micelles. The reactant molecules have a higher effective concentration,[32] and have been shown to undergo a variety of reactions with enhanced yields [33-38] and often altered regio- and stereo-selectivity. We demonstrate in this chapter a simple micelle-templated method to conjugate DNA and DNA amphiphiles to a range of hydrophobic molecules and polymers in aqueous buffer and under mild conditions, with excellent yields and short reaction times. The yields are higher than the positively-charged surfactant method described above,[30] particularly when the molecule

conjugated to DNA has significant hydrophobicity, and the final products can be readily separated and purified.

The method relies on a simple, on column conjugation of DNA with a commercial **1,12-dodecanediol phosphoramidite** (hexaethylene, or **HE** unit) to give DNA-hexaethylene conjugates with sequence- and length control. These amphiphilic conjugates self-assemble in aqueous buffer to form highly monodispersed DNA micelles. We show that these micelles can be used as reaction auxiliaries: a complementary, non-hydrophobically modified DNA strand can hybridize to them, thus orienting its reactive group towards the micelle core, and this sigificantly improves the conjugation yields (the process shown in **Figure 2.1).** We also demonstrate that reactions in these micelles are highly efficient: a range of molecules can be attached directly to the DNA strand and amphiphile components of the micelle, including activated NHS esters of hexadecanoic acid **(C_{16})**, stearic acid **(C_{18})**, behenic acid **(C_{22})**, a branched N,N'-didecyl chain **(NDS)**, the chromophore pyrene and a hydrophobic polymer (polystyrene) via amide formation. Because of the fine sequence control of the DNA-hydrophic conjugates used for templation, we examined the position-dependent reactivity of the functional group inside the micellar **HE** core. This gave us insights into the nature of this hydrophobic environment. Considering the wealth of micelle-promoted reactions and micellar catalysis in organic chemistry, we anticipate that this will be a general method to attach hydrophobic molecules to DNA, as well as increase their complexity through subsequent reactions within the micellar core, thereby increasing the range of applications of DNA conjugates in biomedicine and nanotechnology.

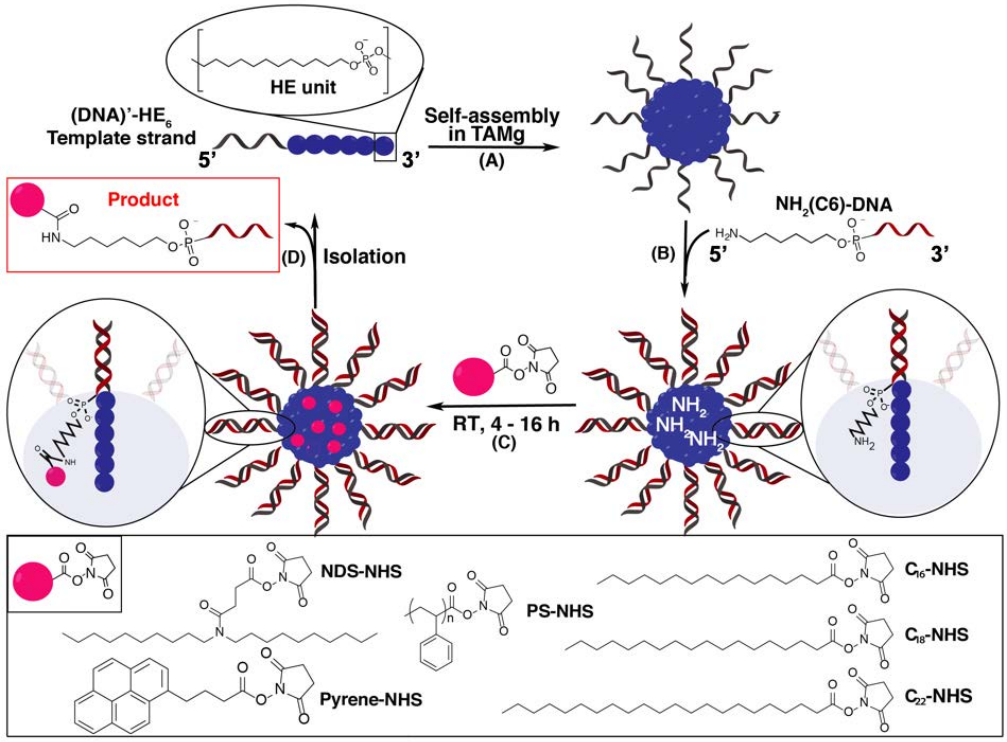

Figure 2.1 | Synthetic methodology for DNA-hydrophobic conjugation using DNA micellar core. **A.** DNA amphiphiles **((DNA)'-HE$_6$)** can self-assemble into micelles in aqueous buffer. **B.** Hybridizing amino-modified DNA (complementary to **(DNA)'**). **C.** Adding activated hydrophobic NHS esters seperately and incubating at room temperature efficiently results in DNA strands covalently modified with the hydrophobic units via amide bond. **D.** Using reverse-phase HPLC (RP-HPLC) with an appropriate gradient, starting material, template strand and conjugate product can be separated easily. By collecting the template strand after RP-HPLC purification, it can be re-used for the next conjugation process.

2.3. Result and discussion

2.3.1. DNA micelles as reaction auxiliaries.

We have recently described a simple method to repeatedly attach the commercially available dimethoxytrityl (DMT)-protected 1,12-dodecanediol phosphoramidite unit **(HE)** **(Figure 2.1)** to DNA on solid support in a sequence- and length-controlled manner. The

obtained DNA amphiphiles can readily self-assemble into highly monodisperse micelles in tris-acetate buffer containing magnesium ions **(TAMg)**.[39] We hypothesized that the hydrophobic cores of these micelles may be suitable as mini-reactors, which can facilitate diffusion of hydrophobic molecules into the core and increase their effective concentrations, resulting in an improvement of the conjugation efficiency. In this work, we functionalized a 19-mer single stranded DNA (we name the DNA sequence "**DNA**") with three different commercially available amino modifiers at the 5'-end, namely Fmoc-Amino-C3-CED phosphoramidite **(NH_2)**, 5'-Amino modifier-C3-TFA **(NH_2(C3))** and 5'-Amino modifier-C6-MMT (**NH_2(C6)**) (see **Figure 2.2** and experimental section **2.5.17** for chemical structures). These amino modified DNA strands can be hybridized to DNA micelles that contain strands of complementary sequence **(DNA)'** and 6 **HE** repeats on the 3' terminus, 5'-**(DNA)'-HE_6**-3'.

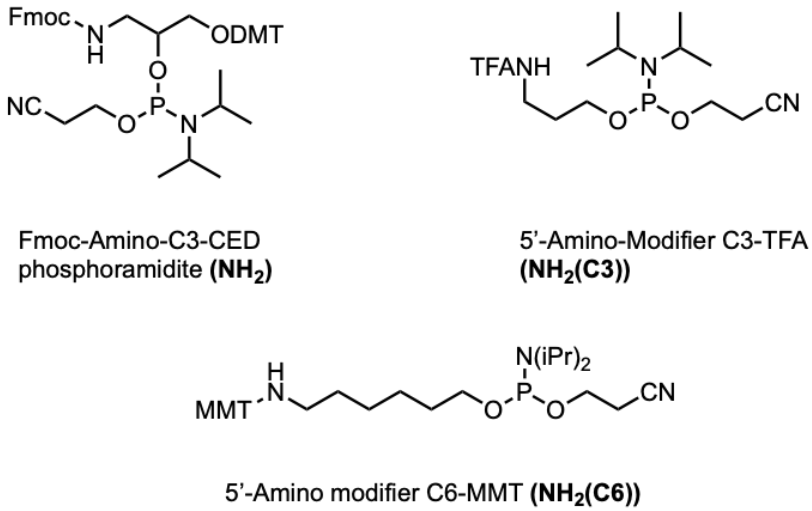

Fmoc-Amino-C3-CED phosphoramidite **(NH_2)**

5'-Amino-Modifier C3-TFA **(NH_2(C3))**

5'-Amino modifier C6-MMT **(NH_2(C6))**

Figure 2.2 | Chemical structures of amino modifications used in this study.

This arrangement will direct the amino group towards the hydrophobic core and thus bring this group into closer proximity to the N-hydroxysuccinimide **(NHS)** guest molecules **(Figure 2.1)**. The amino modified DNA strands and (DNA)'-HE_6 template strands were mixed and assembled into micelles in TAMg buffer by thermally annealing from 95°C to 4°C for 1 hour. Separately, hydrophobic molecules functionalized with a NHS ester group, were dissolved in a small amount of organic solvent (THF or DMSO), then added to the DNA micelles solution. The reaction mixture was then shaken at room temperature for 4 to 16 hours. After the reaction, the conjugated products with hydrophobic molecules can be isolated by reverse-phase HPLC

(RP-HPLC) and the template strand can be potentially recovered and subsequently recycled for the next conjugation process **(Figure 2.1**).

With the micelle-templated approach, we did observe significantly improved conjugation yields. The commercially available amino modified DNA **NH_2(C6)**-DNA resulted in 60 ± 2% conjugation yield with **C_{16}-NHS**, up from 36 ± 5% without templation. 64 ± 4% yield was observed with **C_{18}-NHS**, with only 16 ± 3% without templation. Such lipidic molecules are especially difficult to conjugate to DNA under normal conditions, especially in aqueous media. Interestingly as well, a 20-carbon containing molecule (**NDS-NHS**, see structure in **Figure 2.1**) and pyrene-NHS gave an excellent yield of 88 ± 4% and 95 ± 2 respectively, while it does not react without the micelle auxiliary **(Figure 2.3)**. Finally, the very hydrophobic **C_{22}-NHS** did not result in any conjugation without the template, whereas the yield was 30 ± 3% with micelle templation. Slightly shorter commercially available amino modifiers gave lower yields (18 ± 3% coupling yield **C_{22}-NHS** in case of **NH_2**-DNA and 22 ± 4% with **NH_2(C3)**-DNA- see Figure **2.2** for chemical structures). This is possibly due to the fact that, without a spacer, the terminal amino group on this DNA strand may not be able to reach the micellar core to react with the hydrophobic molecules. Conjugation yields are summarized in **Figure 2.3** (see also Experimental section **2.5.17** for HPLC and MS characterization).

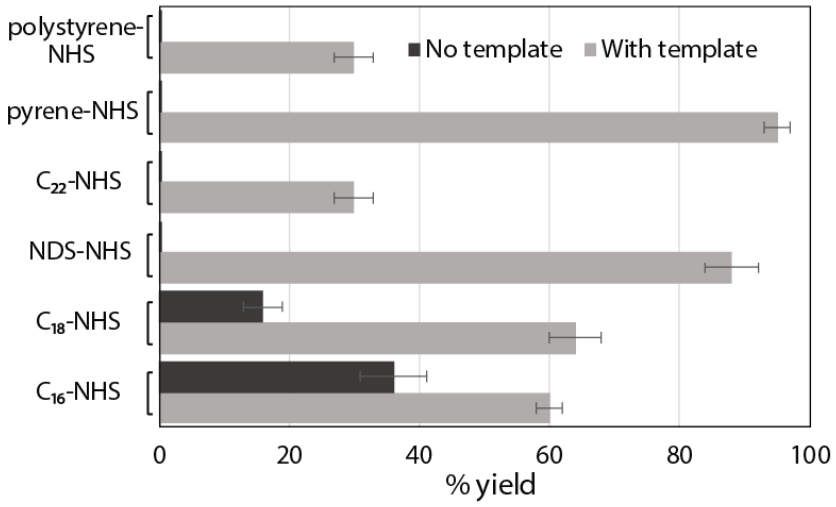

Figure 2.3 | Conjugation yields of **NH_2(C_6)**-DNA with hydrophobic molecules with and without **(DNA)'-HE_6** template. All conjugation reactions were reproduced at least three times.

2.3.2. Reactivity of DNA amphiphiles: hydrophobic length and position of reactive group.

One of the important design elements of the templation approach is to direct the reactive amino group towards the hydrophobic micellar core in order to improve the conjugation efficiency. Therefore, we were interested to examine the dependence of conjugation efficiency on two parameters, including **1)** the position of the amino group inside the micellar core and **2)** the size of the micellar core, to gain better understanding on how DNA micelles can enhance the conjugation efficiency. We deliberately varied positions of the amino group along the hydrophobic chain and lengths of DNA amphiphiles. The 5' end of the DNA strand were functionalized with a specific number of **HE** units and a $\mathbf{NH_2}$ unit as the amino moiety (**Figure 2.4**). Our sequence-controlled synthesis allows the placement of $\mathbf{NH_2}$ group in precise positions along the hydrophobic **HE** backbone, and a detailed assessment of its reactivity. Three classes of DNA amphiphiles were prepared: DNA amphiphiles with **12 HE**, **6 HE** and **0-1 HE** repeats. The first two classes of molecules form stable micelles, while the third does not assemble in aqueous solution and was used as a control. Within these, the position of the amino group was varied by placing it at the end of the hydrophobic chain, in the middle, or at the interface between the DNA strand and the hydrophobic block **(Figure 2.4)**. This position was chosen such that there are at least **6 HE** contiguous repeats, in order not to disrupt the micelle formation.[39] (see experimental section for synthesis and characterization). The DNA amphiphiles were readily assembled into micelles in TAMg buffer and the assembly was verified by dynamic light scattering (**DLS**) and atomic force microscopy **(AFM)**.

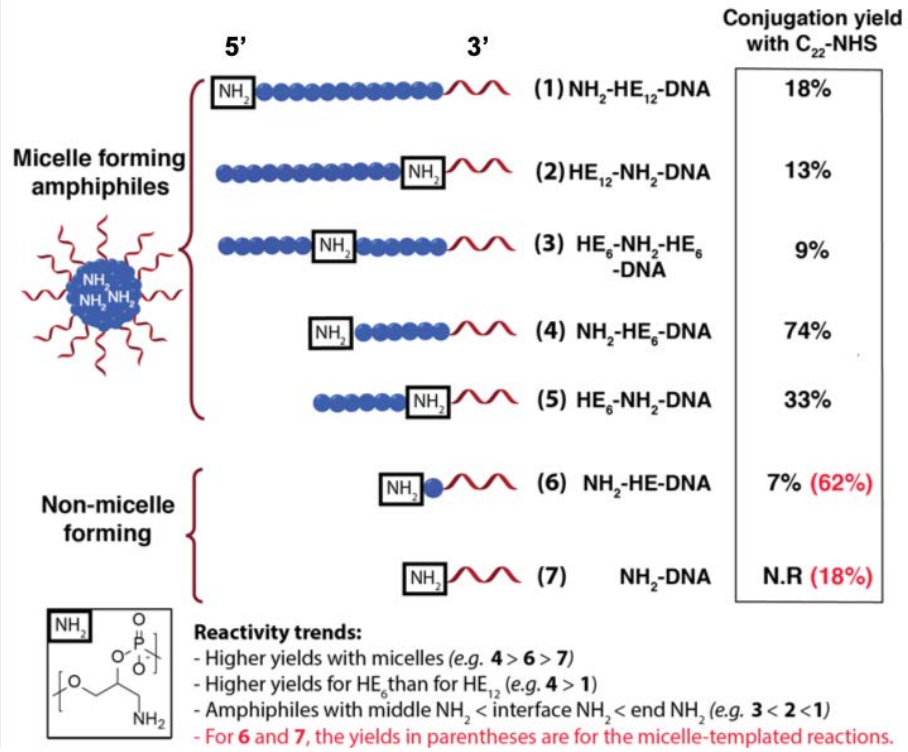

Figure 2.4 | Varying the DNA amphiphile length and position of amino monomer **(NH_2)** on DNA amphiphiles and yield of each strand with C_{22}-NHS (**N.R: No reaction**).

Our investigations were carried out using the hydrophobic NHS molecules described earlier. They allowed us to extract reactivity trends, summarized here:

1. The yields are significantly higher with micelle formation.

For example, for C_{16}-NHS and C_{22}-NHS, DNA amphiphile **NH_2-HE_6-DNA (4)** achieved 87% and 74% yield respectively, while non-micelle-forming **NH_2-DNA (7)** resulted in 0% in both cases (see Experimental section **Figure 2.16** and **Figure 2.4** for C_{16}-NHS).

2. The yields are higher for the HE_6 than for the HE_{12} amphiphiles.

For example, for C_{16}-NHS and C_{22}-NHS, amphiphile (**4**) achieved 87% and 74% yields, while **NH_2-HE_{12}-DNA (1)** gave 40% and 18% yields, respectively (see Experimental Section **Figure 2.20** and **Figure 2.4** for C_{22}-NHS). This is possibly due to increased rigidity of the micellar

core with a higher number of HE repeats, slowing down the diffusion of the small molecules to the reactive units.

3. ***The yields increase in the following order: NH_2 in the middle of the hydrophobic chain < NH_2 at the interface between the polymer and the DNA < NH_2 at the end of the hydrophobic chain.***

For instance, for conjugation with the very hydrophobic C_{22}-NHS, **(1)** gave 18% yield, while **(2)** and **(3)** gave 13% and 9% respectively; **(4)** (74%) is more reactive than **(5)** (33%) **(Figure 2.4)**. This is likely because of the decreased accessibility of the **NH_2** moiety to the reactive hydrophobic molecules when it is in the middle of the chain as compared to the chain end. These observations also allowed us to gain increased understanding on the structure of the alkyl chains in the core.

2.3.3. Position of NH_2 group

One of the important design questions is that where the **NH_2** groups actually locate inside the micellar core. Depending on polyalkyl chain folding, the reactive **NH_2** groups within the **NH_2-HE_6-AT** micelles could either be buried inside the micellar core (if the alkyl chains are folded upon themselves in the core), or on the interface between the micelle core and corona (if the alkyl chains are unfolded) **(Figure 2.5)**.

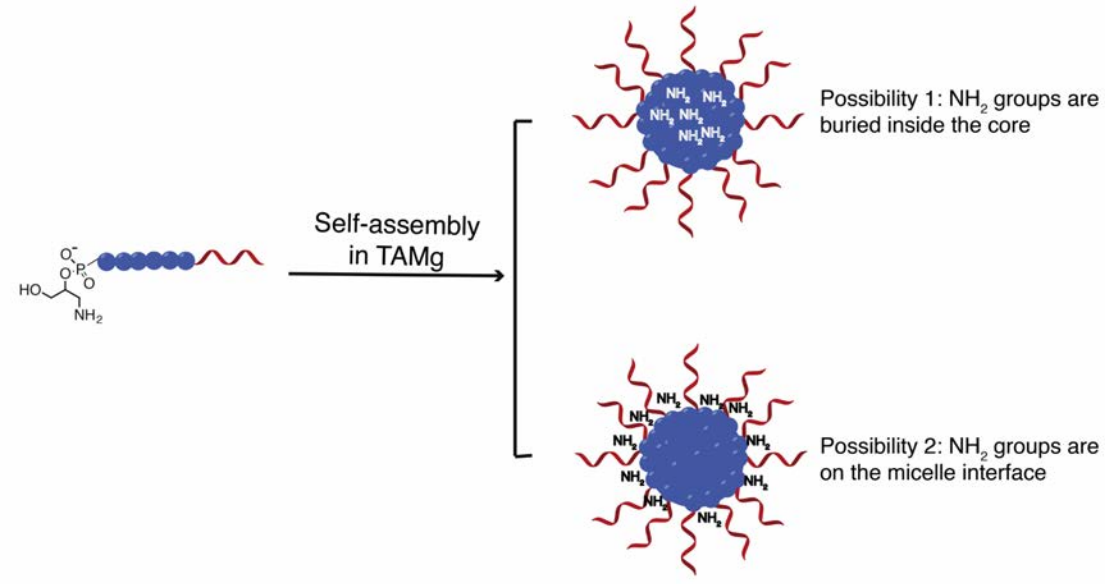

Figure 2.5 | Two possibilities of the positions of **NH_2** groups (inside the core, or on the micelle interface).

We noted above that the **NH_2** group at the chain end is more reactive than the **NH_2** at the micelle interface (e.g., **NH_2-**HE_6-DNA **(4)** and HE_6-**NH_2-**DNA **(5)** in **Figure 2.4**). If the **NH_2** group of **NH_2-**HE_6-DNA were on the micelle interface, then **NH_2-**HE_6-DNA would show similar reactivity to the conjugate HE_6-**NH_2-**DNA. In fact, the reaction of HE_6-**NH_2-**DNA with C_{22}-NHS under the same condition as **NH_2-**HE_6-DNA gave only 33 ± 3% compared to 74 ± 8% in case of **NH_2-**HE_6-DNA (see Experimental Section **Figure 2.20**). In the conjugation reactions with C_{16}-NHS, **NH_2-**HE_6-DNA achieved 87 ± 2% in yield, whereas the yield of **NH_2-**HE_{12}-DNA dropped to 40 ± 4%. Based on these results, we suggest that the **NH_2** groups are likely buried within the hydrophobic core of DNA micelles rather than on the interface, probably due to packing of the alkyl chains in the DNA micellar core. This further supports the improved conjugation yield with spacer length in the auxiliary micelle approach described earlier. We are currently examining the internal structure of the micelle core in greater detail.

2.3.4. Effect of Mg^{2+} concentration and reactivities in other commonly used buffers

Another important insight obtained from the site-specific labeling with **NH_2** was to ascertain that micelle formation is essential to the rate acceleration. We have previously shown that micelle formation in these structures is dependent on the presence of Mg^{2+}, most likely needed to overcome the repulsion in bringing the phosphate units within the core, and that it does not occur in pure water without these ions. We thus compared the reaction of **NH_2-HE_6-**DNA with C_{22}-NHS in Mg-containing buffer and in pure H_2O. Indeed, the reaction in water showed significantly lower yield (20%) compared to the Mg^{2+}-buffer (74%) (**Figure 2.6)**.

So far, all conjugation reactions were carried out in TAMg (Tris, Acetic acid and $MgCl_2$) buffer, and we were interested to probe whether the conjugation efficiency depends on the buffer choice. To examine the effect of each component of the buffer on the reaction efficiency, we compared the conjugation of NH_2-HE_6-AT with C_{22}-NHS in different buffer conditions (**Figure 2.6)** and the corresponding yields were highest with TAMg: TAMg (pH 8, 74±8%) ~ $MgCl_2$ (pH 8, 65±2%; pH 5.5, 61±8%) > TA (tris-acetate, pH 8, 35±8%) ~ H_2O (20±14%). Replacement of tris with non-

nucleophilic (4-(2-hydroxyethyl)-1-piperazineethanesulfonic acid (HEPES) supplemented with $MgCl_2$ gave comparable yield (pH 8, 69±12%) to TAMg (**Figure 2.6).** These suggest that Mg^{2+} is important for efficient conjugation, most likely because it is required for micelle formation. Interestingly, good yields were obtained in Tris buffer although Tris is known to act as a competitor in NHS ester reactions. This suggests that the hydrophobic core of DNA-micelles prevents somehow the interaction of NHS molecules with Tris. To our surprise, commercial non-amine-containing buffers were found to be less effective than amine-containing buffers: phosphate buffered saline (PBS, pH 7.4, 20±8%) and DPBS (Dulbecco's phosphate buffered saline, pH 7.4, 7±3%).

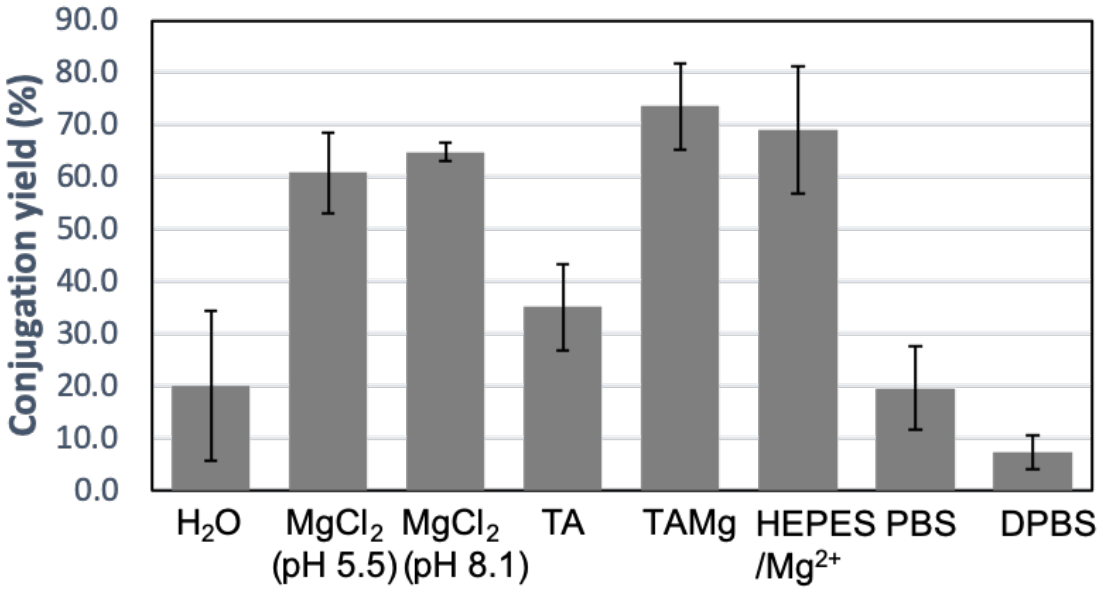

Figure 2.6 | Conjugation yields of **NH_2-HE_6-DNA** with **C_{22}-NHS** in different buffer compositions.

2.3.5. Introducing long spacer between DNA and NH_2 group

With this information, we turned our attention back to the templated micelle approach described earlier **(Figure 2.2 and Figure 2.4, highlighted in red)**. For the **NH_2-**DNA **(7)** with a short serinol amino modification, micelle-templated coupling to C_{22}-NHS gives only 18% yield (**Figure 2.3**, see Experimental Section **Figure 2.42**). Recall that the longer C_6-amino modification gives a higher yield (30%, **Figure 2.2 and Figure 2.3**). Interestingly, introducing a single HE spacer between the DNA strand and the amino group in **(7) (Figure 2.4)** significantly increases the yield of this coupling reaction to 62% (**Figure 2.7**). Thus, directing the amino group deeper into the micellar core by using an amino modification with a longer spacer, or introducing an alkyl spacer allows coupling DNA to extremely hydrophobic units in good yields. For C_{20} or less, the coupling of regular amino-modified DNA occurs with high efficiency.

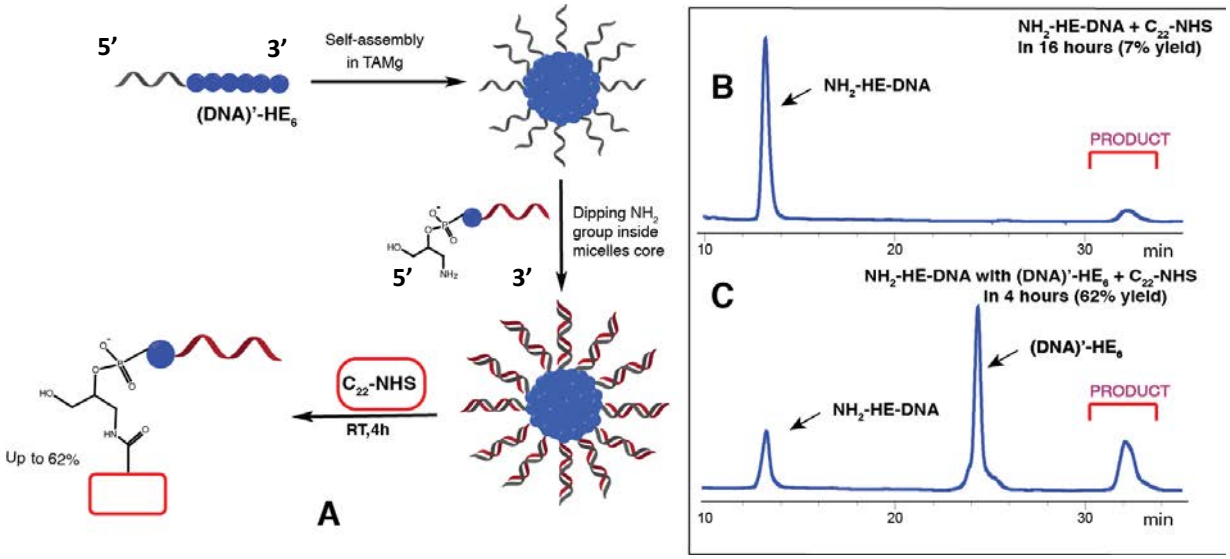

Figure 2.7 | A. Improving coupling efficiency with C_{22}-NHS by introducing a long alkyl spacer between DNA and **NH_2** group. By hybridizing amphiphiles containing **DNA** sequence to its complementary strand **DNA'**, the **NH_2** was dipped inside hydrophobic core of DNA micelles. **B** and **C**. Reported yield of **NH_2-HE-DNA** with **C_{22}-NHS** without and with micelle template.

2.4. Conclusion

In conclusion, this chapter has demonstrated a facile methodology to conjugate hydrophobic molecules to DNA strands in aqueous solution with high yield and under mild conditions. We showed that the micelle can be used as a reaction auxiliary to increase the reactivity of commercially available amino modified DNA. A number of hydrophobic units have been attached to DNA and DNA amphiphiles, ranging from long alkyl chains, branched long alkyls, chromophores like pyrene and a pre-formed polymer (polystyrene). In the mechanistic work, we positioned the reactive groups in different locations within the micelle. This allowed us to optimize the structure of the micelle auxiliary and the location of this reactive group. With a wide range of hydrophobic carboxylic acids from commercially available sources, this synthetic method has the potential to be applied to numerous research problems. It creates the opportunity to synthesize a variety of DNA hybrid materials, which are useful in DNA and small molecule therapeutic delivery, diagnostics, nanopore formation, DNA nanotechnology and material science.

2.5. Experimental Section

2.5.1. General

Unless otherwise stated, all commercial reagents and solvents were used without additional purification. Magnesium sulfate hexahydrate ($MgSO_4 \cdot 6H_2O$), tris(hydroxymethyl)aminomethane (Tris), urea, palmitic acid *N*-hydroxysuccinimide (C_{16}-NHS), chloroform ($CHCl_3$), hexane (Hex), tetrahydrofurane (THF), dimethyl sulfoxide (DMSO), hydrochloric acid (HCl), dichloromethane (DCM), ethyl acetate (EA), decanoic acid, docosahexaenoic acid, *N*-hydroxysuccinimide (NHS), *N*,*N*'-Dicyclohexylcarbodiimide (DCC), 1-Ethyl-3-(3-dimethylaminopropyl)carbodiimide (EDC) and succinic anhydride were used as purchased from Sigma-Aldrich. Carboxy terminated polystyrene (PS-COOH) with M_n of 900 (PDI = 1.5) was purchased from Polymer Source. Acetic acid and boric acid were purchased from Fisher Scientific and used without further purification. GelRed™ nucleic acid stain was purchased from VWR. Acetone ACS reagent grade was

purchased from Fisher. Acrylamide/Bis-acrylamide (40% 19:1 solution), ammonium persulfate and tetramethylenediamine were obtained from Bioshop Canada Inc. and used as supplied. 1 μmol Universal 1000Å LCAACPG supports and standard reagents used for automated DNA synthesis were purchased through Bioautomation. Sephadex G-25 (super fine, DNA grade) was purchased from Glen Research. Analytical thin layer chromatography (TLC) was performed on TLC plates purchased from Sigma-Aldrich. TAMg buffer is composed of 45 mM Tris and 12.5 mM $MgCl_2.6H_2O$ with the pH adjusted to 8.0 using glacial acetic acid. TBE buffer is 90 mM Tris, 90 mM boric acid and 2 mM EDTA with a pH of 8.0. TEAA mobile phase is 50 mM triethylammonium acetate with the pH adjusted to 8.0 using glacial acetic acid.

2.5.2. Instrumentation

Standard automated oligonucleotide solid-phase synthesis was performed on a Mermade MM6 Synthesizer from Bioautomation. HPLC purification was carried out on an Agilent Infinity 1260. DNA quantification measurements were performed by UV absorbance with a NanoDrop Lite spectrophotometer from Thermo Scientific. Gel electrophoresis experiments were carried out on a 20 X 20 cm vertical Hoefer 600 electrophoresis unit. Gel images were captured using a ChemiDocTM MP System from Bio-Rad Laboratories. Thermal annealing of all DNA micelles was conducted using an Eppendorf Mastercycler® 96 well thermocycler. Liquid Chromatography Electrospray Ionization Mass Spectrometry (LC-ESI-MS) was carried out using Dionex Ultimate 3000 coupled to a Bruker MaXis Impact™ QTOF. Column chromatography to purity organic compounds was performed on a CombiFlash® R_f^+ system with RediSep® Silica columns (230-400 mesh) using a proper eluent system. ^{1}H NMR was recorded on 500 MHz AV500 equipped with a 60 position SampleXpress sample changer (Bruker) and 300 MHz Varian Mercury equipped with an SMS-100 sample changer (Agilent). DynaPro (model MS) molecular-sizing instrument was used to measure the particle size distributions. Visualization of TLC was achieved by UV light (254 nm). Chemical shifts were quoted in parts per million (ppM) referenced to the appropriate residual solvent peak or 0.0 ppm for tetramethylsilane. Abbreviations for ^{1}H NMR: s = singlet, d = doublet, t = triplet, q = quartet, quint = quintet, m = multiplet. High-resolution mass spectra were obtained from Exactive Plus Orbitrap Mass Spectrometer (Thermo Scientific).

2.5.3. Synthesis, Purification and Characterization of DNA strands

2.5.3.1. Solid-phase synthesis

DNA synthesis was performed on a 1 μmole scale, starting from the required nucleotide modified 1000 Å LCAA-CPG solid-support. Coupling efficiency was monitored after removal of the dimethoxytrityl (DMT) 5-OH protecting groups. DMT-dodecane-diol (cat.# CLP-1114), Fmoc-Amino-DMT C-3 CED phosphoramidites (cat.# CLP-1661) were purchased from ChemGenes. MMT protected 5'-amino-modifier C6 (cat.# 10-1906-90) and TFA protected 5'-amino-modifier C3 (cat# 10-1923-90) were purchased from Glen Research. Coupling efficiency was monitored by the removal of DMT group on 5'-OH groups. In a glove box under nitrogen atmosphere, DMT-dodecane-diol and Fmoc-Amino-DMT C-3 CED were dissolved in acetonitrile and shaken for 10 mins to achieve final concentration of 0.1 M. The DMT-dodecane-diol amidite was activated with 0.25M 5-(ethylthio)tetrazole in anhydrous acetonitrile and the extended coupling times of 5 minutes were used. The amino modifier amidite was activated by 0.25M 5-(ethylthio)tetrazole in anhydrous acetonitrile but the coupling was performed manually inside the glove box. 3% dichloroacetic acid in dichloromethane was used to remove DMT protecting group on the DNA synthesizer. After the synthesis was completed, CPG was treated with 28% aqueous ammonium hydroxide solution for 16-18 hours at 60°C in water bath. The crude mixture then was concentrated under reduced pressure at 60°C and filtered by 0.22μm centrifugal filter before purifying by RP-HPLC.

Specifically, to generate the micelle template (5'-**DNA'-HE_6**-3'), from CPG Unilinker (1000 Å LCAA), HE unit was incorporated one by one to achieve exactly 6 units. Then, the DNA bases were incorporate as describe above to yield desired sequences.

Table 2.1 | DNA amphiphiles used for reactions inside the micellar core (**D =** dodecane diol, **NH_2** = Amino C-3 CED) (sequence written from 5' to 3' end)

NH_2-HE_{12}-DNA **(1)**	**NH_2-DDDDDDDDDDDD** TTTTTCAGTTGACCATATA
HE_{12}-**NH_2**-DNA **(2)**	**DDDDDDDDDDDD-NH_2**-TTTTTCAGTTGACCATATA

HE_6-**NH_2**-HE_6-DNA **(3)**	**DDDDDD-NH_2-DDDDDD** TTTTTCAGTTGACCATATA
NH_2-HE_6-DNA **(4)**	**NH_2-DDDDDD** TTTTTCAGTTGACCATATA
HE_6-**NH_2**-DNA **(5)**	**DDDDDD-NH_2-** TTTTTCAGTTGACCATATA
NH_2-HE-DNA **(6)**	**NH_2-D** TTTTTCAGTTGACCATATA
NH_2-DNA **(7)**	**NH_2-**TTTTTCAGTTGACCATATA
(DNA)'-HE_{12}	TATATGGTCAACTGAAAAA **DDDDDDDDDDDD**
(DNA)'-HE_6	TATATGGTCAACTGAAAAA **DDDDDD**

2.5.3.2. HPLC purification

All DNA strands with amino-modified monomer (except (DNA)'-HE_6 and (DNA)'-HE_{12}) were purified by RP-HPLC. Two mobile phases were TEAA and HPLC grade acetonitrile. Elution gradient used: amphiphiles with 12 HE units (3-70% acetonitrile over 30 minutes at 60°C and with 0-6 HE units (3-50% acetonitrile over 30 minutes at 60°C). Column used: Hamilton PRP 1 5 µm 2.1x150mm**.** Crude DNA amphiphiles (~0.5 OD) was injected as a 20-50µL solution in Millipore water and then detected using a diode array detector monitoring absorbance at 260nm.

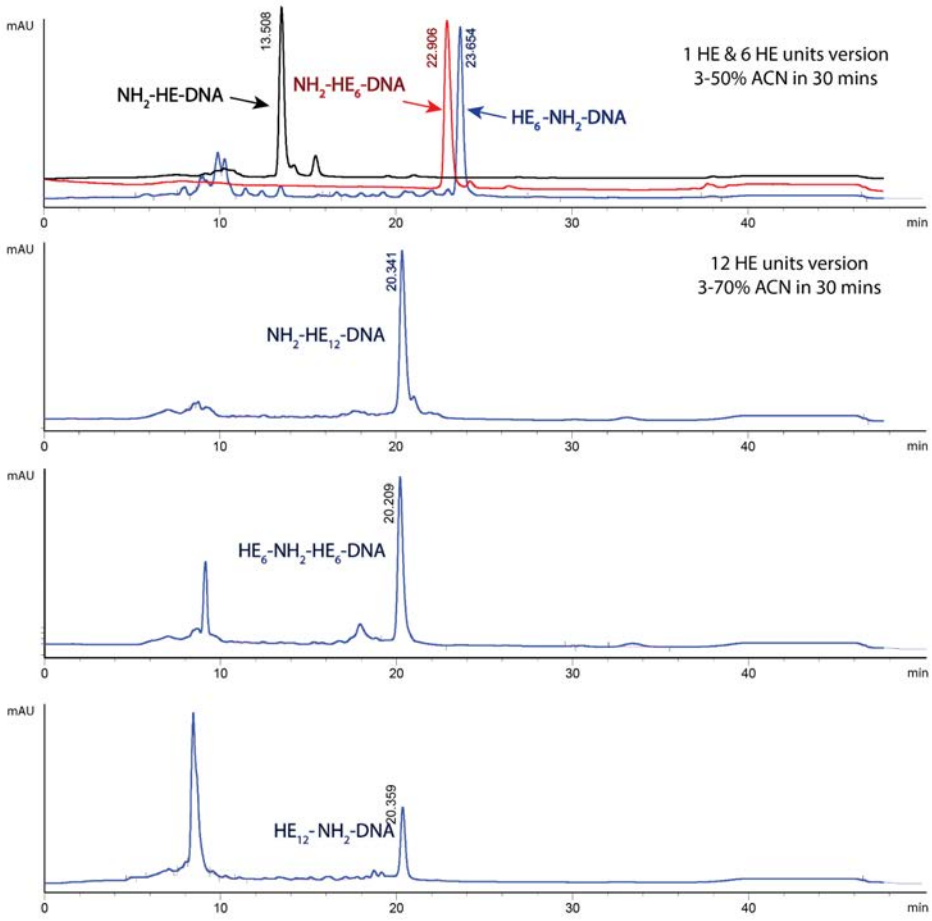

Figure 2.8 | HPLC traces of crude products of the DNA amphiphiles

2.5.3.3. LC-MS characterization of DNA amphiphiles

The oligonucleotides were analyzed by LC-ESI-MS in negative ESI mode. Samples were run through an acclaim RSLC 120 C18 column (2.2µM 120Å 2.1 x 50mm) using a gradient of 98% mobile phase A (100mM 1,1,1,3,3,3-hexafluoro-2-propanol and 5mM triethylamine in water) and 2 % mobile phase B (Methanol) to 40 % mobile phase A and 60% mobile phase B in 8 minutes. The data was processed and deconvoluted using the Bruker DataAnalysis software version 4.1.

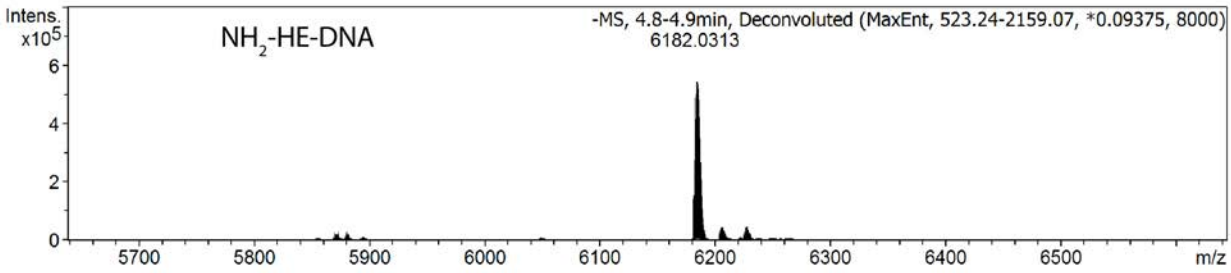
Intens.
x10^5
NH2-HE-DNA
-MS, 4.8-4.9min, Deconvoluted (MaxEnt, 523.24-2159.07, *0.09375, 8000)
6182.0313
m/z

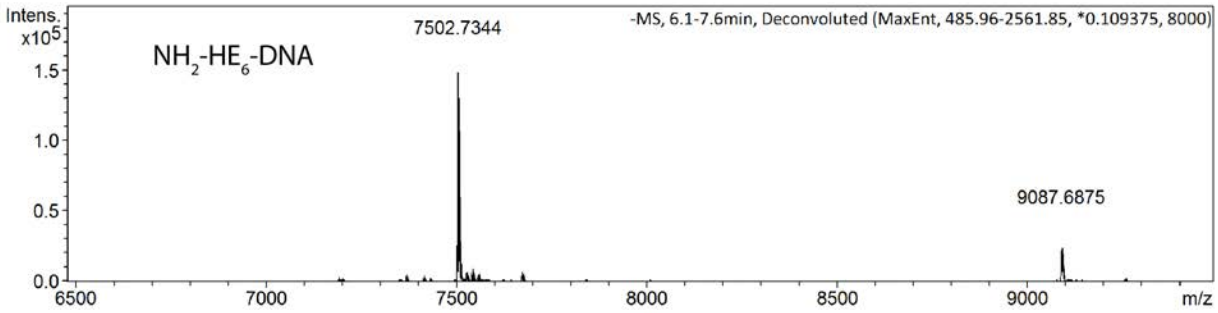
Intens.
x10^5
NH2-HE6-DNA
-MS, 6.1-7.6min, Deconvoluted (MaxEnt, 485.96-2561.85, *0.109375, 8000)
7502.7344
9087.6875
m/z

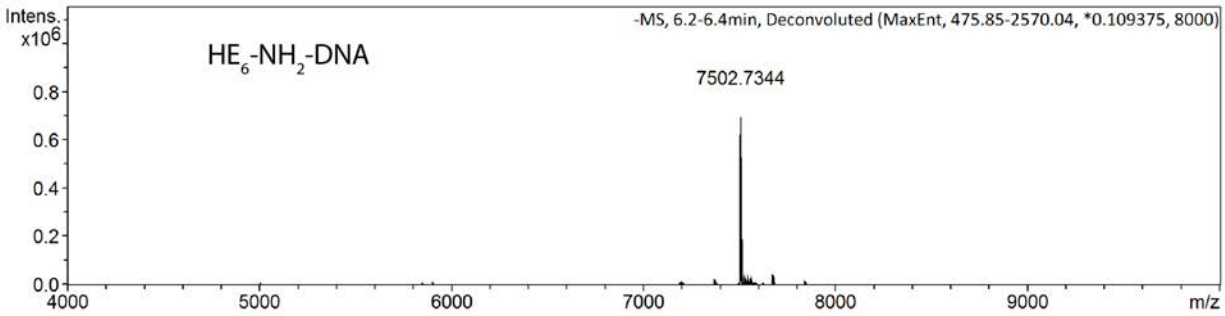
Intens.
x10^6
HE6-NH2-DNA
-MS, 6.2-6.4min, Deconvoluted (MaxEnt, 475.85-2570.04, *0.109375, 8000)
7502.7344
m/z

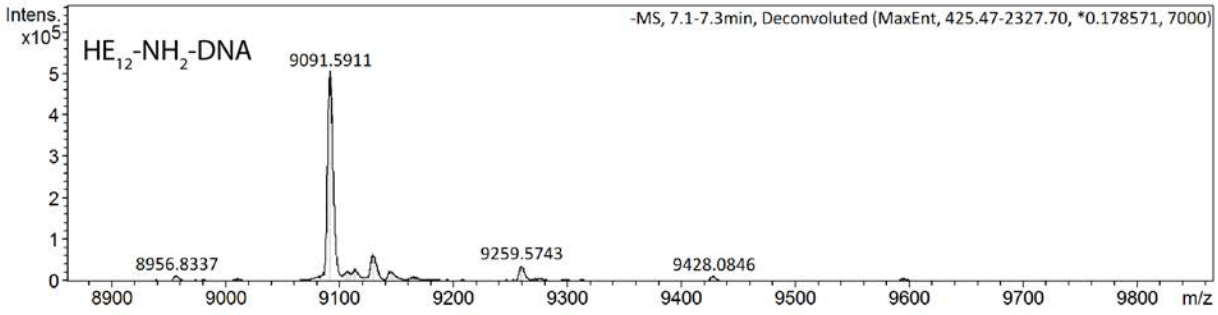
Intens.
x10^5
HE12-NH2-DNA
-MS, 7.1-7.3min, Deconvoluted (MaxEnt, 425.47-2327.70, *0.178571, 7000)
9091.5911
8956.8337
9259.5743
9428.0846
m/z

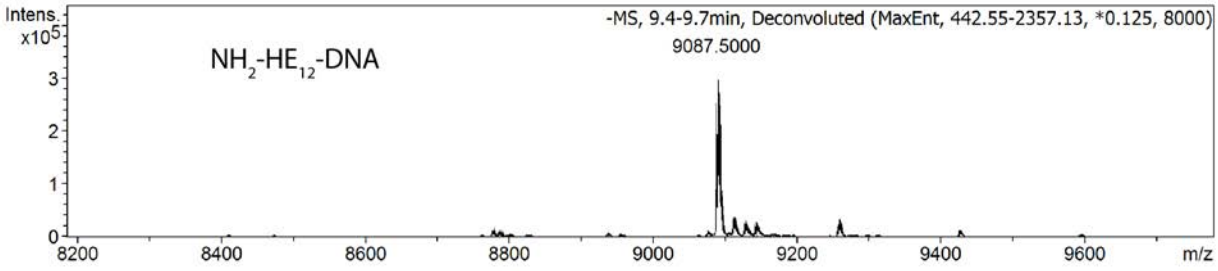
Intens.
x10^5
NH2-HE12-DNA
-MS, 9.4-9.7min, Deconvoluted (MaxEnt, 442.55-2357.13, *0.125, 8000)
9087.5000
m/z

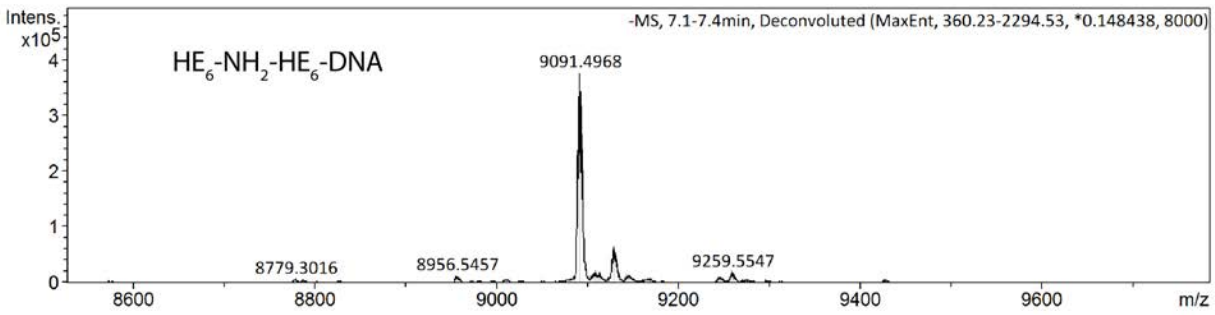

Figure 2.9 | MS characterizations of HPLC purified DNA amphiphiles.

2.5.4. Synthesis of activated NHS-ester molecules

2.5.4.1. Synthesis of decanoic acid- NHS ester (C_{10}-NHS) and docosahexaenoic acid (C_{22}-NHS)

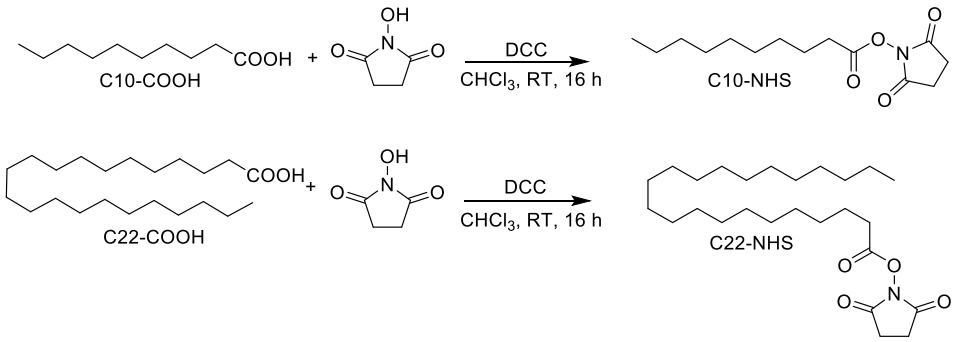

Synthesis of C_{10}-NHS: To a stirred solution of C_{10}-COOH (2 mmol) in $CHCl_3$ was added 2 mmol N-hydroxysuccinimide. Then the mixture was cooled down to 0°C using water bath followed by adding DCC (4 mmol). After adding DCC, the water bath was removed, allowing the mixture to go back to room temperature (22°C). The mixture was stirred overnight for 16 hours. After that, the crude mixture was checked by TLC before filtering to remove urea which formed as by-product, purified by CombiFlash (Ethyl Acetate:Hexane = 1:1) and concentrated under *vacuo* to give desired product as a white solid (C_{10}-NHS) with 80% yield. ^{1}H NMR matches previous reported procedure.

^{1}H NMR (500 MHz, $CDCl_3$) δ 2.85 (s, 4H), 2.54 (t, 2H), 1.54 (quint, 2H), 1.25 (m, 12H), 0.85 (t, 3H); HRMS EI m/z calculated for $C_{14}H_{23}NNaO_4$ $[M+Na]^+$: 292.1519, found: 292.1515.

Synthesis of C_{22}-NHS: Starting from C_{22}-COOH, the synthesis was performed similarly to the

synthesis of C_{10}-NHS described above and a white solid was obtained as product with 70% yield. ^{1}H NMR (500 MHz, $CDCl_3$) δ 2.82 (s, 4H), 2.59 (t, 2H), 1.70 (quint, 2H), 1.24 (m, 36H), 0.85 (t, 3H); HRMS EI m/z calculated for $C_{26}H_{47}NNaO_4$ $[M+Na]^+$: 460.3397, found: 460.3408.

2.5.4.2. Synthesis of 1-pyrenebutyric acid-NHS ester (pyrene-NHS)

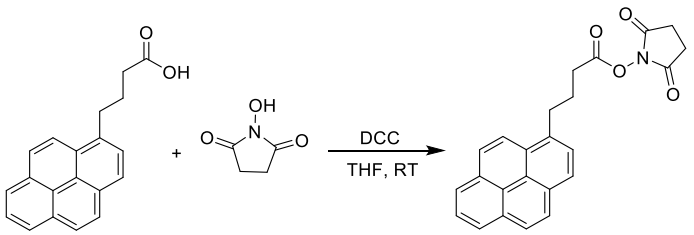

To a stirred solution of 1-pyrenebutyric acid and (1 mmol) in 25 mL THF was added 1 mmol N-hydroxysuccinimide. The mixture was cooled down to 0^{o}C using ice bath followed by dropwise addition of DCC (1 mmol, in 5 mL THF). The ice bath was then removed, allowing the mixture to go back to room temperature. The mixture was stirred overnight. After the reaction, the crude mixture was filtered to remove urea which formed as by-product. The yellow filtrate was collected and concentrated under reduced pressure. The product was purified by recrystallization from ethanol to give desired product as a yellow solid (pyrene-NHS) with 31% yield.

^{1}H NMR (300 MHz, $CDCl_3$) δ 7.88-8.51 (m, 9H), 3.49 (t, 2H), 2.88 (s, 4H), 2.74 (t, 2H), 2.31 (quint, 2H); HRMS EI m/z calculated for $C_{24}H_{19}NNaO_4$ $[M+Na]^+$: 408.1206, found: 408.1192; m/z calculated for $C_{24}H_{19}KNO_4$ $[M+K]^+$: 424.0946, found: 424.0930.

2.5.4.3. Synthesis of N,N-didecylsuccinamide NHS ester (NDS-NHS)

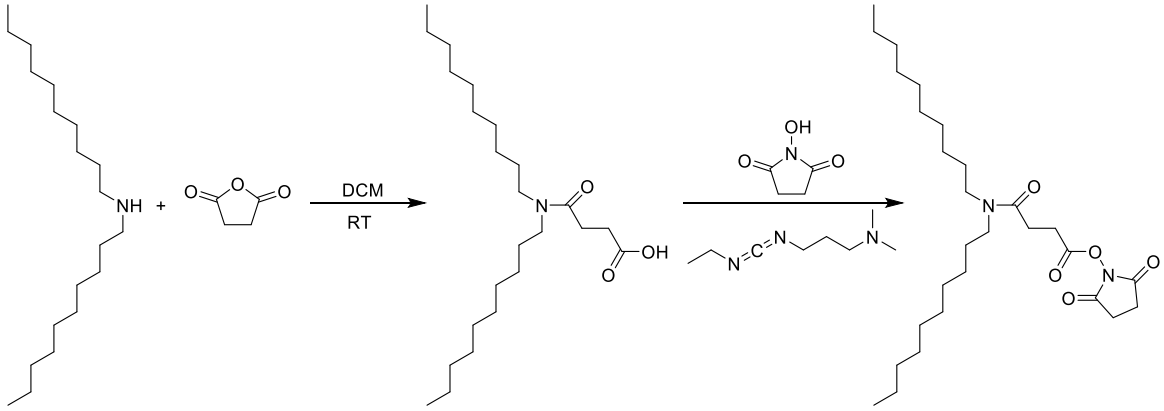

To a stirred solution of succinic anhydride in DCM, didecylamine **(A)** (4 mmol) and triethylamine (8 mmol) were added. The reaction mixture was stirred at 37°C for 16 hours. Then, the crude mixture was added HCl 1M and extracted with diethyl ether followed by drying with $MgSO_4$ and concentrating under *vacuo* to obtain oily product **(B).**

The oily product **(B)** and N-hydroxysuccinimide were dissolved in $CHCl_3$. Then EDC was added to the mixture at 0°C using ice bath. Removal of ice bath brought the mixture to room temperature and it was stirred for 16 hours. After that, the crude mixture was purified by CombiFlash using Hexane:Ethyl Acetate 1:1 and concentrated under *vacuo* to furnished transparent oily product with 25% yield.

^{1}H NMR (500 MHz, $CDCl_3$) δ 3.21 (t, 4H), 2.85 (s, 4H), 3.01 (t, 2H), 2.74 (t, 2H), 1.26 (m, 28H), 0.85 (t, 6H). HRMS EI m/z calculated for $C_{28}H_{50}N_2NaO_5$ $[M+Na]^+$: 517.3612, found: 517.3627.

2.5.5. General procedure for a conjugation reaction

2.5.5.1. Single-stranded system

First, solution of DNA amphiphiles at 5μM concentration was prepared in 1x TAMg buffer. Then, the solution was thermally annealed (95 to 4°C in 1 hour) in order to form micelles. Separately, 10 mM of chosen NHS ester molecule was prepared in organic solvent (DMSO or THF). Then, the reagent was added to micelles solution (1:10 ratio to total volume of micelle solution) and the mixture was shaken for 16 hours at room temperature. The crude mixture after reaction was dried and analyzed by RP-HPLC and LC-MS. Yield of the conjugation product was calculated from the area under the curve ratio obtained from HPLC between the product peak and the sum of starting material and product peak.

2.5.5.2. Double-stranded system

First, solution of DNA amphiphiles ((DNA)'-HE_6 or (DNA)'-HE_{12}) at 10μM concentration was prepared in 1x TAMg followed by thermal annealling (95 to 4°C in 1 hour) in order to pre-form micelles. In another tube, solution of complementary strand with (DNA)' at 10μM in 1x

TAMg and added to pre-formed micelles. Separately, in a glass vial, 10 mM of chosen NHS ester molecule was prepared in organic solvent (DMSO or THF). The reagent was added to micelles solution (1:10 ratio to total volume of micelle solution) and the mixture was shaken for 16 hours at room temperature. The crude mixture after reaction was dried and analyzed by RP-HPLC and LC-MS as single-stranded system. Yield of conjugate reaction was calculated from the area under the curve ratio obtained from HPLC between the product peak and the sum of starting material and product peak.

2.5.6. HPLC analyses of conjugate reactions between DNA amphiphiles and C_{10} NHS-ester molecule

2.5.6.1. Set 1: 12 HE units

A. HPLC traces

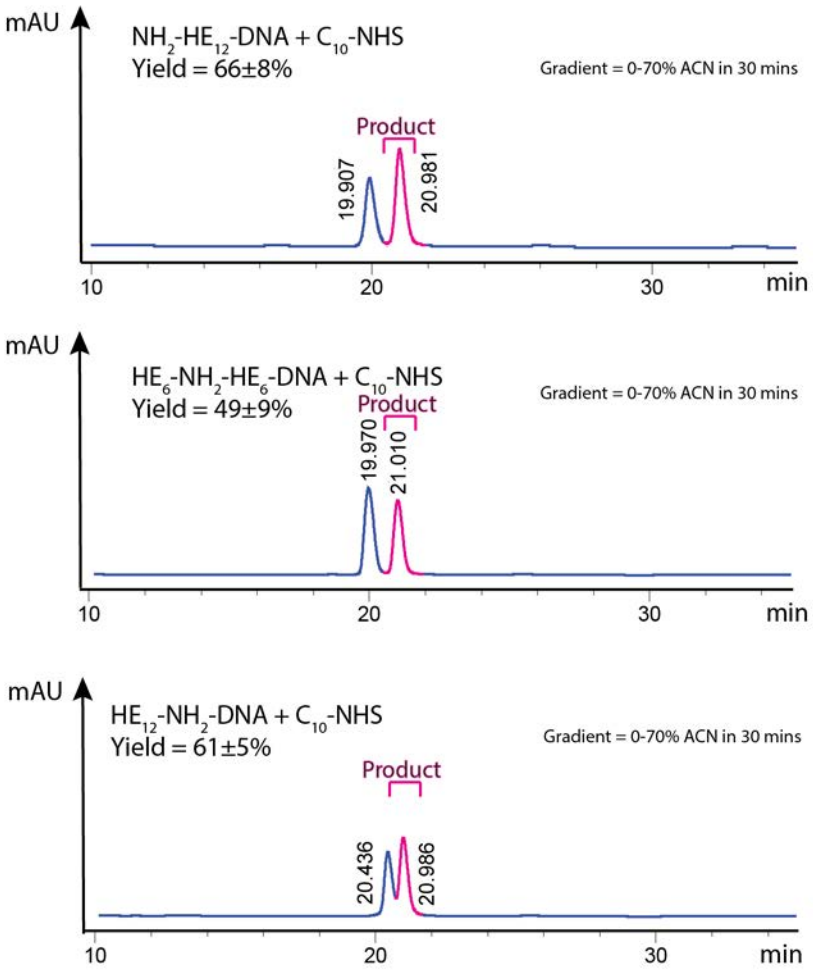

Figure 2.10 | HPLC traces of crude products of the DNA amphiphiles containing 12 HE units with C_{10}-NHS. Peak at **19.907 min** in the 1st HPLC trace is NH_2-HE_{12}-DNA starting material. Peak at **19.970 min** in the 2nd HPLC trace is HE_6-NH_2-HE_6-DNA starting material. Peak at **20.436 min** in the 3rd HPLC trace is HE_{12}-NH_2-DNA starting material.

B. LC-MS characterization

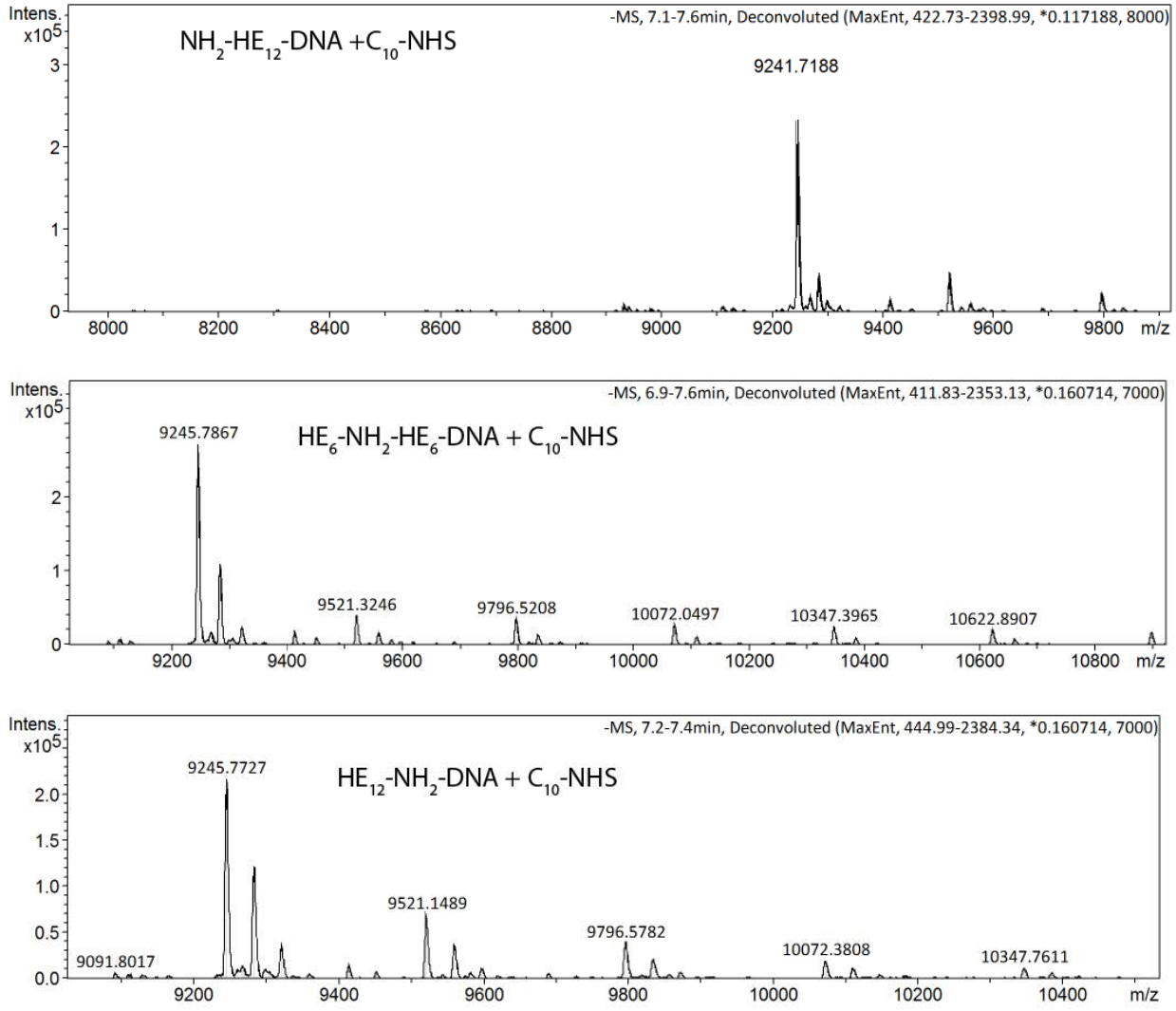

Figure 2.11 | MS characterizations of HPLC purified DNA amphiphiles containing 12 HE units conjugated with C_{10}-NHS. Multiple peaks with a difference of 275.4 correspond to incomplete cleavage of universal linker.

2.5.6.2. Set 2: 6 HE units

A. HPLC traces

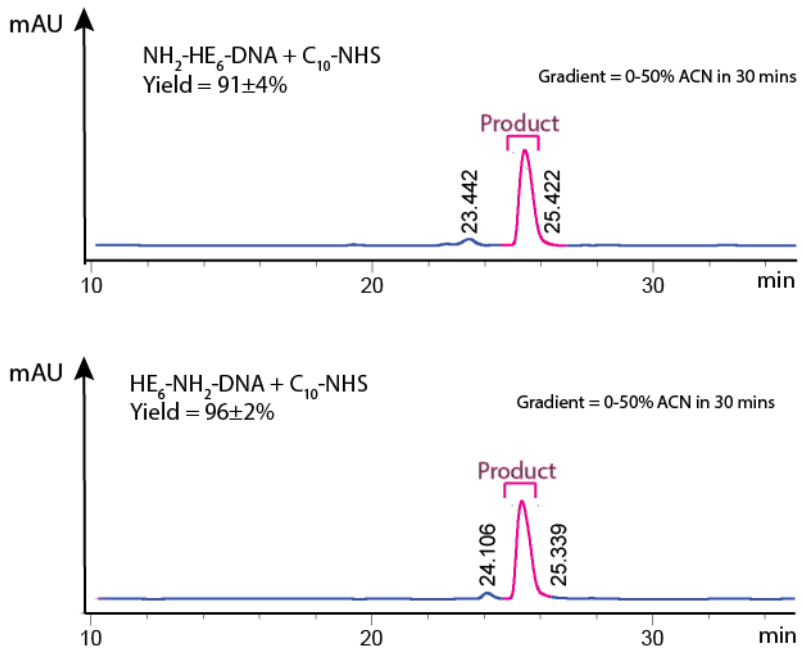

Figure 2.12 | HPLC traces of crude products of the DNA amphiphiles containing 6 HE units with C_{10}-NH. Peak at **23.442 min** in the 1st HPLC trace is NH_2-HE_6-DNA starting material. Peak at 24.106 in the 2nd HPLC trace is HE_6-NH_2-DNA starting material.

B. LC-MS characterization

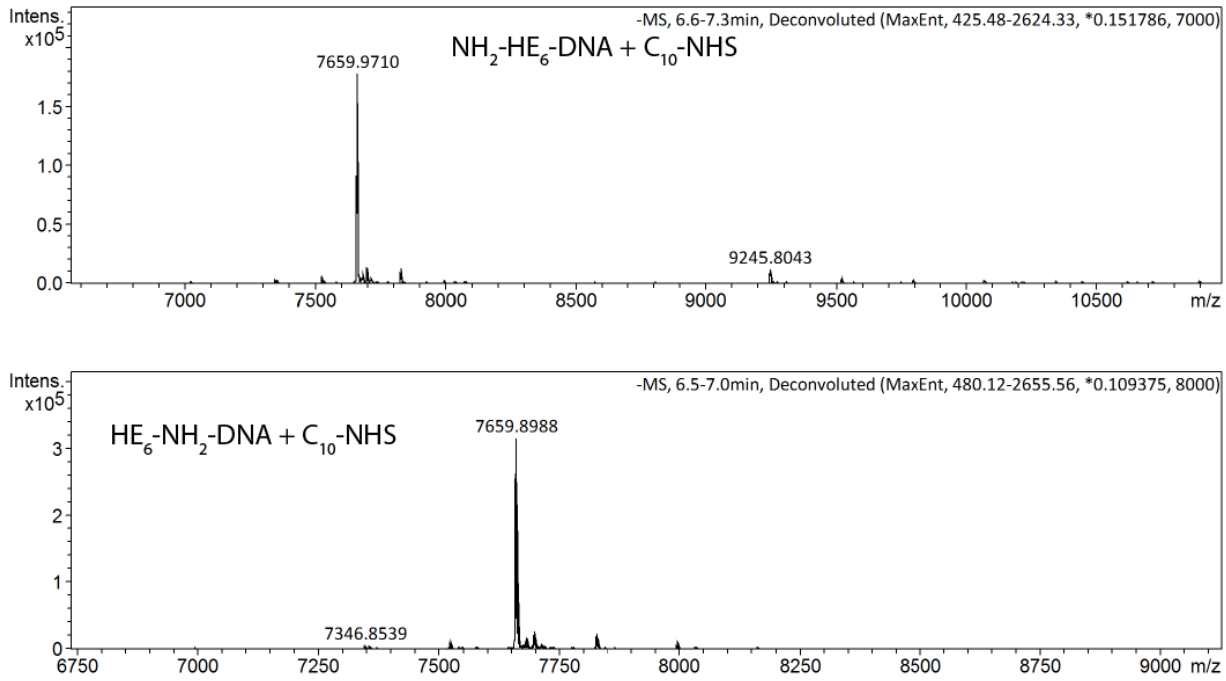

Figure 2.13 | MS characterizations of HPLC purified DNA amphiphiles containing 6 HE units conjugated with C_{10}-NHS.

2.5.6.3. Set 3: 0-1 HE units (Non-micelle forming-control experiment)

A. HPLC traces

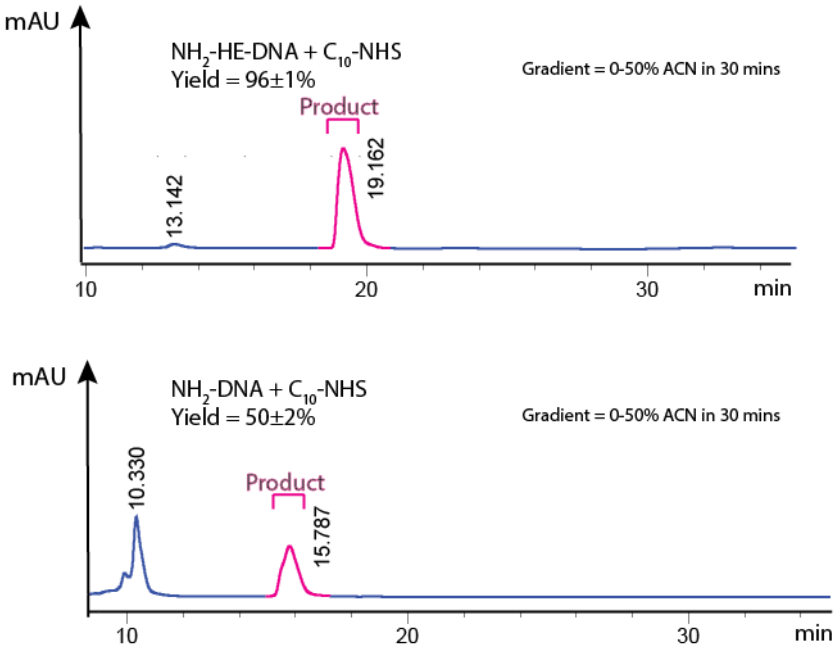

Figure 2.14 | HPLC traces of crude products of the DNA amphiphiles with C_{10}-NHS. Peak at 13.142 min in the 1st HPLC trace is NH_2-HE-DNA starting material. Peak at 10.330 min in the 2nd HPLC trace is NH_2-DNA starting material.

B. LC-MS characterization

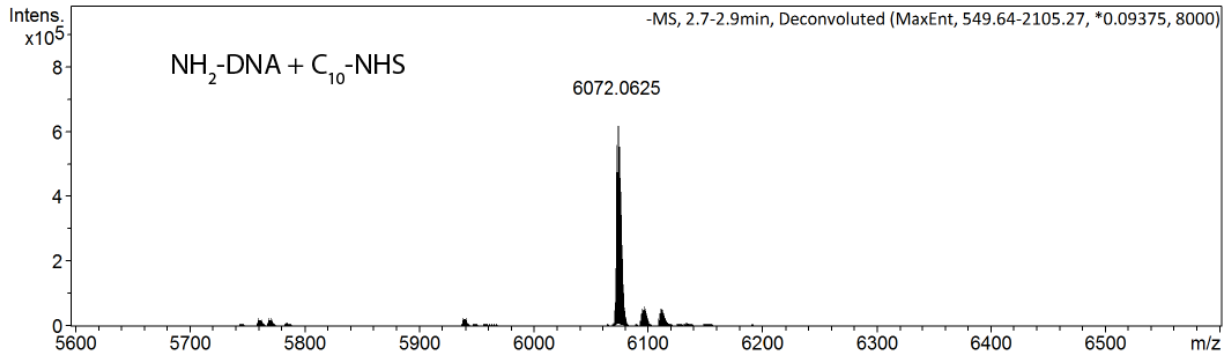

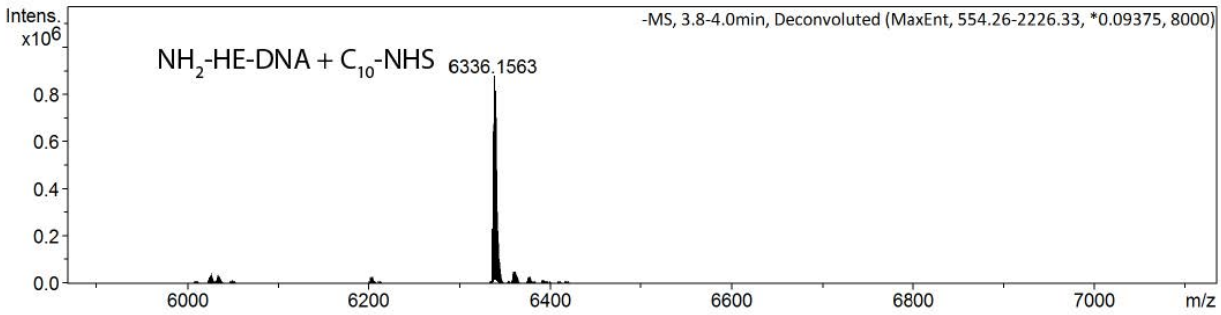

Figure 2.15 | MS characterizations of HPLC purified DNA amphiphiles conjugated with C_{10}-NHS.

2.5.7. HPLC analyses of conjugate reactions between DNA amphiphiles and C_{16} NHS-ester molecule

A. HPLC traces

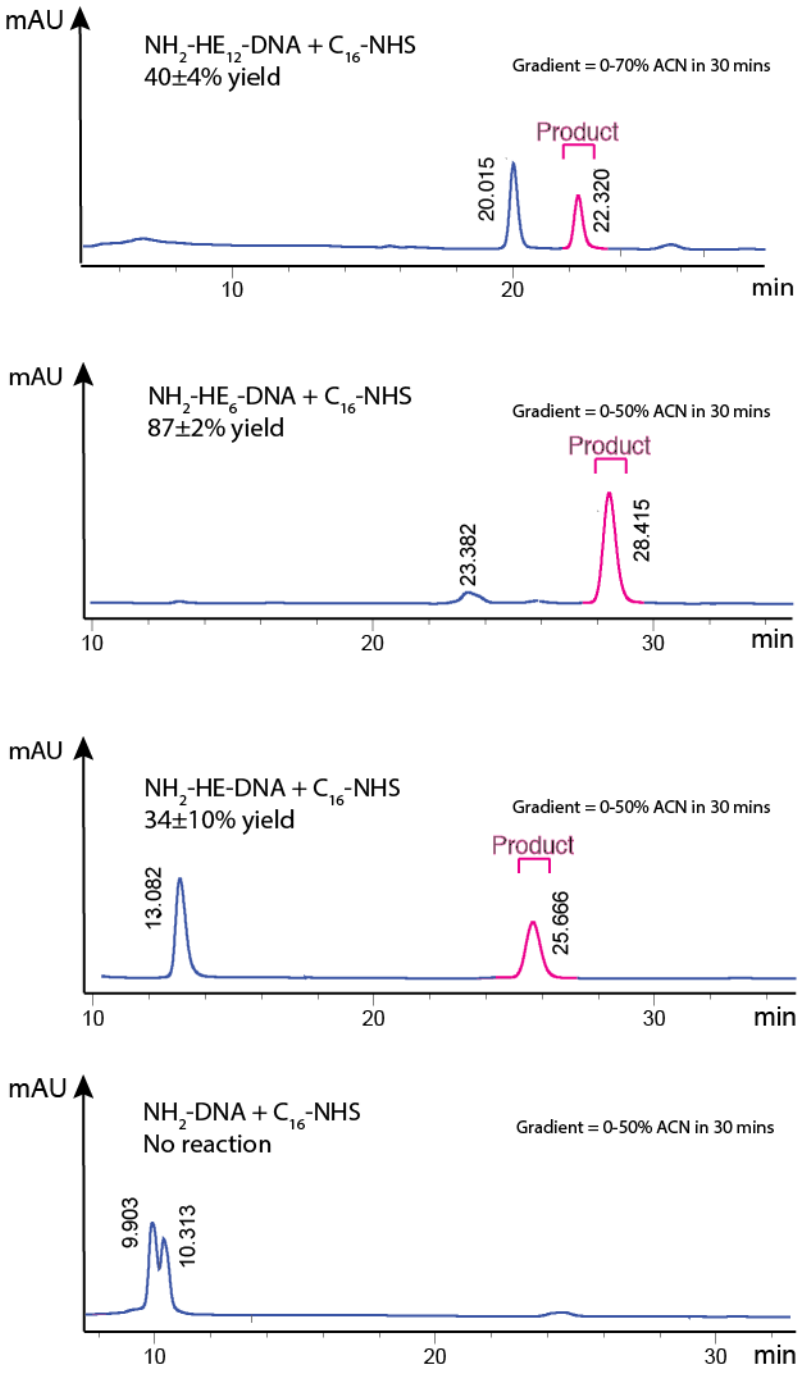

Figure 2.16 | HPLC traces of crude products of the DNA amphiphiles with C_{16}-NHS. Peak at **20.015 min** in the **1st** HPLC trace is NH_2-HE_{12}-DNA starting material. Peak at **23.382 min** in the **2nd** HPLC trace is NH_2-HE_6-DNA starting material. Peak at **13.082 min** in the **3rd** HPLC trace is NH_2-HE-DNA starting material. And lastly, the peak about **10 min** in the **4th** HPLC trace is NH_2-DNA starting material.

B. LC-MS characterization

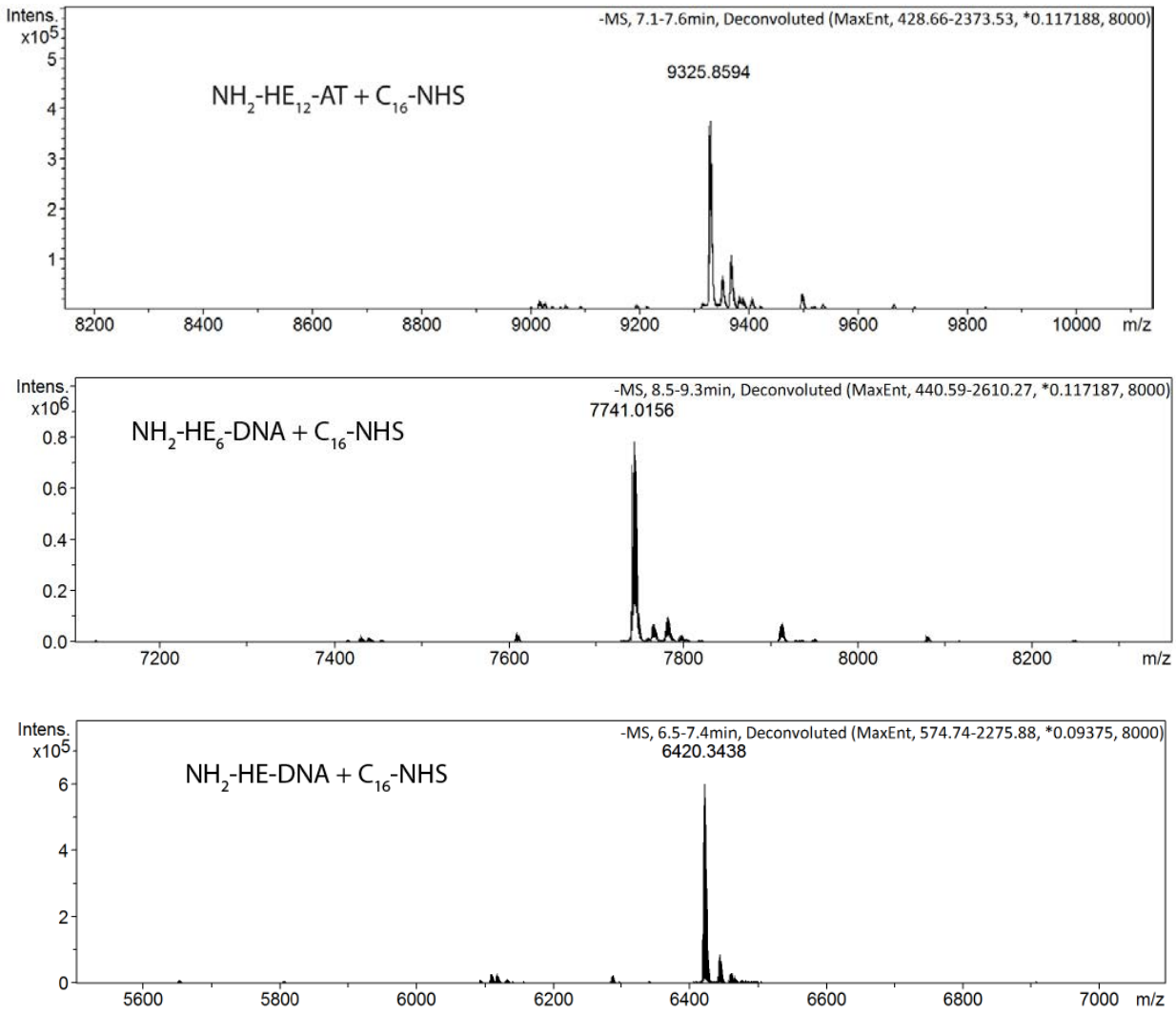

Figure 2.17 | MS characterizations of HPLC purified DNA amphiphiles conjugated with C_{16}-NHS.

2.5.8. HPLC analyses of conjugate reactions between DNA amphiphiles and C_{20} NDS-NHS-ester molecule

A. HPLC traces

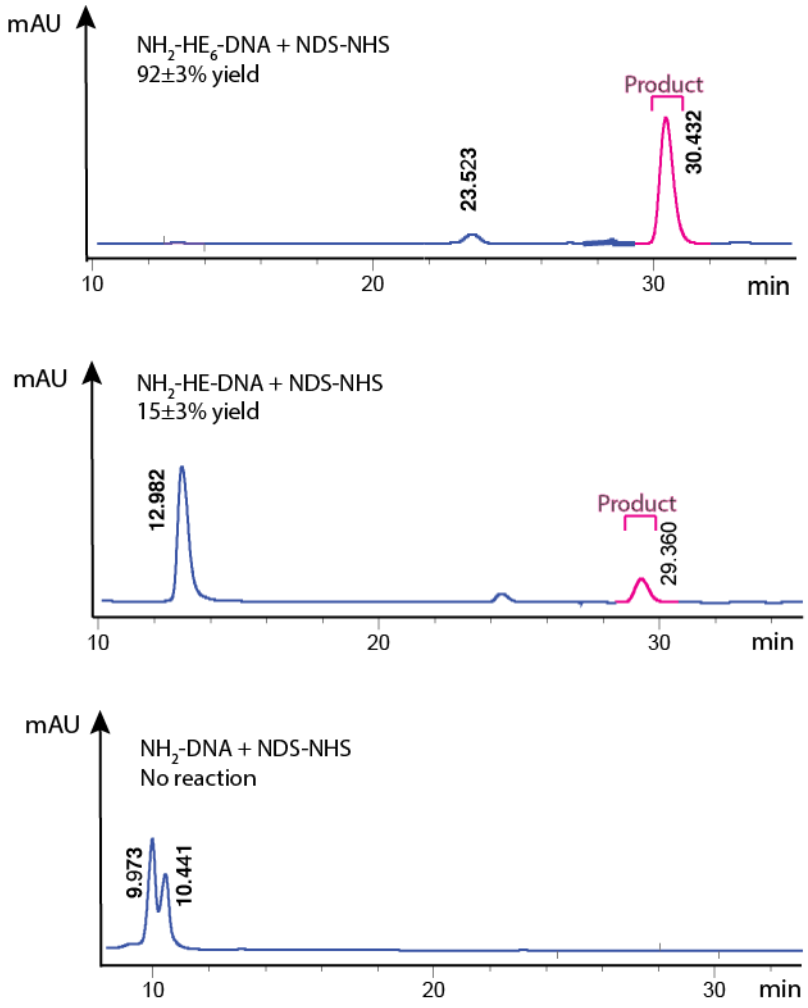

Figure 2.18 | HPLC traces of crude products of the DNA amphiphiles with NDS-NHS. Peak at **23.523 min** in the **1st** HPLC trace is NH_2-HE_6-DNA starting material. Peak at **12.982 min** in the **2nd** HPLC trace is NH_2-HE-DNA starting material. Peak at about **10 min** in the **3rd** HPLC trace is NH_2-DNA crude starting material.

B. LC-MS characterization

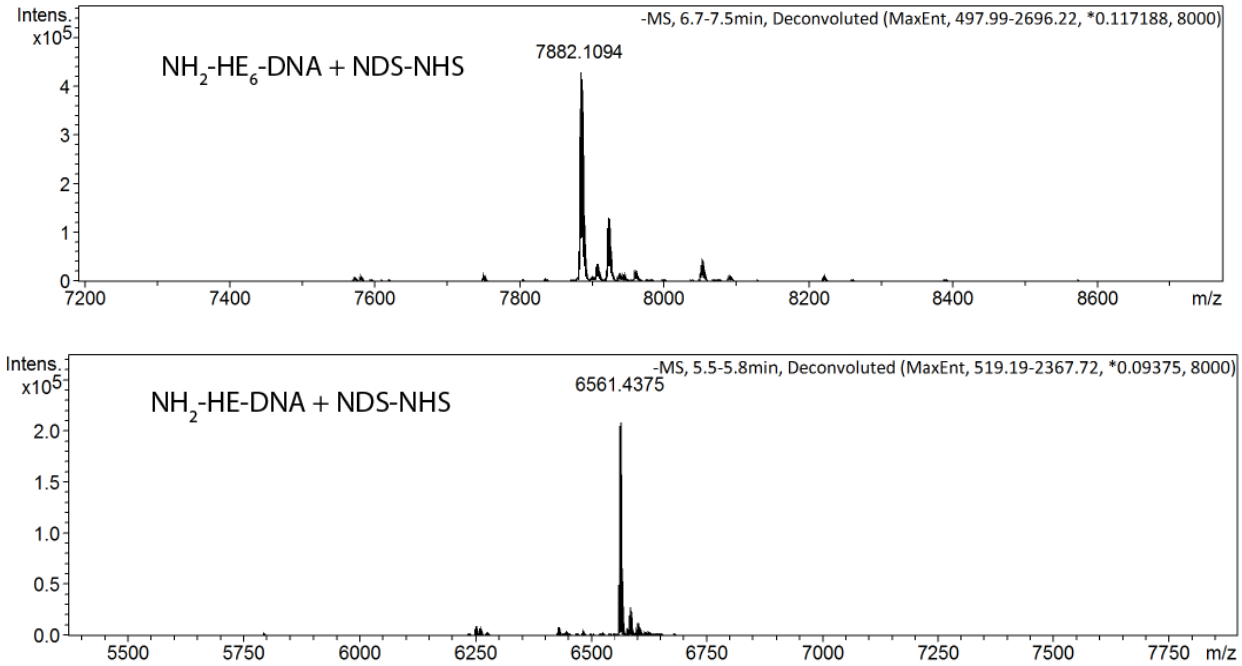

Figure 2.19 | MS characterizations of HPLC purified DNA amphiphiles conjugated with NDS-NHS

2.5.9. HPLC analyses of conjugate reactions between DNA amphiphiles and C_{22} NHS-ester molecule

A. HPLC traces

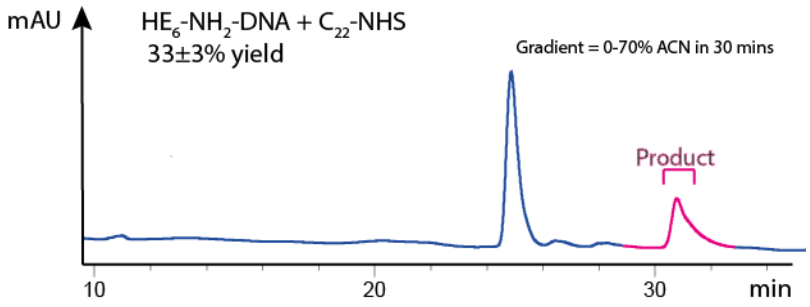

Peak at **25 min** in the HPLC trace is HE_6-NH_2-DNA starting material.

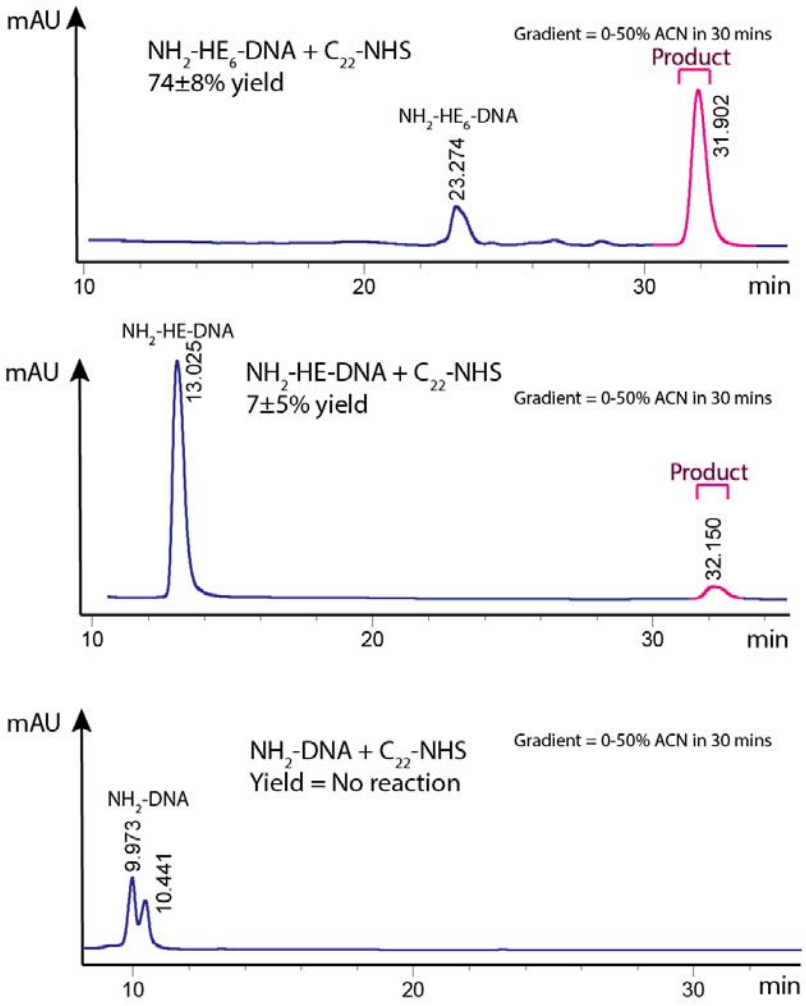
mAU
NH2-HE6-DNA + C22-NHS
74±8% yield
Gradient = 0-50% ACN in 30 mins
Product
NH2-HE6-DNA
23.274
31.902
10
20
30
min
NH2-HE-DNA
13.025
mAU
NH2-HE-DNA + C22-NHS
7±5% yield
Gradient = 0-50% ACN in 30 mins
Product
32.150
10
20
30
min
mAU
NH2-DNA + C22-NHS
Yield = No reaction
Gradient = 0-50% ACN in 30 mins
NH2-DNA
9.973
10.441
10
20
30
min

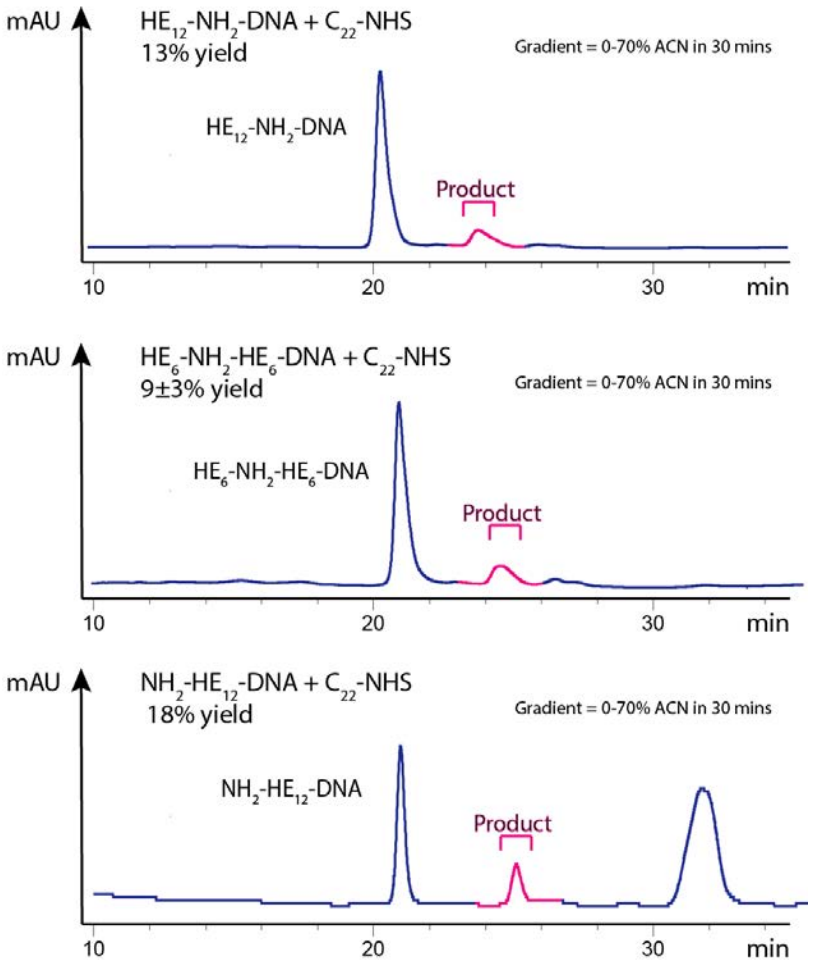

Figure 2.20 | HPLC traces of crude products of the DNA amphiphiles with C_{22}-NHS.

B. LC-MS characterization

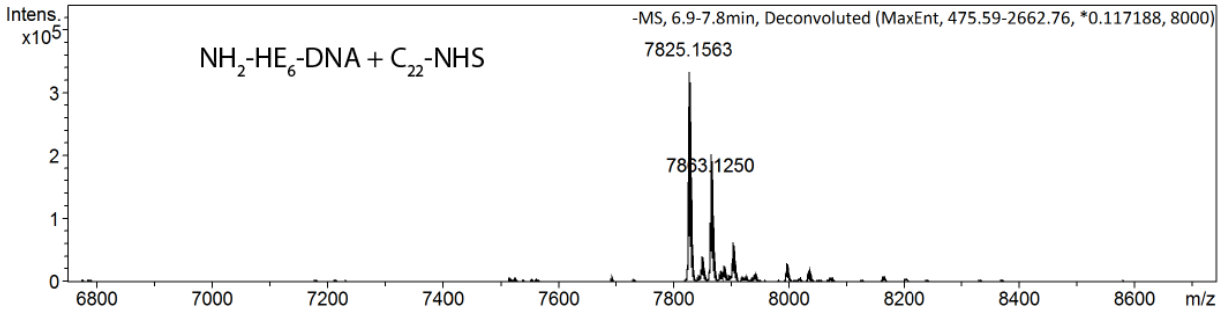

The mass 7863.1250 in this case is $[M+K]^+$

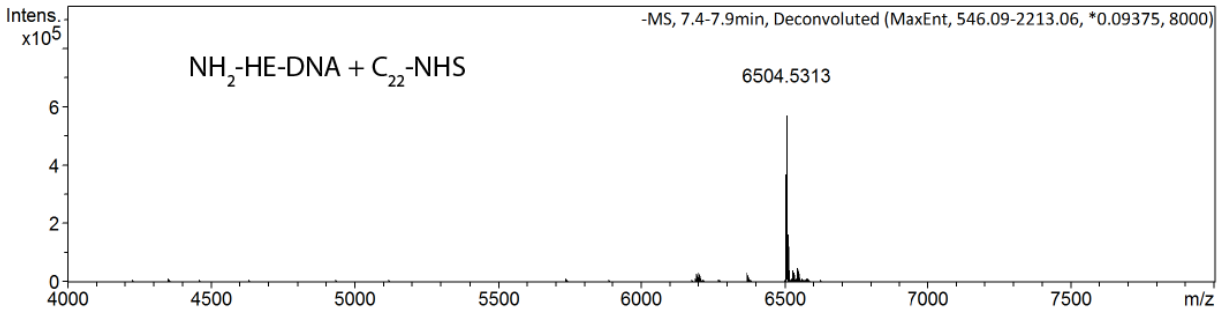

Figure 2.21 | MS characterizations of HPLC purified DNA amphiphiles conjugated with C_{22}-NHS

2.5.10. HPLC analyses of conjugate reactions between DNA amphiphiles and pyrene – NHS ester molecule

A. HPLC traces

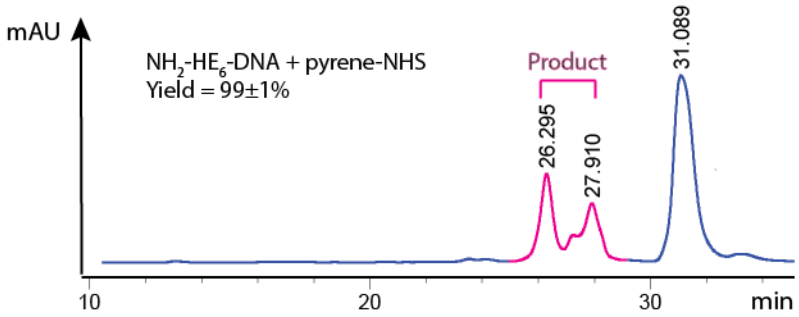

Figure 2.22 | HPLC trace of crude product of the DNA amphiphiles with pyrene-NHS. The big peak at **31.089 min** in the HPLC trace corresponds to small molecule (pyrene) conjugated with tris indicated by MS.

B. LC-MS characterization

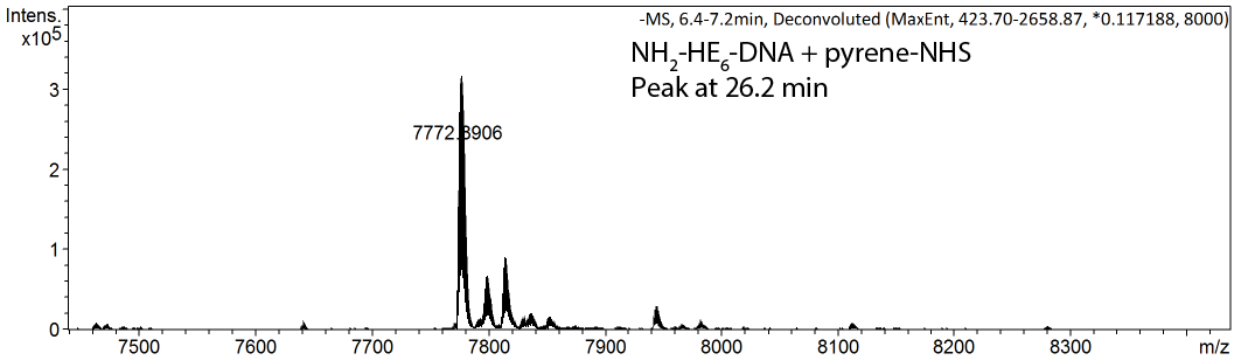

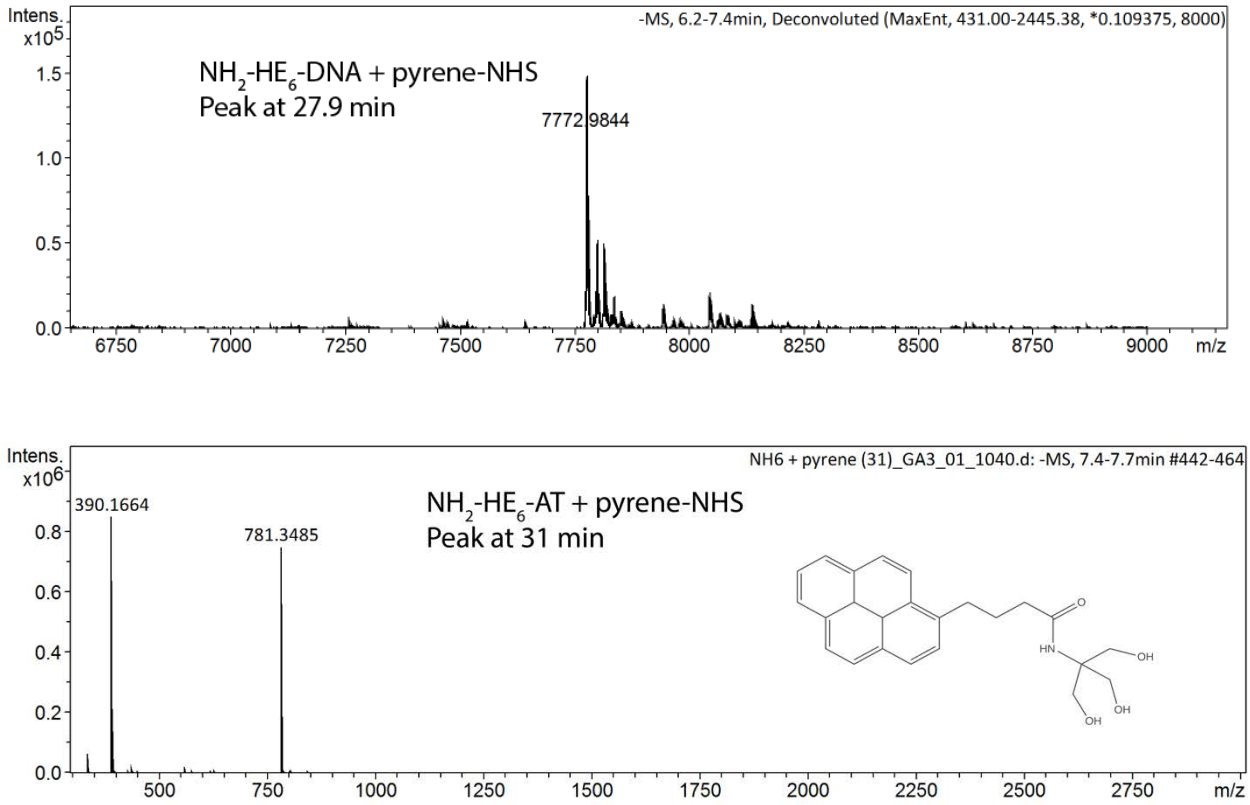

Figure 2.23 | MS characterizations of HPLC purified DNA amphiphiles conjugated with pyrene-NHS.

2.5.11. HPLC analyses of conjugate reactions between DNA amphiphiles and polystyrene - NHS ester molecule

A. HPLC characterization

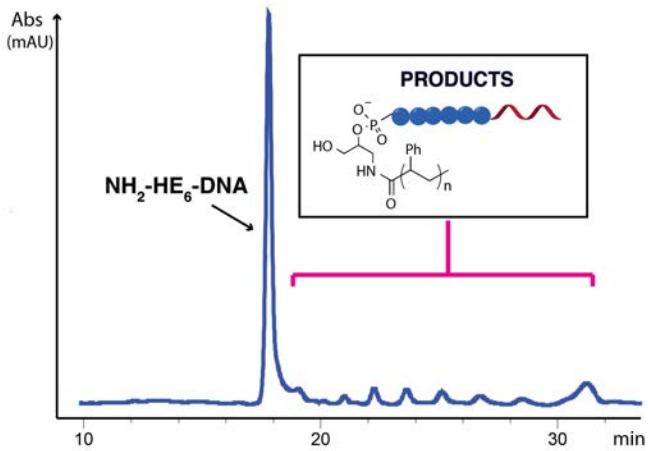

B. LC-MS characterization

The mass spectra results presented here indicated masses of NH_2-HE_6-DNA with polystyrene with different numbers of styrene monomers

a. Peak at 22 min

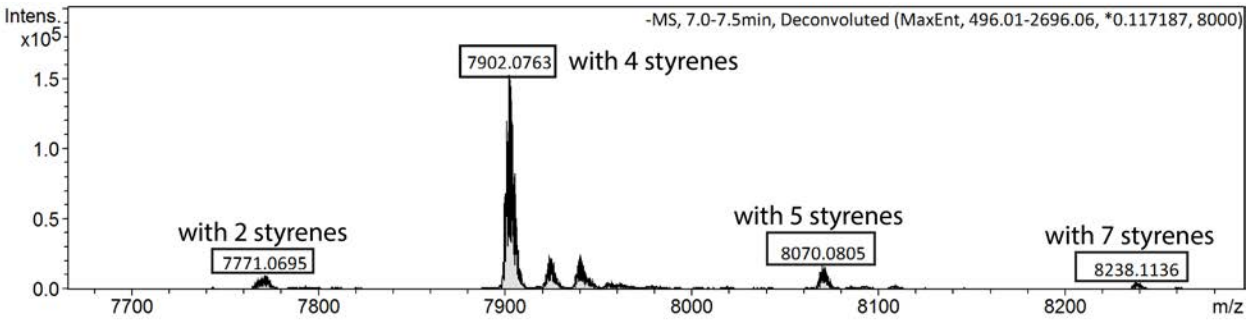

b. Peak at 23 min

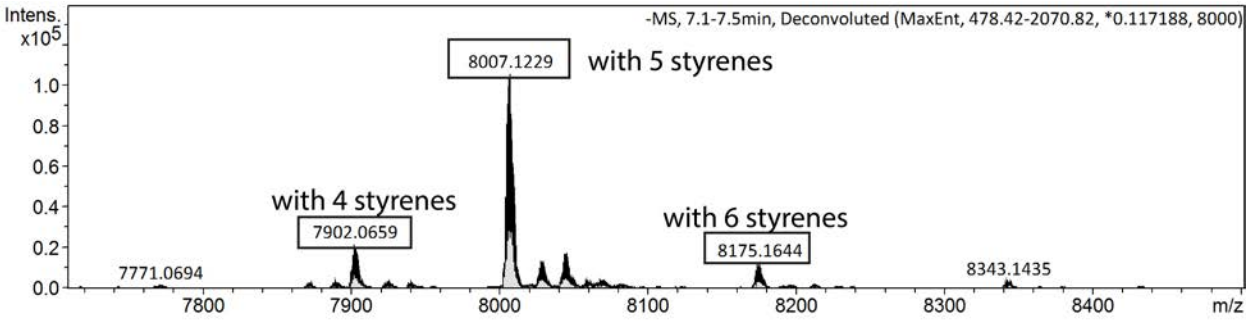

c. Peak at 24 min

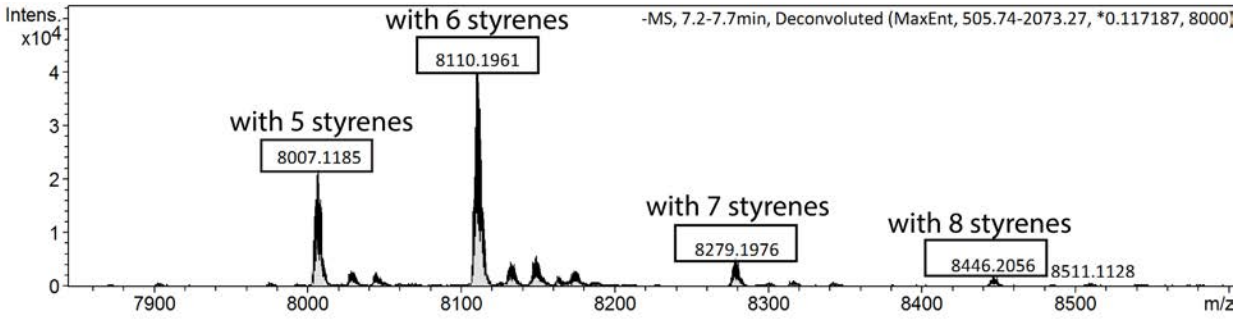

d. Peak at 31 min

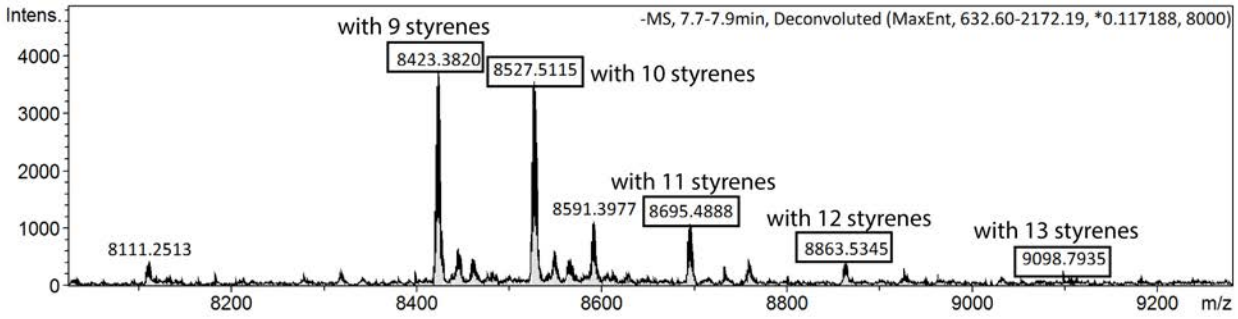

Figure 2.24 | MS characterizations of HPLC purified NH_2-HE_6-DNA conjugated with Polystyrene-NHS

2.5.12. AFM measurements of DNA micelles

5 μM DNA amphiphiles in 1xTAMg was annealed from 95°C to 4°C for 1 hour. The sample was diluted with 1x TAMg to 1.67 μM. Then, 5 μL of sample was deposited on freshly cleaved mica for 5 seconds, and washed three times with 50 μL of H_2O. Excess liquid was brown off by the stream of nitrogen for 30 seconds. The sample was then dried under vacuum for at least 20 minutes prior to imaging. Measurement was acquired in ScanAsyst mode under dry condition using ScanAsyst-Air triangular silicon nitride probe (tip radius = 2 nm, k = 0.4 N/m, f_o = 70kHz; Bruker, Camarillo, CA).

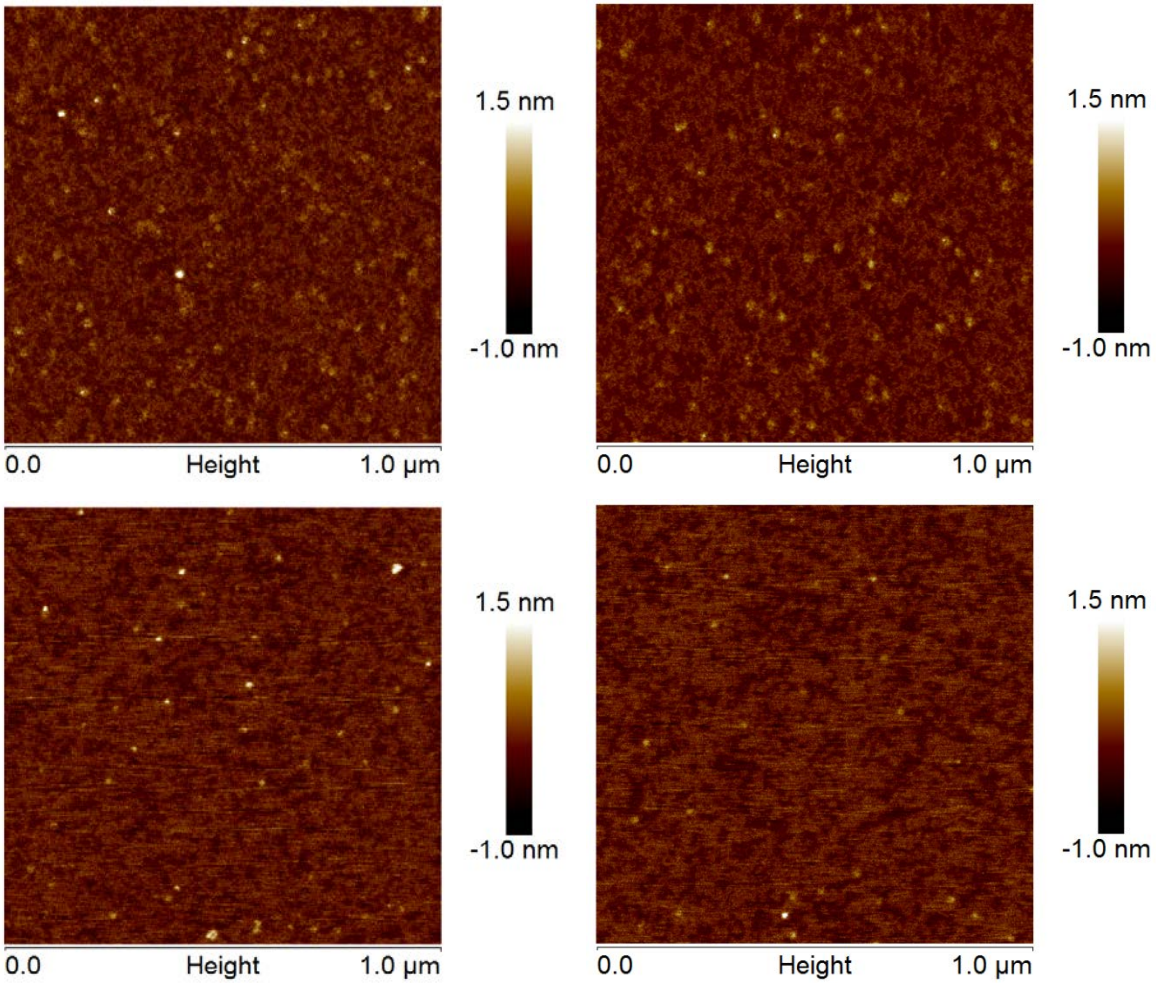

Figure 2.25 | AFM images of NH_2-HE_6-DNA micelles. Spherical structures with the size of 15.5±3.4 nm were observed. The average height was 0.9±0.3 nm.

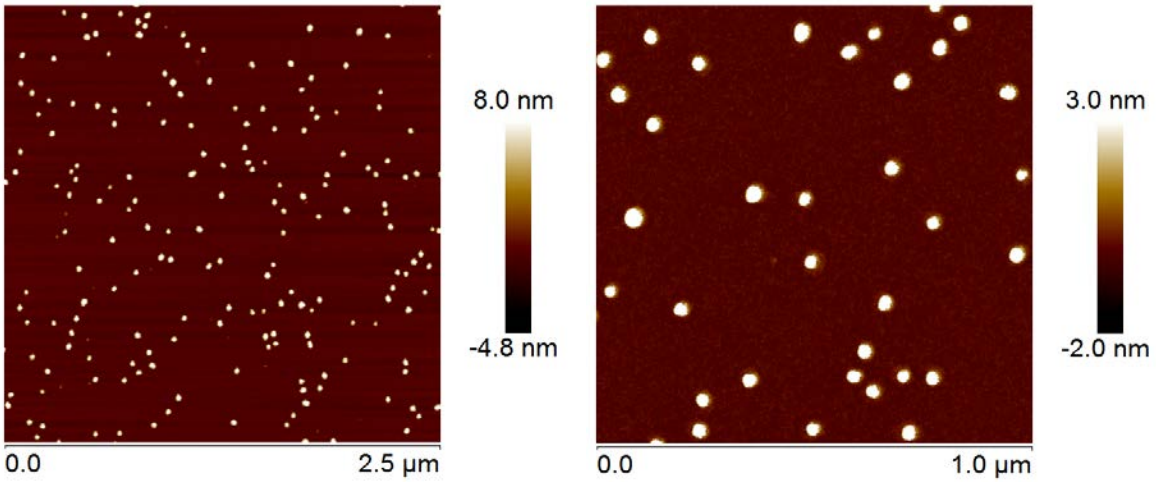

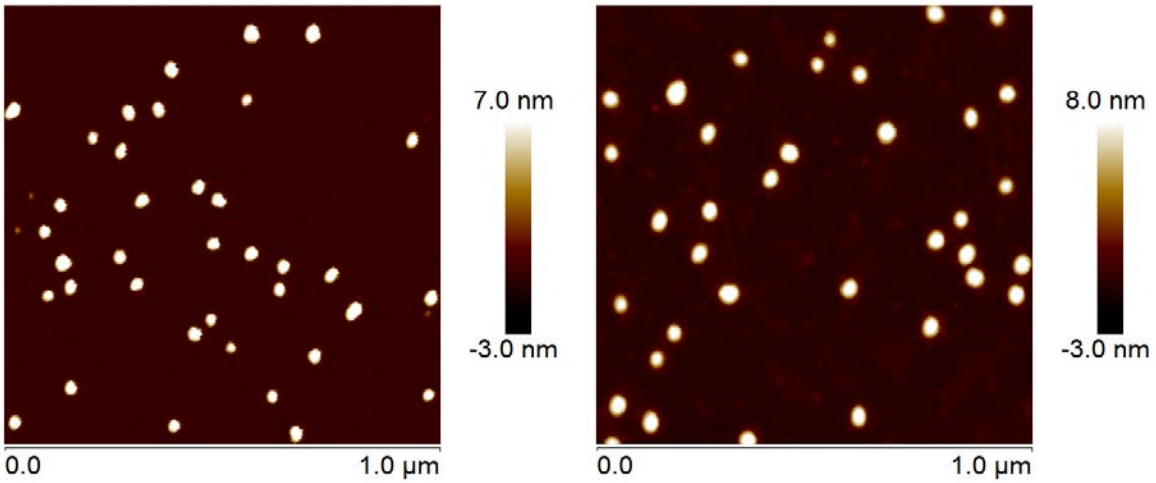

Figure 2.26 | AFM images of HE_6-NH_2-DNA micelles. Spherical structures with the size of 37.0±5.2 nm were observed. The average height was 9.1±1.0 nm.

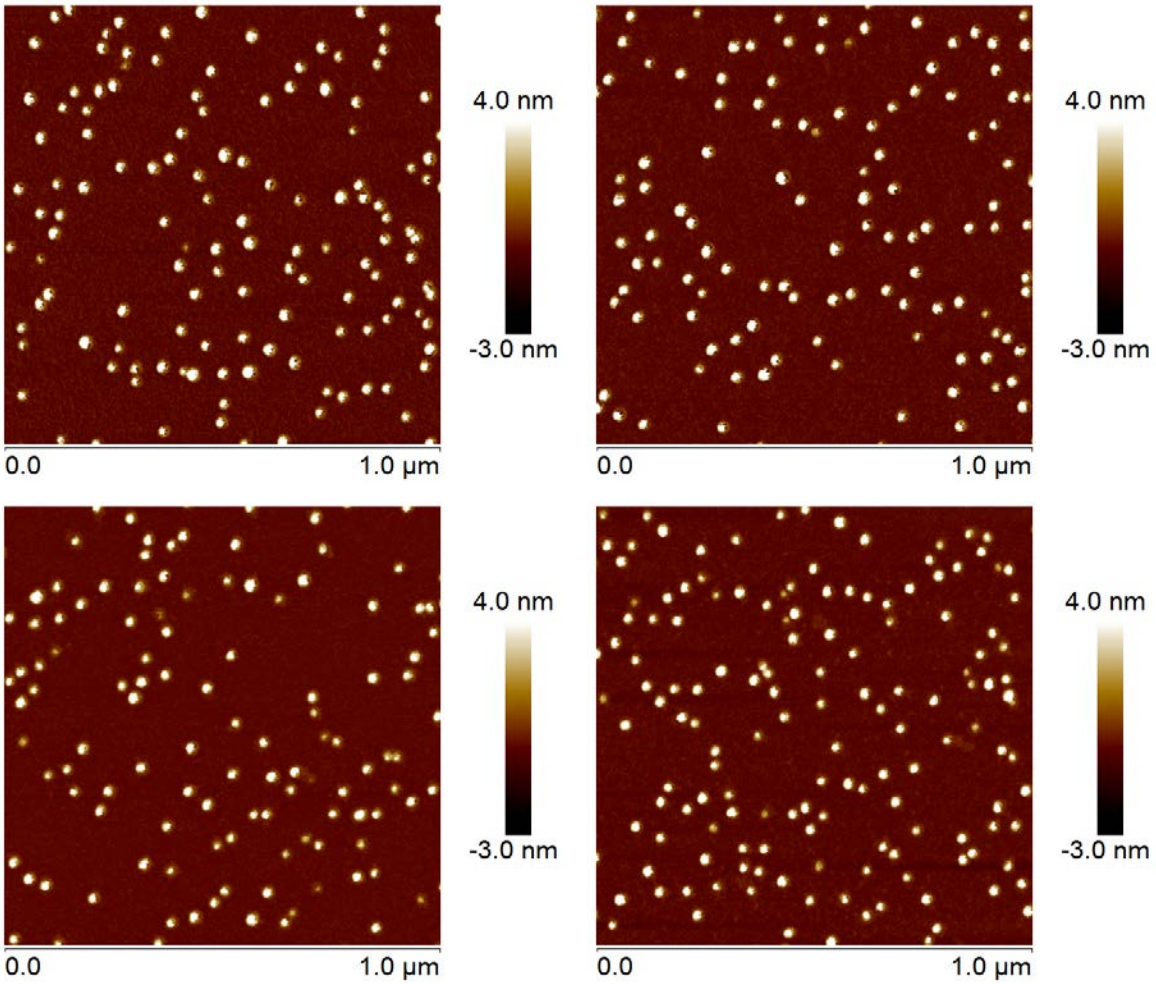

Figure 2.27 | AFM images of NH_2-HE_{12}-DNA micelles. Spherical structures with the size of 26.0±3.4 nm were observed. The average height was 7.0±1.6 nm.

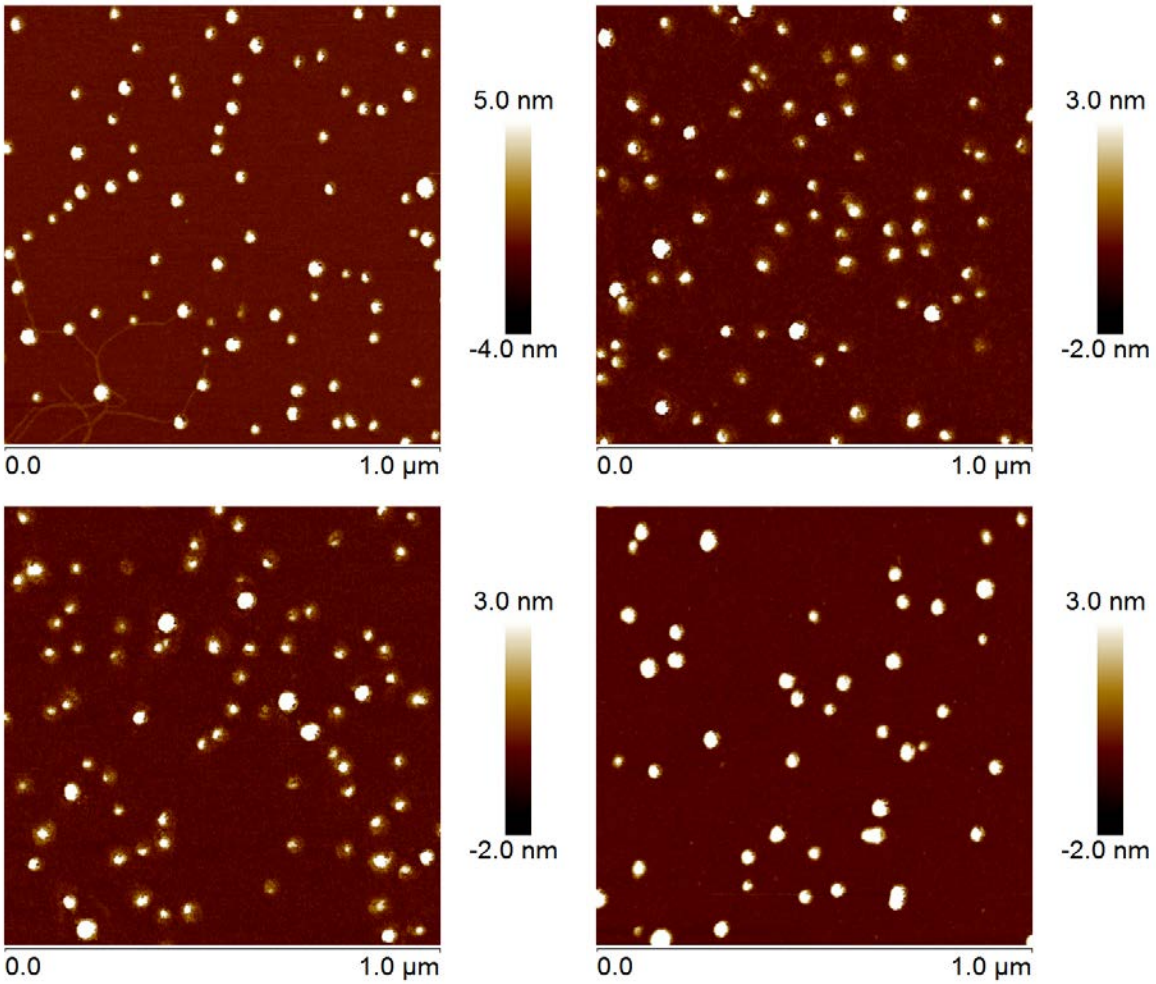

Figure 2.28 | AFM images of HE_{12}-NH_2-DNA micelles. Spherical structures with the size of 27.2±6.5 nm were observed. The average height was 7.2±2.8 nm.

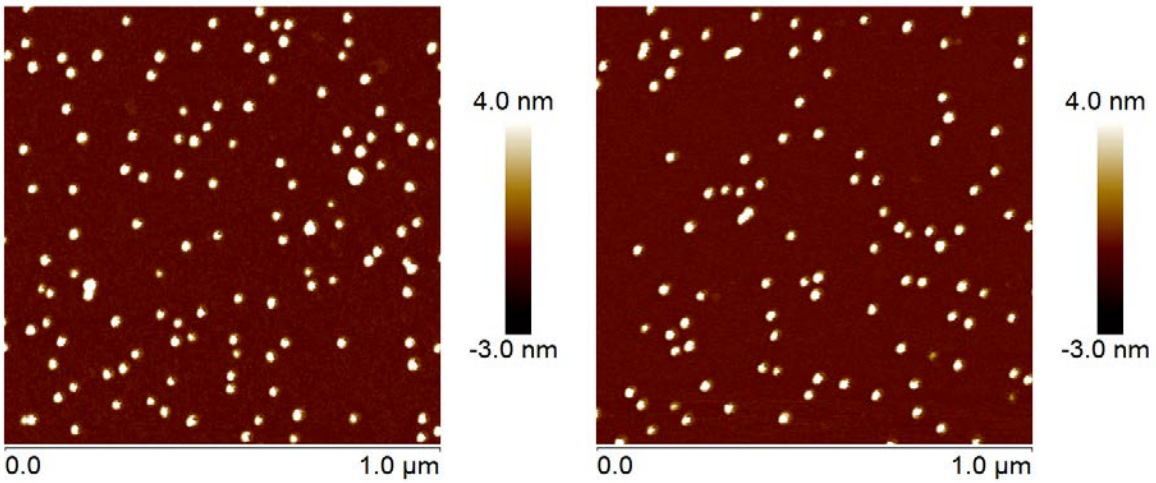

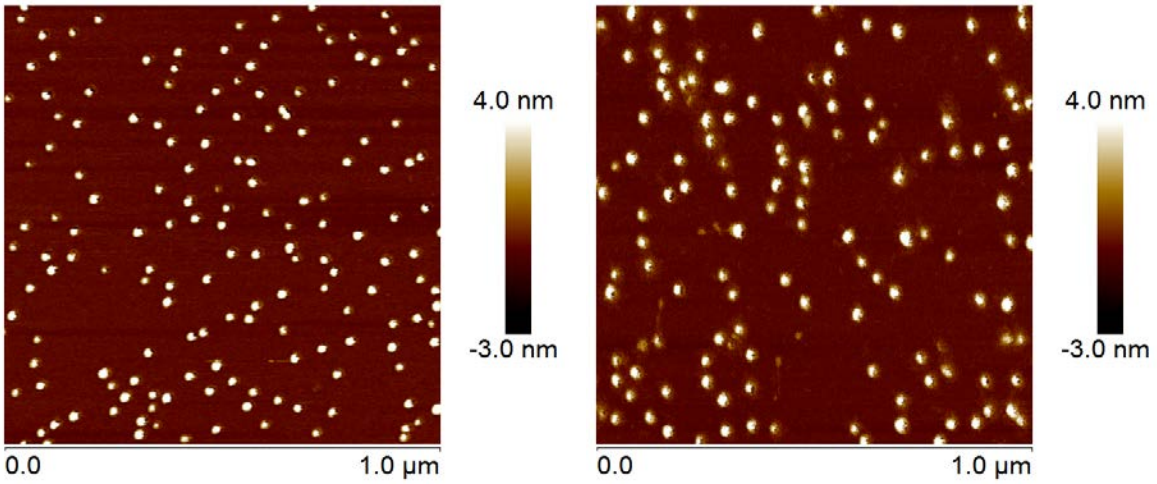

Figure 2.29 | AFM images of HE_6-NH_2-HE_6-DNA micelles. Spherical structures with the size of 25.8±4.5 nm were observed. The average height was 6.7±1.7 nm.

2.5.13. DLS measurements of DNA micelles

20 µL of samples were analyzed on a DynaPro using a laser wavelength of 824 nm at 25°C.

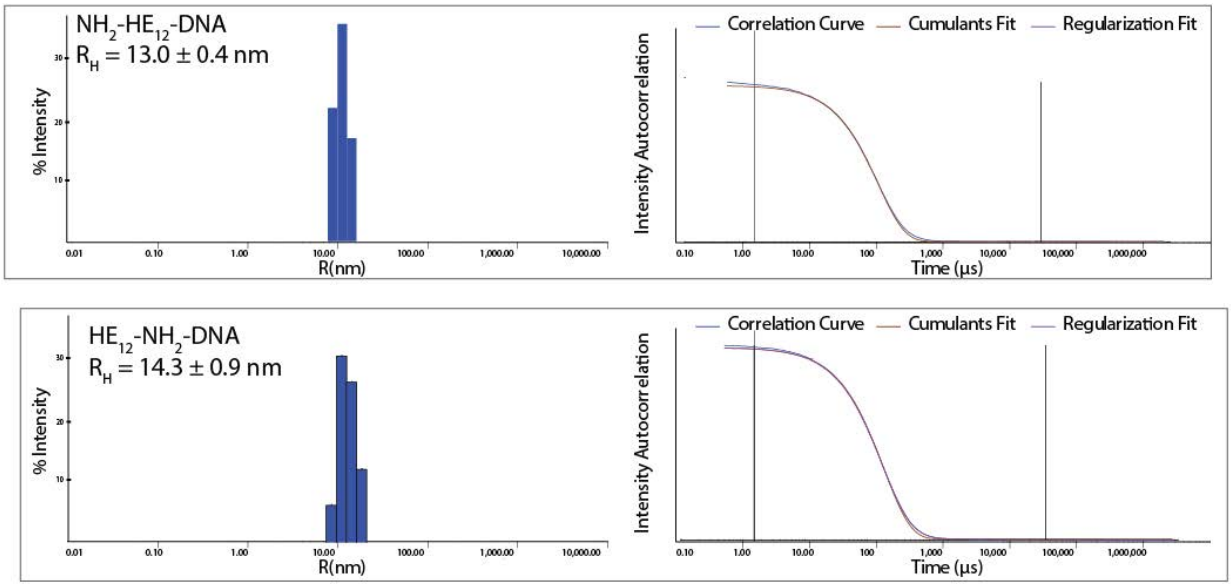

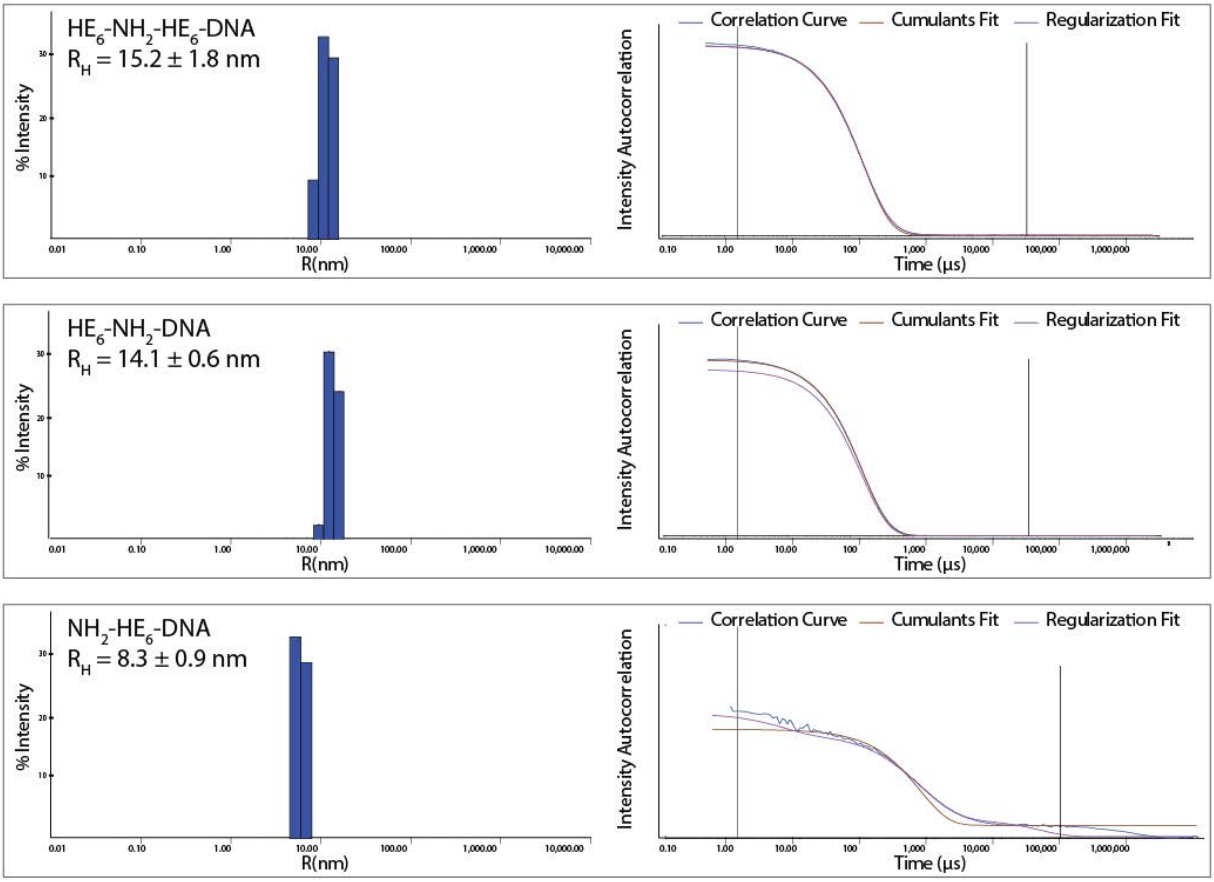

Right: autocorrelation curves of DNA amphiphiles micelles obtained from DLS

Figure 2.30 | DLS measurements of amino-modified amphiphiles self-assembly in aqueous buffer.

2.5.14. Effect of organic solvent on the structures of NH_2-HE_6-DNA micelles

5 µM **NH_2-HE_6**-DNA in 1xTAMg was annealed from 95°C to 4°C for 1 hour. The sample was diluted with 1x TAMg to 1.67 µM then the organic solvents (DMSO and THF) was added in 1/10 volume ratio (i.e. 0.6 µL solvent and 6 µL samples). Then, 5 µL of sample was deposited on freshly cleaved mica for 5 seconds and washed three times with 50 µL of H_2O. Excess liquid was brown off by the stream of nitrogen for 30 seconds. The sample was then dried under vacuum for at least 20 minutes prior to imaging.

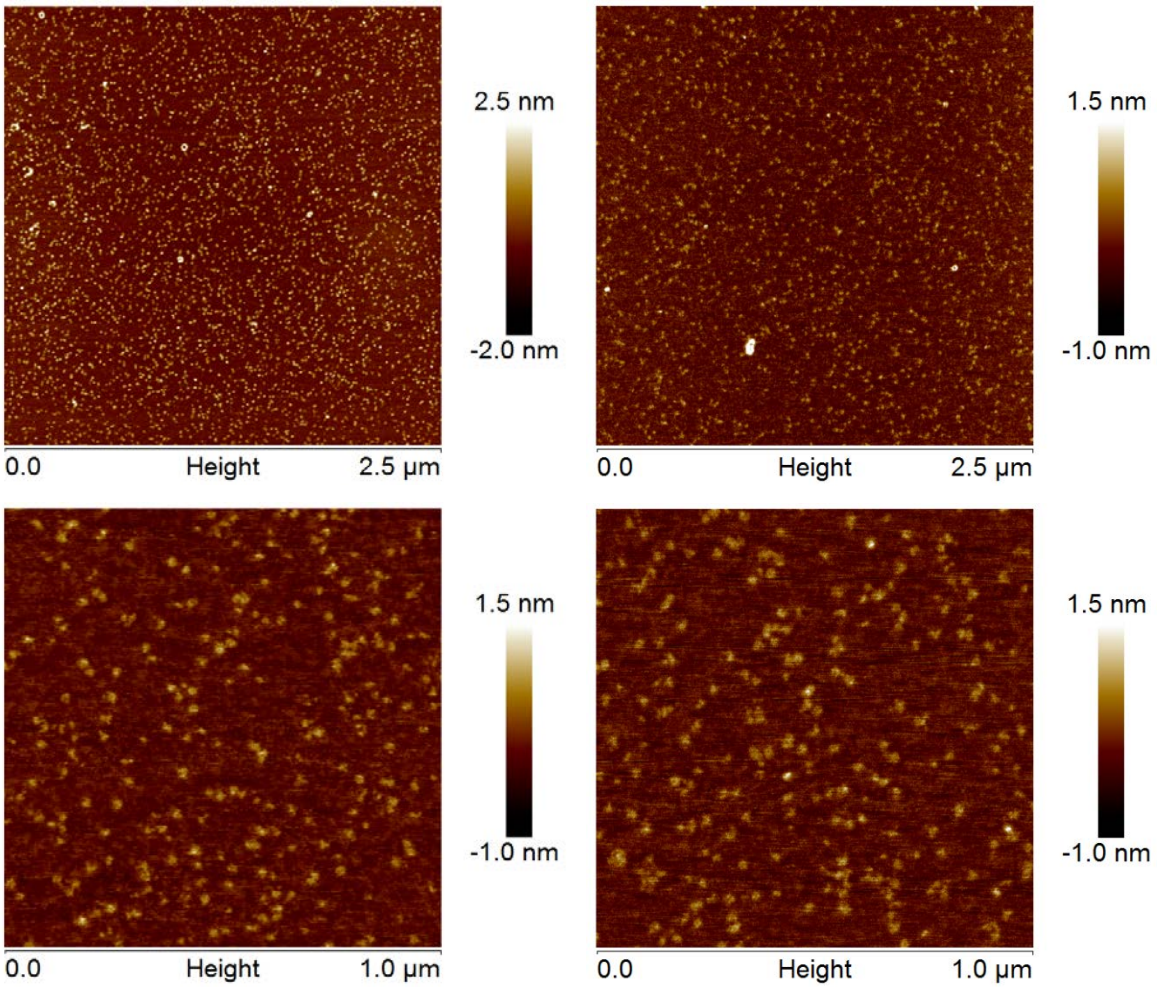

Figure 2.31 | AFM images of NH_2-HE_6-DNA micelles in the presence of DMSO. The morphology of the structure was similar to the micelles without DMSO. The size of the structures was 17.1±4.2 nm and the average height was 1.4±0.5 nm. Although the micelles were relatively larger, the addition of DMSO does not disrupt the stability of preformed micelles.

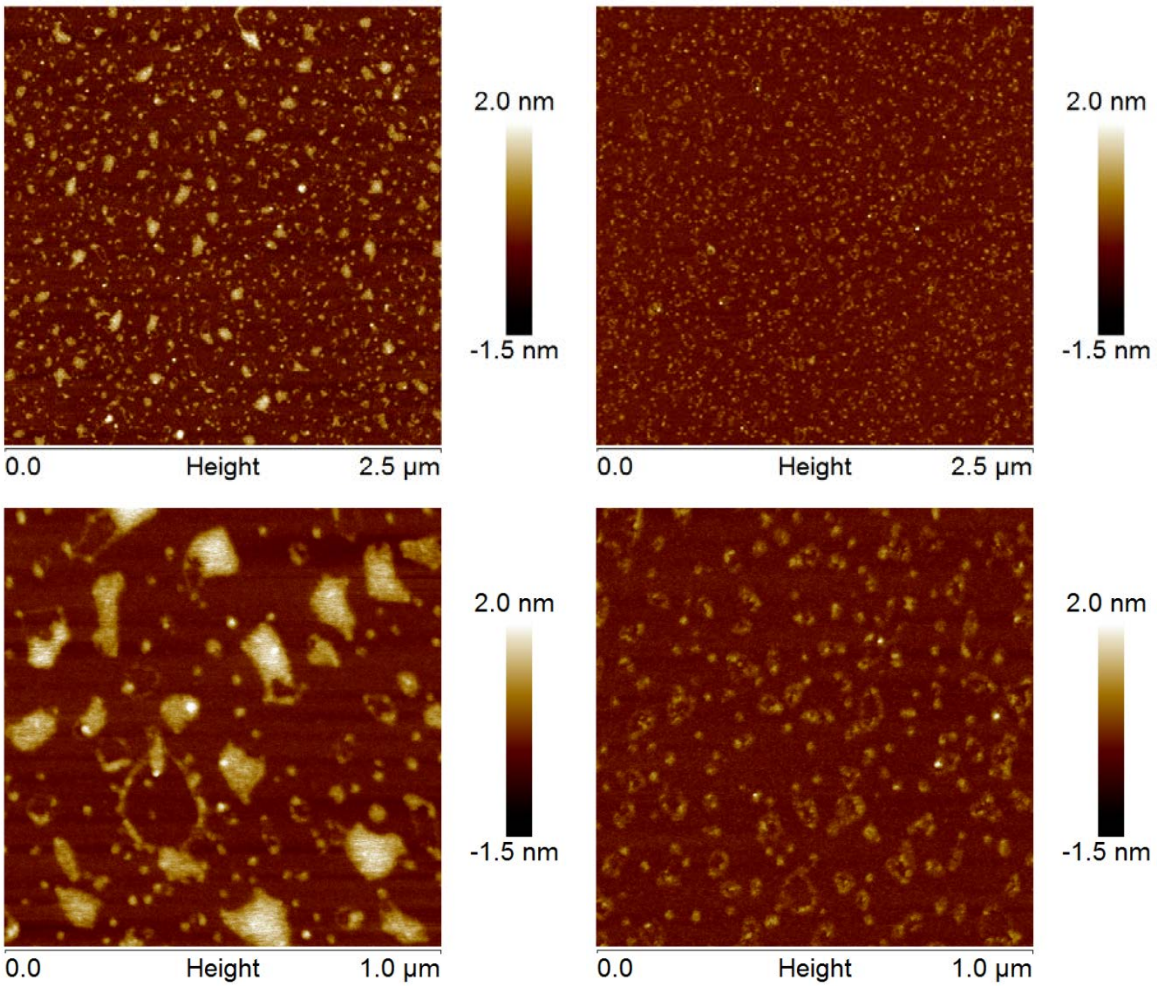

Figure 2.32 | AFM images of NH_2-HE_6-DNA micelles in the presence of THF. Large irregular aggregates and small spherical structures were clearly seen. The presence of the small structures with the size of 19.8±5.8 nm and the height of 0.9±0.2 nm) could suggest that the micelles were considerably stable against addition of THF. Large aggregates could be possibly due to the aggregation of these small structures.

2.5.15. Effect of the buffers on the conjugation efficiency of NH_2-HE_6-DNA with C_{22}-NHS

5μM of NH_2-HE_6-DNA was assembled in 1x buffer and annealed from 95 to 4°C in 1 hour. Separately, 10 mM of C_{22}-NHS in THF was prepared. To 10 volumes of NH_2-HE_6-DNA was quickly added 1 volume of C_{22}-NHS, and the mixture was gently shaken for 16 hours at room temperature. The crude mixture after reaction was dried and analyzed by RP-HPLC. Yield of conjugate reaction was calculated from the area under the curve ratio obtained from HPLC between the product peak and the sum of starting material and product peak. **Table 2.2** summarizes the buffers and their compositions used to compare the conjugation efficiency of NH_2-HE_6-DNA with C_{22}-NHS.

Table 2.2 | Buffer compositions (10x) for the conjugation of NH_2-HE_6-DNA with C_{22}-NHS

Buffers	10x buffer compositions
H_2O	-
$MgCl_2$ (pH 5.5)	125 mM $MgCl_2 \cdot 6H_2O$ (pH 5.5)
$MgCl_2$ (pH 8)	125 mM $MgCl_2 \cdot 6H_2O$ (pH 8.1, adjusted with 1M HCl)
TA	450 mM Tris, 200 mM acetic acid (pH 8.0)
TAMg	450 mM Tris, 200 mM acetic acid, 125 mM $MgCl_2 \cdot 6H_2O$ (pH 8.0)
HEPES/Mg	400 mM HEPES, 125 mM mM $MgCl_2 \cdot 6H_2O$ (pH 8.0, adjusted with 1M HCl)
PBS	10.6 mM KH_2PO_4, 1.6 M NaCl, 29.7 mM $Na_2HPO_4 \cdot 7H_2O$ (pH 7.4)
DPBS	9.0 mM $CaCl_2$, 4.9 mM $MgCl_2 \cdot 6H_2O$, 26.7 mM KCl, 14.7 mM KH_2PO_4, 1.4 M NaCl, 80.6 mM $Na_2HPO_4 \cdot 7H_2O$

2.5.16. Functionalized non-hydrophobically modified DNA using micelles system as auxiliary

2.5.16.1. 5'-Amino-modifier C3-TFA (NH_2(C3)) phosphoramidite purchased from GlenResearch

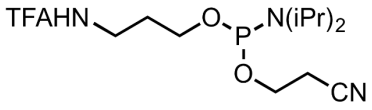

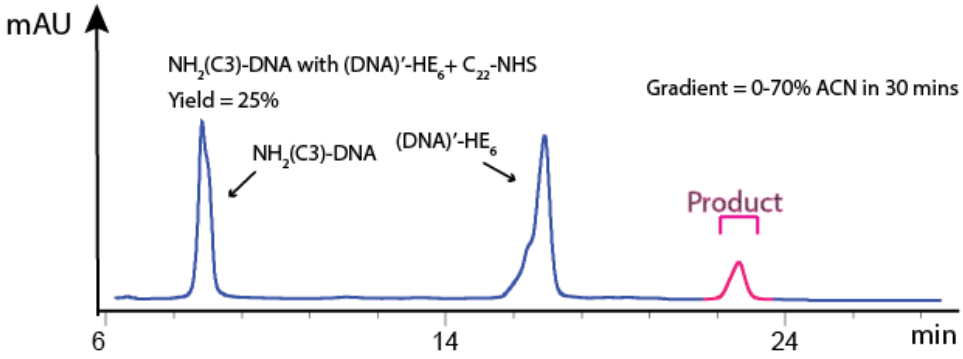

Figure 2.33 | HPLC trace of crude products of the **NH_2(C3)-**DNA + C_{22}-NHS templated by (DNA)'HE_6 micelles

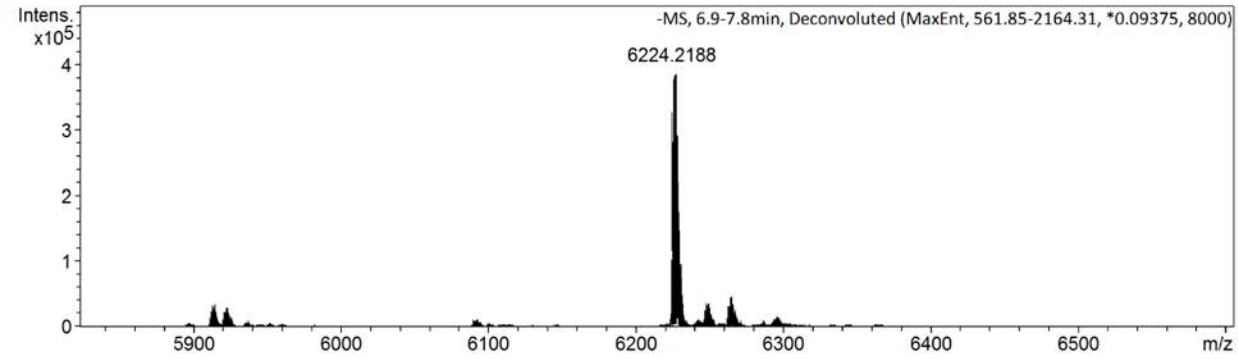

Figure 2.34 | MS characterization of HPLC purified **NH_2(C3)-**DNA + C_{22}-NHS templated by (DNA)'HE_6 micelles

2.5.16.2. 5'-Amino-modifier C6-MMT(NH_2(C6)) phosphoramidite purchased from GlenResearch

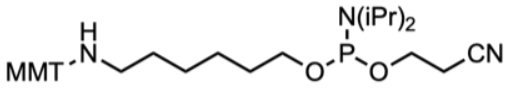

A. Reaction of NH_2(C6)-DNA with C_{18}-NHS

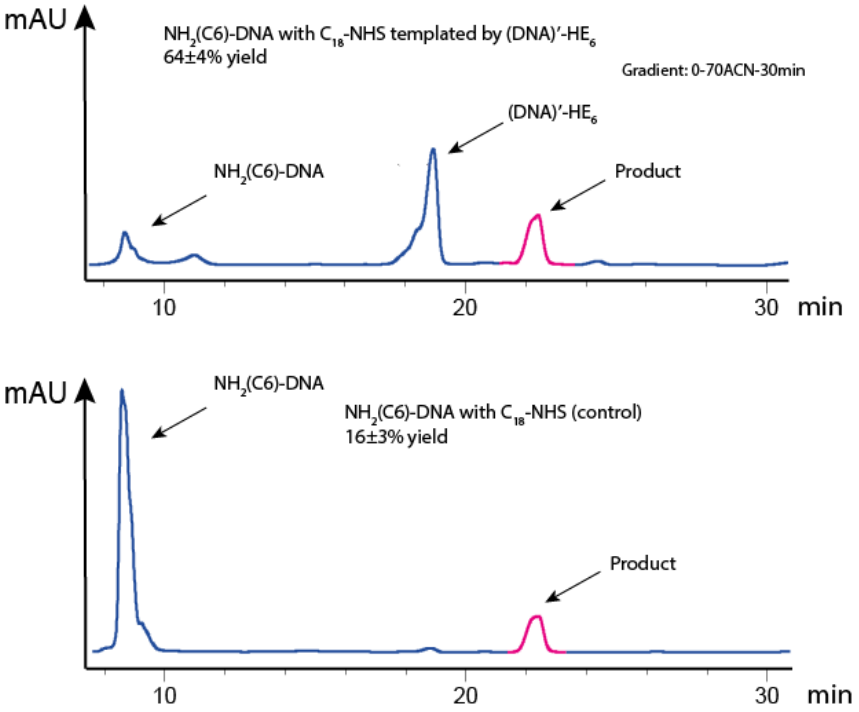

Figure 2.35 | HPLC traces of reaction between NH_2(C6)-DNA with C_{18}-NHS with and without (DNA')-HE_6 template.

B. Reaction of NH_2(C6)-DNA with C_{16}-NHS

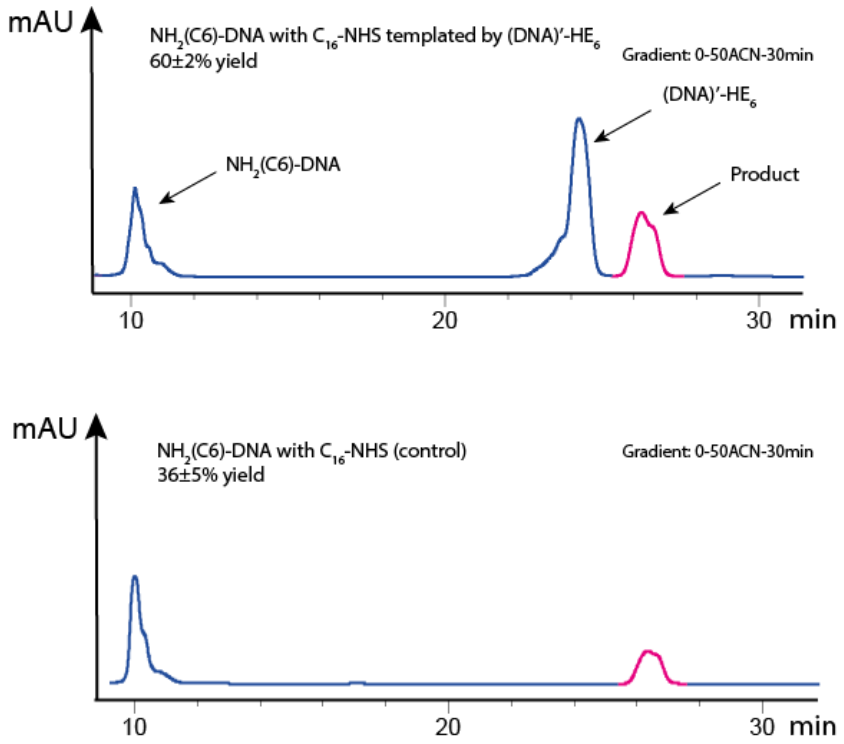

Figure 2.36 | HPLC traces of reaction between NH_2(C6)-DNA with C_{16}-NHS with and without (DNA')-HE_6 template

C. Reaction of NH_2(C6)-DNA with NDS-NHS

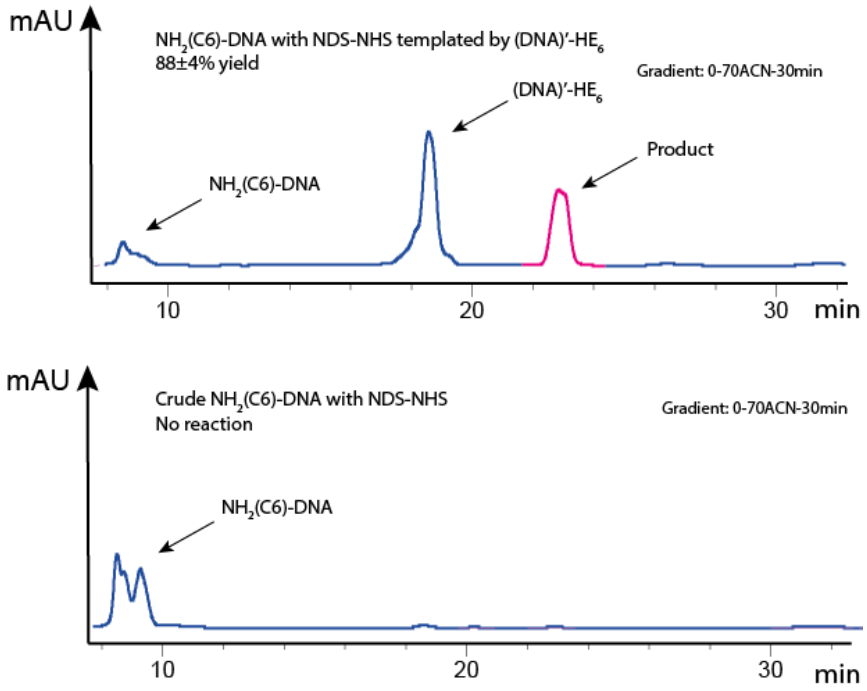

Figure 2.37 | HPLC traces of reaction between **NH_2(C6)-**DNA with NDS-NHS with and without (DNA')-HE_6 template

D. Reaction of NH_2(C6)-DNA with pyrene-NHS

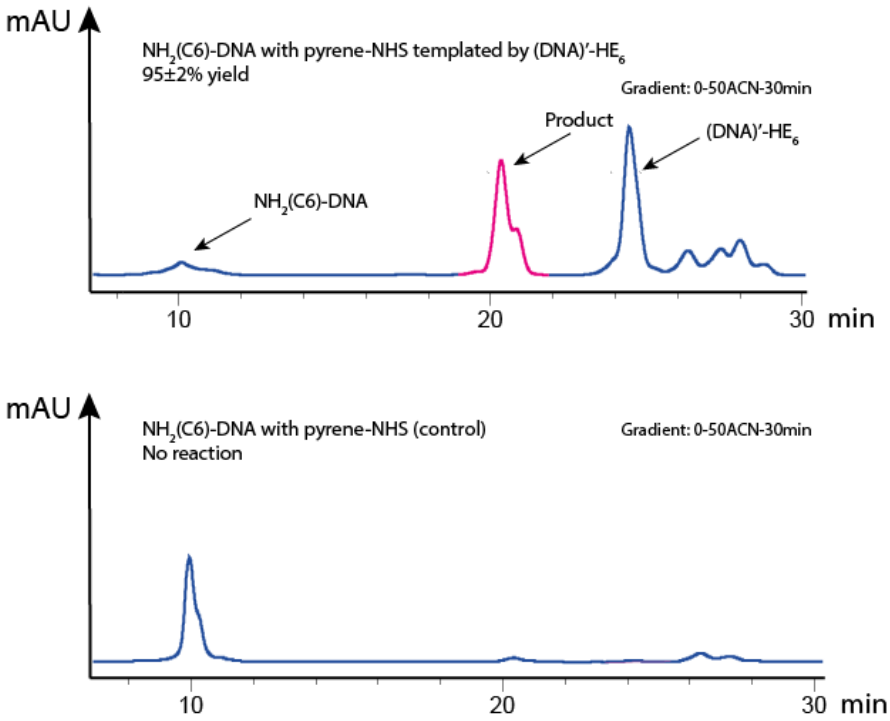

Figure 2.38 | HPLC traces of reaction between **NH_2(C6)-**DNA with pyrene-NHS with and without (DNA')-HE_6 template

E. Reaction of NH_2(C6)-DNA with C_{22}-NHS

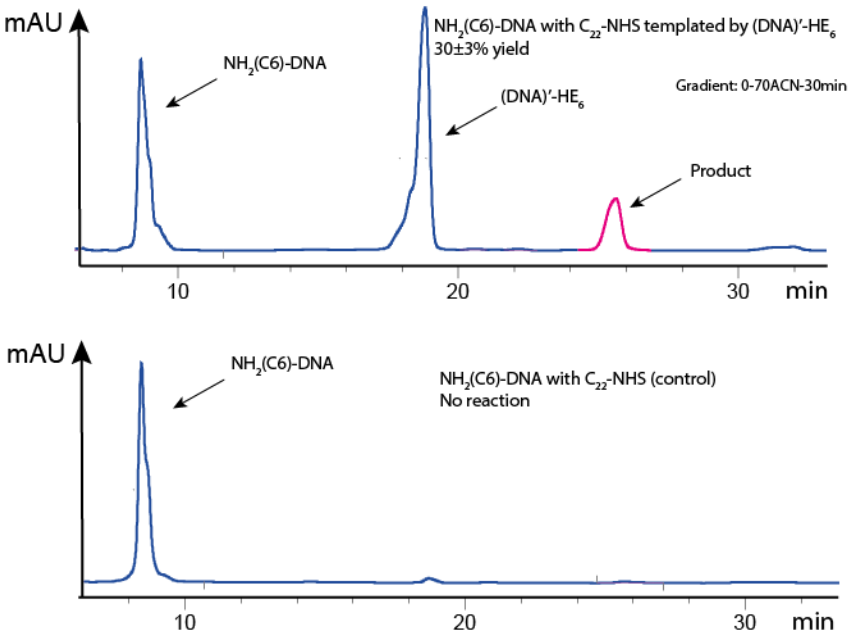

Figure 2.39 | HPLC traces of reaction between NH_2(C6)-DNA with C_{22}-NHS with and without (DNA')-HE_6 template.

F. Reaction of NH_2(C6)-DNA with Polystyrene-NHS (PS-NHS)

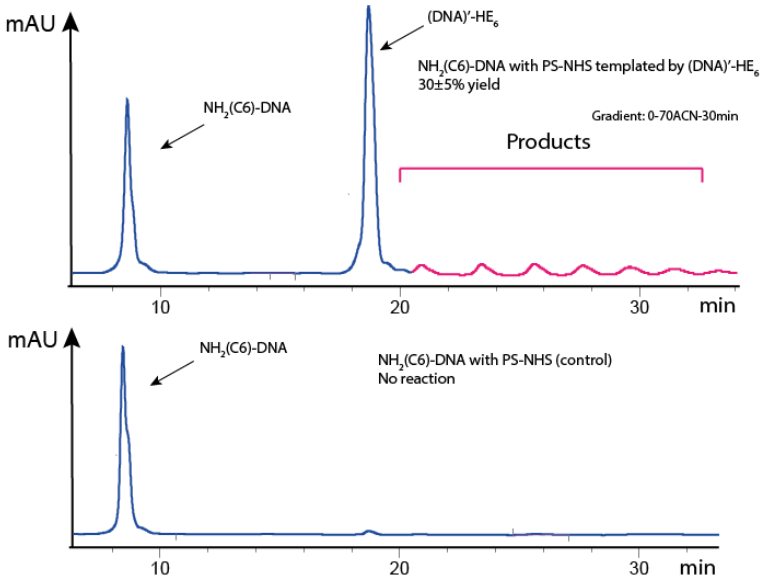

Figure 2.40 | HPLC traces of reaction between **NH_2(C6)-**DNA with PS-NHS with and without (DNA')-HE_6 template

G. MS characterization of conjugate product of NH_2(C6)-DNA and hydrophobic molecules

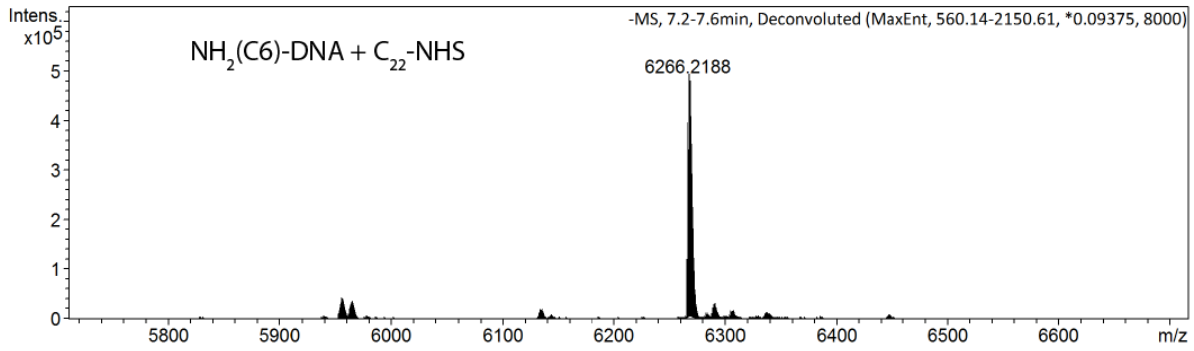
Intens.
x10^5
-MS, 7.2-7.6min, Deconvoluted (MaxEnt, 560.14-2150.61, *0.09375, 8000)
NH2(C6)-DNA + C22-NHS
6266.2188
5800
5900
6000
6100
6200
6300
6400
6500
6600
m/z

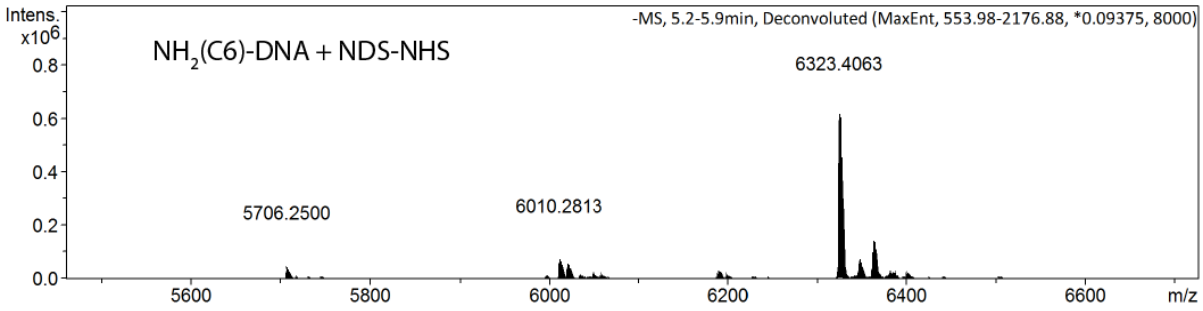
Intens.
x10^6
-MS, 5.2-5.9min, Deconvoluted (MaxEnt, 553.98-2176.88, *0.09375, 8000)
NH2(C6)-DNA + NDS-NHS
6323.4063
5706.2500
6010.2813
5600
5800
6000
6200
6400
6600
m/z

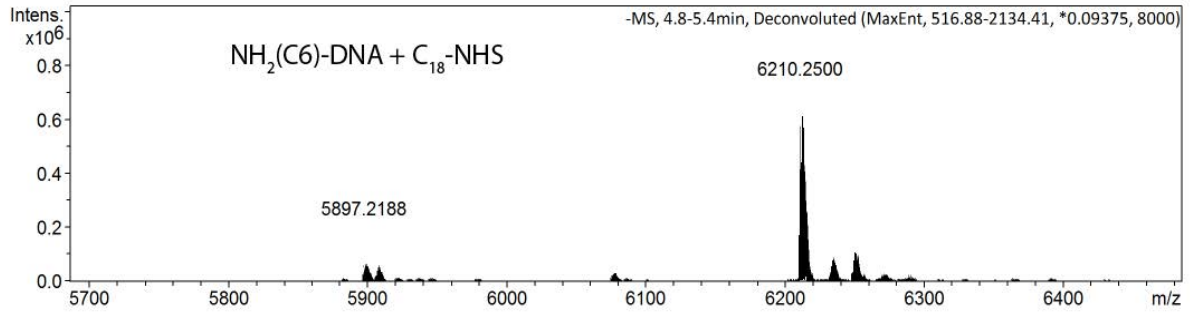
Intens.
x10^6
-MS, 4.8-5.4min, Deconvoluted (MaxEnt, 516.88-2134.41, *0.09375, 8000)
NH2(C6)-DNA + C18-NHS
6210.2500
5897.2188
5700
5800
5900
6000
6100
6200
6300
6400
m/z

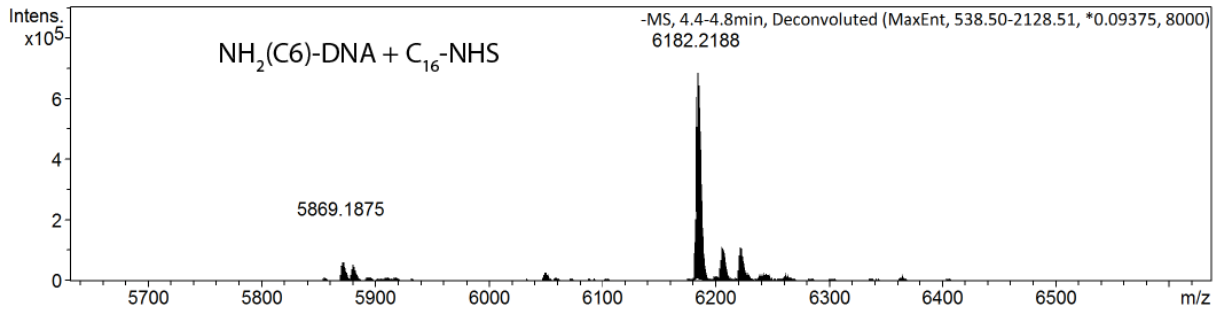

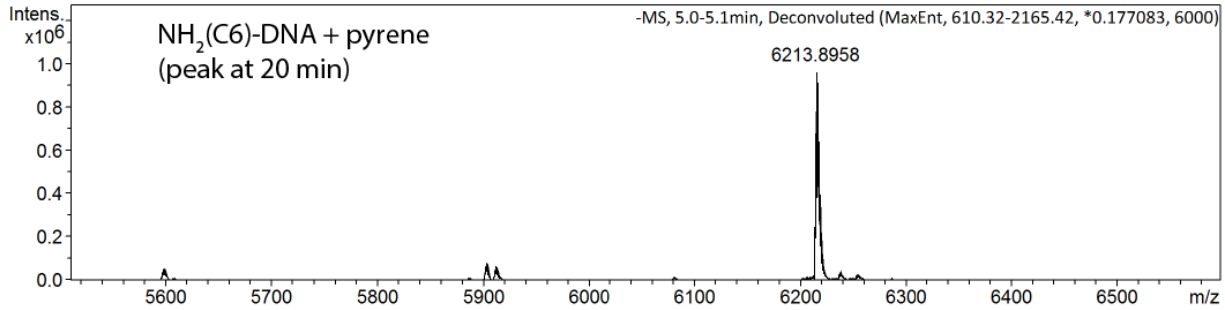

NH_2(C6)-DNA with PS-NHS:

Peak at 21 mins

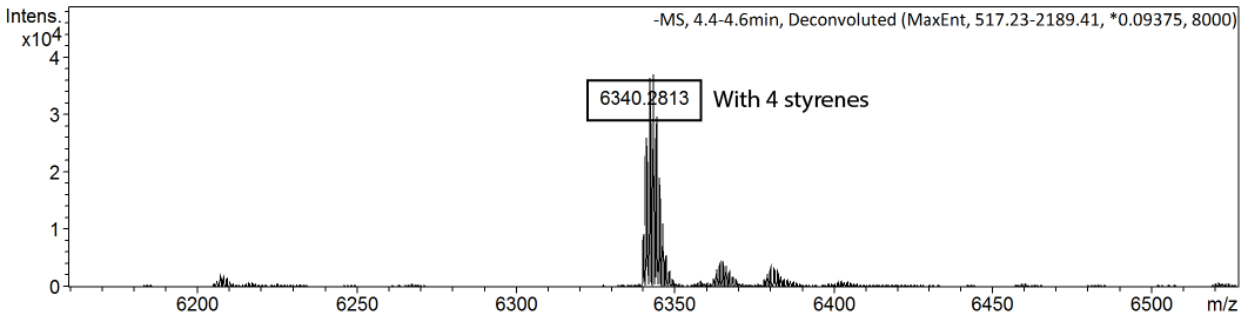

Peak at 23 mins

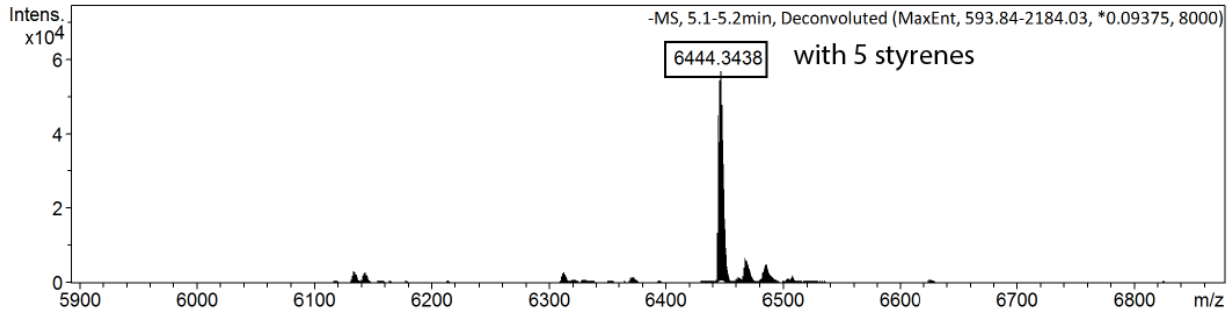

Peak at 27 mins

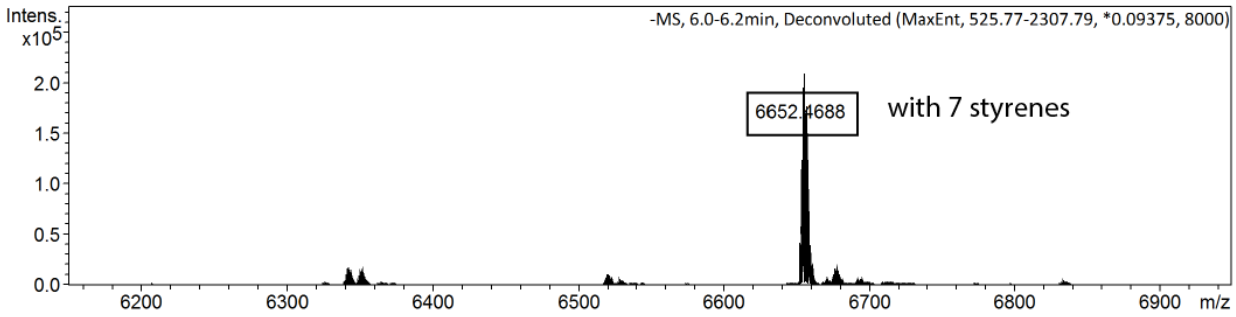

Figure 2.41 | MS characterization of products between NH_2(C6)-DNA with hydrophobic organic molecules.

2.5.17.3. Reaction of NH_2-DNA (Fmoc-C3-CED phosphoramidite) with C_{22}-NHS with DNA

A. HPLC characterization

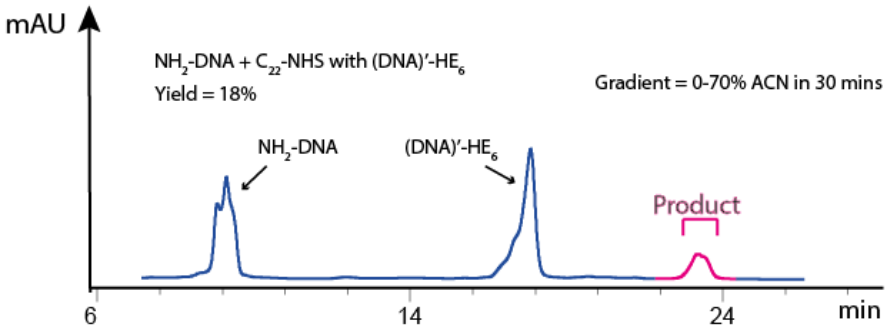

Figure 2.42 | HPLC characterization of products between **NH_2**-DNA with C_{22}-NHS

B. LC-MS characterization

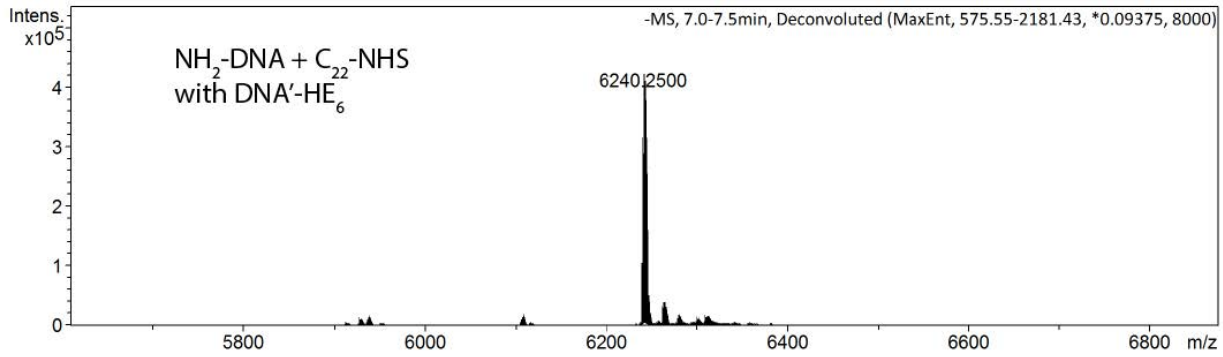

Figure 2.43 | HPLC characterization of products between **NH_2**-DNA with C_{22}-NHS

2.5.18. Note for the purification of NH_2 containing amphiphiles

We observed that a purification of NH_2-containing amphiphiles by the denaturing PAGE with urea generated the impurities which have additional mass of ~43 mass units. The products were further purified by RP-HPLC; however, the desired products and the impurities eluted at the same retention times, so it was difficult to remove the impurities by RP-HPLC.

We believe that the addition of mass is due to the reaction of amino group with the isocyanate, which can potentially form as the gel was heated during the run. The formation of isocyanate and ammonium at high temperature from the hydrolysis of urea is well-known in literature [40] and can induce chemical modification of protein during protein analysis which involves the use of urea as the denaturant.[41] Therefore, it is necessary to avoid the purification techniques involving urea, and we recommend using RP-HPLC or anion-exchange HPLC to separate the desired products.

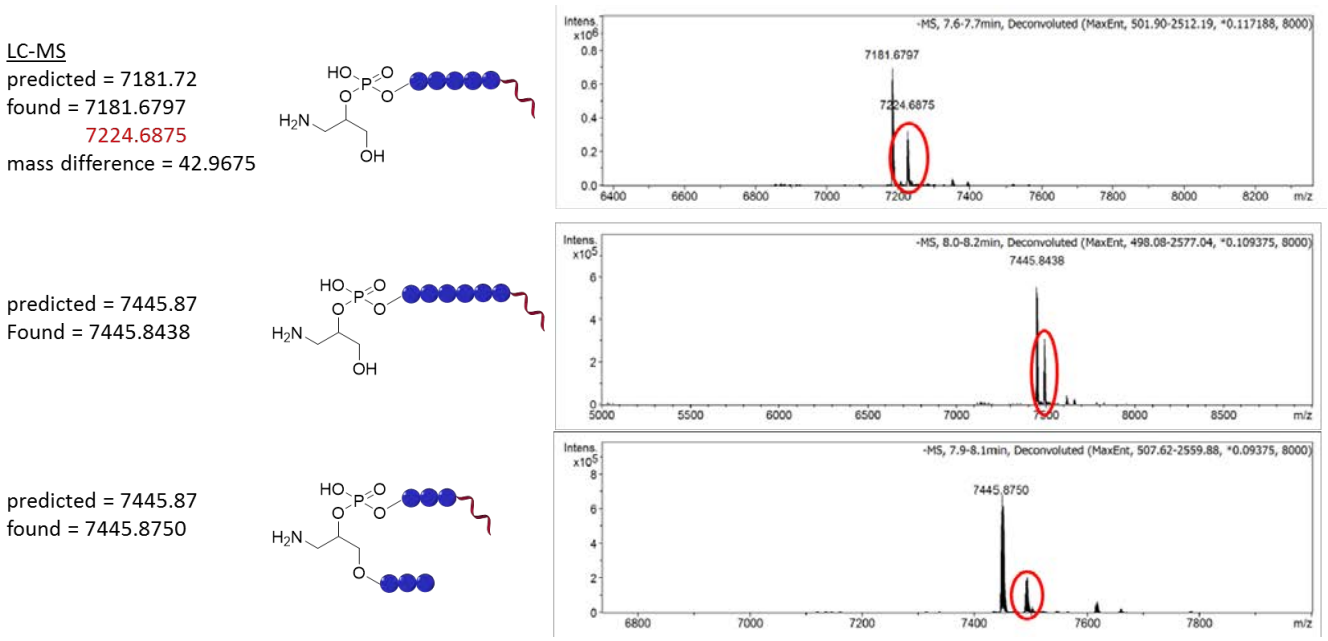

Figure 2.44 | Representative examples of the NH_2-containing amphiphiles which contain adducts of ~43 mass units. The impurities (highlighted in red ovals) could be clearly observed in the mass spectra.

2.6. References

1. Jeong, J. H.; Park, T. G., Novel Polymer−DNA Hybrid Polymeric Micelles Composed of Hydrophobic Poly(d,l-lactic-co-glycolic Acid) and Hydrophilic Oligonucleotides. *Bioconjugate Chem.* **2001,** *12* (6), 917-923.

2. Chabaud, P.; Camplo, M.; Payet, D.; Serin, G.; Moreau, L.; Barthélémy, P.; Grinstaff, M. W., Cationic Nucleoside Lipids for Gene Delivery. *Bioconjugate Chem.* **2006,** *17* (2), 466-472.

3. Zhang, J.; Fan, H.; Levorse, D. A.; Crocker, L. S., Interaction of Cholesterol-Conjugated Ionizable Amino Lipids with Biomembranes: Lipid Polymorphism, Structure–Activity Relationship, and Implications for siRNA Delivery. *Langmuir* **2011,** *27* (15), 9473-9483.

4. Kanasty, R.; Dorkin, J. R.; Vegas, A.; Anderson, D., Delivery materials for siRNA therapeutics. *Nat. Mater.* **2013,** *12* (11), 967-977.

5. Oh, S. S.; Lee, B. F.; Leibfarth, F. A.; Eisenstein, M.; Robb, M. J.; Lynd, N. A.; Hawker, C. J.; Soh, H. T., Synthetic Aptamer-Polymer Hybrid Constructs for Programmed Drug Delivery into Specific Target Cells. *J. Am. Chem. Soc.* **2014,** *136* (42), 15010-15015.

6. Tan, X.; Li, B. B.; Lu, X.; Jia, F.; Santori, C.; Menon, P.; Li, H.; Zhang, B.; Zhao, J. J.; Zhang, K., Light-Triggered, Self-Immolative Nucleic Acid-Drug Nanostructures. *J. Am. Chem. Soc.* **2015,** *137* (19), 6112-6115.

7. Pokholenko, O.; Gissot, A.; Vialet, B.; Bathany, K.; Thiery, A.; Barthelemy, P., Lipid oligonucleotide conjugates as responsive nanomaterials for drug delivery. *J. Mater. Chem. B* **2013,** *1* (39), 5329-5334.

8. Choi, K.-m.; Kwon, I. C.; Ahn, H. J., Self-assembled amphiphilic DNA-cholesterol/DNA-peptide hybrid duplexes with liposome-like structure for doxorubicin delivery. *Biomaterials* **2013,** *34* (16), 4183-4190.

9. Yang, C. J.; Pinto, M.; Schanze, K.; Tan, W., Direct Synthesis of an Oligonucleotide–Poly(phenylene ethynylene) Conjugate with a Precise One-to-One Molecular Ratio. *Angew. Chem.* **2005,** *117* (17), 2628-2632.

10. Immoos, C. E.; Lee, S. J.; Grinstaff, M. W., DNA-PEG-DNA Triblock Macromolecules for Reagentless DNA Detection. *J. Am. Chem. Soc.* **2004,** *126* (35), 10814-10815.

11. Feng, X.; Duan, X.; Liu, L.; Feng, F.; Wang, S.; Li, Y.; Zhu, D., Fluorescence Logic-Signal-Based Multiplex Detection of Nucleases with the Assembly of a Cationic Conjugated Polymer and Branched DNA. *Angew. Chem.* **2009,** *121* (29), 5420-5425.

12. Gibbs, J. M.; Park, S.-J.; Anderson, D. R.; Watson, K. J.; Mirkin, C. A.; Nguyen, S. T., Polymer−DNA Hybrids as Electrochemical Probes for the Detection of DNA. *J. Am. Chem. Soc.* **2005,** *127* (4), 1170-1178.

13. Albert, S. K.; Thelu, H. V. P.; Golla, M.; Krishnan, N.; Chaudhary, S.; Varghese, R., Self-Assembly of DNA–Oligo(p-phenylene-ethynylene) Hybrid Amphiphiles into Surface-Engineered Vesicles with Enhanced Emission. *Angew. Chem. Int. Ed.* **2014,** *53* (32), 8352-8357.

14. Chien, M.-P.; Rush, A. M.; Thompson, M. P.; Gianneschi, N. C., Programmable Shape-Shifting Micelles. *Angew. Chem. Int. Ed.* **2010,** *49* (30), 5076-5080.

15. Ding, K.; Alemdaroglu, F. E.; Börsch, M.; Berger, R.; Herrmann, A., Engineering the Structural Properties of DNA Block Copolymer Micelles by Molecular Recognition. *Angew. Chem. Int. Ed.* **2007,** *46* (7), 1172-1175.

16. Serpell, C. J.; Edwardson, T. G. W.; Chidchob, P.; Carneiro, K. M. M.; Sleiman, H. F., Precision Polymers and 3D DNA Nanostructures: Emergent Assemblies from New Parameter Space. *J. Am. Chem. Soc.* **2014,** *136* (44), 15767-15774.

17. Hong, B. J.; Eryazici, I.; Bleher, R.; Thaner, R. V.; Mirkin, C. A.; Nguyen, S. T., Directed Assembly of Nucleic Acid-Based Polymeric Nanoparticles from Molecular Tetravalent Cores. *J. Am. Chem. Soc.* **2015,** *137* (25), 8184-8191.

18. Bandy, T. J.; Brewer, A.; Burns, J. R.; Marth, G.; Nguyen, T.; Stulz, E., DNA as supramolecular scaffold for functional molecules: progress in DNA nanotechnology. *Chem. Soc. Rev.* **2011,** *40* (1), 138-148.

19. Li, Z.; Zhang, Y.; Fullhart, P.; Mirkin, C. A., Reversible and Chemically Programmable Micelle Assembly with DNA Block-Copolymer Amphiphiles. *Nano Lett.* **2004,** *4* (6), 1055-1058.

20. Teixeira Jr, F.; Rigler, P.; Vebert-Nardin, C., Nucleo-copolymers: oligonucleotide-based amphiphilic diblock copolymers. *Chem. Comm.* **2007,** (11), 1130-1132.

21. Jia, F.; Lu, X.; Tan, X.; Zhang, K., Facile synthesis of nucleic acid-polymer amphiphiles and their self-assembly. *Chem. Comm.* **2015,** *51* (37), 7843-7846.

22. Carneiro, K. M. M.; Hamblin, G. D.; Hanni, K. D.; Fakhoury, J.; Nayak, M. K.; Rizis, G.; McLaughlin, C. K.; Bazzi, H. S.; Sleiman, H. F., Stimuli-responsive organization of block copolymers on DNA nanotubes. *Chem. Sci.* **2012,** *3* (6), 1980-1986.

23. Oishi, M.; Hayama, T.; Akiyama, Y.; Takae, S.; Harada, A.; Yamasaki, Y.; Nagatsugi, F.; Sasaki, S.; Nagasaki, Y.; Kataoka, K., Supramolecular Assemblies for the Cytoplasmic Delivery of Antisense Oligodeoxynucleotide: Polyion Complex (PIC) Micelles Based on Poly(ethylene glycol)-SS-Oligodeoxynucleotide Conjugate. *Biomacromolecules* **2005,** *6* (5), 2449-2454.

24. Oishi, M.; Nagasaki, Y.; Itaka, K.; Nishiyama, N.; Kataoka, K., Lactosylated Poly(ethylene glycol)-siRNA Conjugate through Acid-Labile β-Thiopropionate Linkage to Construct pH-Sensitive Polyion Complex Micelles Achieving Enhanced Gene Silencing in Hepatoma Cells. *J. Am. Chem. Soc.* **2005,** *127* (6), 1624-1625.

25. Fong, R. B.; Ding, Z.; Long, C. J.; Hoffman, A. S.; Stayton, P. S., Thermoprecipitation of Streptavidin via Oligonucleotide-Mediated Self-Assembly with Poly(N-isopropylacrylamide). *Bioconjugate Chem.* **1999,** *10* (5), 720-725.

26. Umeno, D.; Maeda, M., Single stranded DNA-poly(N-isopropylacrylamide) conjugate for affinity precipitation separation of oligonucleotides. *Chem. Comm.* **1998,** (14), 1433-1434.

27. Kwak, M.; Herrmann, A., Nucleic Acid/Organic Polymer Hybrid Materials: Synthesis, Superstructures, and Applications. *Angew. Chem. Int. Ed.* **2010,** *49* (46), 8574-8587.

28. Gosse, C.; Boutorine, A.; Aujard, I.; Chami, M.; Kononov, A.; Cogné-Laage, E.; Allemand, J. F.; Li, J.; Jullien, L., Micelles of Lipid−Oligonucleotide Conjugates: Implications for Membrane Anchoring and Base Pairing. *J. Phys. Chem. B* **2004,** *108* (20), 6485-6497.

29. Lee, J. K.; Jung, Y. H.; Tok, J. B. H.; Bao, Z., Syntheses of Organic Molecule−DNA Hybrid Structures. *ACS Nano* **2011,** *5* (3), 2067-2074.

30. Liu, K.; Zheng, L.; Liu, Q.; de Vries, J. W.; Gerasimov, J. Y.; Herrmann, A., Nucleic Acid Chemistry in the Organic Phase: From Functionalized Oligonucleotides to DNA Side Chain Polymers. *J. Am. Chem. Soc.* **2014,** *136* (40), 14255-14262.

31. Lipshutz, B. H.; Ghorai, S., "Designer"-Surfactant-Enabled Cross-Couplings in Water at Room Temperature. *Aldrichimica Acta* **2012,** *45* (1), 3-16.

32. La Sorella, G.; Strukul, G.; Scarso, A., Recent advances in catalysis in micellar media. *Green Chem.* **2015,** *17* (2), 644-683.

33. Zhang, Q.-Q.; Cai, B.-X.; Gang, H.-Z.; Yang, S.-Z.; Mu, B.-Z., A family of novel bio-based zwitterionic surfactants derived from oleic acid. *RSC Adv.* **2014,** *4* (72), 38393-38396.

34. Wang, L.-M.; Jiao, N.; Qiu, J.; Yu, J.-J.; Liu, J.-Q.; Guo, F.-L.; Liu, Y., Sodium stearate-catalyzed multicomponent reactions for efficient synthesis of spirooxindoles in aqueous micellar media. *Tetrahedron* **2010,** *66* (1), 339-343.

35. Kumar, D.; Seth, K.; Kommi, D. N.; Bhagat, S.; Chakraborti, A. K., Surfactant micelles as microreactors for the synthesis of quinoxalines in water: scope and limitations of surfactant catalysis. *RSC Advances* **2013,** *3* (35), 15157-15168.

36. Bica, K.; Gartner, P.; Gritsch, P. J.; Ressmann, A. K.; Schroder, C.; Zirbs, R., Micellar catalysis in aqueous-ionic liquid systems. *Chem. Comm.* **2012,** *48* (41), 5013-5015.

37. Alemdaroglu, F. E.; Ding, K.; Berger, R.; Herrmann, A., DNA-Templated Synthesis in Three Dimensions: Introducing a Micellar Scaffold for Organic Reactions. *Angew. Chem. Int. Ed.* **2006,** *45* (25), 4206-4210.

38. Li, X.; Liu, D. R., DNA-Templated Organic Synthesis: Nature's Strategy for Controlling Chemical Reactivity Applied to Synthetic Molecules. *Angew. Chem. Int. Ed.* **2004,** *43* (37), 4848-4870.

39. Edwardson, T. G.; Carneiro, K. M.; Serpell, C. J.; Sleiman, H. F., An efficient and modular route to sequence-defined polymers appended to DNA. *Angew. Chem. Int. Ed.* **2014,** *53* (18), 4567-71.

40. Marier, J. R.; Rose, D., Determination of cyanate, and a study of its accumulation in aqueous solutions of urea. *Analytical Biochemistry* **1964,** *7* (3), 304-314.

41. Stark, G. R.; Stein, W. H.; Moore, S., Reactions of the Cyanate Present in Aqueous Urea with Amino Acids and Proteins. *J. Biol. Chem* **1960,** *235* (11), 3177-3181.

| 3 |

DNA pattern transfer to small molecules using 2D DNA structures

This chapter is composed mainly of the work published as " "Printing" DNA strand patterns on small molecules with control of valency, directionality, and sequence" by Tuan Trinh, Daniel Saliba, Chenyi Liao, Donatien de Rochambeau, Alexander Lee Prinzen, Jianing Li, and Hanadi F. Sleiman in Angewandte Chemie International Edition, 2019, **58**, 3042-3047.

Author contributions:

Tuan Trinh helped design the project, developed the concept, primarily contributed to the production of experimental data from DNA synthesis, HPLC, gel electrophoresis, AFM imaging and mass spectroscopy and wrote the paper. **Daniel Saliba** helped to synthesize several DNA strands, generated "temporal growth" backbones and carried out all PCR amplification experiments. **Chenyi Liao** and **Jianing Li** (the University of Vermont) carried out molecular modelling of the junction. **Donatien de Rochambeau** synthesized alkyne modification for DNA synthesis. **Alexander Lee Prinzen** synthesized tetra-azido functionalized small molecule. **Hanadi F. Sleiman** designed the project, guided interpretation of data and result discussion, co-wrote the paper and provided funding for the project.

3.1. Preface

In chapter 2, highly monodispersed DNA micelles were shown to serve as new platform for efficiently templating DNA functionalization with hydrophobic molecules in aqueous media. DNA or DNA amphiphiles can be conjugated directly to hydrophobic molecules in a facile manner via amide bond formation, without the need of heavily modified small molecules. Chapter 3 seeks to expand the capability of DNA-template reaction in generating asymmetric branched DNA-small molecule structures. The incorporation of synthetic molecules as corner units in DNA structures has been of interest over the last two decades. We present a facile method to generate branched small molecule-DNA hybrids with controllable valency, different sequences and directionalities (**5'-3'**) using a "printing" process from a simple 3-way junction structure in one step. This strategy provides opportunities to achieve new structural motifs in DNA nanotechnology and introduce new functionalities to DNA nanostructures.

3.2. Introduction

DNA base-pairing is one of the most reliable and programmable interactions in nature. These remarkable properties make this molecule a unique template to finely organize and control matter at the nanoscale.[1-2] Most current approaches, such as DNA tile assembly or DNA origami, rely on DNA base-pairing, and use unmodified DNA strands to guide the assembly process.[3-8] An attractive complementary approach involves the use of branched small molecule-DNA hybrids, composed of multiple DNA strands covalently attached to small molecule cores, as building blocks for DNA nanostructures.[9-12] Using organic vertices with specific geometries in DNA nanostructures can significantly reduce the number of strands required, greatly influence assembly outcome, and increase DNA stability and assembly cooperativity,[9, 13-16] which is inaccessible with non-modified DNA.[17] Moreover, by simply changing the small molecule core in the building block, new functionalities can be brought into the structure.[18] Branched DNA structures can be used for hydrogel[19] and nanoparticle formation,[20] DNA metallization,[21-22] DNA networks formation [23-24] and DNA crystallization.[25-26] However, despite their significant promise, branched DNA hybrid structures have not been extensively examined as building blocks for DNA nanotechnology, in comparison to methods such as DNA origami or tile assembly. This is largely due to synthetic challenges in generating these structures. Branched DNA-small molecules with identical arms have been generated previously using solid- or solution-phase synthesis.[12, 27-30 31 32] Over the past years, our group [10] and others [12, 33-36] have attached two different DNA strands on synthetic vertices using solid-phase phosphoramidite chemistry, and used them in various applications. However, the attachment of three or more different DNA strands on a molecular core requires the laborious synthesis of molecules with multiple orthogonal protecting groups, followed by sequential build-up of DNA strands, and suffers from low yield and tedious purification. Moreover, controlling DNA (5'-3') directionality using previous methods is difficult,[37] and has been limited to costly and low-yielding reverse amidites.[38] To the best of our knowledge, there is no previous report of a facile synthetic methodology to covalently link different DNA strands to small molecules with controllable valency, sequences and directionalities.

In this chapter, we describe a simple method to covalently "print" different DNA strands from a self-assembled three-way junction to a small molecule core using copper-catalyzed alkyne-azide

"click" chemistry (**Figure 3.1**). DNA-templated synthesis has evolved considerably over the past few decades as a powerful method to control and enable reactivity of synthetic molecules.[39-40] Our proposed method relies on using a DNA template to ensure high effective concentration of reactive units in the middle of the junction, hence facilitating conjugation reactions. As a proof of concept, we transfer three and four different DNA sequences on triazide- and tetraazide-functionalized cores, respectively. We show that the isolated products have exactly pre-determined numbers and DNA sequences and can be tuned with respect to DNA directionality and length. Each arm of the asymmetric branched DNA-small molecule product can be elongated separately to different lengths in high yield using the polymerase chain reaction (PCR). The elongated structure can be can serve as a unique scaffold for nanomaterial organization in 2D. Finally, we then use these branched DNA structures as templates for high-yielding chemical replication to generate "daughter" branched structures, thus increasing the scalability of this approach. Our strategy offers several distinct advantages compared to the previous methods: **1)** It uses commercially available starting materials and does not need heavily modified small molecule cores, **2)** uses end-modified DNA strands and does not require an in-house DNA synthesizer (i.e. modified DNA strands can be purchased directly from providers such as IDT, Chemgenes and Glen Research), **3)** has short reaction time (about 2 hours), **4)** is easy to purify and **5)** importantly, it is highly modular, allowing the incorporation of different DNA sequences with controllable directionalities, length and valency onto different synthetic molecules.

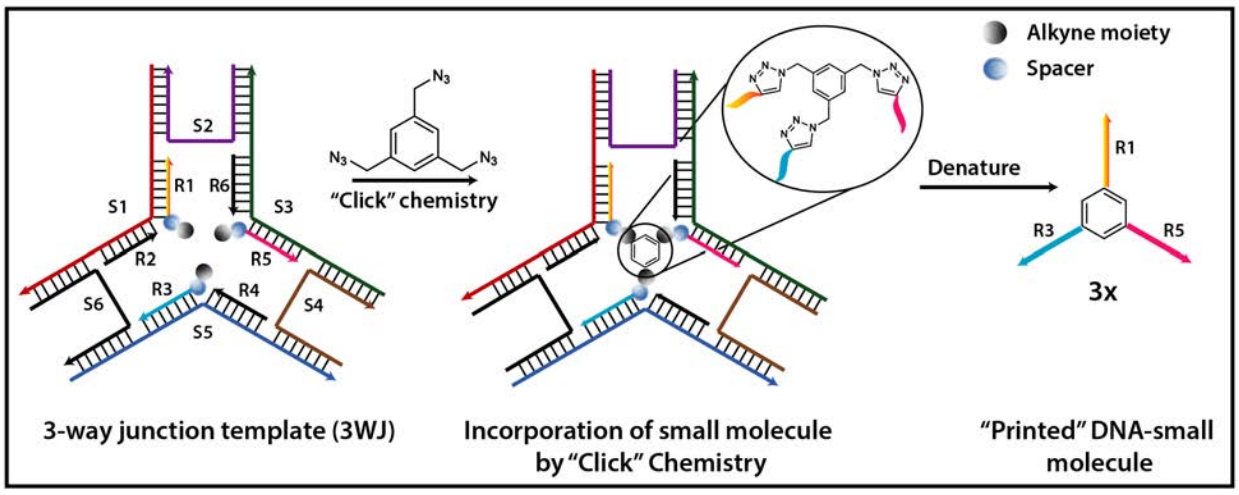

Figure 3.1 | Schematic representation of the overall design approach.

3.3. Result and Discussion

3.3.1. Design of the template

Our strategy utilizes a self-assembled 3-way junction **(3WJ)** as a template (**Figure 3.1)** containing six scaffold strands namely **S1** to **S6** in addition to single-stranded DNAs **(ssDNAs)** hybridized to the middle region of the junction **(R1** to **R6)**. Unlike a typical DNA tile,[41] we break the long middle strand into six individual strands with three pointing their 5'-end and the other three pointing their 3'-end toward the middle region in an alternating fashion. In this region, we hybridize two types of DNA strands: reactive and rigidifying strands. A reactive strand contains an alkyne functional group at its end and is separated from the DNA part by a commercially available hexaethylene (**C12)** spacer (**Figure 3.2**), while the rigidifying strands without functional groups are hybridized to increase the junction's geometric definition. Once all the reactive and rigidifying strands are in pre-designated positions, we anticipate that this region has a high local concentration of the reactive groups and a small molecule would be able to react and "pick" up the alkyne-functionalized DNA strands covalently. The resulting DNA-small molecule product can be then released from the junction template by denaturation **(Figure 3.1)**. **Figure 3.2b** shows a native polyacrylamide gel electrophoresis **(PAGE)** as the outcome of the stepwise 3WJ assembly. Lane **12** shows a quantitative formation of the junction, which is robust enough to not fall apart at room temperature.

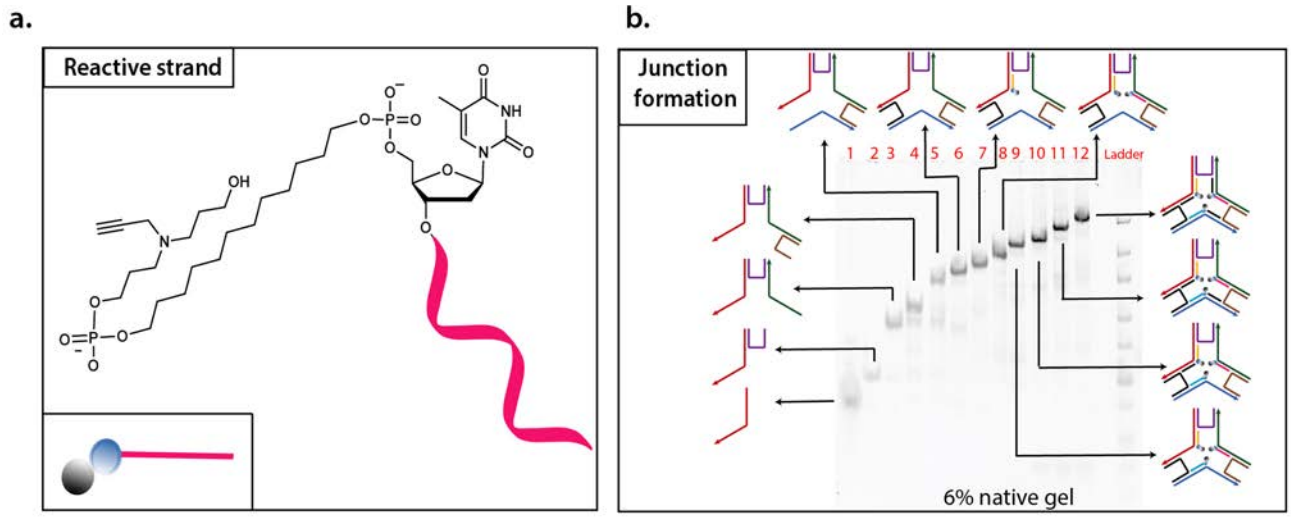

Figure 3.2 | a. Chemical structure of reactive strand having 12-carbon organic spacer and alkyne group. **b.** 6% native PAGE shows stepwise assembly of the 3WJ.

3.3.2. Transfer of DNA patterns to a tris-azido functionalized molecule

To examine our hypothesis, we first attempted to "print" three unique DNA strands (19 bases each) from a designed 3WJ to a 1,3,5-tris(azidomethyl)benzene core. Previously, this core has been used to connect to different DNA strands using solid-phase synthesis.[11, 36] However, instead of going through multi-step synthesis of small molecule core, our method allows simple preparation of the core as well as the template from commercially available materials. The middle part is functionalized with three DNA strands having an alkyne functional group at their 5' end, namely **R1, R3** and **R5**, and 3 rigidifying strands *without* functional group, namely **R2**, **R4** and **R6 (Figure 3.1**). The denaturing gel in **Figure 3.3a** shows that the trimer with 3 different DNA sequences (**R1, R3** and **R5**) **(3x)** was formed with an approximate 30% yield after 2 hours (equivalent to ~70% yield for each "click" reaction), along with rigidifying strands, scaffold strands **(S)** and side products (i.e. monomer and dimer). Note that there was low or no yield of trimer formation in the absence of template under the same reaction conditions (Experimental Section **3.5.9**). In order to characterize the sequence asymmetry of **3x**, 3 fully complementary strands (**R1', R3'** and **R5'**) which hybridize with each of the arms of **3x** were added sequentially. **Figure 3.3b** reveals a gradual decrease in mobility shift of the structures, suggesting the successful

hybridization of the individual complementary strands (see Experimental Section Figure **3.17** for mass spectrometry confirmation).

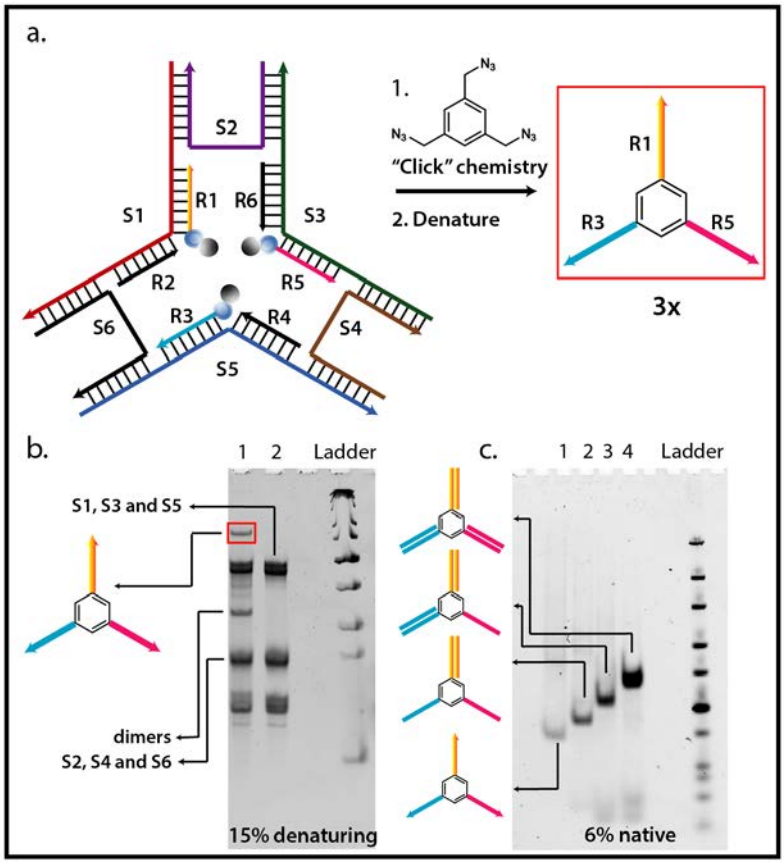

Figure 3.3 | Pattern transfer to a 3-arm molecule. a. Schematic representation of the approach **b.** 15% denaturing PAGE for trimer formation. Lane 1: crude reaction mixture between fully assembled 3WJ with triazide molecules. Lane 2: fully assembled 3WJ in denaturing condition **c.** Stepwise addition of complementary strands to **3x**.

3.3.3. Changing directionalities of DNAs in trimer structure

We were then interested in changing the directionality (5'-3') of the transferred DNA strands onto the core. The 3WJ allows us to easily switch the reactive alkyne groups to the 3' ends of the three other strands (**R2, R4** and **R6**), pointing toward the core of the 3WJ. Now, **R1, R3** and **R5** acts as rigidifying strands. We obtained a similar yield of the reverse direction trimer (with the

3'-ends of the DNA strands connected to the small molecule core) that would be difficult to achieve using previously reported methods (**Figure 3.4**).[31-32, 36-37] Moreover, we were able to covalently link three DNA strands with different lengths (19 mers, 36 mers and 41 mers) to the benzene core (see below).

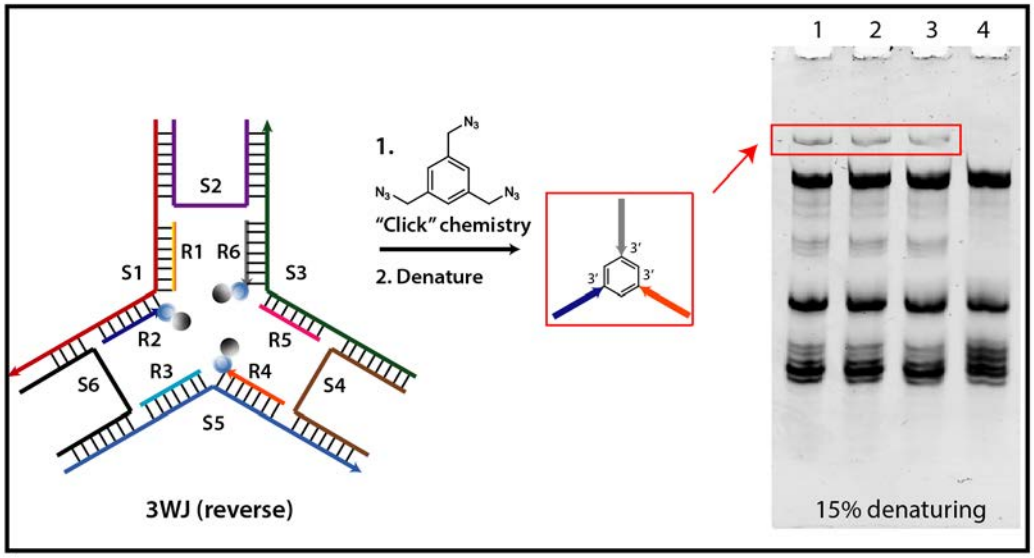

Figure 3.4 | Changing directionalities of DNAs in trimer. Lane 1: 3WJ reverse + triazide molecule (1:1 ratio), Lane 2: 3WJ (reverse)+ triazide molecule (1:3 ratio), lane 3: 3WJ (reverse) + triazide molecule (1:8 ratio) and lane 4: 3WJ (reverse) (control).

3.3.4. Expanding the scope to 4-arm molecule

To broaden the scope of this approach, we examined the transfer of four unique DNA strands onto a flexible tetraazide-functionalized molecule. We hybridized 4 reactive strands (*three of them having alkynes at their 5'-ends and 1 of them having an alkyne at its 3'-end*) and 2 rigidifying strands to the 3WJ (**Figure 3.5a**). The denaturing gel in **Figure 3.5b** reveals the formation of the tetramer product **(4x)** with an efficiency of 26%. Similar to **3x**, the sequential decrease in mobility shift when hybridizing to its complementary strands is shown in the native gel in **Figure 3.5c**, which confirms that **4x** indeed has 4 different strands grafted on the core. This approach thus offers full control over the number, sequences, and directionalities of the DNA strands transferred to the small molecule core.

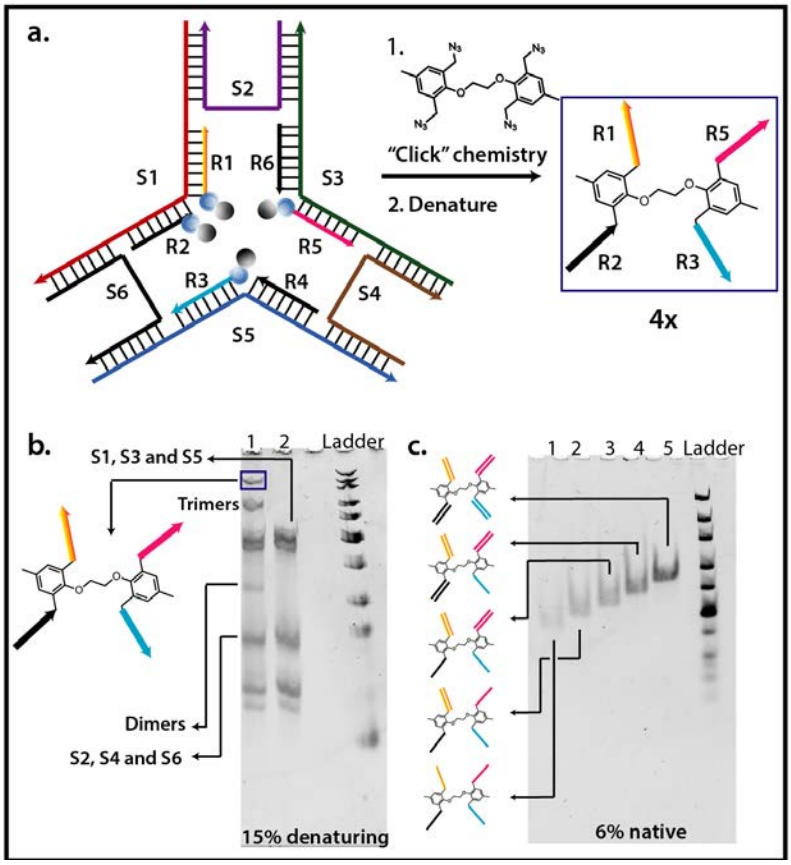

Figure 3.5 | Pattern transfer to 4-arm molecule. **a.** Schematic representation of the process to tetra-azide molecule **b.** 15% denaturing gel for the tetramer formation. Lane 1: crude reaction mixture between 3WJ and tetra-azide molecule. Lane 2: 3WJ control. **c**. 6% native gel show the process of adding complementary strands to the tetramer.

3.3.5. Effect of linker length on the transfer process

We were then interested in studying the effect of linker length, connecting the DNA portion to the alkyne moiety, on the efficacy of the transferring process. Interestingly, we observed that the trimer formation efficiency significantly decreased to 7% and 17%, by shortening the 12-carbon linker to a 3-carbon and 6-carbon spacer, respectively. When we completely removed the organic spacer and connected the DNA strand directly to the alkyne monomer, there was no trimer formation observed **(Figure 3.6)**. We hypothesized that the length of the spacer plays a critical

role in bringing the alkyne groups near the azides on the small molecule that will be investigated using molecular simulation in the next section.

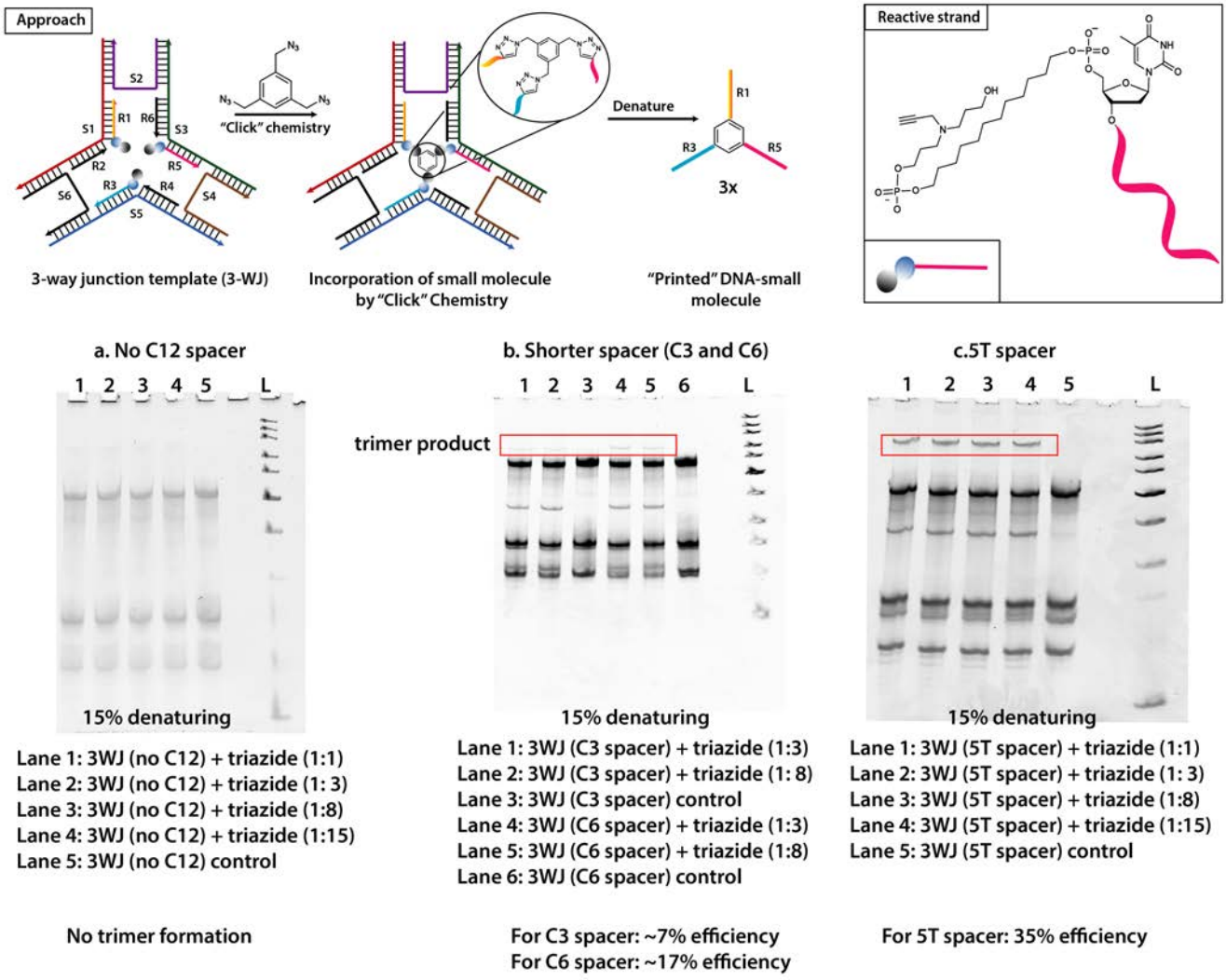

Figure 3.6 | Effect of linker length on the trimer formation.

3.3.6. Molecular dynamics simulations of the 3WJ

Molecular dynamics **(MD)** simulations of the 3WJ (**Figure 3.7**) were performed by Chenyi Liao and Jianing Li at the University of Vermont to gain insight into the molecular level and validate our hypothesis on the spacer length. To understand the regulation of the reactive strands

in the junction to the final small-molecule products, we simulated the 3WJ consisting three reactive-strand models:

1) the C12 spacer (~18 Å) connecting the DNA and the alkyne modifier;
2) without the C12 linker; and
3) a longer spacer consisting of 5 thymine bases (~24.5 Å).

The simulations show that the length of the spacer indeed affects the inter-reactive strand distance towards the yield of products. Within 30 ns, there is at least one pair of reactive units on each strand within ~15 Å measured by nitrogen-nitrogen distance (in alkyne modifier) in the **C12** spacer system (Experimental Section **3.5.13**). In contrast, in the no-C12 spacer system, no reactive strands were found to maintain within 15 Å. When we replaced the C12 spacer with a longer 5-thymidine spacer, three reactive strands were able to reside closely together within ~15 Å. Thus, we predicted a spacer with length ~18 Å is essential to produce our desired products. In some cases, having a long organic linker is not highly desirable (e.g. in terms of flexibility and hydrophobicity). Based on our simulation results, we experimentally examined trimer formation by directly linking alkyne-functionalized DNA (no organic spacer) to the organic core. We substituted the C12 spacer with a 5-thymidine spacer and we observed the formation of the trimer with ~35% efficiency, which is slightly improved compared to that using 12-carbon linker **(Figure 3.6)**. These results demonstrate that the length of spacer is crucial for the process.

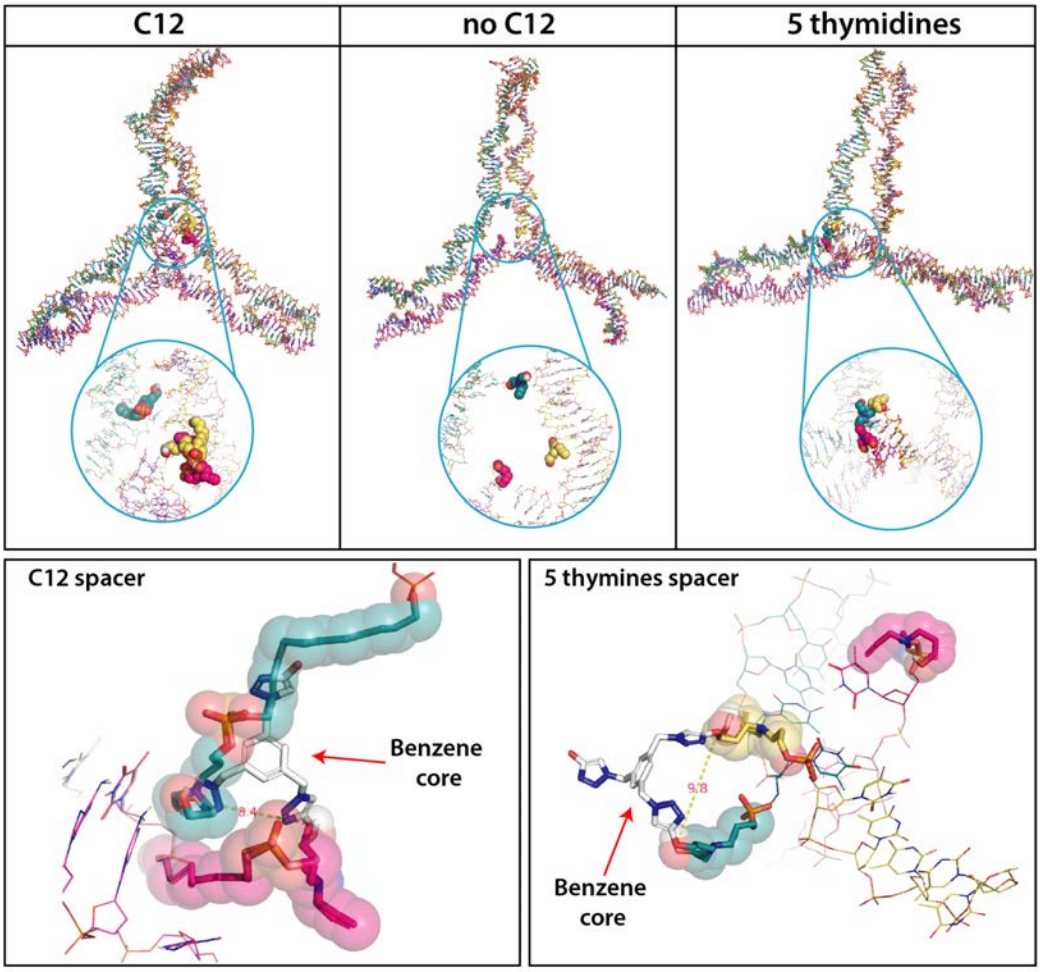

Figure 3.7 | MD simulations of the 3WJ. 3WJ models with 3 different reactive strands in the center with room-in top/side views on the right.

3.3.7. Expanding the approach to four-way junction (4WJ)

In the previous sections, we showed that by using a simple three-way junction (3WJ), tri- or tetra-azide functionalized small molecules can be "printed" with different DNA patterns with controllable DNA valency, directionality and sequences. However, in the case of tetra-azide small molecule, it was not possible to "print" all four strands having the same directionalities when using the 3WJ template, thereby potentially limiting the use of the DNA-imprinted small molecule in self-assembly. In order to address this issue, we expanded the scope of our approach to a four-way junction **(4WJ)** structure as it allows positioning of up to four reactive DNA strands with the same

directionalities in the middle of the junction. The 4WJ structure is an expanded version of the 3WJ, consisting of 8 scaffold strands (**S1** to **S8**) and 8 short strands in the middle of the junction (**R1** to **R8**) (**Figure 3.8**). Step-wise assembly revealed the formation of 4WJ with high efficiency (more than 90% assembly yield) (Experimental Section **3.5.14**).

As revealed in the MD simulation, the linker between the alkyne group and the DNA part plays a critical role in the transfer process. Based on our crude estimate on the geometry of the 4WJ compared to the previously used 3WJ, we hypothesized the linker should have approximately 18-carbon to 20-carbon in length in order to enable the process. Therefore, we first used a commercially available linker hexaethylene glycol (HEG) phosphoramidite in order to incorporate to alkyne-functionalized DNA strands. However, the formation of the desired tetramer was not observed in this case **(Figure 3.8b)**. We predicted that HEG linker might wrap around the cations presenting in solution in an 18-crown-6-like conformation, thus hindering the "printing" process. We then decided to move away from organic linkers and use 7-base linkers instead. Four alkyne-functionalized DNA strands were synthesized appending a random 7-base spacer **(sp7)**, namely **sp7-R1, sp7-R3**, **sp7-R5** and **sp7-R7**. **Figure 3.8c** showed the formation of tetramer **(4WJ-4x)** consisting of four unique DNA strands with the same directionalities (pointing the 5'-end towards the small molecule core). The efficiency of this process is comparable to the case of 3WJ. With the success of using 4WJ as a template, the method can potentially be realized with other multi-way junctions, provided the linker length is sufficient with respect to each geometry.

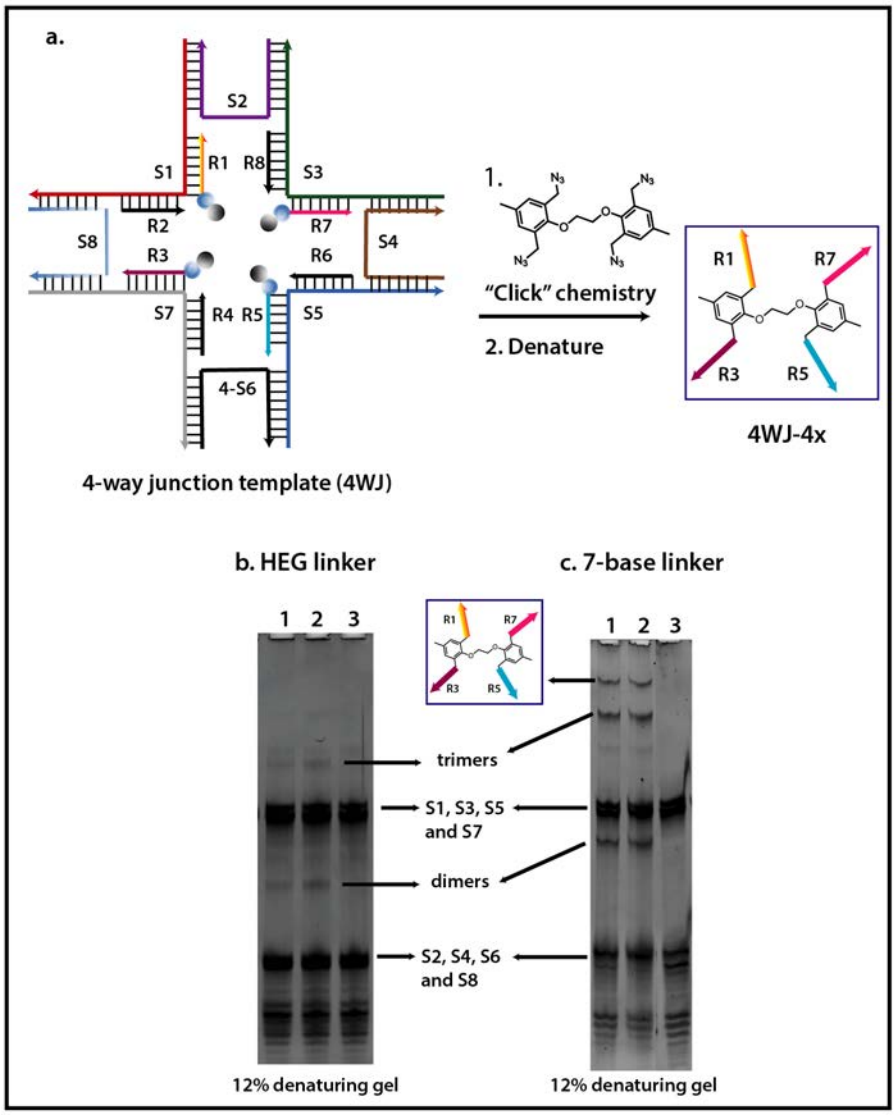

Figure 3.8 | Expanding the approach to 4WJ. a. Schematic representation of the approach using **4WJ. b.** Using HEG linker in reactive strands. **Lane 1:** 4WJ (HEG) + tetra-azide molecule (1:3 ratio). **Lane 2:** 4WJ (HEG) + tetra-azide molecule (1:8 ratio). **Lane 3**: 4WJ (HEG) **c.** Using 7-base linker in reactive strands. **Lane 1:** 4WJ (7-base) + tetra-azide molecule (1:3 ratio). **Lane 2**: 4WJ (7-base) + tetra-azide molecule (1:8 ratio). **Lane 3**: 4WJ (7-base).

3.3.8. Asymmetric elongation of DNA-imprinted small molecule's arms

Long strands of DNA with controlled sequences are of interest for a variety of applications including data storage, material organization and molecular electronics.[42-43] However, only up to

200 bases ssDNA can be practically synthesized using conventional solid-phase synthesis. One reliable method to amplify a DNA strand is by using PCR. Previously, the Bao group at Stanford University has demonstrated that DNA arms can be symmetrically elongated to micron-sized structures from different small molecule cores, but the asymmetrical elongation of DNA arms is still of a great challenge.[44-46] Asymmetric DNA elongation can significantly enhance the complexity and information content of a DNA-small molecule building block, that can potentially serve as a unique scaffold for DNA metalation and for organizing precisely different materials (e.g. quantum dots and/or gold nanoparticles).

In order to probe the utility of our method, we set out to elongate 2 arms (**R1** and **R3)** of the asymmetric trimer building block simultaneously to different lengths using PCR. The PCR experiment was performed by Daniel Saliba. Since our method enables the full control over the sequences and the lengths of the DNA strands grafted on the small molecule, we were able to synthesize a benzene core (called **trimer-2primers** – **Figure 3.9a**) connected to 3 different DNA arms: a 41-nucleotide **(nt)** arm containing a forward primer 1 (**R1-primer1**), a 36-nt arm containing a forward primer 2 (**R3-primer2**) and a 19-nt arm (**R5**). Two different long double-stranded DNA **(dsDNA)** were used as templates. One of the sequences was generated using "temporal growth", a process that was previously developed by our lab, while the other one was synthesized using standard phosphoramidite DNA synthesis.[42] Lane **7** in the agarose gel **(Figure 3.9c)** revealed the formation of the PCR desired product with a yield of 70-80% (3 repeats). Then, the band of interest was excised and further characterized by atomic force microscopy (AFM) under dry conditions. To facilitate visualization by AFM, we hybridized the third arm with an 82 bases double-stranded DNA (dsDNA). Unambiguously, the AFM images confirmed that the product has exactly three arms and each of them possesses a different length (**Figure 3.9b**). The length of the longest arm was measured to be 119.42 ± 9 nm (N=100), which is in accordance with the expected length of 120.70 nm. Similarly, the two other arms were measured with length of 45.66 ± 5.07 nm (N=100, theoretical length for 132 bp dsDNA is about 44.88 nm) and 28.40 ± 3.95 nm (N=100, theoretical length for 85 bp dsDNA is about 28.90 nm), respectively (see **Figure 3.26** for gel characterization). This is the first time a branched DNA-small molecule motif has been elongated asymmetrically using PCR.

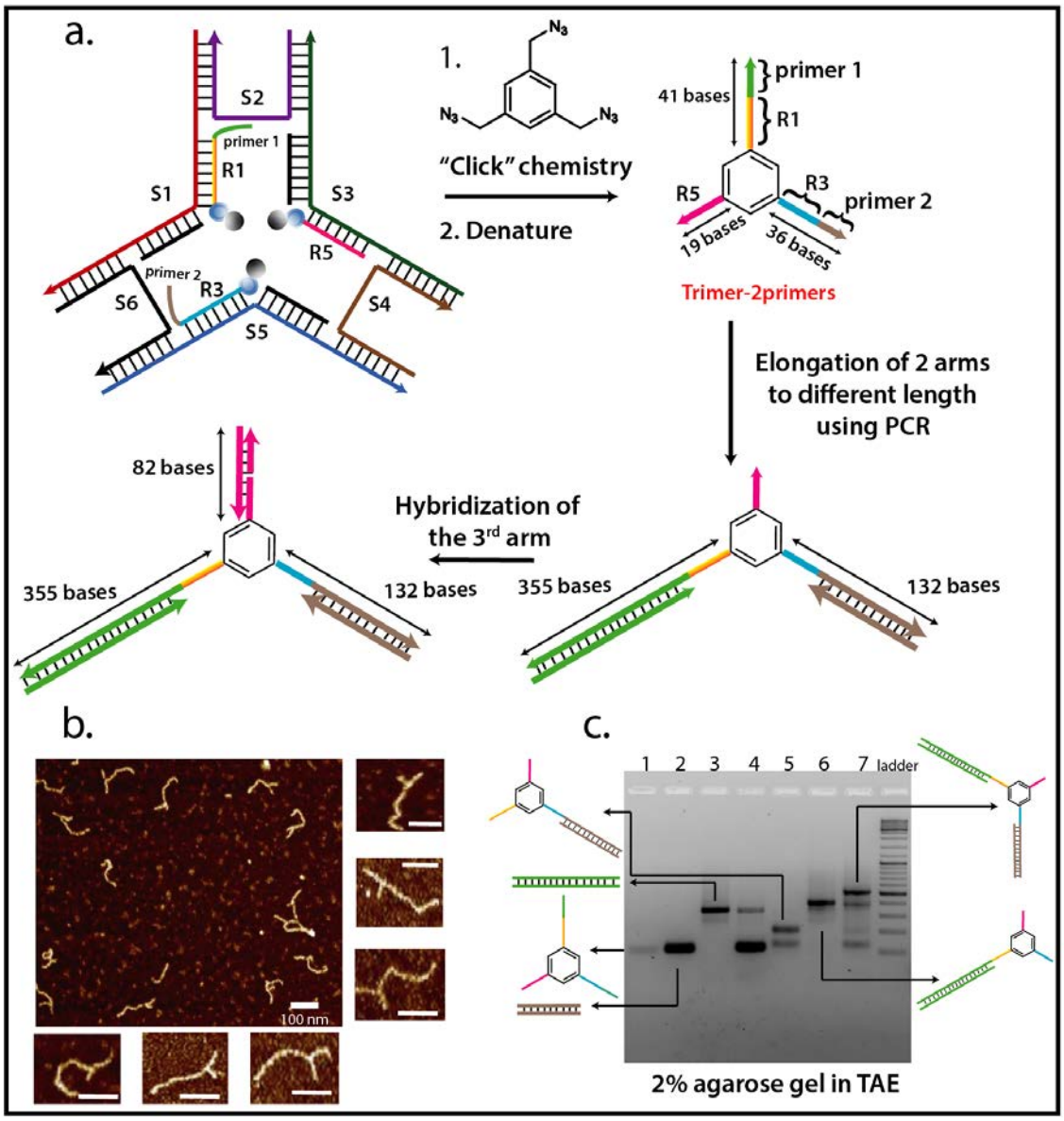

Figure 3.9 | Elongation of 2 arms in 3x simultaneously. a. Scheme for DNA arm elongation using PCR **b.** AFM images (in dry condition) confirm that the elongated trimer structure has exactly 3 arms of different lengths **c.** 2% agarose gel in TAE buffer confirms the elongation of the DNA trimer structure. **Lane 1:** trimer-2primers (control); **Lane 2:** PCR product of ssDNA (113 bases**); Lane 3**: PCR product of ssDNA (336 bases); **Lane 4:** PCR products of both ssDNA (113 bases) and ssDNA (336 bases) in the same mixture; **Lane 5:** Elongation of 1 arm in trimer to 132 bases in length; **Lane 6:** Elongation of 1 arm in trimer to 355 bases in length; **Lane 7**: Elongation of 2 arms simultaneously in trimer. Scale bar: 100 nm.

3.3.9. Elongated 3x as a platform for nanomaterial organization in 2D

Following the success of the simultaneous elongation of two different arms in the **3x** structure, we seek to extend the method to elongate three arms of **3x** simultaneously using PCR. It allows us to transform **3x** into a unique platform for selectively organizing nanomaterials. First, using the same approach, we were able to generate a trimer containing three forward primers (**trimer-3primers**). The **trimer-3primers** contains three unique DNA strands: a 42-nt arm having forward primer AB (**R1-ABprimer**), a 39-nt arm having forward primer CD (**R3-CDprimer**) and a 42-nt arm having forward primer EF (**R5-EFprimer**). 12% denaturing gel in **Figure 3.10c** revealed the formation of the trimer-3primers. The band of interest was excised and recovered by electroelution. Having the **trimer-3primers** in hand, we then performed PCR reactions on each arm. Similar to section **3.3.8**, three different dsDNA templates generated by the "temporal growth" method, namely **AB[10], CD[6]** and **EF[8],** were used (see the structure of strands below). Note that the **Pf** and **Pr** regions (each contains 21 nucleotides (nts)) are designed for forward and reverse primers to bind in subsequent PCR amplification reactions **(Figure 3.10a)**. The PCR experiments was performed by Daniel Saliba. 2% agarose gel electrophoresis **(AGE)** in TAE in **Figure 3.10d** showed the formation of the desired PCR product and the band was characterized further by AFM in air showing the PCR product has exactly three different arms with expected lengths. Since the arms are made of long double-stranded DNAs with more than 250 bases in length, they are expected to have a high degree of flexibility, which is undesirable in applications for nanomaterials organization.

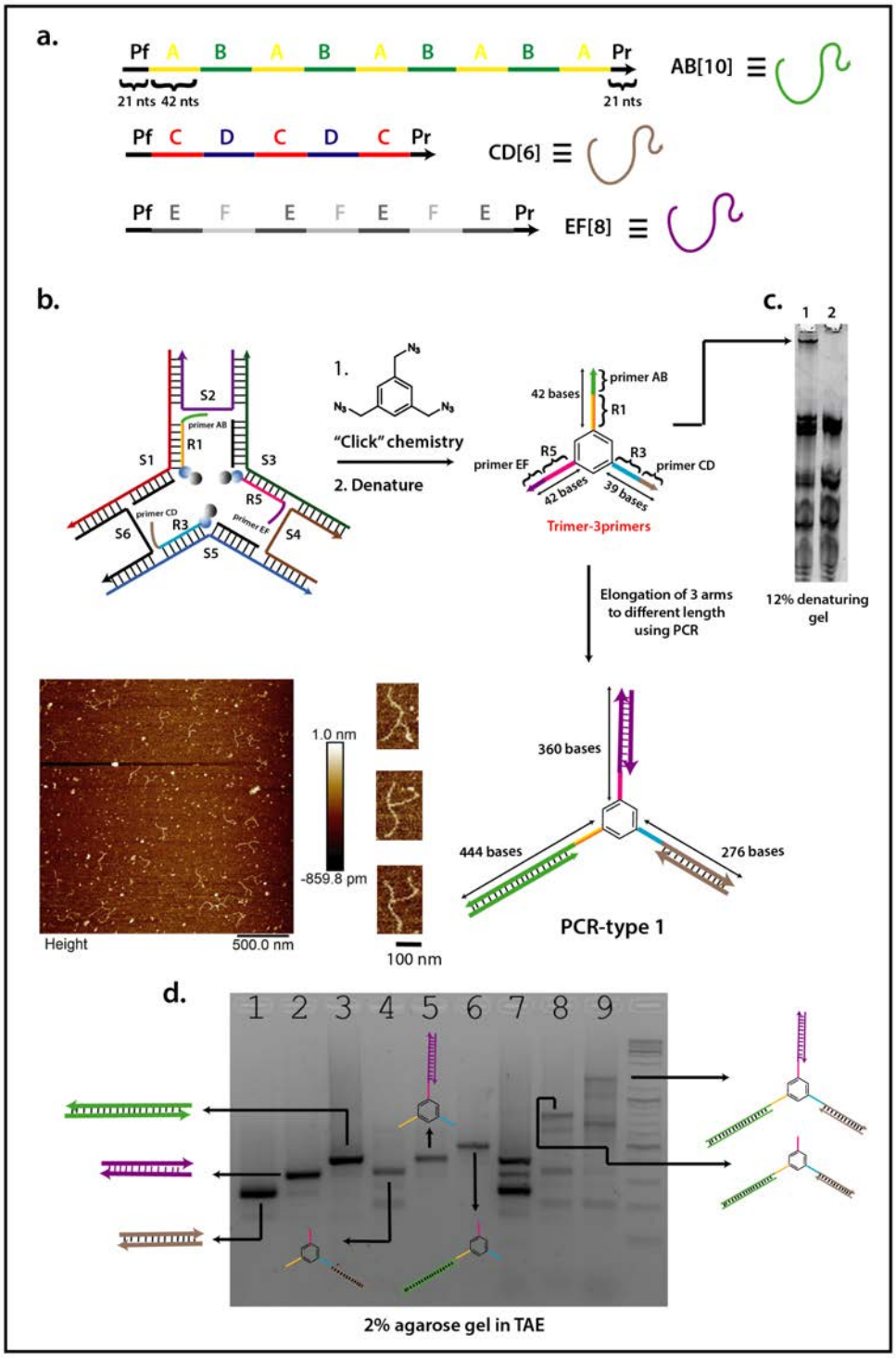

Figure 3.10 | Elongation of 3 arms simultaneously in 3x. a. Structures of "temporal growth" backbone, AB[10], CD[6] and EF[8] **b.** Schematic representation of trimer-3primers formation and the elongation of 3 arms in trimer-3primers to yield **PCR-type 1** structure **c.** 12% denaturing gel showed the formation of trimer-3primers**. Lane 1:** crude reaction mixture after adding triazide molecule to the **3WJ, lane 2: 3WJ**

control **d.** 2% agarose gel in TAE buffer showed the elongation of trimer-3primers structure. **Lane 1**: PCR product of single-stranded CD[6] (252 bp); **lane 2:** PCR product of single-stranded EF[8] (336 bp); lane 3: PCR product of single-stranded AB[10] (420 bp); **lane 4:** Elongation of 1 arm in trimer-3primers to 276 bases in length; **lane 5:** Elongation of 1 arm in trimer-3primers to 360 bases in length; **lane 6:** Elongation of 1 arm in trimer-3primers to 444 bases in length; **lane 7:** PCR products of a mixture of AB[10], CD[6] and EF[8]; **lane 8:** Elongation of 2 arms to 276 bases and 444 bases in length; **lane 9:** Elongation of 3 arms of trimer-3primers. Scale bar of zoom-in structure: 100 nm.

Therefore, we set out to rigidify each arm of the elongated **trimer-3primers** using DX tiles. DX tiles can offer geometric rigidity and stability and are estimated to be twice as stiff as normal duplexes. To do that, the double-stranded **PCR-type 1 (Figure 3.11)** product was first denatured to yield the single-stranded form with the use of a denaturing agarose gel. The single-stranded form of the **PCR-type 1** was then decorated DX tiles on each arm in order to provide rigidity. DX tiles was designed by the co-author Daniel Saliba. Undoubtedly, AFM images revealed that the arms of **PCR-type 2** structure are significantly more rigid than those in the **PCR-type 1** structure. We noticed that the structure of **PCR-type 2** still has single-stranded region right next to the benzene core (dashed circle region in **Figure 3.11b**) that might cause flexibility. Hence, we further rigidify the structure with DX tiles near the benzene core to yield **PCR-type 3** structure.

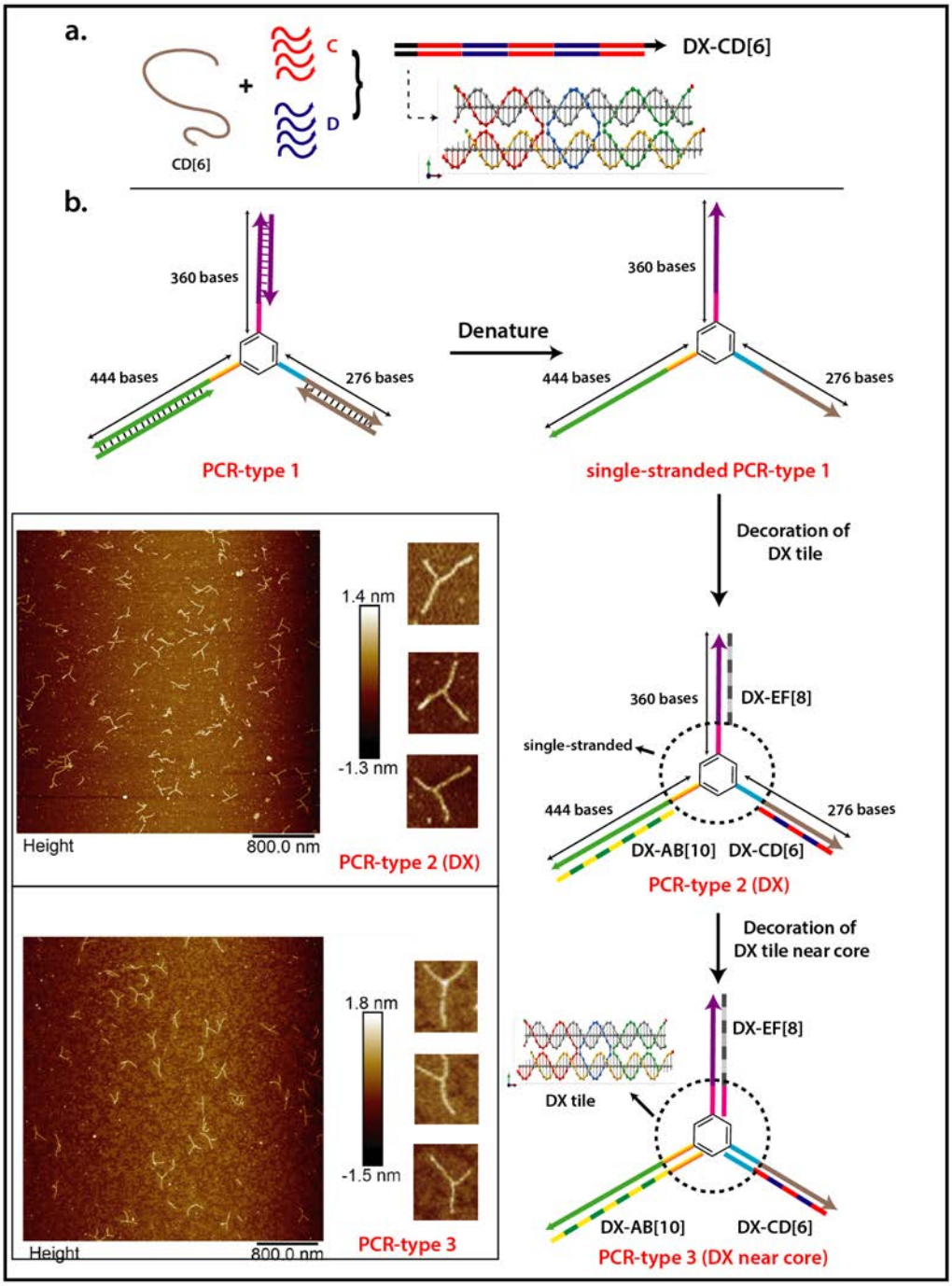

Figure 3.11 | Rigidifying the elongated structure. a. Scheme of DX decoration on a temporal growth backbone **b.** Denaturation of **PCR type 1** from double-stranded to single-stranded form and decoration of DX tiles on the elongated structure.

The arms of the **PCR-type 3** structure are relatively long and more importantly, they are completely unique and addressable. Such 2D structures are of great interest for templated nanowires, and as scaffold for protein arrays. As a proof of concept, we demonstrate the power of our approach in selective material organization on each arm of the elongated structure (**PCR-type 3)** using biotin-streptavidin interactions. Each individual arm consists of two different building blocks, which are components of a long repetitive template strand (e.g. A and B blocks on **AB [10]**, C and D blocks on **CD [6]** and E and F blocks on **EF [8]**). As such, they allow the selective functionalization of biotin molecules at the building block of interest without interfering with other blocks on different arms. **Figure 3.12a** demonstrates the positions of biotin molecules on each arm. For instance, if the C block is functionalized with biotin, it results in periodic biotin functionalization in all three C blocks on **DX-CD[6]** arm. Upon addition of streptavidin, elongated structures had three streptavidins precisely residing on the **DX-CD[6]** arm that can be observed clearly by AFM imaging with more than 90% yield **(Figure 3.12b)**. Similarly, AFM images showed that we were able to selectively pattern exactly four streptavidins on the **EF[8]** arm with the yield of 85% **(Figure 3.12c)**. We observed some crosslinked structure due to multiple binding sites of streptavidin molecules. The approach can be further expanded to aperiodic and periodic patterning nanomaterias within any elongated structures (e.g. 3-arm, 4-arm or even 5-arm molecule).

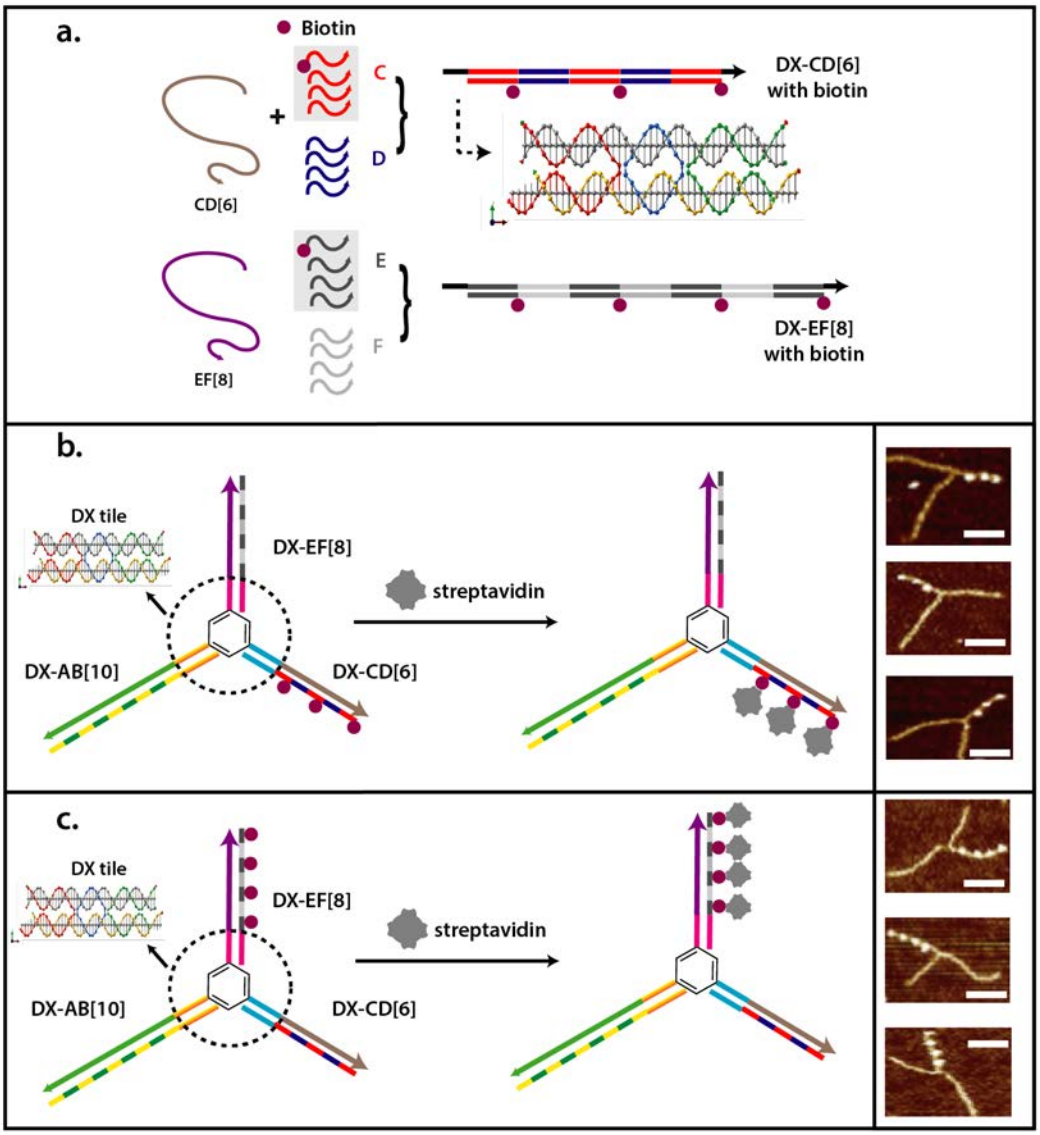

Figure 3.12 | Material organization on the DX-elongated structure. a. Functionalization of biotin moieties on "temporal growth" backbone **DX-CD[6]** and **DX-EF[8] b.** Decoration of streptavidin on the **DX-CD[6]** arm c. Decoration of streptavidin on the **DX-EF[8]** arm. Scale bar: 100 nm.

3.3.10. Chemical copying of the DNA-imprinted small molecule

DNA is one of the most classical examples of self-replication - the ability to make its own copies in nature. This concept has been recently transferred from living cells to DNA

nanotechnology to replicate DNA tiles and DNA origami rafts.[47-48] Working towards this path may solve the problem of DNA structure scalability. Therefore, we would like to see if our asymmetric branched trimer structure (**trimer-2primers** in **Figure 3.13**) can serve as a mother template to produce daughter generations chemically. Previously, von Kiedrowski *et al.* introduced this concept using a symmetrical junction.[49] First, we hybridized alkyne-functionalized **T2-R1comp, T3-R3comp** and **T4-R5comp** to the "mother" template (**trimer-2primers**), followed by the addition of the triazide molecule. After denaturation, the "daughter" structure, characterized by a higher mobility shift, was formed (**Figure 3.13b**-lane **1**), and the biotinylated "mother" template was recovered using streptavidin-functionalized magnetic beads. The product appeared as a tight band by gel electrophoresis, suggesting that a single trimer product was formed with a yield exceeding 90% (**Figure 3.13b**-lane **3**). Control experiments in the absence of the template under the same reaction conditions showed no branched trimer formation **(Figure 3.13b** – lane **2**). In addition, after 3 rounds of replication **(Figure 3.13a)**, the daughter was amplified 3 times more than the amount produced in a single cycle (Experimental Section **3.5.13)**.

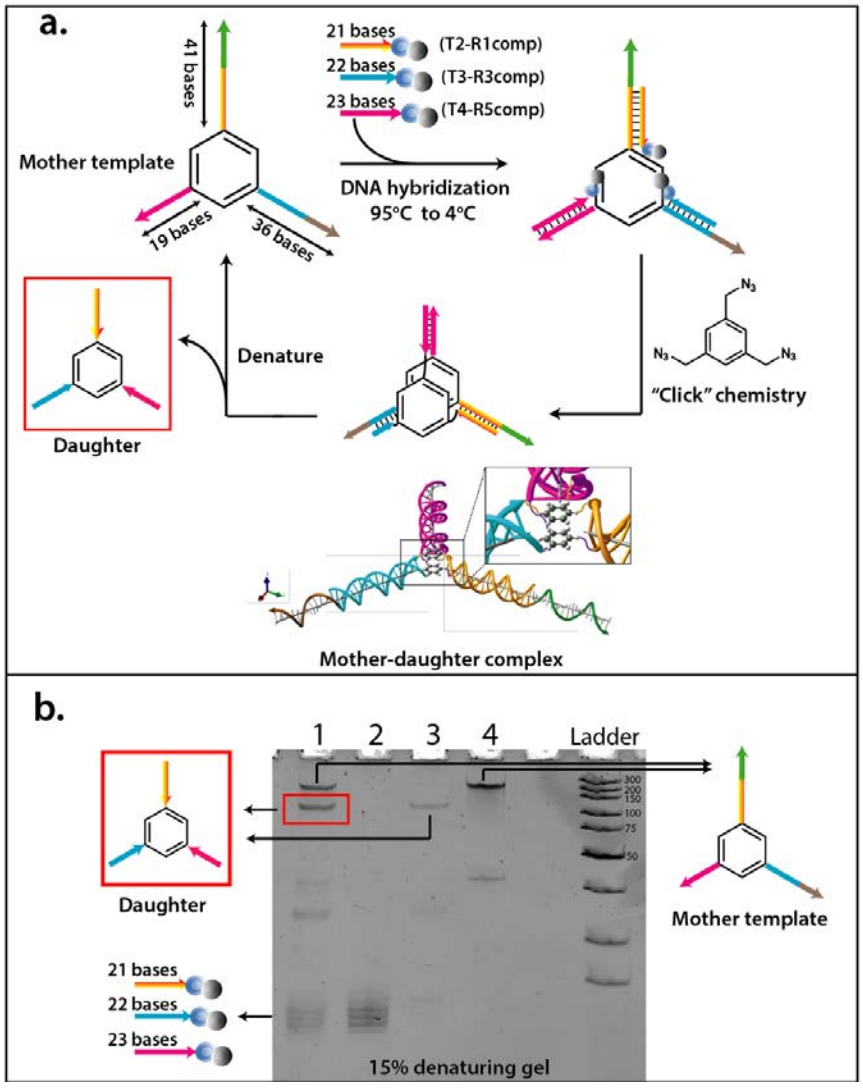

Figure 3.13 | a. Making a copy from mother template (**trimer-2primers**) **b.** denaturing PAGE monitors the process. **Lane 1**: crude reaction mixture containing mother template, daughter, excess complementary ssDNA. **Lane 2:** control sample prepared under the same reaction condition without the mother template. **Lane 3:** reaction mixture after removing mother template and excess ssDNA complementary using streptavidin- magnetic bead. **Lane 4:** mother template **(trimer-2primers)** (control).

3.4. Conclusion

Overall, this chapter demonstrated a facile method to transfer different DNA strands onto a small molecule core with controllable valency, DNA directionalities and sequences. While we

initially used a 12-carbon spacer, we showed using MD simulations and experiments that DNA strands can be directly attached to the core. The DNA-imprinted small molecule can be extended asymmetrically using PCR and it can be chemically self-replicated to make a daughter generation. The ease with which multivalent DNA-small molecule hybrids can be synthesized and purified will make them useful in the field of DNA nanotechnology as building blocks for wireframe DNA nanoobjects, branching staple strands in DNA origami and tunable templates for material organization. By blending together DNA with synthetic molecules, DNA nanotechnology can acquire new structural motifs and can impart functionality to its typically passive DNA structures.

3.5. Experimental Section

3.5.1. General

Unless otherwise stated, all commercial reagents and solvents were used without additional purification. Magnesium sulfate hexahydrate (**$MgSO_4 \cdot 6H_2O$**), tris(hydroxymethyl)aminomethane (Tris), urea, dimethyl sulfoxide (**DMSO**), copper (II) sulfate **($CuSO_4$)**, Tris(3-hydroxypropyltriazolylmethyl) amine (**THPTA**) were used as purchased from Sigma-Aldrich. Glacial acetic acid and boric acid were purchased from Fisher Scientific. GelRed™ nucleic acid stain was purchased from Biotium Inc. Acrylamide/Bis-acrylamide (40% 19:1 solution), ammonium persulfate and tetramethylenediamine were obtained from Bioshop Canada Inc. and used as supplied. 1 μmol Universal 1000Å LCAA-CPG supports and standard reagents used for automated DNA synthesis were purchased through Bioautomation. Sephadex G-25 (super fine, DNA grade) was purchased from Glen Research. DMT-1,12-dodecane-diol (HE, cat. # CLP-1114) was purchased from ChemGenes Corporation. Spacer phosphoramidite C3 and spacer phosphoramidite C6 and 5'-Hexynyl phosophoramidite were purchased from Glen Research Corporation. TAMg buffer is composed of 45 mM Tris and 12.5 mM $MgCl_2.6H_2O$ with the pH adjusted to 8.0 using glacial acetic acid. TBE buffer is 90 mM Tris, 90 mM boric acid and 2 mM EDTA with a pH of 8.0. TEAA mobile phase is 50 mM triethylammonium acetate with the pH adjusted to 8.0 using glacial acetic acid.

3.5.2. Instrumentation

Standard automated oligonucleotide solid-phase synthesis was performed on a Mermade MM6 synthesizer from Bioautomation. HPLC purification was carried out on an Agilent Infinity 1260. DNA quantification measurements were performed by UV absorbance with a NanoDrop Lite spectrophotometer from Thermo Scientific. Gel electrophoresis experiments were carried out on a 20x20 cm vertical Hoefer 600 electrophoresis unit. Gel images were captured using a ChemiDocTM MP System from Bio-Rad Laboratories. Thermal annealing of all DNA structures was conducted using an Eppendorf Mastercycler® 96 well thermocycler. Electroelution employed an Elutrap Electroelution System from Whatman®. Liquid Chromatography Electrospray Ionization Mass Spectrometry (LC-ESI-MS) was carried out using Dionex Ultimate 3000 coupled to a Bruker MaXis Impact™ QTOF. Gels were imaged by BioRad ChemiDoc MP. Multimode 3 scanning probe microscope and Nanoscope V controller (Bruker, Santa Barbara, CA) was used to acquire AFM images.

3.5.3. Synthesis, Purification of DNA strands

DNA synthesis was performed on a 1 μmol scale, starting from the required nucleotide modified 1000 Å LCAA-CPG solid-support. Coupling efficiency was monitored after removal of the dimethoxytrityl (DMT) 5'-OH protecting groups. Coupling efficiency was monitored by the removal of DMT group on 5'-OH groups.

- **For alkyne-functionalized DNA**: In order to couple modified monomers, in a glove box under nitrogen atmosphere, DMT-dodecane-diol and alkyne phosphoramidite were separately dissolved in acetonitrile and shaken for 10 mins to achieve final concentration of 0.1 M. The DMT-dodecane-diol amidite, was activated with 0.25 M 5-(ethylthio)tetrazole in anhydrous acetonitrile and the extended coupling times of 10 minutes were used. 3% dichloroacetic acid in dichloromethane was used to remove DMT protecting group on the DNA synthesizer. After the synthesis was completed, CPG was treated with 28% aqueous ammonium hydroxide solution for 16-18 hours at 60°C in water bath. The crude mixture then was concentrated under reduced pressure at 60°C and filtered by 0.22 μm centrifugal filter before purifying by RP-HPLC (3-30% ACN in 50 mins).

- **For DNA template strand (S1-S6)**: DNA was synthesized using Mermade MM6 DNA synthesizer. Coupling efficiency was monitored after removal of the DMT 5-OH protecting group. After deprotection step using aqueous NH_4OH solution (28%), the crude product was isolated, dried, and re-suspended in 1:1 8 M urea before loading to polyacrylamide/urea gel (15% denaturing PAGE). The gel was run at 250 V for 30 minutes followed by 500 V for 45-60 minutes in 1x TBE as the running buffer. The gel was then imaged and excised on TLC plate under a UV lamp. The solution was dried to approximately 1 mL before loading to Sephadex G-25 column. The purified DNA was quantified by the absorbance at 260 nm.

3.5.4. DNA Sequences for 3-way Junction

Sequences are listed from **5'** to **3'** (**Alk** = alkyne-modified phosphoramidite, **HE** = 1,12-dodecanediol phosphoramidite). All clip strands were synthesized using Mermade MM6 on 1 μmol scale and purified by 15% denaturing PAGE.

Name	Sequence (5' → 3')
W1AB (S1)	AAATCTCGAACACA TTTATATGGTCAACTGAAAAA AAAAAGTAATACCAGATGGTT CTAGTCGGCACTTC
W2HE (S3)	TTAACCGGCGGCCT TTTCTTCTATACTGGCAAAAA AAAAACAGGATTAGCAGAGTT ACAACCAATGGCTT
W3DI (S5)	AGATAGTGTACCGC TTTGGCCTTGGTCCATAAAAA AAAAAACCGCGACTGCGAGTT TGCGCCACACCGTA
D1 (S2)	GAAGTGCCGACTAG AGGCCGCCGGTTAA
D2 (S4)	AAGCCATTGGTTGT GCGGTACACTATCT
D3 (S6)	TACGGTGTGGCGCA TGTGTTCGAGATTT
Alk-HE-AT (R1)	Alkyne-HE-TTTTTCAGTTGACCATATA
Alk-HE-DT (R3)	Alkyne-HE-TTTTTATGGACCAAGGCCA
Alk-HE-HT (R5)	Alkyne-HE-TTTTTGCCAGTATAGAAGA
TB-HE-Alk(R2)	CCATCTGGTATTACTTTTT-HE-Alkyne

TE-HE-Alk(R6)	TCTGCTAATCCTGTTTTT-HE-Alkyne
TI-HE-Alk(R4)	CGCAGTCGCGGTTTTTT-HE-Alkyne
Alk-HE-Primer1-AT (primer1-R1)	Alkyne- HE-TTTTTCAGTTGACCATATAACCAGTCTAGATGTGCTATTCT
Alk-HE-Primer2-DT (primer2-R3)	Alkyne-HE-TTTTTATGGACCAAGGCCATATTTAACGCCGCCGTC

Non-modified DNA (e.g. **AT (R1), DT (R3), HT (R5), TB (R2), TE (R6), TI (R4)**) were obtained from IDT (standard desalting) and used directly for assembly experiment without further purification.

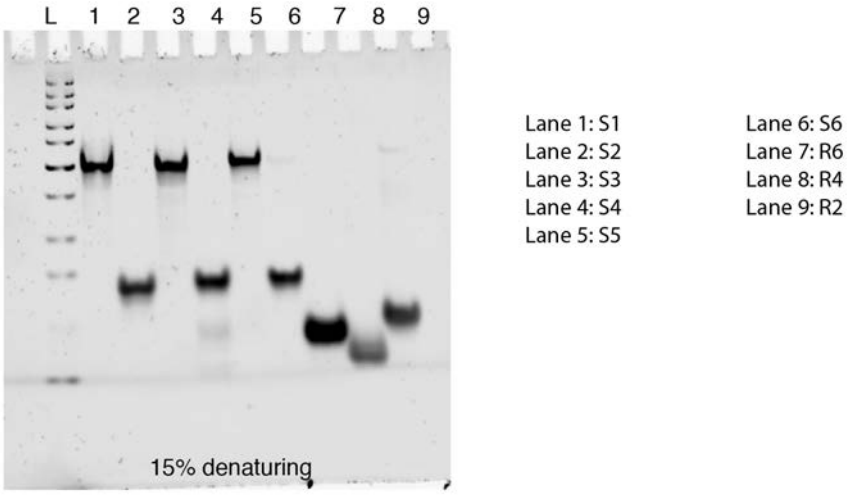

Figure 3.14 | Gel characterization of 3WJ strands.

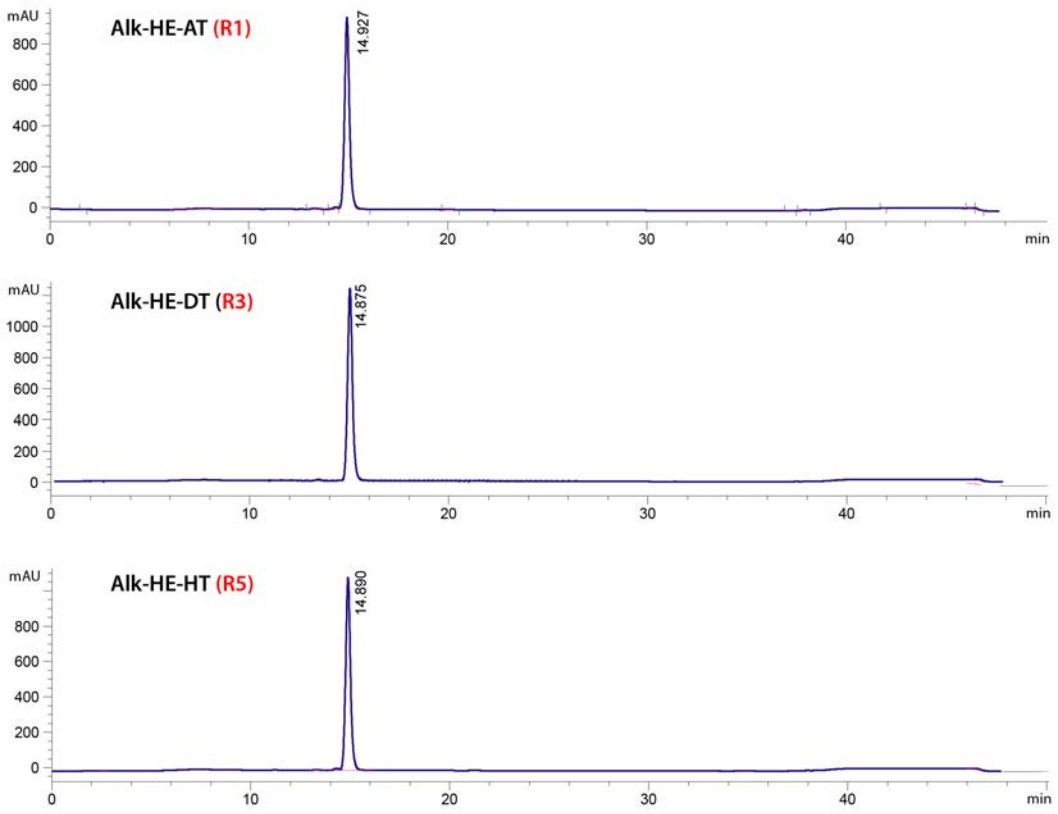

Figure 3.15 | HPLC characterization of all reacting strands

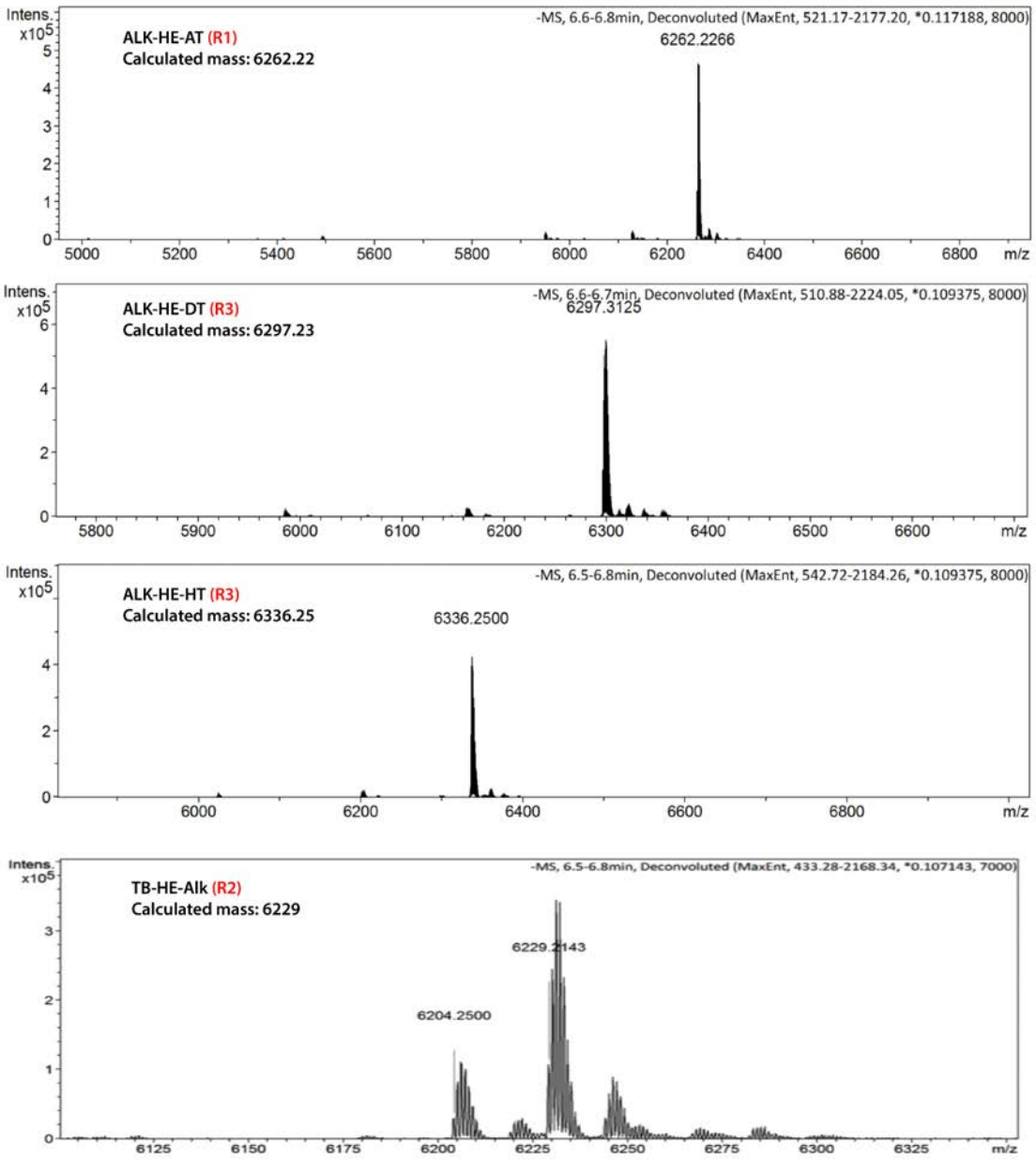

Figure 3.16 | MS characterization of all reacting strands.

3.5.5. DNA Sequences for Temporal Growth and PCR Experiment

Name	Sequence (5' → 3')
A1P	AGGTTAGTGGCGATCAGAAGAAATCTGGCTGCGCTTGAAACAACGGAAG GTCATGCTTTAGGA
A2P	TGACCTTCCGTTGTTTCAAGCGCAGCCAGATTTCTTCTGATCGCCACTAA CCT
B1P	AATCTGGCTGCGCTTGAAACAACGGAAGGTCATGCTTTAGGAGAATAGC ACATCTAGACTGGT
B2P	ACCAGTCTAGATGTGCTATTCTCCTAAAGCATGACCTTCCGTTGTTTCAA GCGCAGCCAGATTTCTTCTGATC
A1	AATCTGGCTGCGCTTGAAACAACGGAAGGTCATGCTTTAGGA
A2	TGACCTTCCGTTGTTTCAAGCGCAGCCAGATTTCTTCTGATC
B1	ATCAAACCAAAGTTCAGCAACAGGCCGTTAAGGATCAGAAGA
B2	CTTAACGGCCTGTTGCTGAACTTTGGTTTGATTCCTAAAGCA
ss8AB	AGGTTAGTGGCGATCAGAAGAAATCTGGCTGCGCTTGAAACAACGGAAGGTC ATGCTTTAGGAATCAAACCAAAGTTCAGCAACAGGCCGTTAAGGATCAGAAG AAATCTGGCTGCGCTTGAAACAACGGAAGGTCATGCTTTAGGAATCAAACCA AAGTTCAGCAACAGGCCGTTAAGGATCAGAAGAAATCTGGCTGCGCTTGAAA CAACGGAAGGTCATGCTTTAGGAATCAAACCAAAGTTCAGCAACAGGCCGTT AAGGATCAGAAGAAATCTGGCTGCGCTTGAAACAACGGAAGGTCATGCTTTA GGAGAATAGCACATCTAGACTGGT
ss8AB comp	ACCAGTCTAGATGTGCTATTCTCCTAAAGCATGACCTTCCGTTGTTTCAAGCGC AGCCAGATTTCTTCTGATCCTTAACGGCCTGTTGCTGAACTTTGGTTTGATTCC TAAAGCATGACCTTCCGTTGTTTCAAGCGCAGCCAGATTTCTTCTGATCCTTAA CGGCCTGTTGCTGAACTTTGGTTTGATTCCTAAAGCATGACCTTCCGTTGTTTC AAGCGCAGCCAGATTTCTTCTGATCCTTAACGGCCTGTTGCTGAACTTTGGTTT GATTCCTAAAGCATGACCTTCCGTTGTTTCAAGCGCAGCCAGATTTCTTCTGAT CGCCACTAACCT
V	CTCAGCAGCGAAAAACCGCTTTACCACATTCGAGGCACGTTGTACGTCCACAC TTGGAACCTCATCGCACATCCGCCTGCCACGCTCTTAGCATAGGACGGCGGCG TTAAATA

Vcomp	TATTTAACGCCGCCGTCCTATGCTAAGAGCGTGGCAGGCGGATGTGCGATGAG GTTCCAAGTGTGGACGTACAACGTGCCTCGAATGTGGTAAAGCGGTTTTTCGC TGCTGAG
M	GCGTACTCGTTATCACGAACATAAGATATTATGCTTCCGACTGATCTCTGTGTC GGCAGACTTCTTCTATACTGGCAAAAA
Mcomp	AGTCTGCCGACACAGAGATCAGTCGGAAGCATAATATCTTATGTTCGTGAT AACGAGTACGC
Forward primer V	CTCAGCAGCGAAAAACC
Reverse Primer V	TATTTAACGCCGCCGTC
Forward primer [ds8]	AGGTTAGTGGCGATCAGA
Reverse primer [ds8]	ACCAGTCTAGATGTGCTATTCT

3.5.6. Mass spectroscopy characterization of trimer and tetramer structure

- Trimer structure has 3 different DNA strands, namely **R1, R3** and **R5**.

Calculated mass: 19138.88

Found mass: 19147.8184

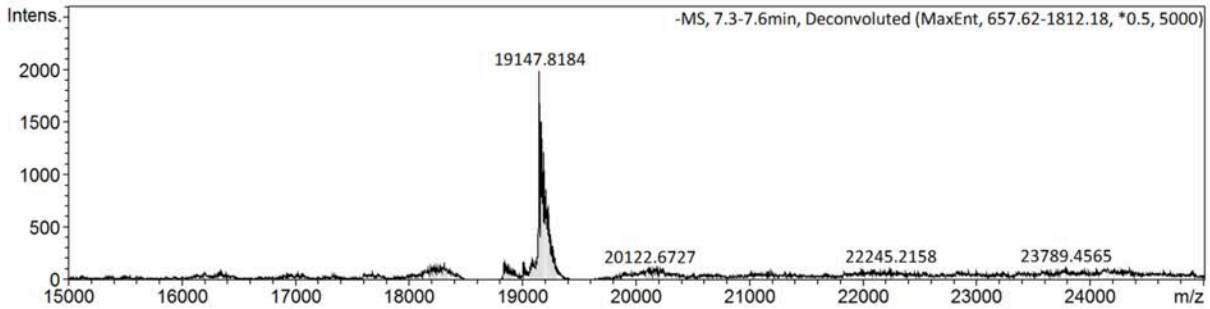

Figure 3.17 | MS result of trimer structure containing R1, R3 and R5

- Tetramer structure has 4 different DNA strands, namely **R1, R3, R5** and **R2**

Calculate mass: 25587.1688

Found mass: 25599.1157

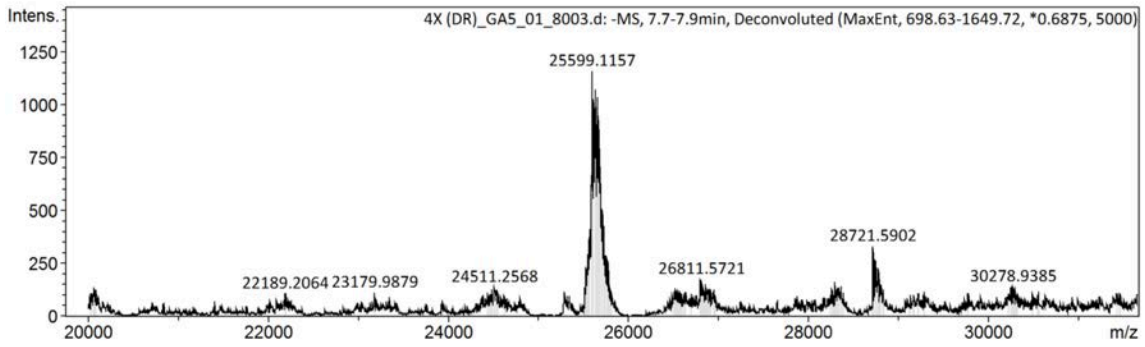

Figure 3.18 | MS result of tetramer structure containing R1, R3, R5 and R2.

3.5.7. Synthesis of tetraazide molecule core (performed by the co-author Alexander L. Prinzen)

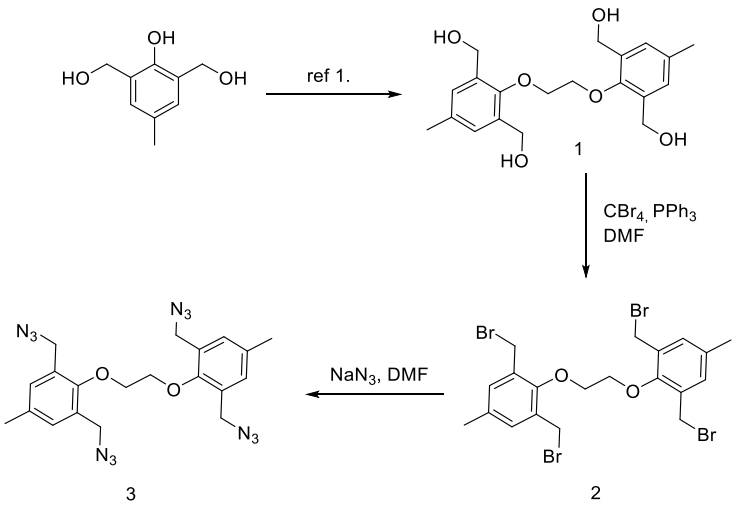

Compound 2

Compound **1** (500 mg, 1.38 mmol) was dissolved in DMF (20 ml) and the solution cooled to 0ºC. CBr_4 (3.7 g, 11.03 mmol) was then added, followed by the addition of PPh_3 (2.90 g, 11.03 mmol). The reaction mixture was allowed to warm to room temperature and stirred for 24 hours. The solution was then diluted with H_2O (100ml) and extracted with ethyl acetate (3 x 100 ml). The collected organic phase was then washed with 1M HCl (200 ml), saturated $NaHCO_3$ (200 ml), and saturated NaCl (200 ml). The organic phase was then dried on $MgSO_4$, filtered and concentrated *in vacuo*. The collected oil was then purified by column chromatography (EtOAc/Hex 5:95) to give compound **2** (550 mg, 65%). Characterization matched literature.

Compound 3

Compound 2 (500 mg, 0.81 mmol) was dissolved in DMF (10 ml). NaN_3 (850 mg, 13.07 mmol) was then added, and the solution was heated to 60ºC for 24 hours. The solution was then cooled to room temperature and diluted with H_2O (100 ml). This mixture was then extracted with ethyl acetate (3 x 100ml). The organic phase was then combined and washed with, 1M HCl (200 ml), saturated $NaHCO_3$ (200 ml), and saturated NaCl (200 ml). The organic phase was then dried on $MgSO_4$, filtered and concentrated *in vacuo*. No further purification was required resulting in compound 3 (75 mg, 20%). **^{1}H NMR (500 MHz, $CDCl_3$)**: δ = 7.17 (s, 4H), 4.47 (s, 8H), 4.22 (s, 4H), 2.37 (s, 6H) **^{13}C NMR (125 MHz, $CDCl_3$)**: δ = 153.1, 134.9, 131.5, 129.3, 74.3, 49.6, 20.9. **HRMS (EI):** calc. for $[C_{20}H_{22}N_{12}NaO_2]^+$ $[M]^+$: 485.1881 found 485.1877

Reference: Richards, T. I.; Layden, K.; Warminski, E. E.; Milburn, P. J.; Haslam, E., The shikimate pathway. Part 7. Chorismate mutase: towards an enzyme model. *Journal of the Chemical Society, Perkin Transactions 1* **1987,** (0), 2765-2773

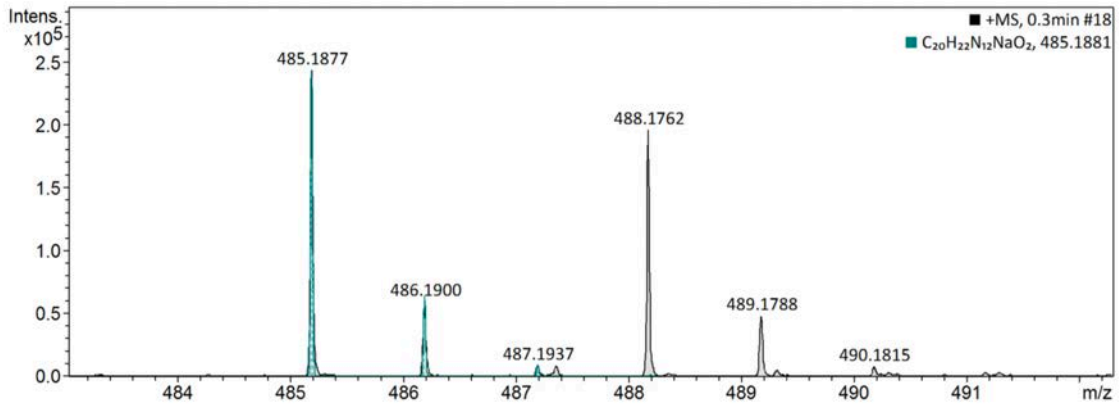

Figure 3.19 | ESI-MS of tetraazide small molecule.

3.5.8. Procedure for trimer/tetramer construction

The 3-way junction (**3WJ)** was assembled using 6 strands (**W1AB, W2HE, W3DI, D1, D2** and **D3**) in 1xTAMg at final concentration 1μM. Then, 1.25 times excess of each single alkyne-functionalized strand (i.e. **R1, R3** and **R5**) and each of ssDNA (**R2, R4** and **R6**) was added to the mixture. The mixture was annealed from 95ºC to 4ºC over 4 hours followed by the addition of triazide small molecule in DMSO (**24mM** final), **$CuSO_4$/THPTA** solution in H_2O (**6mM** as final concentration) and Na-ascobate (**6mM** as final concentration). At least a solution of 5:1 **THPTA:$CuSO_4$** was made, in order to prevent the degradation of DNA. The reaction mixture was stirred RT for 2 hours before being analyzed by denaturing gel.

3.5.9. Control experiment of trimer formation

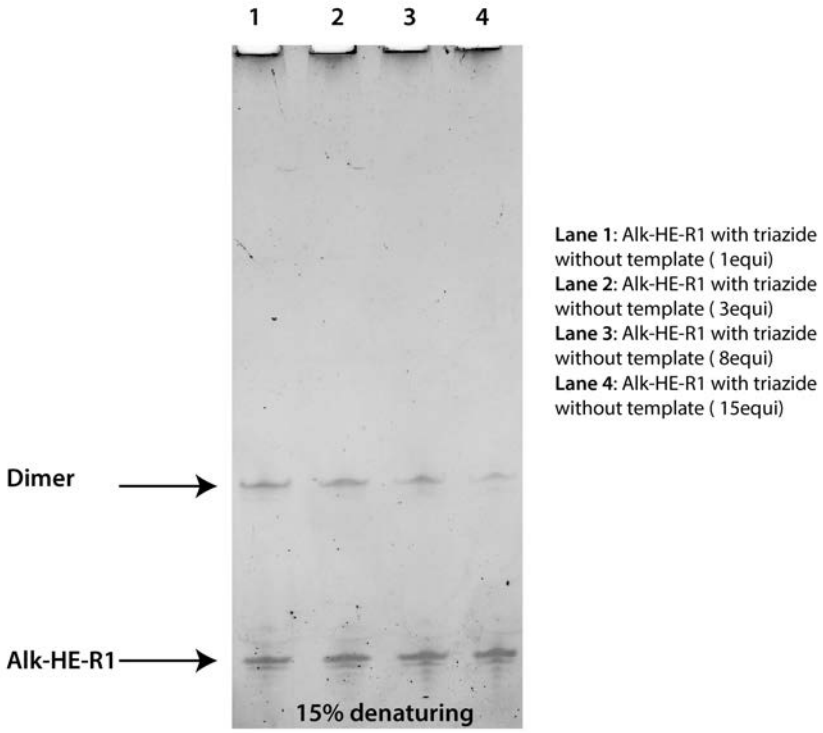

Figure 3.20 | Control experiment of trimer formation without 3WJ template.

3.5.10. Synthesis of trimers incorporating primers

We incorporated DNA strands having primers in three different **3WJ** versions. All versions of **3WJ** were assembled as above and annealed from 95ºC to 4ºC over 4 hours in 1xTAMg buffer. There are three of them:

1) **3WJ (R1-primer1)** having three alkyne-functionalized strands, namely **Alkyne-HE-R1-primer1, Alkyne-HE-R3 and Alkyne-HE-R5.**

2) **3WJ (R3-primer2)** having three alkyne-functionalized strands, namely **Alkyne-HE-R1, Alkyne-HE-R3-primer2 and Alkyne-HE-R5.**

3) **3WJ (2 primers)** having three alkyne-functionalized strands, namely **Alkyne-HE-R1-primer1, Alkyne-HE-R3-primer2 and Alkyne-HE-R5.**

After the **3WJs** were formed, triazide small molecule was added in the presence of Cu^{2+} catalyst as describe above at room temperature for 2 hours before being analyzed by denaturing gel.

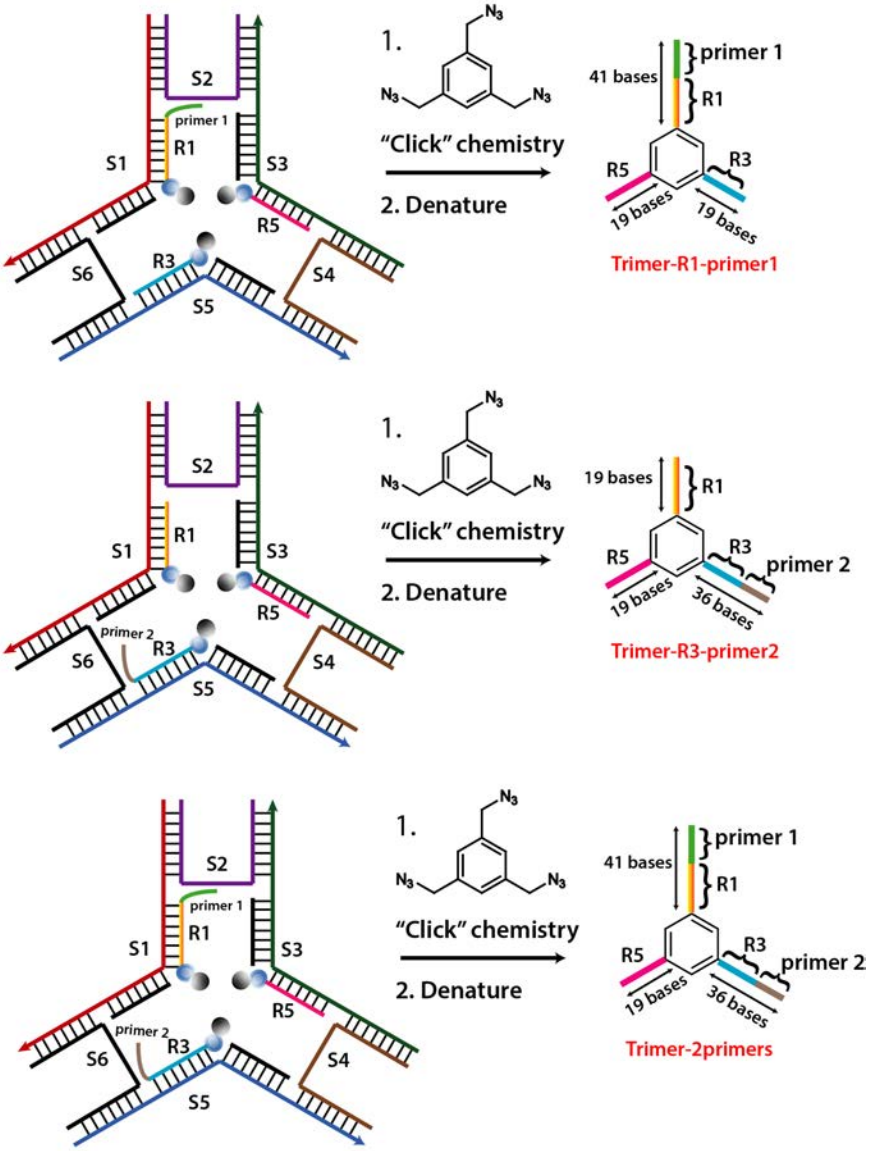

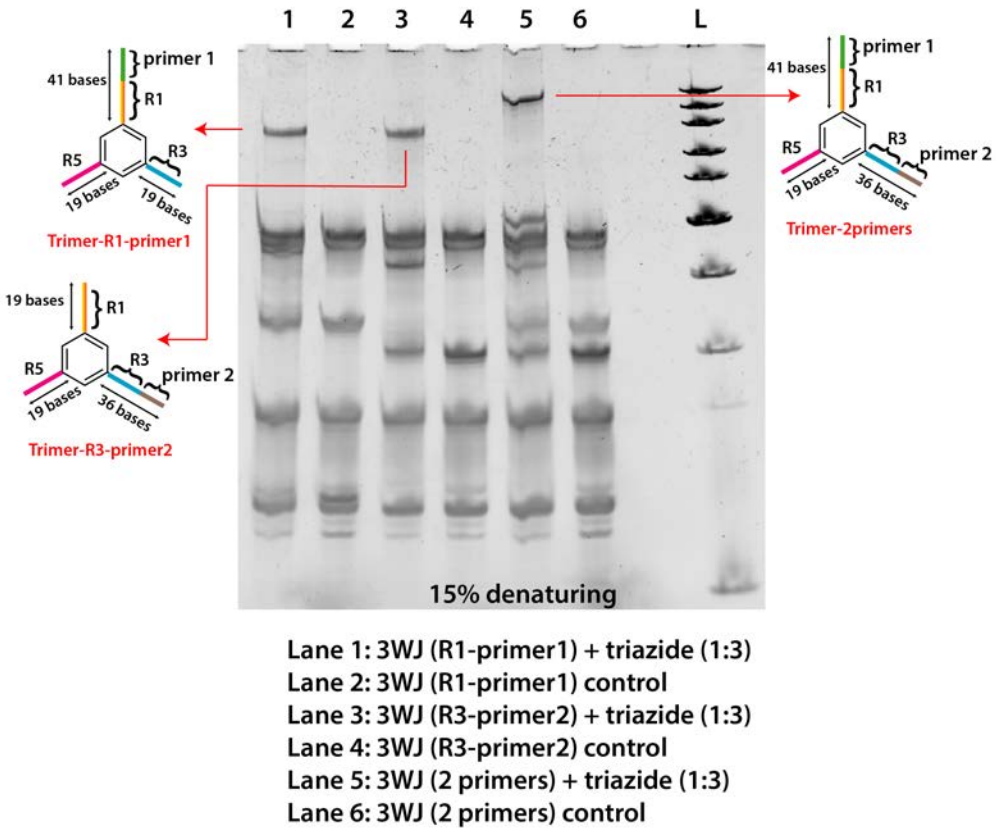

Figure 3.21. **Synthesis of trimers incoprorating primers.**

3.5.11. AFM characterization

The sample was diluted with 1xTAMg from 25 nM to 12-18 nM. 5µL of sample was deposited on freshly cleaved mica for 30 seconds and washed four times with 50 µL of filtered H_2O. Excess liquid was blown off by the stream of nitrogen for 45 seconds. The sample was then dried under vacuum for at least 20 minutes prior to imaging. Measurement was acquired in ScanAsyst mode under dry condition using ScanAsyst-Air triangular silicon nitride probe (tip radius = 2 nm, k = 0.4 N/m, fo = 70 kHz; Bruker, Camarillo, CA). Images were processed by NanoScope Analysis 1.40 Software. The data was treated with flattening to correct tilt, bow and scanner drift.

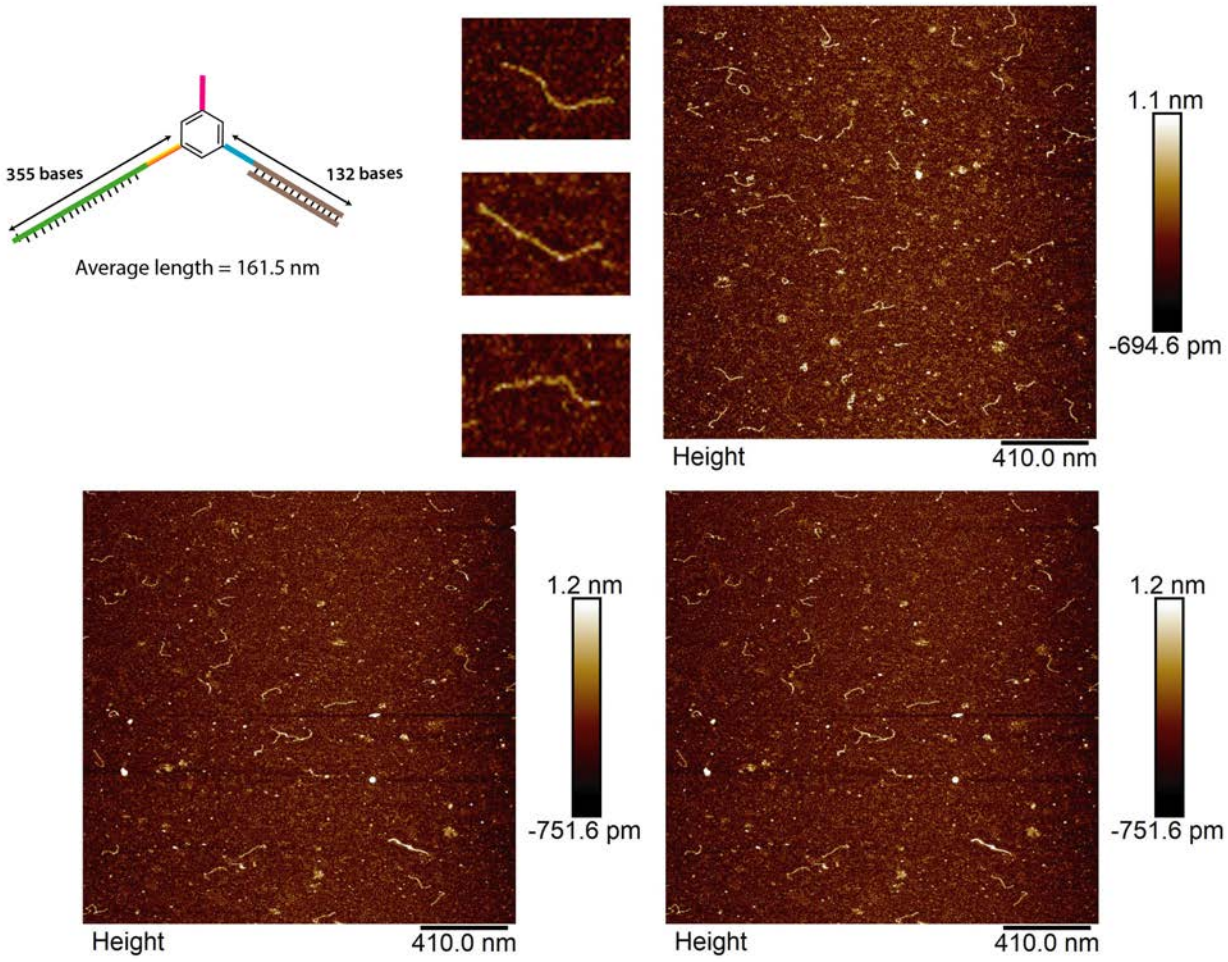

Figure 3.22 | AFM characterization of trimer extending 2 arms simultaneously.

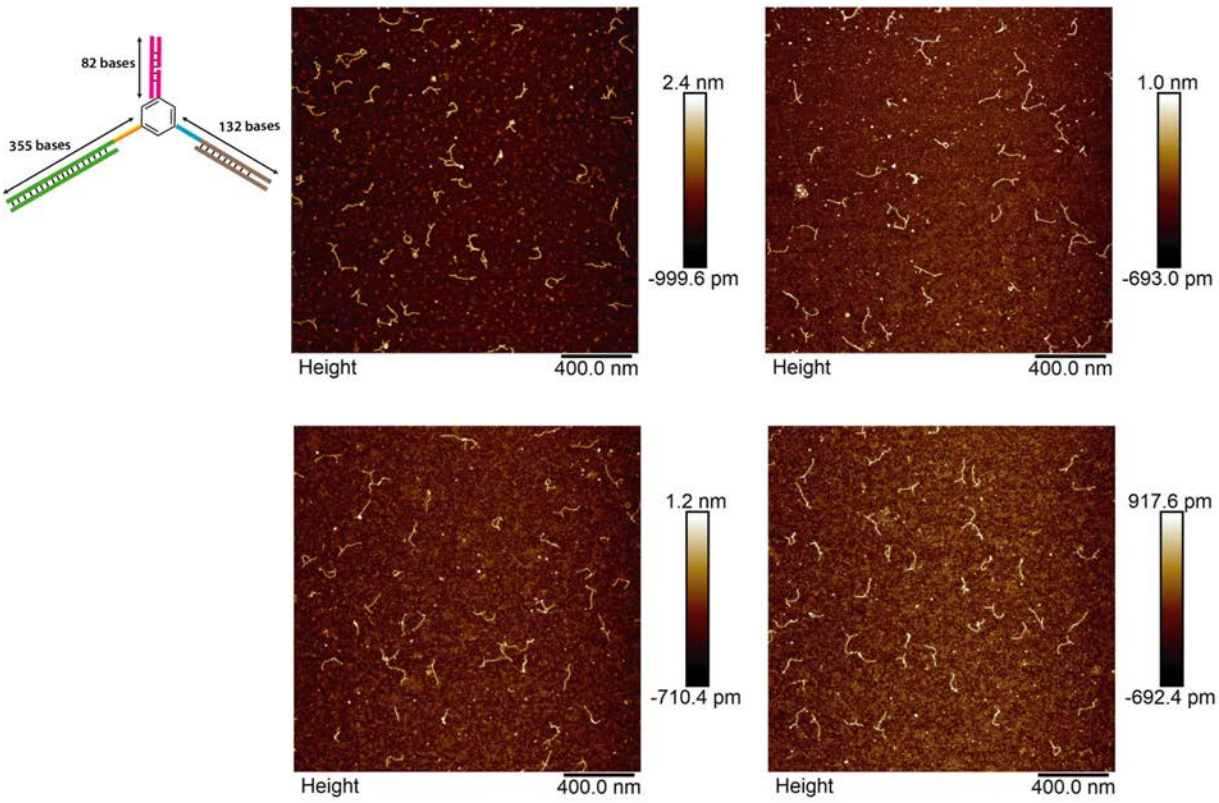

Figure 3.23 | AFM characterization of trimers having 3 arms extended.

3.5.12. Procedure for temporal growth and PCR

3.5.12.1. Procedure of temporal growth (performed by Daniel Saliba):

Temporal growth was performed following the previously reported protocol (***G. D. Hamblin, J. F. Rahbani, H. F. Sleiman, Nat. Comm. 2015, 6, 7065***). Briefly, all the component strands with an internal 5'end (all strands except **A1P** and **B2P**) were phosphorylated using T4 polynucleotide kinase (**T4PNK**). Each strand concentration was adjusted to 10 μM, in the presence of 2.5 mM adenosine triphosphate (**ATP**), **1xT4PN**K buffer and 0.1 $U.\mu L^{-1}$ of **T4PNK**. The mixtures were incubated at 37 ^{o}C after which the enzyme was heat-inactivated for 10 min at 65 ^{o}C. Next, equal volumes of each the complementary strands (**A1/A2, B1/B2, A1P/A2P** and **B1P/B2P**) of the building blocks were mixed together and left for 5 min at room temperature. Then, an equal volume of 2x Quick ligase (**QL**) buffer was added so that the final concentration

is 1x QL buffer. The temporal growth was achieved by combining equal amount of the duplex stock solutions as follows:

1) A1P-A2P + B1-B2 + Quick ligase + A1-A2 + B1-B2 (AP-A1B2)

2) B1P-B2P + B1-B2 + Quick ligase + A1-A2 (BP-A1B1)

After each addition, the mixture was incubated for 5 min to allow both for hybridization of the sticky ends and for ligation. Quick ligase was added (10 $U.\mu L^{-1}$) after the second addition of building blocks and the mixture was incubated for another 5 min at room temperature. Then both fractions (1 and 2) were combined and incubated for 10 min at room temperature. The final mixture was loaded on a 2% 1xTAE gel (80 V, 90 min) (**Figure 3.24A**) to isolate the product of interest, namely [ds8]. Note that the gel was pre-stained with 1xSybrSafe DNA Gel Stain to allow the visualization of the band of interest that was excised and purified using a QIAquick gel extraction Kit.

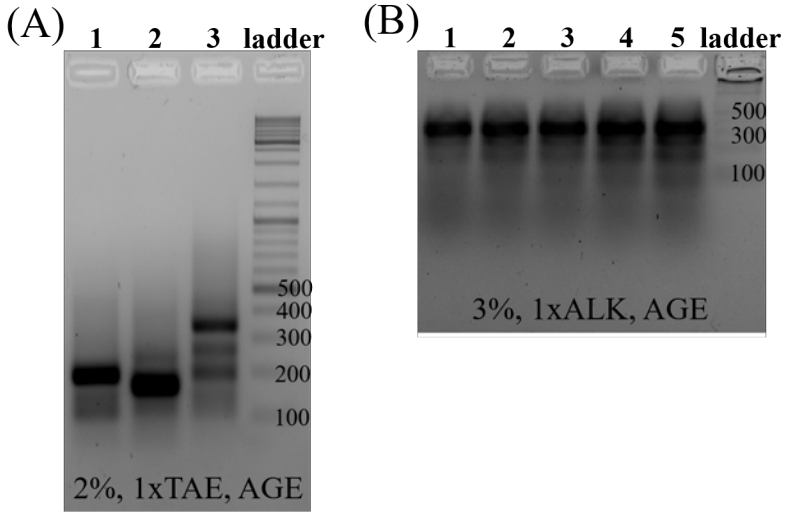

Figure 3.24 | Temporal growth and PCR products characterized by agarose gel electrophoresis. **(A)** 2% TAE native AGE: **lane 1:** AP-A1B2, **lane 2:** BP-A1B1, **lane 3:** [ds8] (336 bp) and **lane 4:** OGen ruler. **(B)** First round of PCR optimization of the isolated temporal growth backbone AP-A2B3-BP or [ds8] showing different annealing temperature: **lane 1:** T=65 °C (optimal temperature), **lane 2**: T=64.5 °C, lane 3: T=64 °C, lane 4: T=63.6 °C and lane 5: T=63.1 °C.

3.5.12.2. Polymerase Chain Reaction (PCR) (performed by Daniel Saliba):

Polymerase chain reaction (PCR) was carried out using the MyTaq™ HS Red Mix PCR kit. The reaction was performed in a batch of 200 µL, using 0.15 ng.µL^{-1} of [ds8] template, 0.6 µM of each of the [ds8] forward and reverse primers, and a final concentration of 1x MyTaq™ HS Red Mix. The mixture was then heated at 95 ºC for 1 minute and was followed by 30 cycles of: 1) 95 ºC for 15 seconds, 2) 65 ºC (temperature was optimized **(Figure 3.25B**)) for 15 seconds, and 3) 72 ºC for 15 seconds. After PCR, the sample was purified by 3% denaturing agarose gel electrophoresis (AGE) with 1x alkaline (**ALK**) running buffer. The gel was run for 2 hours after which it was neutralized (1 minute in distilled water followed by 15 minutes in 2xSSC), stained with SYBR Gold (15 minutes in 1xSSC) and de-stained in 1xTAE for 15 minutes. The full-length non-nicked product (336mer, **Figure 3.25B**) was excised and purified using Freeze 'N Squeeze™ DNA Gel Extraction Spin Columns (manufacturer protocol was followed). Besides, **V** and **Vcomp** were synthesized using the standard protocol of solid-phase synthesis.

To selectively extend one of the sequences that were added on the trimer, a DNA sequence that matches the reverse primer previously used in temporal growth was added to the 3' end of the **R1** sequence resulting in **R1-primer1**. Next, PCR was performed using the **[ds8]** backbone as a template (PCR conditions: the template concentration was 0.15 ng.µL^{-1} while each primer had a concentration of 0.6 µM both in 1x MyTaq™ HS Red Mix). The heating cycles are the same as described above. Same experimental conditions were used to extend the **R3-primer2** sequence that holds on its **3'** end the sequence of the **V** strand reverse primer. After each of the PCR cycles, the samples were loaded on a 2%, 1xTAE AGE **(Figure 3.25A** below).

The simultaneous extension of the **R1-primer1** and **R3-primer2** arms on the same trimer, performed under the same PCR conditions as above**,** resulted in the formation of 2 sub-products corresponding to the extension of the arms individually (**R1-primer1** extended or **R3-primer2** extended sequences) in addition to the product of interest (**Figure 3.25A, B**). Besides, the yield of the **R1-primer1** extended sub-product was relatively higher than that of the **R3-primer2** extended sub-product even though both primers were designed to have same melting temperature (**T= 62.9ºC**) under PCR conditions. The yield's optimization was performed by decreasing the ratio of

the trimer-R1-primer1-R3-primer2/reverse primers concentration (**Figure 3.25B**). A concentration decrease of 4 folds (0.15 μM) of the trimer concentration resulted in a yield increase from 20% to around 70-80%.

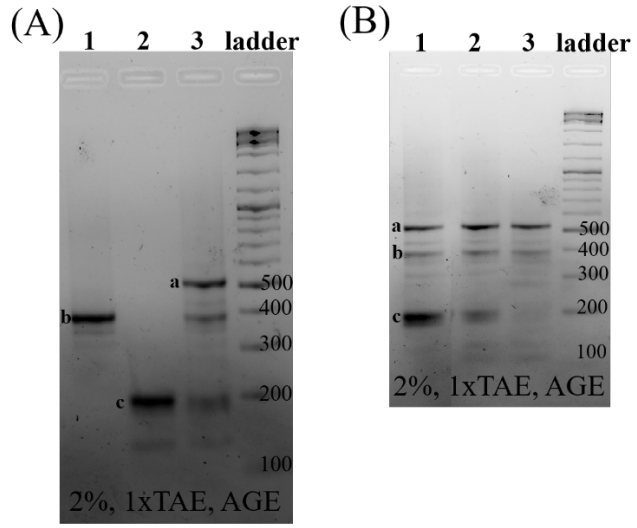

Figure 3.25 | PCR optimization of the double extended DNA trimer (**R1-primer1-R3-primer2 extended. (A)** PCR performed using [ds8] **(lane 1),** V/Vcomp **(lane 2)** and both [ds8] and V/Vcomp **(lane 3)** as template and in the presence of the DNA trimer. (B) The ratio of equivalents between the trimer and both reverse primers were varied from 1:1 (lane 1) to 1:2 (lane 2) to 1:3 (lane 3). Lane 3 gave the highest yield of the product of interest (indicated as "**a**") in comparison to the sub-products noted as "**b**" and "**c**" and corresponding to the **R1-primer1** extended and **R3-primer2** extended sequences, respectively.

The hybridization of the 81mer to the third arm of the trimer was performed by annealing the double stranded sticky ended **M/Mcomp** to the extended trimer from **44 to 20**^{o}C over 1 hour at a final concentration of 25 nM. The 5% native **PAGE** showed a decrease in the mobility shift upon hybridization of the **M/Mcomp** to the third arm (**Figure 3.26**).

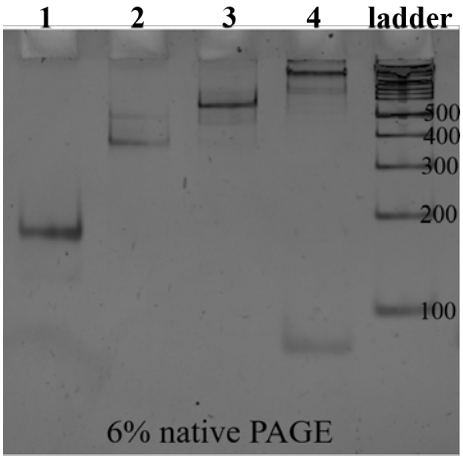

Figure 3.26 | 6% native PAGE showing the successful isolation and purification (via excision and freeze and squeeze) of the individually extended DNA trimer arms (**R1-primer1** extended (lane 2) and **R3-primer2** extended (lane 3) sequence) in addition to the double extended DNA trimer (lane 3). Lane 4 represents the successful hybridization of the sticky-ended M/Mcomp sequence that reveals a lower mobility shift in comparison to the product in lane 3.

3.5.13. Modelling (performed by Dr. Chenyi Liao and Prof. Jianing Li)

Model Preparation. All the models were constructed using the program Maestro (Schrödinger, Inc.). To build the 3-way junction DNA model, three segments of double-stranded DNA were initially generated by a web tool (http://structure.usc.edu/make-na/server.html, James Stroud 2004, 2011) based on the sequence design. After deleting extra bonding and nucleotides, each DNA strand was rotated by the phosphate group of the middle nucleotide to generate ~120 degree bending. With three strands carefully positioned as edges of the 3-way junction, we linked them together at the connecting phosphate groups. The reactive strand consists the 12-carbon spacer (C12) and(or) the alkyne modifier. To understand the regulation of the reactive strands in the complex center to the final products, we have first simulated the 3-way junction DNA complex with two reactive-strand models: (1) the C12 spacer **(~18 Å**) connects the DNA and the alkyne modifier; (2) without the C12 linker. Base on the results of model (1) and (2), a longer spacer as 5 thymine bases **(~24.5 Å**) was used to substitute the C12. Each model was solvated in a periodic simulation box of ~**278×59×245 Å^3** with SPC water molecules, counter ions, and $MgCl_2$ to mimic the experimental condition, totaling around 365366~389520 atoms.

Simulation Setup. All simulations were performed with the OPLS3 force field in NPT ensemble (1 bar, Martyna-Tobias-Klein coupling scheme) with a time step of 2 fs. The particle mesh Ewald technique was used for the electrostatic calculations. The van der Waals and short-range electrostatics were cut off at 9.0 Å. Hydrogen atoms were constrained using the SHAKE algorithm.

Visualization and Analysis. Using our local Tcl and Python tools, we calculated the distance of the nitrogen-nitrogen atoms pair between every two alkyne-modifiers

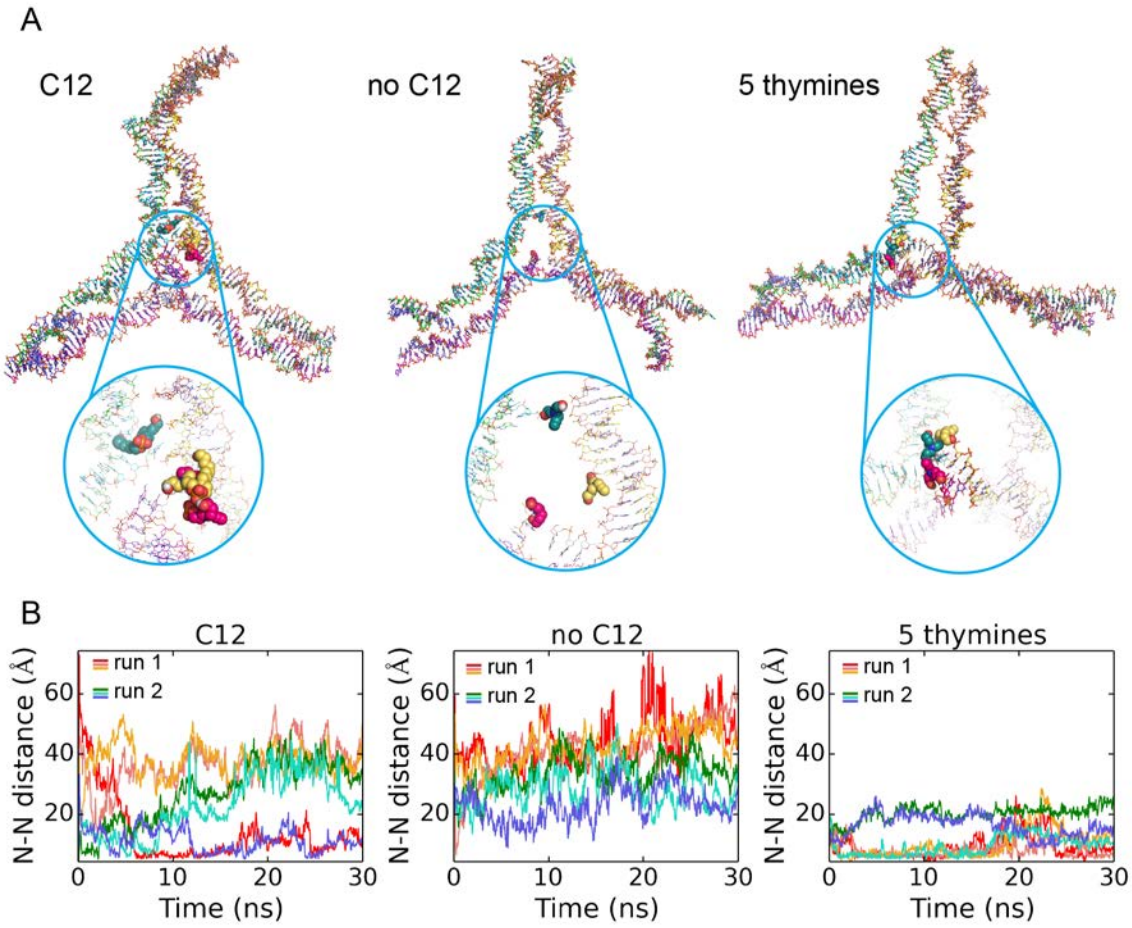

Figure 3.27 | Molecular modelling of 3WJ. **A)** Final snap-shots of 3-way junction DNA models with three different reactive strands in the center with room-in top views. **B)** Time evolutions of nitrogen-nitrogen distances of three nitrogen pairs in three different reactive strands. Two replicas were carried out for C12 and no C12 systems.

3.5.14. Self-assembly of 4WJ

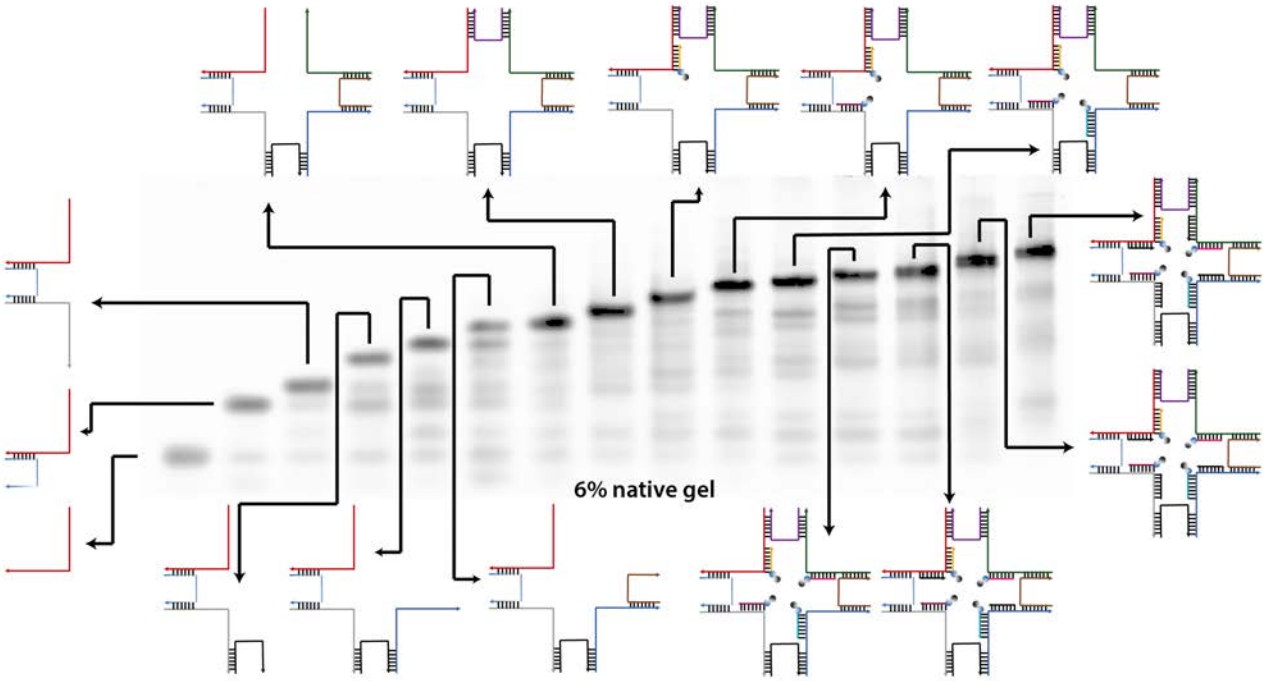

Figure 3.28 | Step-wise assembly of the 4WJ.

3.5.15. Self-replication of mother template.

The mother template **(trimer-2primers**) was prepared using above procedure. We used 3 alkyne-functionalized strands hybridized to the 3WJ: **Alkyne-HE-R1-primer1, alkyne-HE-R3-primer2 and alkyne-HE-R5**. The trimer has exactly 3 arms (41 bases, 36 bases and 19 bases). To characterized if the mother template has 3 different arms, we hybridized each arm with complementary strands.

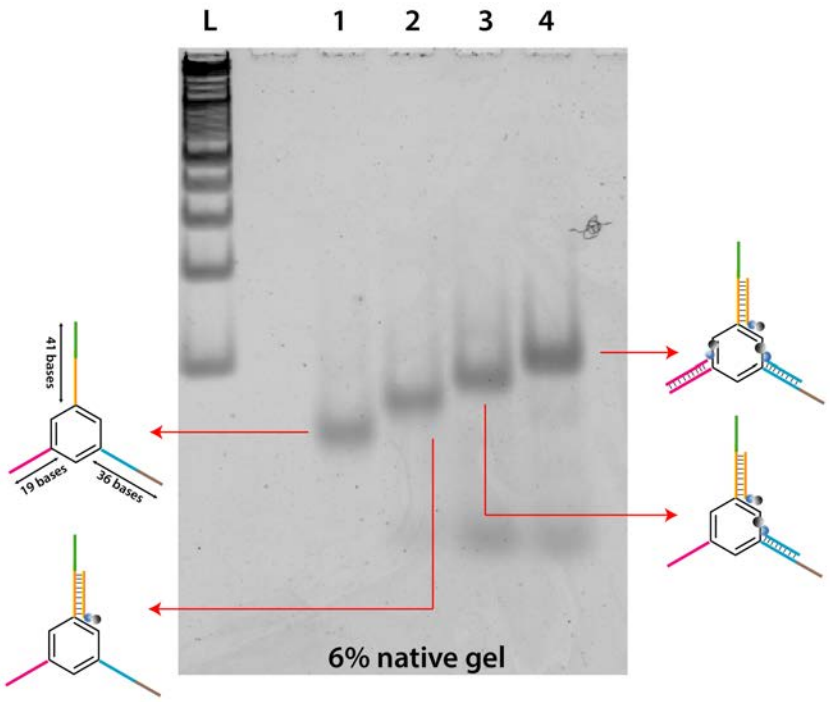

Figure 3.29 | Hybridizing trimer-2primers to complementary strands sequentially.

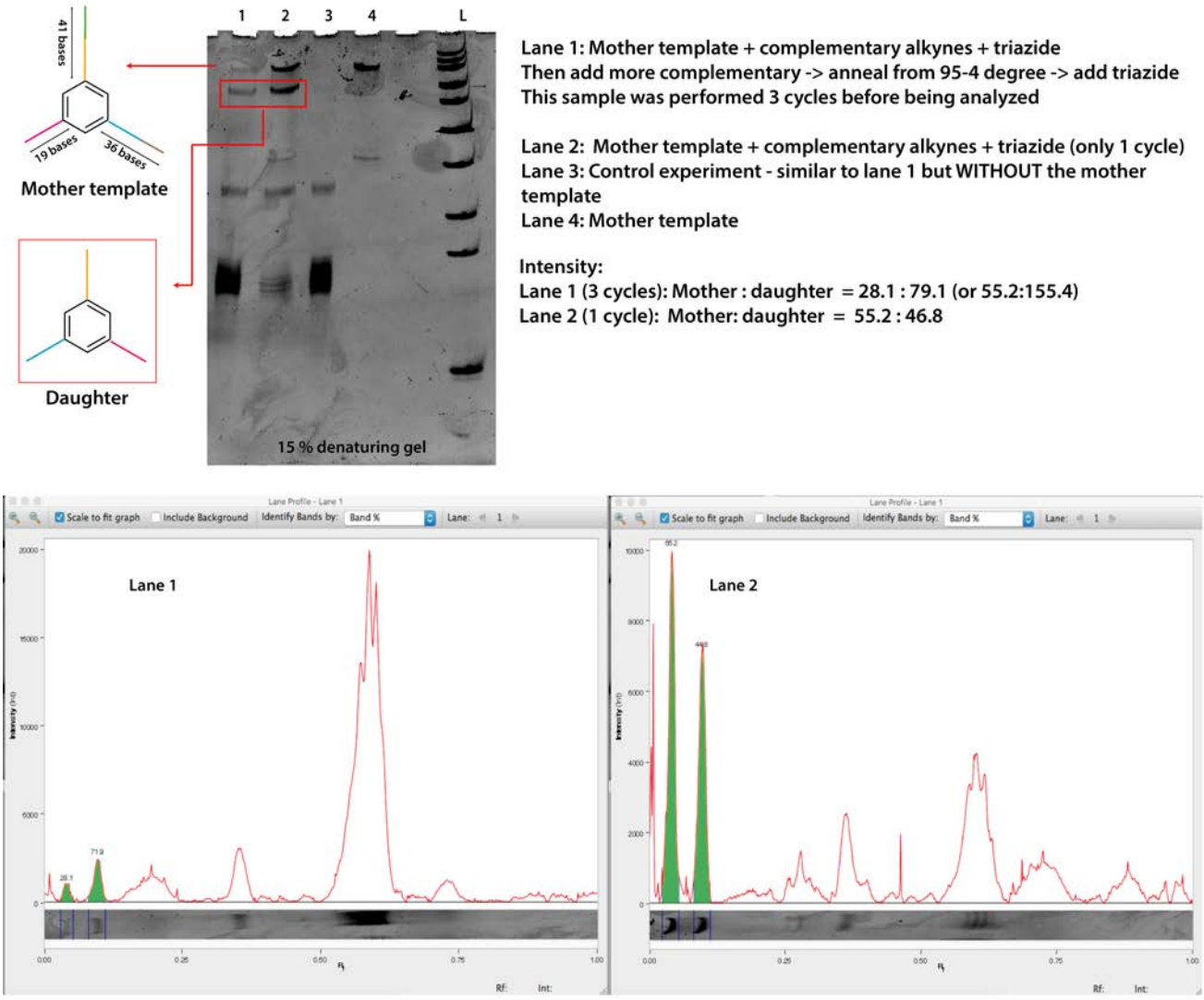

Figure 3.30 | Self-replication of daughter structure using mother template.

3.5.15. AFM characterization of streptavidin-decorated structure

3.5.15.1. Decorating 3 streptavidin molecules on the CD[6] arm of the extended structure.

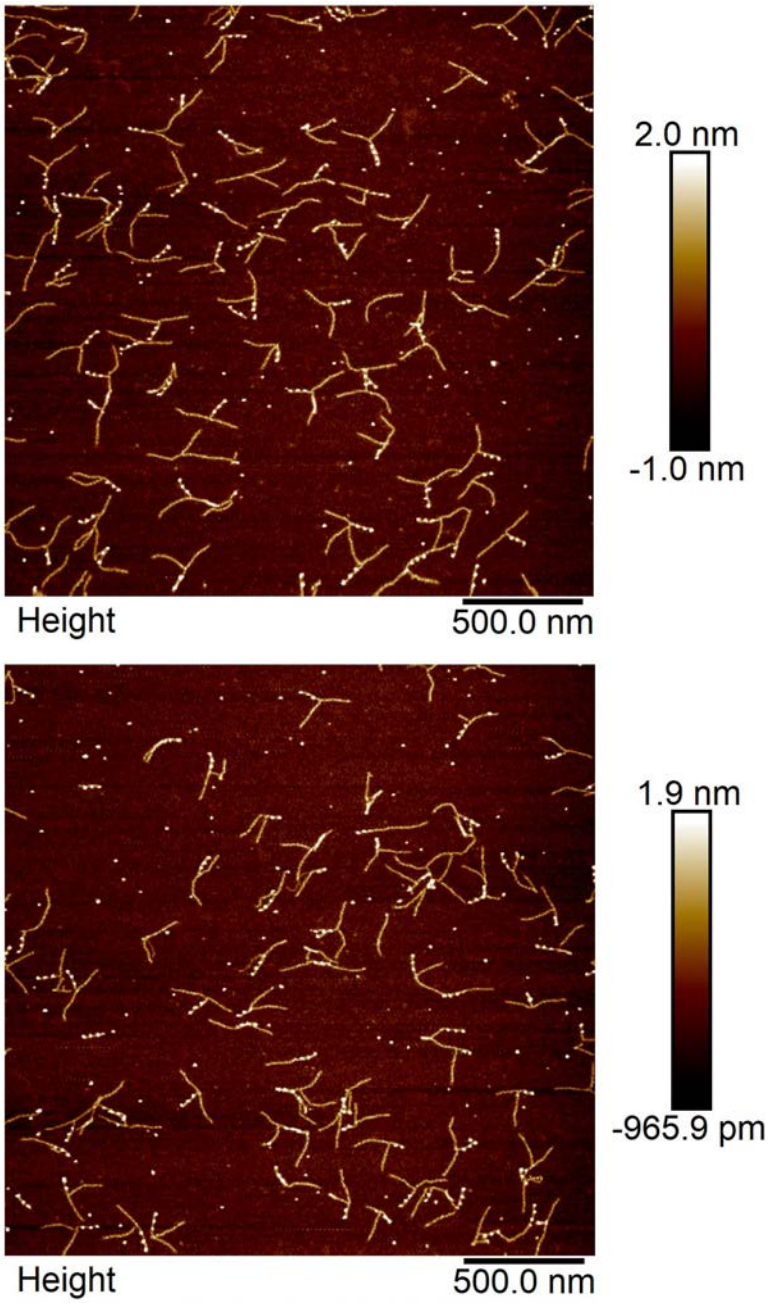

Figure 3.31 | Decorating 3 streptavidin molecules on the CD[6] arm of the extended structure

3.5.15.2. Decorating 4 streptavidin molecules on the EF[8] arm of the extended structure.

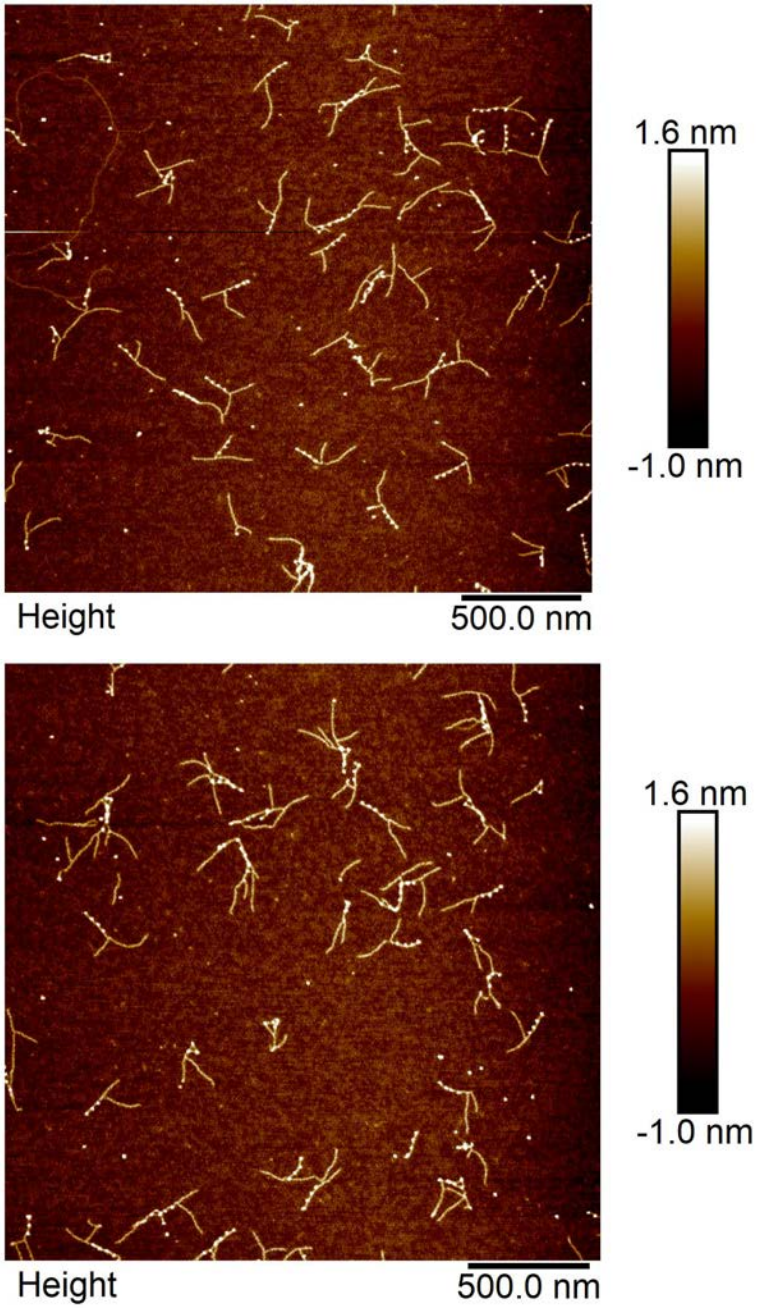

Figure 3.32 | Decorating 4 streptavidin molecules on the EF[8] arm of the extended structure.

3.6. References

1. Yan, H.; Park, S. H.; Finkelstein, G.; Reif, J. H.; LaBean, T. H., DNA-Templated Self-Assembly of Protein Arrays and Highly Conductive Nanowires. *Science* **2003,** *301* (5641), 1882-1884.

2. Sharma, J.; Chhabra, R.; Cheng, A.; Brownell, J.; Liu, Y.; Yan, H., Control of Self-Assembly of DNA Tubules Through Integration of Gold Nanoparticles. *Science* **2009,** *323* (5910), 112-116.

3. Rothemund, P. W. K., Folding DNA to create nanoscale shapes and patterns. *Nature* **2006,** *440*, 297.

4. Wei, B.; Dai, M.; Yin, P., Complex shapes self-assembled from single-stranded DNA tiles. *Nature* **2012,** *485*, 623.

5. Ke, Y.; Ong, L. L.; Shih, W. M.; Yin, P., Three-Dimensional Structures Self-Assembled from DNA Bricks. *Science* **2012,** *338* (6111), 1177-1183.

6. Winfree, E.; Liu, F.; Wenzler, L. A.; Seeman, N. C., Design and self-assembly of two-dimensional DNA crystals. *Nature* **1998,** *394*, 539.

7. Douglas, S. M.; Dietz, H.; Liedl, T.; Högberg, B.; Graf, F.; Shih, W. M., Self-assembly of DNA into nanoscale three-dimensional shapes. *Nature* **2009,** *459*, 414.

8. Benson, E.; Mohammed, A.; Gardell, J.; Masich, S.; Czeizler, E.; Orponen, P.; Högberg, B., DNA rendering of polyhedral meshes at the nanoscale. *Nature* **2015,** *523*, 441.

9. Greschner, A. A.; Toader, V.; Sleiman, H. F., The Role of Organic Linkers in Directing DNA Self-Assembly and Significantly Stabilizing DNA Duplexes. *J. Am. Chem. Soc* **2012,** *134* (35), 14382-14389.

10. McLaughlin, C. K.; Hamblin, G. D.; Sleiman, H. F., Supramolecular DNA assembly. *Chem. Soc. Rev.* **2011,** *40* (12), 5647-5656.

11. Zimmermann, J.; Cebulla, M. P. J.; Mönninghoff, S.; Kiedrowski, G. v., Self-Assembly of a DNA Dodecahedron from 20 Trisoligonucleotides with C3h Linkers. *Angew. Chem. Int. Ed.* **2008,** *47* (19), 3626-3630.

12. Gothelf, K. V.; Brown, R. S., A Modular Approach to DNA-Programmed Self-Assembly of Macromolecular Nanostructures. *Chem. Eur. J* **2005,** *11* (4), 1062-1069.

13. Eryazici, I.; Prytkova, T. R.; Schatz, G. C.; Nguyen, S. T., Cooperative Melting in Caged Dimers with Only Two DNA Duplexes. *J. Am. Chem. Soc* **2010,** *132* (48), 17068-17070.

14. Aldaye, F. A.; Sleiman, H. F., Modular Access to Structurally Switchable 3D Discrete DNA Assemblies. *J. Am. Chem. Soc* **2007,** *129* (44), 13376-13377.

15. Masayuki, E.; C., S. N.; Tetsuro, M., DNA Tube Structures Controlled by a Four-Way-Branched DNA Connector. *Angew. Chem. Int. Ed.* **2005,** *44* (37), 6074-6077.

16. Greschner, A. A.; Bujold, K. E.; Sleiman, H. F., Intercalators as Molecular Chaperones in DNA Self-Assembly. *J. Am. Chem. Soc* **2013,** *135* (30), 11283-11288.

17. Seeman, N. C.; Sleiman, H. F., DNA nanotechnology. *Nat. Rev. Mat.* **2017,** *3*, 17068.

18. Yang, H.; McLaughlin, C. K.; Aldaye, F. A.; Hamblin, G. D.; Rys, A. Z.; Rouiller, I.; Sleiman, H. F., Metal–nucleic acid cages. *Nat. Chem.* **2009,** *1*, 390.

19. Hartman, M. R.; Yang, D.; Tran, T. N. N.; Lee, K.; Kahn, J. S.; Kiatwuthinon, P.; Yancey, K. G.; Trotsenko, O.; Minko, S.; Luo, D., Thermostable Branched DNA Nanostructures as Modular Primers for Polymerase Chain Reaction. *Angew. Chem.* **2013,** *125* (33), 8861-8864.

20. Hong, B. J.; Eryazici, I.; Bleher, R.; Thaner, R. V.; Mirkin, C. A.; Nguyen, S. T., Directed Assembly of Nucleic Acid-Based Polymeric Nanoparticles from Molecular Tetravalent Cores. *J. Am. Chem. Soc* **2015,** *137* (25), 8184-8191.

21. Becerril, H. A.; Stoltenberg, R. M.; Wheeler, D. R.; Davis, R. C.; Harb, J. N.; Woolley, A. T., DNA-Templated Three-Branched Nanostructures for Nanoelectronic Devices. *J. Am. Chem. Soc* **2005,** *127* (9), 2828-2829.

22. Rudiuk, S.; Venancio-Marques, A.; Hallais, G.; Baigl, D., Preparation of one- to four-branch silver nanostructures of various sizes by metallization of hybrid DNA–protein assemblies. *Soft Matter* **2013,** *9* (38), 9146-9152.

23. Richa, P.; Andreas, M., An Adamantane-Based Building Block for DNA Networks. *Chem. Asia J.* **2011,** *6* (6), 1450-1455.

24. Bußkamp, H.; Keller, S.; Robotta, M.; Drescher, M.; Marx, A., A new building block for DNA network formation by self-assembly and polymerase chain reaction. *Beilstein J. Org. Chem.* **2014,** *10*, 1037-1046.

25. Martin, M.; Carolin, A.; Matthias, B.; Oliver, P.; A., S. S.; Arunoday, S.; Thierry, M.; Wolfgang, W.; Stefan, B.; Clemens, R., Two Base Pair Duplexes Suffice to Build a Novel Material. *ChemBioChem* **2009,** *10* (8), 1335-1339.

26. Singh, A.; Tolev, M.; Meng, M.; Klenin, K.; Plietzsch, O.; Schilling, C. I.; Muller, T.; Nieger, M.; Bräse, S.; Wenzel, W.; Richert, C., Branched DNA That Forms a Solid at 95 °C. *Angew. Chem. Int. Ed.* **2011,** *50* (14), 3227-3231.

27. Ponomarenko, A. I.; Brylev, V. A.; Sapozhnikova, K. A.; Ustinov, A. V.; Prokhorenko, I. A.; Zatsepin, T. S.; Korshun, V. A., Tetrahedral DNA conjugates from pentaerythritol-based polyazides. *Tetrahedron* **2016,** *72* (19), 2386-2391.

28. Clave, G.; Chatelain, G.; Filoramo, A.; Gasparutto, D.; Saint-Pierre, C.; Le Cam, E.; Pietrement, O.; Guerineau, V.; Campidelli, S., Synthesis of a multibranched porphyrin-oligonucleotide scaffold for the construction of DNA-based nano-architectures. *Org. Biomol. Chem.* **2014,** *12* (17), 2778-2783.

29. Hudson, R. H. E.; Damha, M. J., Nucleic acid dendrimers: novel biopolymer structures. *J. Am. Chem. Soc* **1993,** *115* (6), 2119-2124.

30. Hudson, R. H. E.; Robidoux, S.; Damha, M. J., Divergent solid-phase synthesis of nucleic acid dendrimers. *Tetrahedron Letters* **1998,** *39* (11), 1299-1302.

31. Thaner, R. V.; Eryazici, I.; Farha, O. K.; Mirkin, C. A.; Nguyen, S. T., Facile one-step solid-phase synthesis of multitopic organic-DNA hybrids via "click" chemistry. *Chem. Sci.* **2014,** *5* (3), 1091-1096.

32. Okochi, K. D.; Monfregola, L.; Dickerson, S. M.; McCaffrey, R.; Domaille, D. W.; Yu, C.; Hafenstine, G. R.; Jin, Y.; Cha, J. N.; Kuchta, R. D.; Caruthers, M.; Zhang, W., Synthesis of Small-Molecule/DNA Hybrids through On-Bead Amide-Coupling Approach. *J. Org. Chem.* **2017,** *82* (20), 10803-10811.

33. Endo, M.; Sugiyama, H., Chemical Approaches to DNA Nanotechnology. *ChemBioChem* **2009,** *10* (15), 2420-2443.

34. Gothelf, K. V.; Thomsen, A.; Nielsen, M.; Cló, E.; Brown, R. S., Modular DNA-Programmed Assembly of Linear and Branched Conjugated Nanostructures. *J. Am. Chem. Soc* **2004,** *126* (4), 1044-1046.

35. Panagiotidis, C.; Kath-Schorr, S.; Kiedrowski, G. v., Flexibility of C3h-Symmetrical Linkers in Tris-oligonucleotide-Based Tetrahedral Scaffolds. *ChemBioChem* **2016,** *17* (3), 254-259.

36. Utagawa, E.; Ohkubo, A.; Sekine, M.; Seio, K., Synthesis of Branched Oligonucleotides with Three Different Sequences Using an Oxidatively Removable Tritylthio Group. *J. Org. Chem.* **2007,** *72* (22), 8259-8266.

37. Eckardt, L. H.; Naumann, K.; Matthias Pankau, W.; Rein, M.; Schweitzer, M.; Windhab, N.; von Kiedrowski, G., Chemical copying of connectivity. *Nature* **2002,** *420*, 286.

38. Eryazici, I.; Yildirim, I.; Schatz, G. C.; Nguyen, S. T., Enhancing the Melting Properties of Small Molecule-DNA Hybrids through Designed Hydrophobic Interactions: An Experimental-Computational Study. *J. Am. Chem. Soc* **2012,** *134* (17), 7450-7458.

39. Li, X.; Liu, D. R., DNA-Templated Organic Synthesis: Nature's Strategy for Controlling Chemical Reactivity Applied to Synthetic Molecules. *Angew. Chem. Int. Ed.* **2004,** *43* (37), 4848-4870.

40. Trinh, T.; Chidchob, P.; Bazzi, H. S.; Sleiman, H. F., DNA micelles as nanoreactors: efficient DNA functionalization with hydrophobic organic molecules. *Chem. Comm.* **2016,** *52* (72), 10914-10917.

41. He, Y.; Ye, T.; Su, M.; Zhang, C.; Ribbe, A. E.; Jiang, W.; Mao, C., Hierarchical self-assembly of DNA into symmetric supramolecular polyhedra. *Nature* **2008,** *452*, 198.

42. Hamblin, G. D.; Rahbani, J. F.; Sleiman, H. F., Sequential growth of long DNA strands with user-defined patterns for nanostructures and scaffolds. *Nat. Comm.* **2015,** *6*, 7065.

43. Lau, K. L.; Sleiman, H. F., Minimalist Approach to Complexity: Templating the Assembly of DNA Tile Structures with Sequentially Grown Input Strands. *ACS Nano* **2016,** *10* (7), 6542-6551.

44. Lee, J. K.; Jung, Y. H.; Tok, J. B. H.; Bao, Z., Syntheses of Organic Molecule−DNA Hybrid Structures. *ACS Nano* **2011,** *5* (3), 2067-2074.

45. Lee, J. K.; Jung, Y. H.; Stoltenberg, R. M.; Tok, J. B. H.; Bao, Z., Synthesis of DNA−Organic Molecule−DNA Triblock Oligomers Using the Amide Coupling Reaction and Their Enzymatic Amplification. *J. Am. Chem. Soc* **2008,** *130* (39), 12854-12855.

46. K., L. J.; Frank, J.; E., M. W.; Zhenan, B., Micrometer-sized DNA–Single-Fluorophore–DNA Supramolecule: Synthesis and Single-Molecule Characterization. *Small* **2009,** *5* (21), 2418-2423.

47. Wang, T.; Sha, R.; Dreyfus, R.; Leunissen, M. E.; Maass, C.; Pine, D. J.; Chaikin, P. M.; Seeman, N. C., Self-replication of information-bearing nanoscale patterns. *Nature* **2011,** *478*, 225.

48. He, X.; Sha, R.; Zhuo, R.; Mi, Y.; Chaikin, P. M.; Seeman, N. C., Exponential growth and selection in self-replicating materials from DNA origami rafts. *Nat. Mater.* **2017,** *16*, 993.
49. von Kiedrowski, G.; Eckardt, L. H.; Naumann, K.; Pankau, W. M.; Reimold, M.; Rein, M., Toward replicatable, multifunctional, nanoscaffolded machines. A chemical manifesto. In *Pure Appl. Chem.*, 2003; Vol. 75, p 609.

| 4 |

3D DNA nanostructures as scaffolds for DNA pattern transfer to polymeric materials

This chapter is composed mainly of the work published as "DNA-Imprinted Polymer Nanoparticles with Monodispersity and Prescribed DNA Strand Patterns" by Tuan Trinh, Chenyi Liao, Violeta Toader, Maciej Barłóg, Hassan S. Bazzi, Jianing Li and Hanadi F. Sleiman in Nature Chemistry, 2018, **10**, 184-192.

Author contributions:

Tuan Trinh helped design the project, developed the concept, primarily contributed to production of experimental data from DNA synthesis, HPLC, gel electrophoresis, AFM imaging, dynamic light scattering and mass spectroscopy and wrote the paper. **Chenyi Liao** and **Jianing Li** carried out modelling for the cube with DNA amphiphiles. **Violeta Toader, Maciej Barlog** and **Hassan S. Bazzi** synthesized hexaethylene phosphoramidite for DNA synthesis. **Hanadi F. Sleiman** designed the project, guided interpretation of data, result discussion, co-wrote the paper and provided funding for the project.

4.1. Preface

DNA nanostructures are promising scaffolds for DNA functionalization and DNA pattern transfer as shown in chapter 2 and 3. Chapter 3 specifically discussed mainly on the transfer of DNA patterns from a DNA multi-way junction to azide-functionalized small molecules. However, the transfer of molecular recognition was carried out in 2D. Chapter 4 seeks to expand the pattern transfer process onto new structures, namely polymeric material, and in three-dimensions.

As colloidal self-assembly increasingly approaches the complexity of natural systems, an ongoing challenge is to generate non-centrosymmetric structures. For example, patchy, Janus, or living crystallization particles have significantly advanced the area of polymer assembly. It has remained very challenging however to devise polymer particles that associate in a directional manner, with controlled valency and recognition motifs. The present chapter introduces a method to transfer DNA patterns from a DNA cage to a polymeric nanoparticle encapsulated inside the cage in 3D. These printed particles assemble with programmability and directionality. Interestingly, the

number, orientation and sequence of DNA strands grafted onto the polymeric core can be controlled during the process, and the resulting DNA-polymer particles may be of use for a variety of applications**.**

4.2. Introduction

Through their reliable, reversible hybridization, nucleic acids can guide the assembly of nanostructures with unparalleled precision.[1-3] While the predictability of Watson-Crick DNA base pairing makes it possible to generate anisotropic and monodisperse nanostructures with a great degree of complexity, from two-dimensional patterns to three-dimensional objects such as tubes or polyhedra, the functionality of these structures is still limited.[4-11] Synthetic polymers, on the other hand, provide stability and ease of functionalization, yet lack the high degree of programmability, predictability and monodispersity that DNA offers. As such, DNA amphiphilic polymer conjugates have recently received much attention as promising hybrid materials arising from the combination of the programmability and predictability of DNA with the stability and functionality of polymers. They have found use in numerous applications ranging from drug delivery to nanoelectronics.[12-16]

The self-assembly of DNA amphiphilic polymers mostly gives rise to symmetrical structures such as micelles and vesicles based on microphase separation of the two polymeric blocks.[17-19] On the other hand, the creation of discrete and asymmetric nanostructures using DNA-polymer building blocks has not been examined, due to the difficulty in controlling the number, directionality and relative orientation of DNA strands grafted onto the polymeric core. Although polymeric micelles are now being manipulated with greater precision, both by varying their shapes and introducing anisotropy (e.g. Janus, patchy particles or particles obtained by living crystallization), the current challenge still remains in generating a library of polymer nanoparticles, capable of directional bonding.[20-26] This has been recently pursued with DNA-functionalized inorganic nanoparticles (NPs) where the development of new strategies to control valency and bond anisotropy of NPs is underway.[27-41] Our group, as well as Fan *et al.* have recently proposed strategies to transfer DNA patterns from three-dimensional (3D) DNA nanostructures or DNA origami onto gold NPs (AuNPs).[42-43] The number of DNA strands and relative arrangement of DNA patterns in 2D can

be controlled based on the Au-sulfur interactions. However, to our knowledge, 3D-DNA pattern transfer, and more generally, DNA pattern transfer to polymeric particles has not been previously reported.

In this chapter, we describe a method to transfer 3D DNA motifs from DNA cube structures, generating DNA-polymer particles using covalent chemistry. The DNA-imprinted particle **(DIP**) is "molded" on the inside of a DNA nanostructure and composed of a monodisperse polymer core and a prescribed number of DNA strands in specific orientations **(Figure 4.1**). As a proof of concept, we "print" a specific pattern of 6 unique strands directly from a DNA cube scaffold to a polymeric core. We show that **DIPs** are stable under thermal, denaturing conditions and can be precisely controlled in terms of the number of DNA strands and their directionality, whilst preserving sequence anisotropy. These polymeric particles can self-assemble into well-defined structures using DNA base-pair recognition. **DIPs** provide additional directional and programmable control and can potentially find numerous biological and materials applications.

4.3. Results and Discussions

4.3.1. Design and working principle

Our patterning process relies on a DNA cube scaffold **(Cb)** as a template (**Figure 4.1**) and DNA-polymer amphiphiles complementary to the sides of this cube. We have previously shown that, when 8 amphiphiles are positioned on **Cb**, they undergo an intra-scaffold "handshake" to create an internal hydrophobic pocket.[44-46] We hypothesized that, if the polymer portions on the inside of the cube were covalently crosslinked, this would produce polymeric particles that are covalently conjugated to the DNA strands hybridized to the cube. This DNA-imprinted particle **(DIP**) can then be released from the cubic scaffold by denaturation. Its core is defined by the number of strands, the nature and the length of the polymer, which are precisely controlled (see below); it is functionalized with DNA strands of different sequences, presenting on its exterior in well-defined numbers and directions.

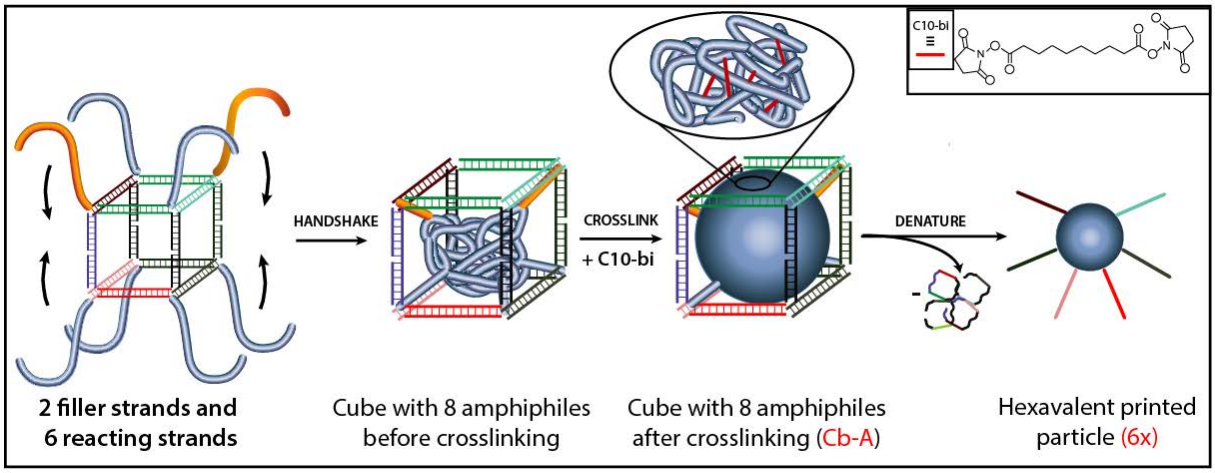

Figure 4.1 | Overview of the approach. An intra-scaffold hydrophobic pocket is formed upon introducing 8 amphiphiles to the cube. Sebacic acid bis(N-succinimidyl) ester **(C10-bi)** is then used to crosslink the hydrophobic core via amide bond formation. Under denaturing conditions, the printed particle **(6x)** is purified.

The cube scaffold **(Cb)** was prepared using a "clip-by-clip" approach as previously reported from our lab (**Figure 4.2**).[45-46] This scaffold was chosen because it presents several attractive features: **1)** it has up to 8 different binding regions (four on top and four on bottom) and **2**) it is possible to generate **DIPs** with different patterns (e.g. number of DNA strands, sequences and directionality) using only one scaffold.

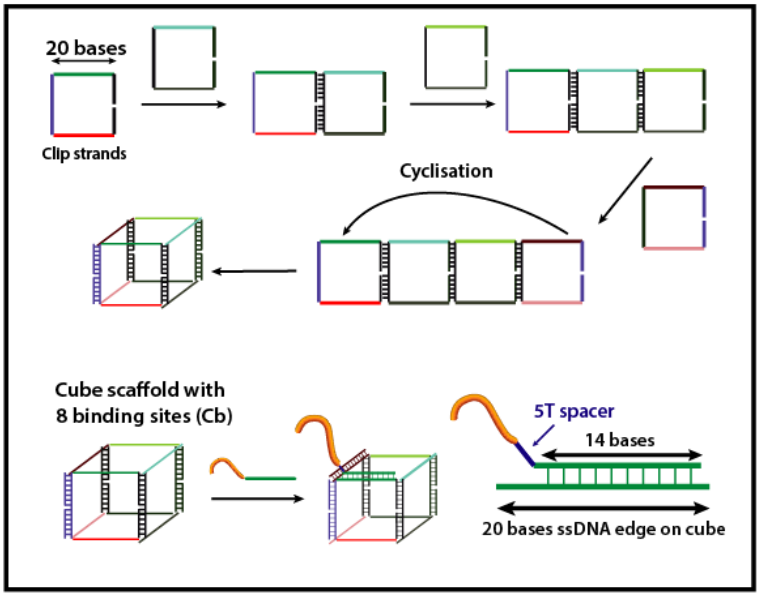

Figure 4.2 | Design of cube scaffold. "Clip-by-clip" assembly approach for a cube scaffold (**Cb**). **Cb** has 8 single-stranded regions (4 on top and 4 at the bottom), which can be used to decorate it with DNA or amphiphiles.

Another component required in the process are DNA amphiphilic polymers. They were prepared using automated solid-phase phosphoramidite synthesis.[18] We functionalized DNA strands with hydrophobic alkyl chains and reactive amine moieties at precise numbers and positions. The units consist of a hexa-ethylene **(HE**) segment and an amino groups **(Am)** which both feature an end phosphate group through which they can connect to each other as well as to the DNA strand **(**Figure **4.3).** The resulting DNA-polymer amphiphile structure was optimized (by changing the numbers and positions of **HE** chains and **Am** units) to maximize the yield of the desired crosslinked product (**Experimental Section 4.5.4**). The optimal strands contain 6 **HE** units and 3 **Am** groups in the sequence **5'-Am-(HE)$_3$-Am-(HE)$_3$-Am-DNA-3'** (i.e., one at the end, one in the middle of the hydrophobic part and one between the DNA and polymeric portions) and are called **"reacting strands" (Figure 4.3)**.

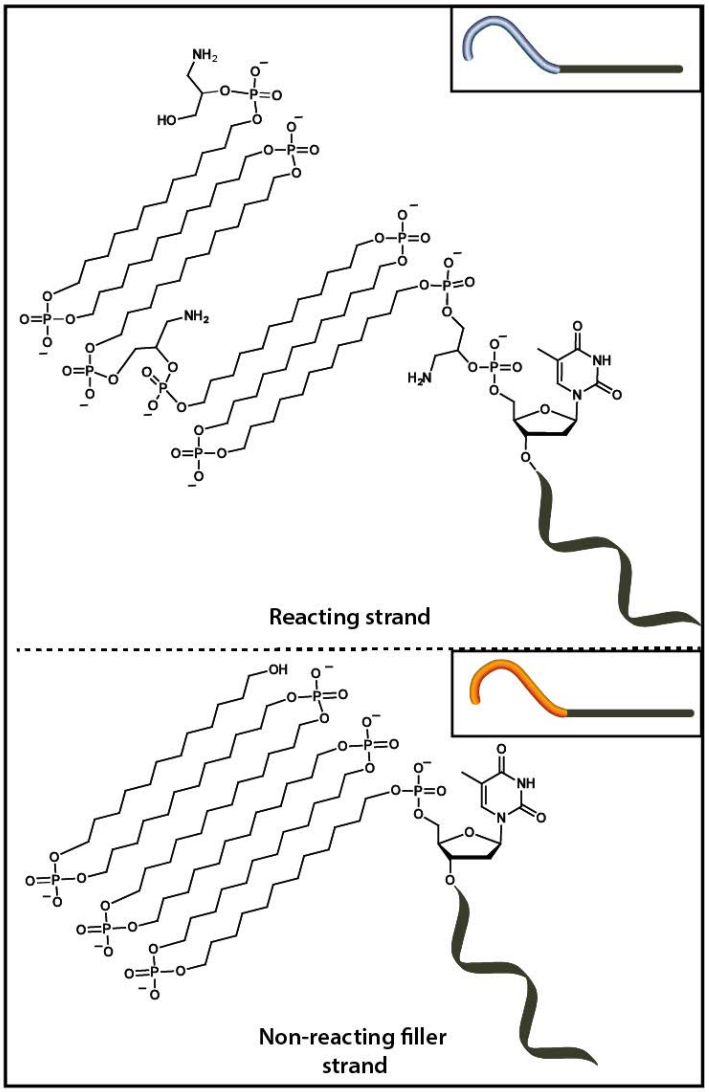

Figure 4.3 | Design of DNA amphiphilic polymer. Hydrophobic portion of the reacting DNA-polymer strand has exactly 6 hexaethylene **(HE)** units, with crosslinking amino groups (**Am**) at the beginning, middle and end of the chain; 2 additional unreactive "filler" strands with 6 **HE** units are used to fill the unused portions of the cube (labelled in yellow color).

We showed earlier in chapter 2 of this thesis that the hydrophobic cores of DNA micelles can act as nanoreactors which facilitate the conjugation of DNA with hydrophobic organic molecules in aqueous buffer.[47] Hence, we predicted that the hydrophobic core inside the DNA cube **(Cb)** could serve as a platform to carry out organic reactions that crosslink this core. The result is a polymeric nanoparticle that is covalently bonded to different DNA strands. To make a hexavalent particle inside the cube, 6 reacting strands (with **Am** groups) are needed, leaving 2 single-stranded regions on the scaffold. To form a hydrophobic environment within the cube, all 8 binding sites on **Cb** need to be filled with amphiphiles. Therefore, 2 additional amphiphiles which contain only 6 **HE** units but without any functional groups, called **"filler strands**", are also introduced (**Figure 4.3**).

The 6 DNA reacting strands (with **Am** groups) and 2 non-reacting filler strands (without **Am** groups) on **Cb** are expected to fold in, creating a hydrophobic pocket in the cube with multiple **Am** groups.[46] Then, a crosslinking reagent (sebacic acid bis(N-succinimidyl) ester (**C10-bi**)) is added to covalently "lock" the core via amide bond formation at room temperature **(Figure 4.1)**.

Figure **4.4** shows a native polyacrylamide gel electrophoresis (**PAGE)** as the outcome of this process: **1)** quantitative assembly of **Cb** decorated with 8 amphiphiles (lane **3**) **2)** the structure remains intact after the crosslinking reaction (lane **4**) and **3)** no higher order structures are formed, demonstrating that the crosslinking reactions occur only inside one cube. Interestingly, we observe that when 8 amphiphiles with 6 **HE** units (**HE_6-DNA**) were placed on the cube scaffold, its electrophoretic mobility was higher than that of cube with 8 unfunctionalized complementary DNA strands (**Figure 4.4,** lane **2-3**). This is consistent with our previous observations, and is most likely due to the efficient folding of the hydrophobic chains upon introduction of the **HE** units on the decorating strands, which ultimately leads to a more compact structure (**Figure 4.4**).[46]

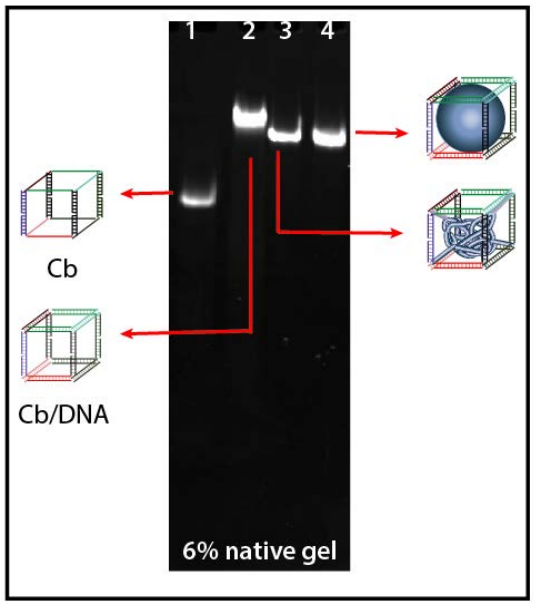

Figure 4.4 | Assembly of DNA cube scaffold. 6% native PAGE shows the assembly of **Cb** which is decorated with 8 DNA-amphiphiles (6 reacting strands and 2 non-reacting filler strands) to form the cube-micelle structure. The structure remains intact after crosslinking (**lane 3** (before crosslinking) and lane **4** (after crosslinking)): **lane 1**: **Cb** (cube scaffold), **lane 2**: **Cb** decorated with 8 unfunctionalized DNA, **lane 3: Cb** decorated with 8 amphiphiles before crosslinking, **lane 4**: crosslinked cube.

Finally, after the crosslinked process, the crude mixture was run on a denaturing PAGE to separate the desired hexavalent product (**6x**) from side-products (divalent (**2x**), trivalent (**3x**), tetravalent (**4x**) and pentavalent (**5x**)) (Figure **4.5a)**. Although **2x**-**5x** are expected to be composed of different

isomers, **6x** should be a single product. The unreacted "filler strands" dissociate from the particle, leaving behind the prescribed number of DNA arms and HE core (**Figure 4.5**). The core of **6x** is equivalent to a polyethylene chain with exactly 216 repeat units, **-(CH_2-CH_2)-$_{216}$**, thus it is monodispersed.

4.3.2. Characterization of the DNA-imprinted particle 6x's formation

The denaturing **PAGE** in Figure **4.5** shows that after crosslinking, a mixture of products with different numbers of DNA strands (from divalent to hexavalent) is formed. The yield of **6x**'s formation is 30% based on band intensity analysis corresponding to at least 88% efficiency in individual reactions between amino group and NHS moieties (Experimental Section **4.5.9**, 40% yield for a **DIP** with 4 DNA strands, see below), and **6x** can be recovered with up to 92% by electroelution after gel extraction. With higher-yielding coupling reactions, we expect this efficiency to further increase. In addition, the formation of the crosslinked **6x** product was confirmed by atomic force microscopy (**AFM**) imaging in air and dynamic light scattering **(DLS)**. Our previous studies showed that **HE_6-DNA** amphiphiles can only self-assemble into spherical micelles in the presence of Mg^{2+}, which compensates for the electrostatic repulsion between phosphate groups.[18] In contrast, **6x** in water (without Mg^{2+}) could still maintain its integrity with a diameter of 22.2 ± 3.8 nm measured by AFM (**Figure 4.5b**) and 30.6 ± 5.7 nm by DLS (Experimental Section **4.5.16**), which strongly supported that **6x** was covalently crosslinked. The difference in size of **6x** obtained by AFM and DLS could be due to repulsion between phosphate backbones in salt-free environment. Despite its high polyethylene content, the particle appears compact in the AFM images, most likely due to its phospholipid-like folding/compaction and from its collapse on the mica surface. Moreover, the "printed" particle was still intact after incubating at 95°C for 2 hours as analyzed by denaturing PAGE (Experimental Section **Figure 4.18**).

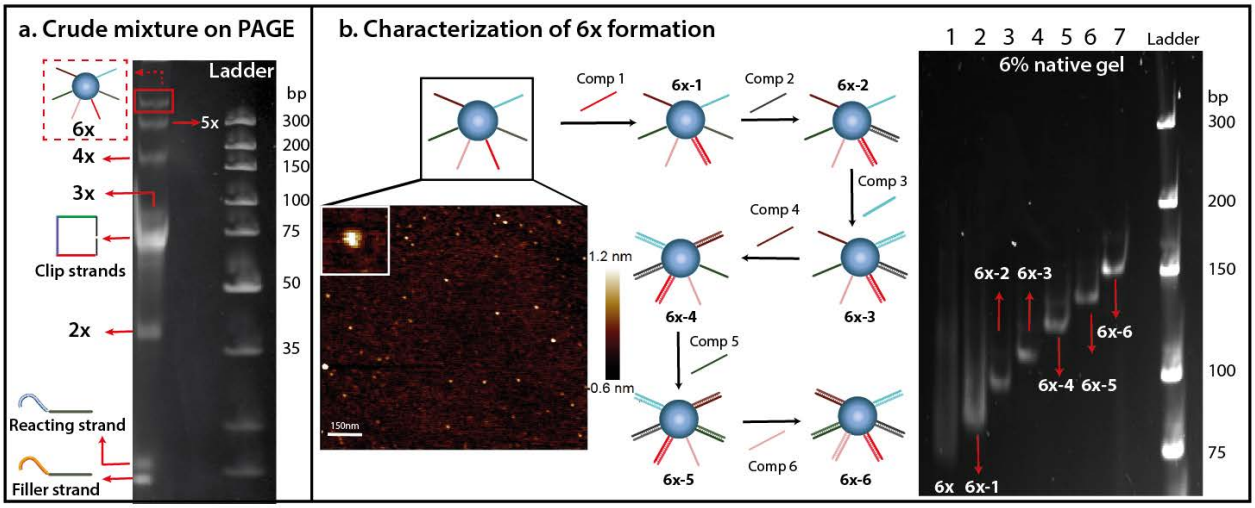

Figure 4.5 | Characterization of "printed" particle. a. 12% denaturing PAGE to separate the desired hexavalent product (**6x**) from other side products (**2x, 3x, 4x** and **5x**) **b.** Characterization of the final product **6x**: **1**) AFM (in air) image of **6x** in Mg^{2+}-free condition. **6x** still maintained its integrity in salt-free environment, suggesting that **6x** was crosslinked. **2**) Adding complementary strands (**comp**) to strands 1 to 6 of **6x** in a stepwise fashion results in lower mobility shifts on 6% native PAGE, consistent with the addressability of each position. **Lane 1**: **6x** (control), **lane 2**: **6x** + comp 1, **lane 3**: **6x** + comp 1-2, **lane 4**: **6x** + comp 1-3, **lane 5**: **6x** + comp 1-4, lane 6: **6x** + comp 1-5, **lane 6**: **6x** + comp 1-6.

To further characterize the number and addressability of the DNA strands transferred onto the crosslinked micelle, six fully complementary strands (**comp 1-6**), which hybridize with each of the 6 DNA unique strands were sequentially added to the printed particles. A sequential decrease in electrophoretic mobility of the structures indicates the successful hybridization of individual **comp 1-6** to **6x** (**Figure 4.5b**, lane **1-7**). In addition, as the complementary strands were added, the width of the band narrowed, likely because the printed particle's polymeric core interacts less with the gel matrix.

4.3.3. Crosslinking reaction inside different cage geometries

Furthermore, the approach can be expanded to different cage geometries (e.g. trigonal prism or pentagonal prism), which tunes the degree of polymerization of the polymer core and demonstrating its versatility **$(-(CH_2-CH_2)-_n$** where e.g., n = 180, 216 or 252). Our previous studies

showed that the pentagonal prism **PP** structure has the largest internal space, followed by cube structure and the trigonal prism **TP** structure has the smallest internal space.[46] More specifically, the internal space of **TP** can accommodate 6 amphiphiles having 5 hexaethylen**e (HE)** units each (capacity = 30 HE units, equivalent to **–$(CH_2\text{-}CH_2)_{180}$**, degree of polymerization (DP)=180); Cube can accommodate 8 amphiphiles having 6 HE units each (capacity = 48 HE units, equivalent to –**$(CH_2\text{-}CH_2)_{288}$**, DP =288) and **PP** can accommodate up to 10 amphiphiles having up to 7 HE units each (capacity = 70 HE units, equivalent to **$(CH_2\text{-}CH_2)_{420}$** , DP = 420).

We positioned DNA amphiphiles on each cage structure to make **6x** as follows:

- For **TP** (having 6 binding sites in total): decorate **6 x** Am-HE_5-Am-DNA (**5 HE** units in each amphiphile); equivalent to a polyethylene chain **–$(CH_2\text{-}CH_2)_{180}$**, degree of polymerization (DP)=180.

- For **Cube** (having 8 binding sites in total): decorate 6 x Am-HE_3-Am-HE_3-Am-DNA (reacting strand) and 2 x HE_6-DNA (non –reacting filler strand) (**6 HE** units in each amphiphile); equivalent to a polyethylene chain **–$(CH_2\text{-}CH_2)_{216}$**, DP=216 in hexavalent printed particle.

- For **PP** (having 10 binding sites in total): decorate 6 x Am-HE_3-Am-HE_4-Am-DNA (reacting strand) and 4 x HE_7-DNA (non- reacting filler strand) (**7 HE** units in each amphiphile); equivalent to a polyethylene chain **–$(CH_2\text{-}CH_2)_{252}$**, DP=252 in hexavalent printed particle.

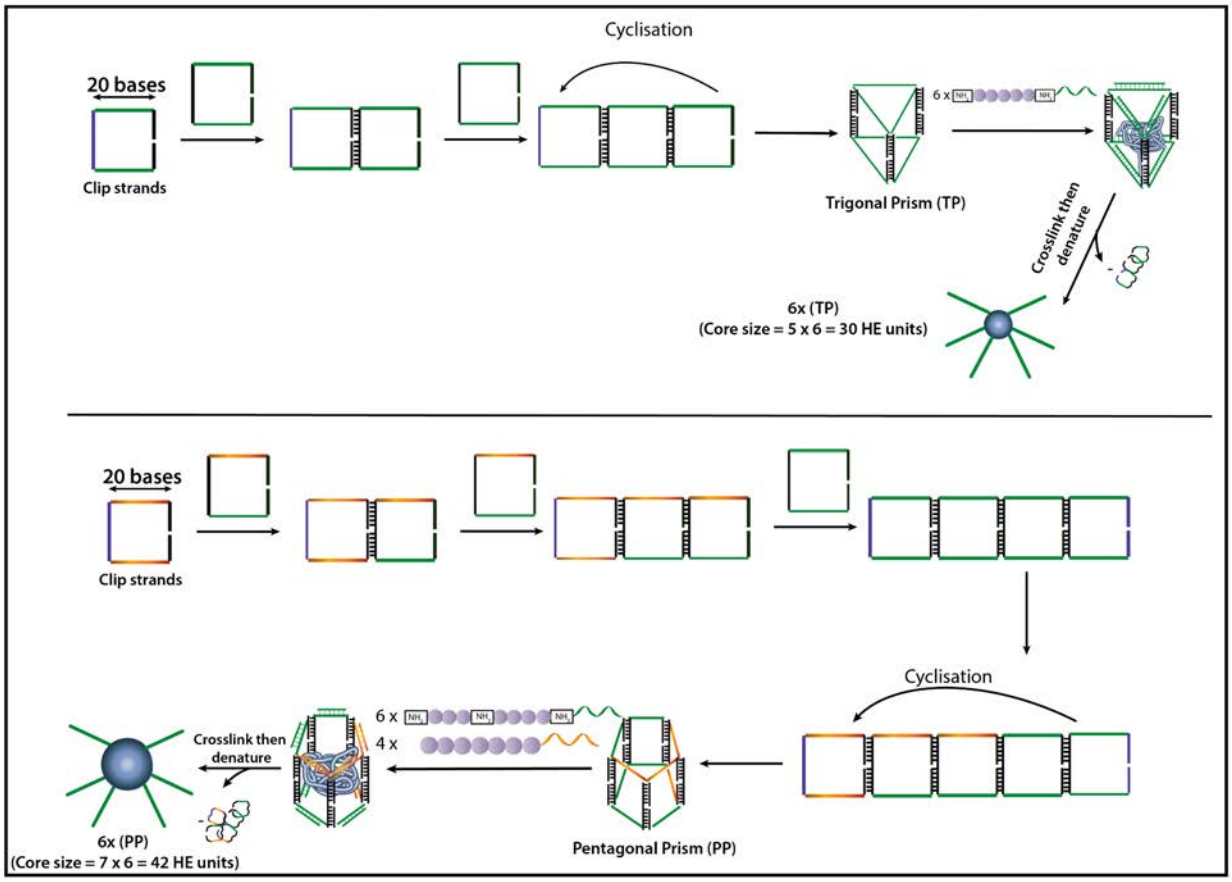

Figure 4.6 | Scheme of crosslinking reaction inside trigonal prism and pentagonal prism.

The retardation in gel mobility shift on native gel suggested that there is an increase in size from **TP** to **PP** structure (**Figure 4.7a).** Based on the denaturing gel of reaction mixtures in different cages shown below, up to hexavalent product (**6x**) was formed in each case (lane **1-3** (squared in yellow) **Figure 4.7b).** This experiment demonstrates the approach's versatility as it can also be used in different geometrical cages other than the cube. Interestingly, there is a decrease in mobility shift of crosslinked products having the same number of DNA arms (same number of bases in total) formed by **TP**, **cube** and **PP**. For example, in the gel Figure **4.7b** below, we have placed a blue box around the **4x** product from the **TP**, **cube** and **PP** (lane **1**, **2** and **3** respectively). the difference in mobility is mainly due to different core size of the particle formed by different cages (for example**,** there are **20 HE (DP = 120)**, **24 HE (DP = 144)** and **28 HE (DP = 168)** units in the core of **4x** formed by **TP**, **cube** and **PP**, respectively). Therefore, the size of the particle can be changed by changing the number of clip strands in the formation of scaffold (more clips = larger

cage). To our knowledge, this is the first example of a monodisperse DNA-polymeric particle featuring a specific number of unique and addressable DNA sequences.

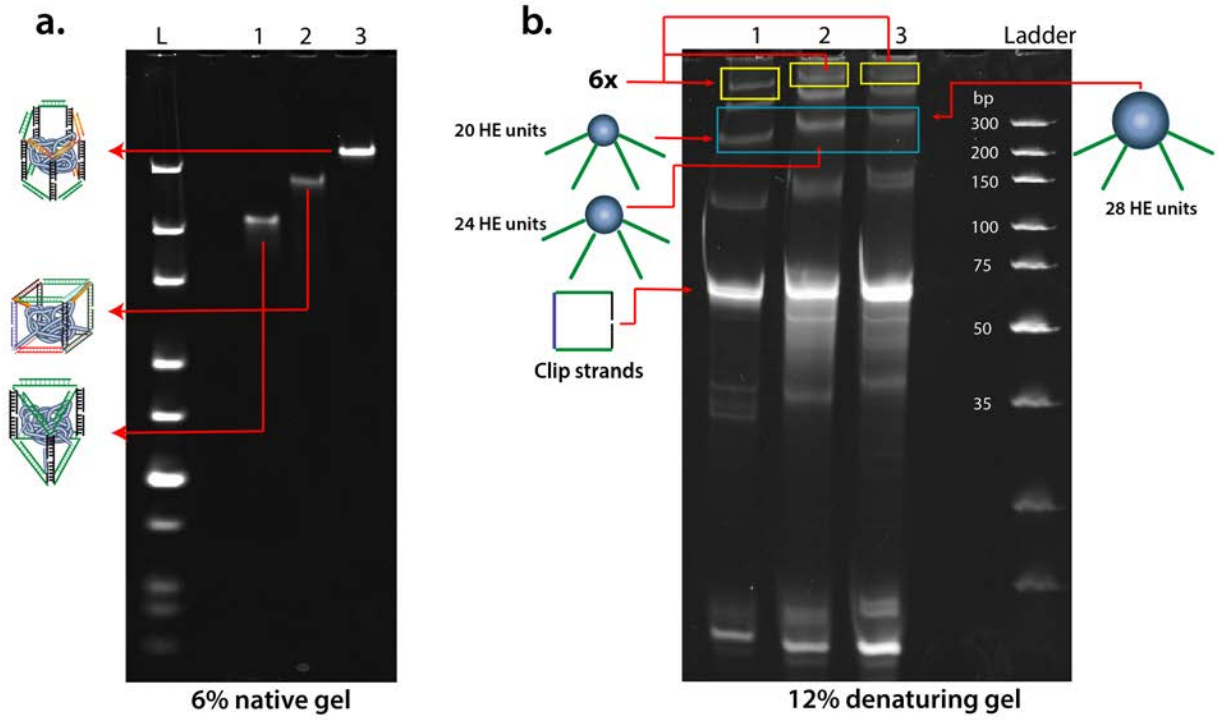

Figure 4.7 | Pattern transfer in different cage geometries. a. 6% native gel shows successful assembly of different structures. **b.** 12% denaturing gel analyzes reaction crude mixtures in each cage.

4.3.4. Rebinding 6x to the "correct" and "incorrect" scaffolds

Following the formation of **6x**, we sought to determine if the relative orientations of DNA strands were maintained after our patterning process. To do this, we carried out a series of rebinding experiments of crosslinked **6x** to the cube scaffold.[42] First, the correct cube scaffold **(Cb)**, whose sequences and geometry match **6x**, was prepared separately, then incubated with **6x** (in excess) at room temperature for 16 hours. Two **HE_6-DNA** strands complementary to the remaining cube sides were also added ("**filler strands"**), in order to fill all 8 binding regions on **Cb** and trigger the intra-scaffold handshake (step **1, Figure 4.8a**). The 6% native PAGE in Figure **4.8d** shows a single band for the resulting rebinding product (**RP**) (lane **2**), indicating high rebinding efficiency. Moreover, **RP** has the same mobility as a control crosslinked cube structure

(Cb-A), implying that it has the same compaction degree and a similar structure (see Experimental Section **Figure 4.5.13** for additional verification). This suggests that the printed particle has its 6 DNA strands bound to their correct positions on the cube.

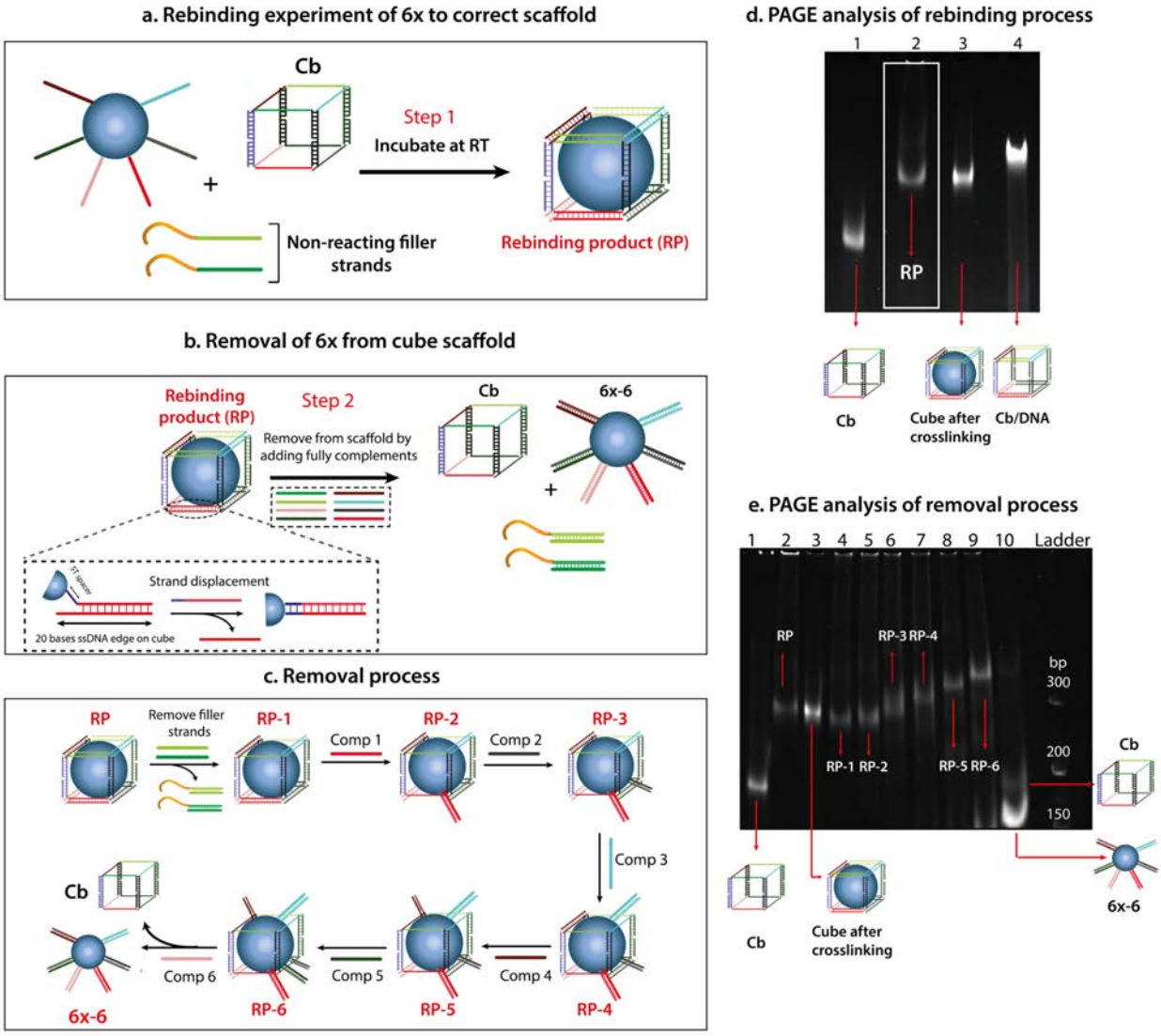

Figure 4.8 | Rebinding experiment of "printed" particle 6x to cube scaffold (Cb). This experiment consists of 2 steps. In the first step, **6x** is rebound to cube scaffold (**Cb)** by incubating at room temperature over 16 hours to form the rebinding product **(RP)**. In the second step, **6x** is removed from **Cb** by adding fully complementary strands (strand displacement) to the **RP. a.** Rebinding experiment of **6x** to **Cb**: **Cb** was incubated with **6x** (in excess) and 2 non-reacting filler strands in order fill up all 8 binding sites on **Cb (Step 1). b** and **c.** Scheme outlining the removal of **6x** from **Cb** using strands that are fully complementary

to **6x (Step 2) d.** 6% native PAGE analysis of the rebinding experiment (**Step 1**): **Lane 1**: Cb scaffold, **lane 2:** rebinding product, **lane 3**: Cb-A (cube after crosslinking), **lane 4**: Cb/DNA (cube with 8 unfunctionalized DNA). **RP** has the same mobility shift as a control crosslinked cube, indicating that **6x** bound completely to **Cb e.** After removal of **6x** from **Cb**, **Cb** was reformed along with the fully double-stranded micelle, **6x-6**, and non-reacting filler strands are hybridized to their complements **(comp-temp)**: 6% native PAGE analysis of the removal experiment **(Step 2)**: **lane 1**: **Cb**, **lane 2**: rebinding product **(RP), lane 3**: **Cb** with amphiphiles after crosslinking (control), **lane 4**: RP + non-reacting filler strand complements (**comp-temp**) which remove the two filler strands, **lanes 5-10: RP** + comp-temp + sequential addition of the complementary strands to **6x** and outlined in **c**.

As the amphiphiles have a 5T spacer and are hybridized to only 14 bases of 20-base edges on the DNA cube, a strand displacement strategy can be used. DNA strands with fully complementary sequences to the strands of **6x** were added to **RP** sequentially. This results in the liberation of **6x** hybridized with 6 complementary strands **(6x-6)** from **Cb** (**Figure 4.8c**). Indeed, only after the addition of all 6 complementary strands (**comp 1-6**) to **RP**, we observed full dissociation of the particle from the cube scaffold (**Figure 4.8e**, lane **10**). This unambiguously confirms that **6x** rebound completely to each of its 6 binding regions on **Cb**. Interestingly, we observed that **6x** could recognize fully the cube scaffold even after being heated at higher temperature (Experimental Section **Figure 4.18** and **4.19**). This implies that the DNA pattern of **6x** is still maintained at higher temperature.

To further verify the asymmetric nature of our "printed" particle (**6x**), we designed a rebinding experiment in which **6x** was incubated with an "incorrect" scaffold. This scaffold (**Cb-wrong**) contains 6 complementary binding regions to **6x,** but they are presented in a different spatial arrangement than the correct template cube (**Cb**), such that only 3 contiguous binding sites on **Cb-wrong** can be accessed by **6x**. Interestingly, **6x** could not bind completely to the wrong scaffold due to its different spatial arrangement; instead, two **6x** particles partially bound to the incorrect cube as characterized by non-denaturing PAGE, DLS and several control experiments (**Figure 4.9**, Experimental Section **4.5.14**-**4.5.16**).

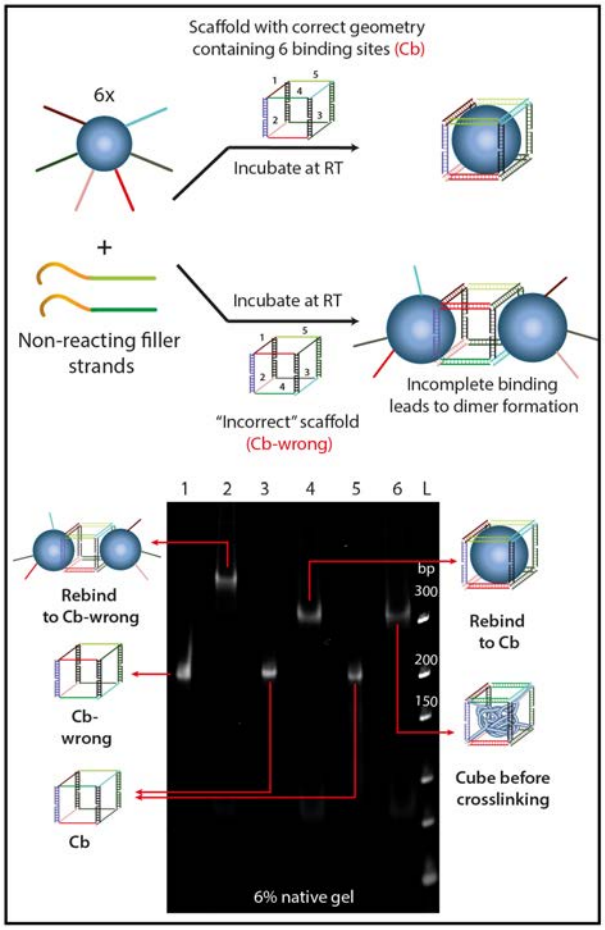

Figure 4.9 | Rebinding experiment to wrong scaffold and molecular simulation. Rebinding experiment of **6x** to wrong cube scaffold **(Cb-wrong).** Due to the difference in configuration, **6x** could not bind completely to **Cb-wrong (**lane **2).** Instead, two printed particles bound partially to the wrong scaffold.

4.3.5. Molecular mechanism of polymer self-assembly and crosslinking inside the DNA cube (peformed by Chenyi Liao and Jianing Li)

To gain insight at the molecular level, we performed computer modeling with molecular dynamics simulations of our cube scaffold (**Cb)** decorated with amphiphiles. Our simulations started from two distinct conformations: **Cb** scaffold with pre-folded hydrophobic portion (control) and with the scaffold with extended hydrophobic portion of amphiphiles. The latter may better represent the annealing conditions of the experiment. Within 20 ns, we observed simultaneous fast-folding and self-assembly of the **HE** chains in the simulations starting from the

extended hydrophobic portion, but relatively slow self-assembly in the simulations starting from the pre-folded hydrophobic portion (**Figure 4.10**).

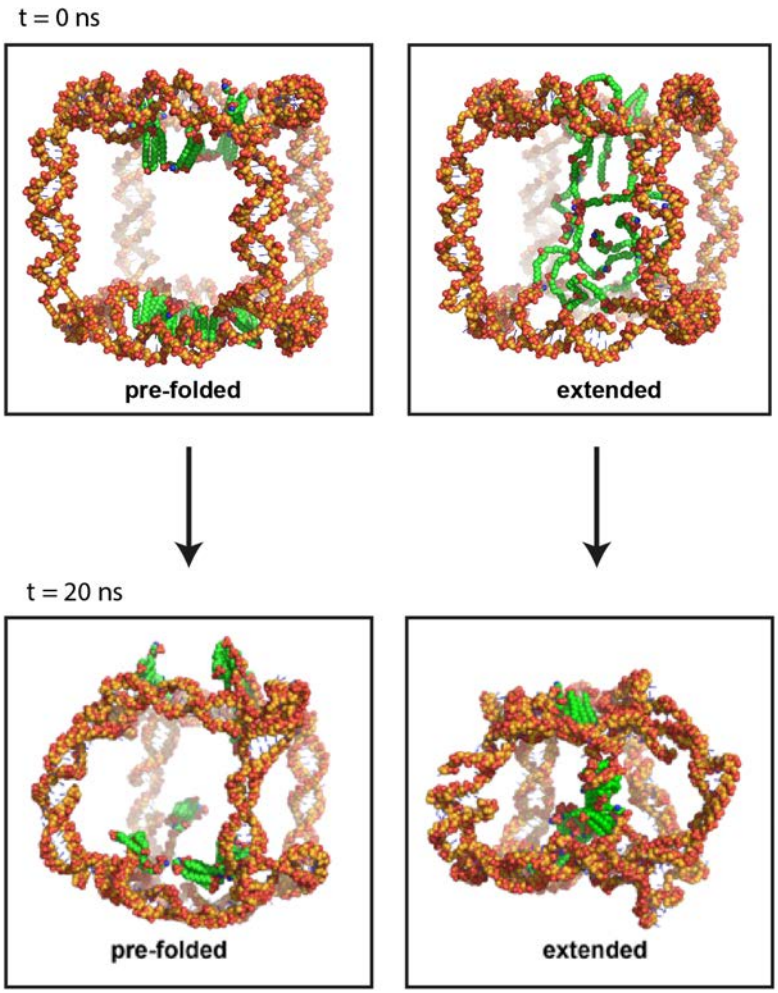

Figure 4.10 | Molecular simulation of cube/amphiphiles structure. Initial and final snapshots at t = 20 ns of two molecular models showing the intramolecular hydrophobic "handshake": one with previously folded hydrophobic chains ("pre-folded") and the second (which better reflects the experimental conditions, "extended") with unfolded hydrophobic chains. Within 20 ns, fast-folding and self-assembly of **HE** chains occurred in the latter case, in accordance with our earlier discussion about scaffold compaction. DNA strands are in orange color; non-reacting and reacting hydrophobic units are in green color.

With the help of the cube, it is likely that the extended **HE** chains can easily form a hydrophobic core inside the cube, which is further stabilized by rearrangements of the charged and hydrophobic groups during the polymer folding (Experimental Section **4.5.21**). To our surprise, this phenomenon is quite different from many natural peptides, in which the self-assembly occurs faster than folding.[48] We also showed that, by significantly reducing the diffusion, the cube facilitates the polymer self-assembly as well as crosslinking. Interestingly, during the self-assembly process, we observed the distortion in length of DNA cubic edges, which further supports our discussion earlier about the compaction of the cube (**Figure 4.10** and Experimental Section

Figure 4.34). Along with the self-assembly process, there is an increasing probability that the **Am** groups from hydrophobic portions are within 15 Å separation, a distance that allows crosslinking. Toward the last 1 ns of the simulations starting from the extended **HE** chains, almost each **Am** group on the reacting strands has another one in the distance range that is ready for crosslinking (Experimental Section **Figure 4.5.21**).

4.3.6. Controlling the valency of "printed" particle

We were interested in controlling the number of DNA strands transferred onto the polymeric core. Although it has been previously examined with gold nanoparticles, [29] it is still a great challenge to control precisely the DNA valency and sequences grafted onto a polymeric core. The ability to control the number and sequences of DNA strands on a nanostructured object is of great importance e.g., to drug delivery, in controlling the nature and number of cell targeting ligands on a nanomaterial.[29] By deliberately hybridizing a predefined number of reacting strands (e.g. x strands where $x \leq 8$) and 8-x non-reacting filler strands (**HE_6-DNA**) on the cube scaffold, after crosslinking using **C10-bi**, an x-valent product was formed and purified (**Figure 4.11a**). Our cube scaffold could be potentially recovered and re-used for "printing" to increase scalability. We were particularly interested in making printed patterns having 2 to 6 unique DNA arms because the synthesis of these structures is not trivial. The divalent (**2x**), trivalent **(3x)**, tetravalent **(4x)** and pentavalent **(5x)** products were formed with 60%, 51%, 40% and 35% yield, respectively (**Figure 4.11b**, see Experimental Section **4.5.17** for gel characterization and **4.5.22** ((**8x)** formation).

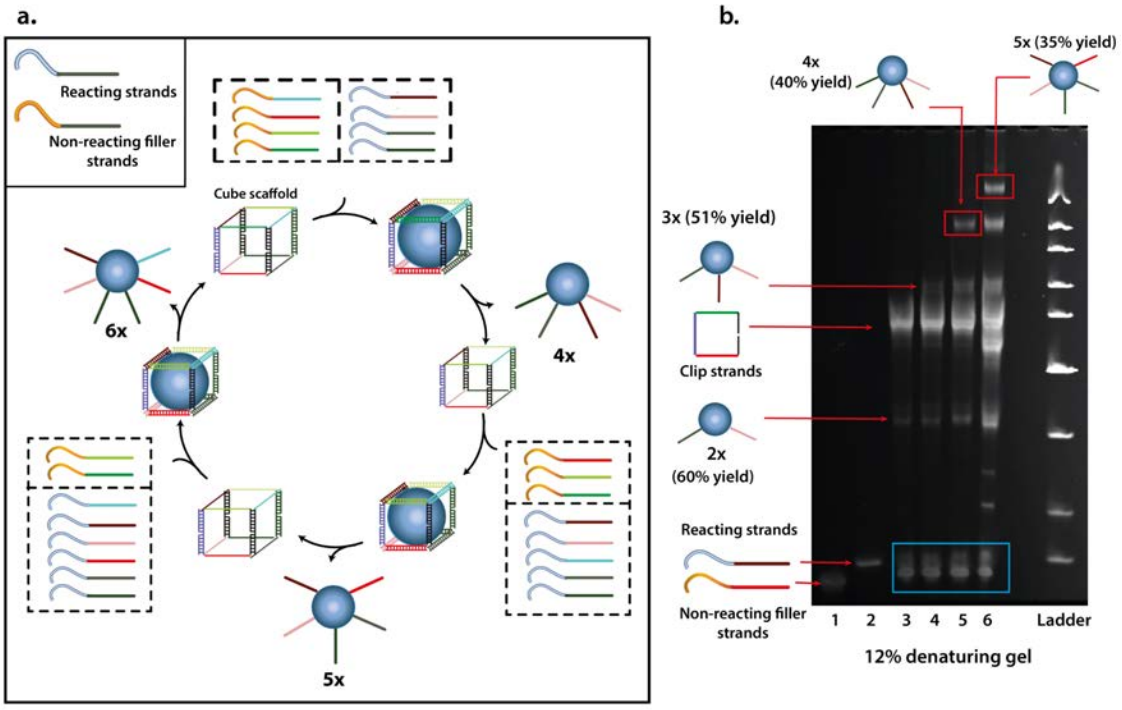

Figure 4.11 | **Controlled valency of DNA-imprinted particles. a.** Overall process of controlling the number of DNA strands transferred from DNA cube scaffold. By decorating the scaffold with pre-defined number of reacting and filler strands, polymeric particles with desired valency can be formed. Our cube scaffold could be potentially recovered and re-used in another "printing" process, thus increasing the scalability of this approach. **b.** Denaturation of the cube after crosslinking results in non-reacting filler strands, cube clip strands and a mixture of printed products with different valency. Indeed, the unreacted "filler strands" dissociate from the particle (squared in blue box in Figure **4.11**) leaving behind the prescribed number of DNA arms and HE core. 12% denaturing PAGE: **Lane 1**: non-reacting filler strand without functional groups (HE_6 amphiphile) (control), **lane 2**: reacting strand with 3 **Am** group (control), **lanes 3-5**: denatured crosslinked cubes which produced divalent (2x, **lane 3**), trivalent (3x, **lane 4**), tetravalent (4x, **lane 5**) and pentavalent (5x, **lane 6**) products.

4.3.7. Self-assembly of printed particles 6x into higher-order discrete structures

An important challenge is to generate complex and well-defined polymeric structures by self-assembly.[49-50] Therefore, we were motivated to explore the possibility of using them as new building blocks in assembling nanostructures based on polymeric particles. We thus set out to create a dimer and a trimer from the printed particle **6x** as a proof of concept. **Connector 1**, which

is a 42 base-pair DNA duplex with 14-base sticky ends at both ends, was introduced to bring together two **DIPs** with a designed configuration, separated by 70 bases, leading to the formation of dimer product (Figure **4.12**). To make DIPs trimer, we further added more **DIP** and **connector 2** (same design as **connector 1)**. This allows the positioning of two other **DIPs** in adjacent relative positions on the central particle (**Figure 4.12** and **4.13** for positioning). Native PAGE revealed the successful assembly as demonstrated by the decrease in mobility shifts (Experimental Section Figure **4.30**). Dimer and trimer assembled structures were further characterized by AFM (in air) in 2 separate experiments with yields of 68% (N=196) and 45% (N=345), respectively (**Figure 4.12** and Experimental Section **4.5.23)**. The difference in yield compared to PAGE is most likely due to AFM sample preparation. Moreover, the distance between two printed particles was measured to be 22.0±2.5 nm (N=100), which is in accordance with the expected length of a 70 DNA base pairs duplex connecting the particles (~23.8 nm).

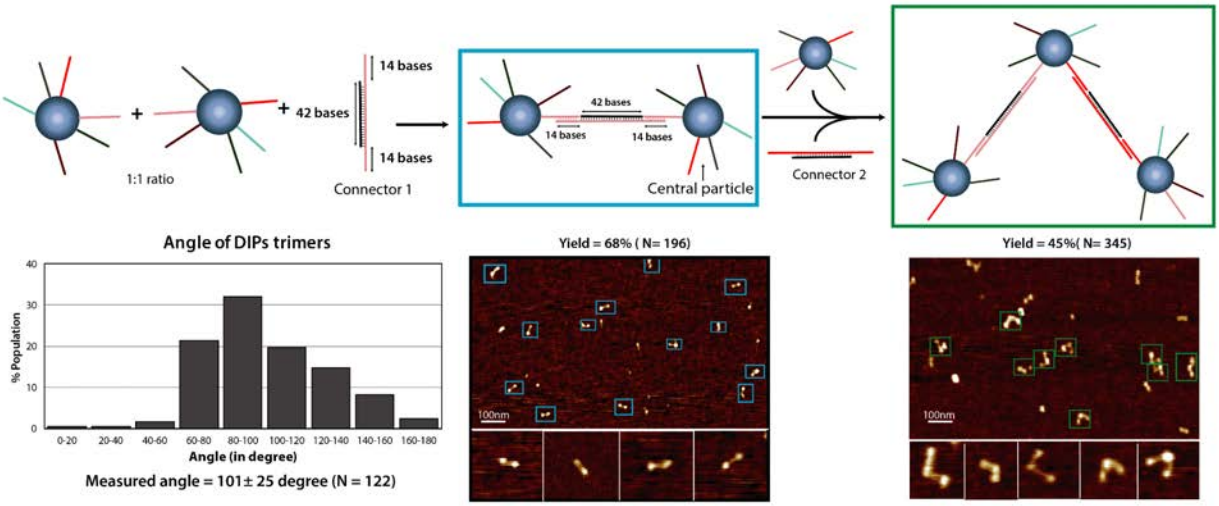

Figure 4.12 | **Self-assembly of DIPs into dimer and trimer and angle analysis of DIPs trimer**. AFM images under dry condition in 2 separate experiments showed the structure of dimer and trimer **DIPs** with yields of 68% and 45%, respectively. The inter-particle distance was measured to be 22.0±2.5 nm (N=100) and can be finely tuned. Measured angle of trimer **DIPs** is approximately 101 ± 25 degree (N=122).

The asymmetric nature of the **6x** was further examined using AFM for the construction of trimer structures. The central particle allows us to place 2 other particles in the "opposite" positions to

each other (by using 2 DNA arms transferred from 2 opposite cube edges), resulting in wider observed angles of the trimers (**Figure 4.13** and Experimental Section **Figure 4.29**).

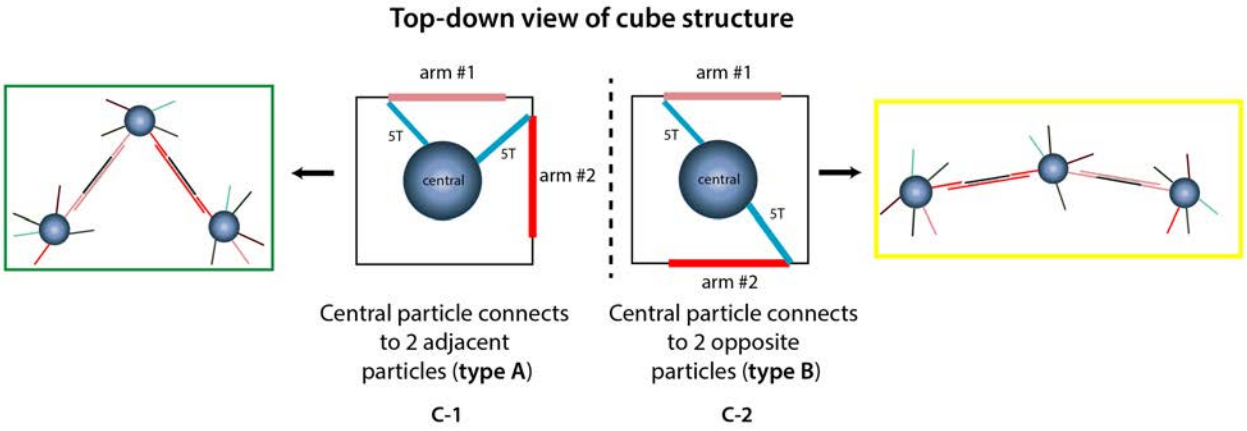

Figure 4.13 | Representation of 2 different types of self-assembled DIPs trimers.

We expect that if the relative placement is maintained, we should observe a wider angle in **type B**-trimer compared to **type A**-trimer (**Figure 4.13**). Indeed, by analyzing angular distributions in each type of trimer structure, we observed the trimers with configuration **B** have wider angles than the trimers having configuration **A** (Figure **4.12** and **4.14**).

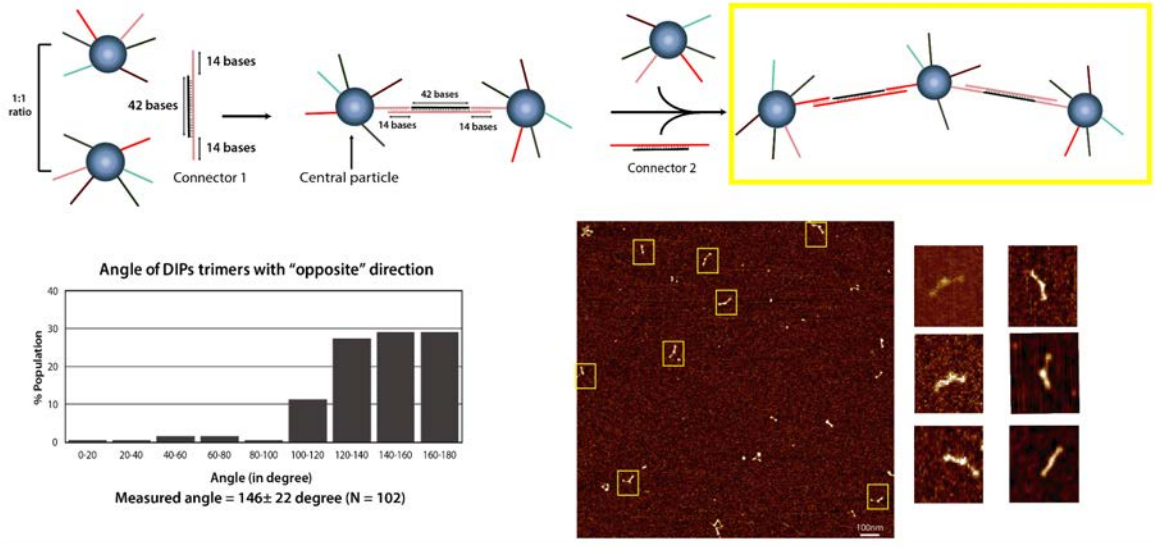

Figure 4.14 | Self-assembly of DIPs trimers with 2 particles in "opposite" position and angle analysis. Measured angle of trimer "opposite" **DIPs** is approximately 146 ± 22 degree (N=102).

Finally, self-assembled tetramer structures based on **DIPs** were prepared with yield of 40% (N=183), where 3 particles were connected to the central particle by adding more **DIP** and **connector 3**. Unambiguously, a wider angle between particle **1** and **3** (2 DNA arms are originally from opposite edges of the cube**)** compared to angles between particles **1** and **2** or between particles **2** and **3** (2 DNA arms are originally from adjacent edges of the cube) are observed in tetramer (Figure **4.15** and Experimental Section **4.5.20**). Moreover, the angle between particles **1** and **2** is statistically similar to the angle between particles **2** and **3,** reflecting the adjacent positions of the DNA strands on the printed particles. This further confirms the retention of the relative geometric patterns after being transferred from the cube scaffold. For our statistical analysis, we only counted tetramer species presenting all 3 arms on the mica surface. The yield of 40% tetramer may reflect the manner in which the structures land on the mica surface, as their arms can be turned towards the surface and may thus appear to have fewer arms (e.g., they may look like trimers while they are tetramers).

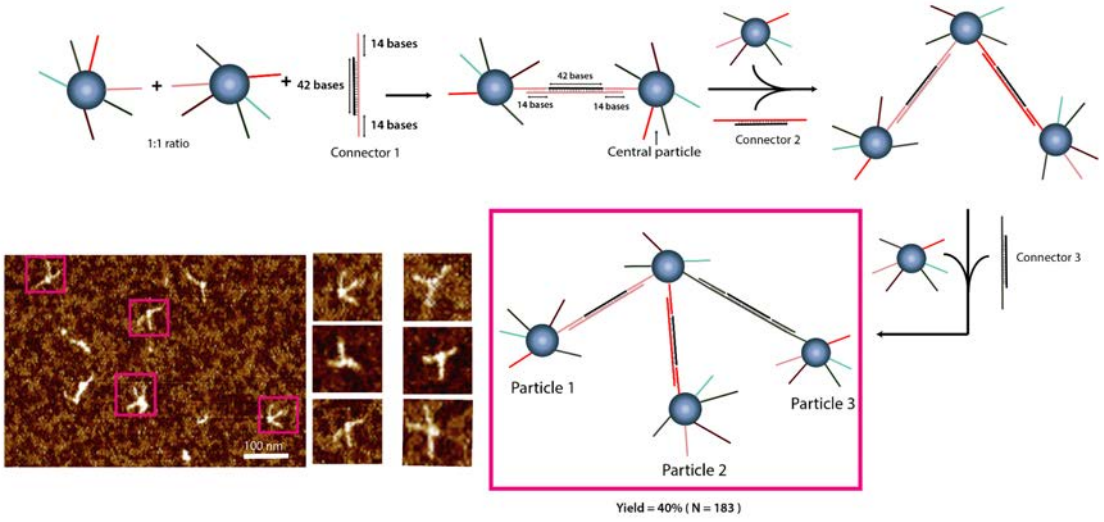

Figure 4.15 | Self-assembly of DIPs tetramers with 3 particles connected to the central particle.

4.4. Conclusion

In this chapter, we have demonstrated the first method to transfer DNA patterns in 3D, directly from a DNA cubic scaffold to well-defined polymeric particles. We have shown that our

printed particle (**6x)** has exactly 6 unique DNA strands grafted on its **HE** core and that its valency can be controlled exactly. The polymer nanoparticle is "molded" inside the cage, with a precise and tunable number of repeat units. More importantly, the hexavalent printed particles preserve the orientation and sequence anisotropy obtained from the DNA cubic scaffold, which was demonstrated using scaffold rebinding as well as hierarchical assembly experiments. We anticipate that this method will serve in the self-assembly of colloidal particles in which the printed particles can serve as precisely-defined "6-arm junctions" to create highly complex nanostructures in a predictable manner. As well, this method can be used in targeted delivery and diagnostics in the future due to the addressability and monodispersity of the resulting particles. More specifically, our "printed" particle could potentially be functionalized with targeting moieties with chosen 3D orientations, which is of great importance in polyvalent receptor recognition.[51] Applications such as drug delivery vehicles, asymmetrically substituted nanomaterials to control cellular processes, barcoded diagnostics or building blocks for non-centrosymmetric polymer patterning are anticipated. These directions of research as well as scaling-up the printed product (e.g. by immobilizing the scaffold on bead) will be our main focus in the future.

4.5. Experimental Section

4.5.1. General

Unless otherwise stated, all commercial reagents and solvents were used without additional purification. Magnesium sulfate hexahydrate ($MgSO_4 \cdot 6H_2O$), tris(hydroxymethyl)aminomethane (Tris), urea, sebacic acid bis (*N*-hydroxysuccinimide) (C10-bi), chloroform ($CHCl_3$), tetrahydrofurane (THF) were used as purchased from Sigma-Aldrich and used without further purification. Glacial acetic acid and boric acid were purchased from Fisher Scientific and used without further purification. GelRed™ nucleic acid stain was purchased from Biotium Inc. Acrylamide/Bis-acrylamide (40% 19:1 solution), ammonium persulfate and tetramethylenediamine were obtained from Bioshop Canada Inc. and used as supplied. 1 μmol Universal 1000Å LCAACPG supports and standard reagents used for automated DNA synthesis were purchased through Bioautomation. Sephadex G-25 (super fine, DNA grade) was purchased

from Glen Research. DMT-hexaethyloxy-glycol (HEG, cat.# CLP-9765) and Fmoc-Amino-DMT C-3 CED (cat.# CLP-1661) phosphoramidites were purchased from ChemGenes Corporated. TAMg buffer is composed of 45 mM Tris and 12.5 mM $MgCl_2.6H_2O$ with the pH adjusted to 8.0 using glacial acetic acid. TBE buffer is 90 mM Tris, 90 mM boric acid and 2 mM EDTA with a pH of 8.0. TEAA mobile phase is 50 mM triethylammonium acetate with the pH adjusted to 8.0 using glacial acetic acid.

4.5.2. Instrumentation

Standard automated oligonucleotide solid-phase synthesis was performed on a Mermade MM6 synthesizer from Bioautomation. HPLC purification was carried out on an Agilent Infinity 1260. DNA quantification measurements were performed by UV absorbance with a NanoDrop Lite spectrophotometer from Thermo Scientific. Gel electrophoresis experiments were carried out on a 20 X 20 cm vertical Hoefer 600 electrophoresis unit. Gel images were captured using a ChemiDocTM MP System from Bio-Rad Laboratories. Thermal annealing of all DNA structures was conducted using an Eppendorf Mastercycler® 96 well thermocycler. Electroelution employed an Elutrap Electroelution System from Whatman®. Liquid Chromatography Electrospray Ionization Mass Spectrometry (LC-ESI-MS) was carried out using Dionex Ultimate 3000 coupled to a Bruker MaXis Impact™ QTOF. Gels were imaged by BioRad ChemiDoc MP. Multimode 3 and multimode 8 scanning probe microscope and Nanoscope V controller (Bruker, Santa Barbara, CA) was used to acquire AFM images. DLS measurements were carried out using Zetasizer Nano Z obtained for Malvern Instruments.

4.5.3. Synthesis, Purification of DNA strands

DNA synthesis was performed on a 1 μmol scale, starting from the required nucleotide modified 1000 Å LCAA-CPG solid-support. Coupling efficiency was monitored after removal of the dimethoxytrityl (DMT) 5-OH protecting groups. DMT-hexaethyloxy-glycol (HEG, cat.# CLP-9765) and Fmoc-Amino-DMT C-3 CED phosphoramidites (cat.# CLP-1661) were purchased from ChemGenes. Coupling efficiency was monitored by the removal of DMT group on 5'-OH groups.

+ For DNA amphiphiles: In order to couple modified monomers, in a glove box under nitrogen atmosphere, DMT-dodecane-diol and Fmoc-Amino-DMT C-3 CED phosphoramidite were dissolved in acetonitrile and shaken for 10 mins to achieve final concentration of 0.1 M. The modifiers were activated with 200 uL of 0.25M 5-(ethylthio)tetrazole in anhydrous acetonitrile and the extended coupling times of 10 minutes were used. 3% dichloroacetic acid in dichloromethane was used to remove DMT protecting group on the DNA synthesizer. After the synthesis was completed, CPG was treated with 28% aqueous ammonium hydroxide solution for 16-18 hours at 60^{o}C in water bath. The crude mixture then was concentrated under reduced pressure at 60^{o}C and filtered by 0.22μm centrifugal filter before purifying by RP-HPLC (3-50% ACN in 30 mins).

+ For DNA clip strands: DNA was synthesized using Mermade MM6 DNA synthesizer. DMT-hexaethyloxy-glycol amidite was dissolved in anhydrous acetonitrile to 0.1 M final concentration. Coupling efficiency was monitored after removal of the DMT 5-OH protecting group. After deprotection step using aqueous NH_4OH solution (28%), the crude product was isolated, dried, and re-suspended in 1:1 8M urea before loading to polyacrylamide/urea gel (15% denaturing PAGE). The gel was run at 250 V for 30 minutes followed by 500 V for 45-60 minutes in 1x TBE as the running buffer. The gel was then imaged and excised on TLC plate under a UV lamp. The solution was dried to approximately 1 mL before loading to Sephadex G-25 column. The purified DNA was quantified by the absorbance at 260 nm.

4.5.4. DNA Sequences

A. Clip strands:

Sequences are listed from 5' to 3' (**6** = DMT-hexaethyloxy-glycol (**HEG**, cat.# CLP-9765)). All clip strands were synthesized using Mermade MM6 on 1umol scale and purified by 15% denaturing PAGE.

1AB:

TCGCTGAGTA6TCCTATATGGTCAACTGCTC6GCAAGTGTGGGCACGCACAC6GTAGT
AATACCAGATGGAGT6CACAAATCTG

2AC:

CTATCGGTAG6TCCTATATGGTCAACTGCTC6TACTCAGCGACAGATTTGTG6GTAGT AATACCAGATGGAGT 6 CAACTAGCGG

3AD:

CACTGGTCAG6TCCTATATGGTCAACTGCTC6CTACCGATAGCCGCTAGTTG6GTAGT AATACCAGATGGAGT 6 GGTTTGCTGA

4AE: CCACACTTGC 6 TCCTATATGGTCAACTGCTC 6 CTGACCAGTGTCAGCAAACC 6 GTAGTAATACCAGATGGAGT 6 GTGTGCGTGC

1AA: TCGCTGAGTA 6 TCCTATATGGTCAACTGCTC 6 GCAAGTGTGGGCACGCACAC 6 TCCTATATGGTCAACTGCTC 6 CACAAATCTG

2AA: CTATCGGTAG 6 TCCTATATGGTCAACTGCTC 6 TACTCAGCGACAGATTTGTG 6 TCCTATATGGTCAACTGCTC 6 CAACTAGCGG

3AA:

CACTGGTCAG6TCCTATATGGTCAACTGCTC6CTACCGATAGCCGCTAGTTG6TCCTA TATGGTCAACTGCTC 6 GGTTTGCTGA

4AA:

CCACACTTGC6TCCTATATGGTCAACTGCTC6CTGACCAGTGTCAGCAAACC6TCCTA TATGGTCAACTGCTC 6 GTGTGCGTGC

TP3-AA:

CCACACTTGC6TCCTATATGGTCAACTGCTC6CTACCGATAGCCGCTAGTTG6TCCTA TATGGTCAACTGCTC 6 GTGTGCGTGC

PP4-AA:

TACCGGATCG6TCCTATATGGTCAACTGCTC6CTGACCAGTGTCAGCAAACC6TCCTA TATGGTCAACTGCTC6CCGTAATTGC

PP5-AA:

CCACACTTGC6TCCTATATGGTCAACTGCTC6CGATCCGGTAGCAATTACGG6TCCTA TATGGTCAACTGCTC 6 GTGTGCGTGC

1BA:

TCGCTGAGTA 6 GTAGTAATACCAGATGGAGT 6 GCAAGTGTGGGCACGCACAC 6 TCCTATATGGTCAACTGCTC 6 CACAAATCTG

2BA:

CTATCGGTAG 6 GTAGTAATACCAGATGGAGT 6 TACTCAGCGACAGATTTGTG 6 TCCTATATGGTCAACTGCTC 6 CAACTAGCGG

3BA:

CACTGGTCAG6GTAGTAATACCAGATGGAGT6CTACCGATAGCCGCTAGTTG6TCCTA TATGGTCAACTGCTC 6 GGTTTGCTGA

4BA:

CCACACTTGC6GTAGTAATACCAGATGGAGT6CTGACCAGTGTCAGCAAACC6TCCT ATATGGTCAACTGCTC6GTGTGCGTGC

2CD:

CTATCGGTAG6AAAACTCTGCCGTAAGAGGA6TACTCAGCGACAGATTTGTG6GCCT GGCCTTGGTCCATTTG 6 CAACTAGCGG

3AE:

CACTGGTCAG6TCCTATATGGTCAACTGCTC6CTACCGATAGCCGCTAGTTG6TAACA GGATTAGCAGAGCGA6GGTTTGCTGA

4IH:

CCACACTTGC6GTAACCGCGACTGCGAGAGT6CTGACCAGTGTCAGCAAACC6TCCT CTTCTATACTGGCCTC 6 GTGTGCGTGC

4HI:

CCACACTTGC6TCCTCTTCTATACTGGCCTC6CTGACCAGTGTCAGCAAACC6GTAAC CGCGACTGCGAGAGT6GTGTGCGTGC

3EC:

CTATCGGTAG6GCCTGGCCTTGGTCCATTTG6TACTCAGCGACAGATTTGTG6AAAAC TCTGCCGTAAGAGGA6CAACTAGCGG

- **Connect 1**, **connect 2, A42** were obtained from IDT (standard desalting) and used directly for assembly experiment.

Connect 1 (connect via B sequence):

GTAATACCAGATGGTTTTTTTTTTTTTTTTTTTTTTTTTTTTTTTTTTTTTTTTTGTAAT ACCAGATGG

Connect 2 (connect via D sequence):

TCTTCTATACTGGCTTTTTTTTTTTTTTTTTTTTTTTTTTTTTTTTTTTTTTTTTATCTTC TATACTGGC

A42:

AAAAAAAAAAAAAAAAAAAAAAAAAAAAAAAAAAAAAA

B. DNA amphiphiles

Sequences are listed from 5' to 3' direction. (**X** = DMT-dodecane-diol phosphoramidite (cat.# CLP-1114), **Am** = Fmoc-Amino-DMT C-3 CED (cat.# CLP-1661) phosphoramidite). DNA

amphiphiles were synthesized as listed above. The crude products were purified using RP-HPLC using Agilent 1260 Infinity HPLC. The purity of DNA amphiphiles used was determined by HPLC and LC-MS.

HE_6-AT: XXXXXX - TTTTTCAGTTGACCATATA

Am-HE_3-Am-HE_3-Am-AT: Am-XXX-Am-XXX-Am-TTTTTCAGTTGACCATATA

Am-HE_3-Am-HE_3-Am-BT: Am-XXX-Am-XXX-Am-TTTTTCCATCTGGTATTAC

BT- Am-HE_3-Am-HE_3-AG: CCATCTGGTATTACTTTTT- Am-XXX-Am-XXX-Am

Am-HE_3-Am-HE_3-Am-CT: Am-XXX-Am-XXX-Am-TTTTTTCTTACGGCAGAGT

Am-HE_3-Am-HE_3-Am-DT: Am-XXX-Am-XXX-Am-TTTTTATGGACCAAGGCCA

DT-Am-HE_3-Am-HE_3-Am: ATGGACCAAGGCCATTTTT Am-XXX-Am-XXX-Am

Am-HE_3-Am-HE_3-Am-ET: Am-XXX-Am-XXX-Am-TTTTTCTCTGCTAATCCTG

Am-HE_3-Am-HE_3-Am-IT: Am-XXX-Am-XXX-Am- TTTTTCTCGCAGTCGCGGT

Am-HE_3-Am-HE_3-Am-HT: Am-XXX-Am-XXX-Am-TTTTTGCCAGTATAGAAGA

HT- Am-HE_3-Am-HE_3-Am: GCCAGTATAGAAGATTTTT-Am-XXX-Am-XXX-Am

<u>For optimization of crosslinking yield:</u>

Am-HE_5-Am-AT: Am-XXXXX-Am-TTTTTCAGTTGACCATATA

Am-HE_6-Am-AT: Am-XXXXXX-Am-TTTTTCAGTTGACCATATA

HE-Am-HE_4-Am-HE-AT: X-Am-XXXX-Am-X-TTTTTCAGTTGACCATATA

HE-Am-HE-Am-HE_3-AT: X-Am-X-Am-XXX-TTTTTCAGTTGACCATATA

4.5.5. HPLC purification and LC-MS characterizations of DNA amphiphiles

- **HPLC purification:** Solvent system: A: Triethylamine-acetic acid buffer, B: Acetonitrile. TEAA buffer (50mM Triethylammonium acetate, pH 8.0) was filtered through 0.22 μm cellulose membrane before use. All DNA strands with amino-modified monomer were purified by RP-HPLC. Two mobile phases were TEAA and and HPLC grade acetonitrile. Elution gradient used: 3-50% acetonitrile over 30 minutes at 60ºC. Column used: Hamilton PRP 1 5 μm 2.1x150mm**.** Approximately 0.5-0.75 OD_{260} of crude amphiphiles was injected as a 20-50μL solution in Milipore water and then detected using a diode array detector monitoring absorbance at 260nm.
- **LC-MS characterization of DNA amphiphiles:** The oligonucleotides were analyzed by LC-ESI-MS in negative ESI mode. Samples were run through an acclaim RSLC 120 C18 column (2.2μM 120Å 2.1 x 50mm) using a gradient of 98% mobile phase A (100mM 1,1,1,3,3,3-hexafluoro-2-propanol and 5mM triethylamine in water) and 2 % mobile phase B (Methanol) to 40 % mobile phase A and 60% mobile phase B in 8 minutes. The data was processed and deconvoluted using the Bruker DataAnalysis software version 4.1.

Am-HE_3-Am-HE_3-Am-BT:

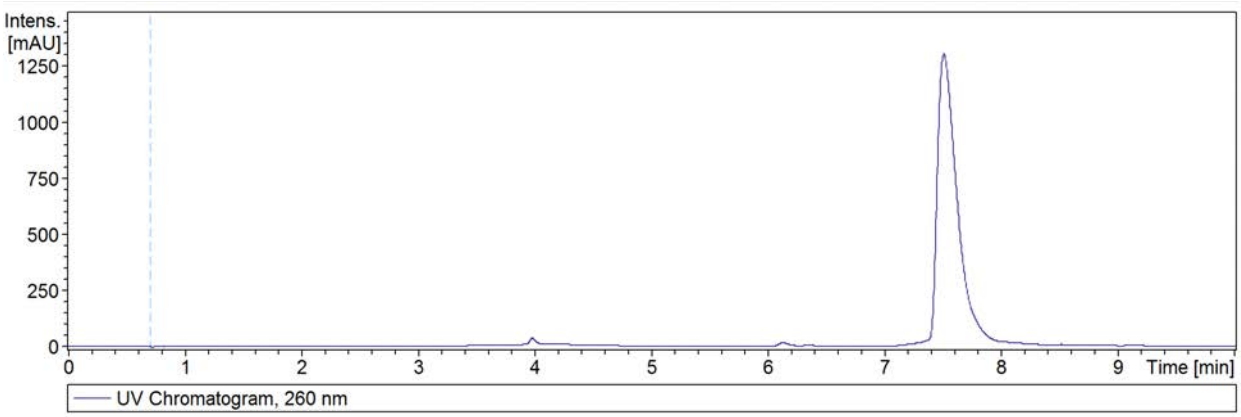

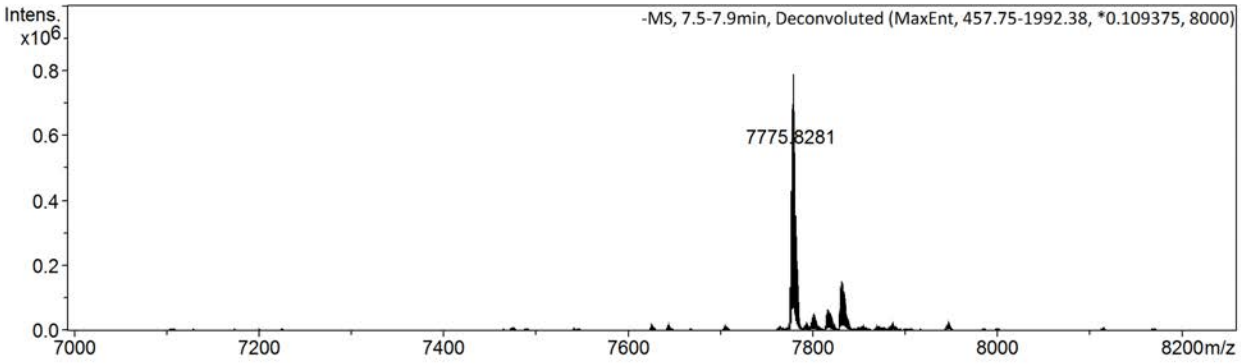

Am-HE$_3$-Am-HE$_3$-Am-CT:

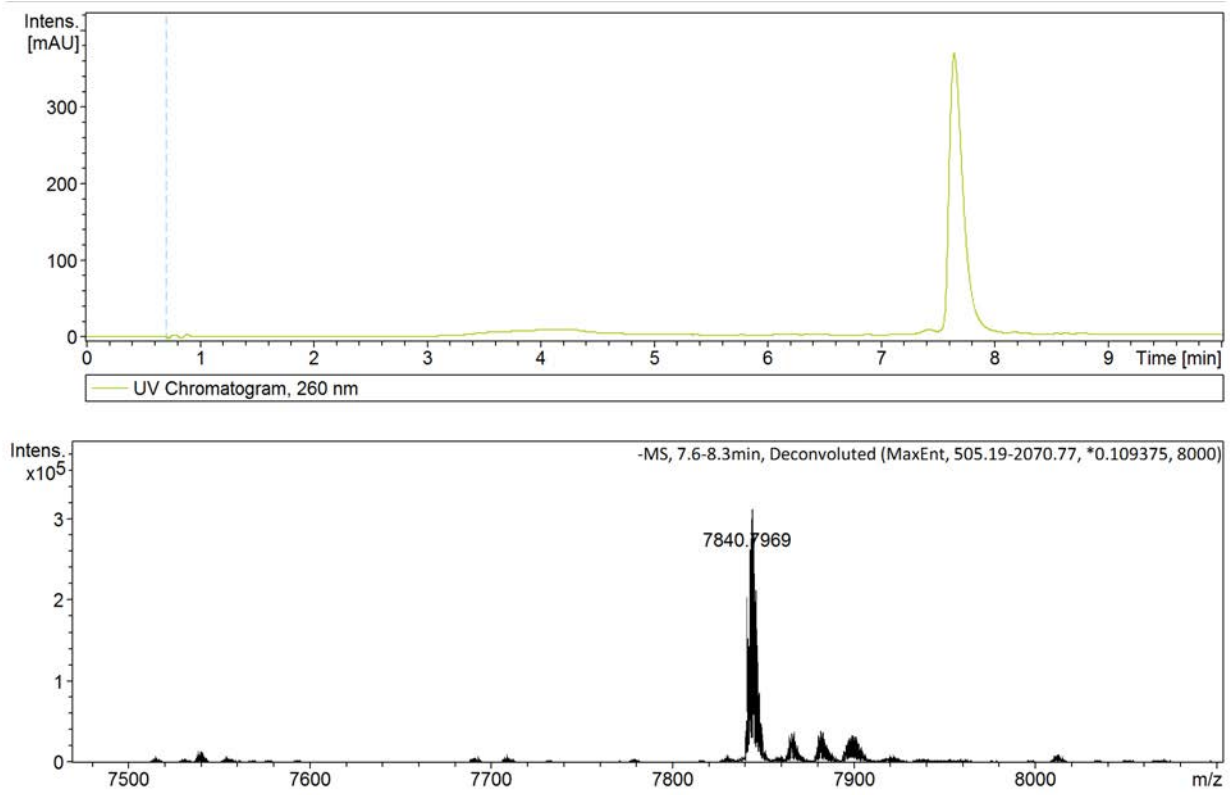

Am-HE$_3$-Am-HE$_3$-Am-DT:

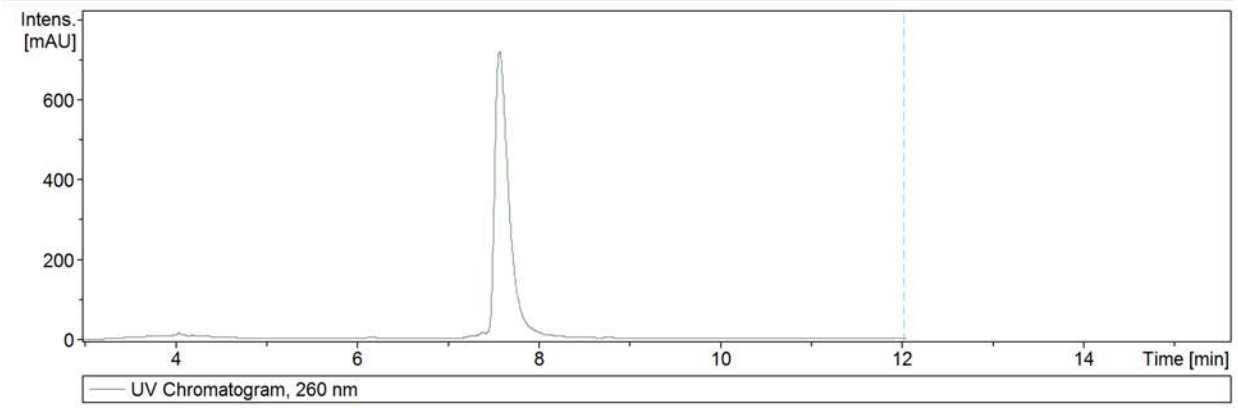

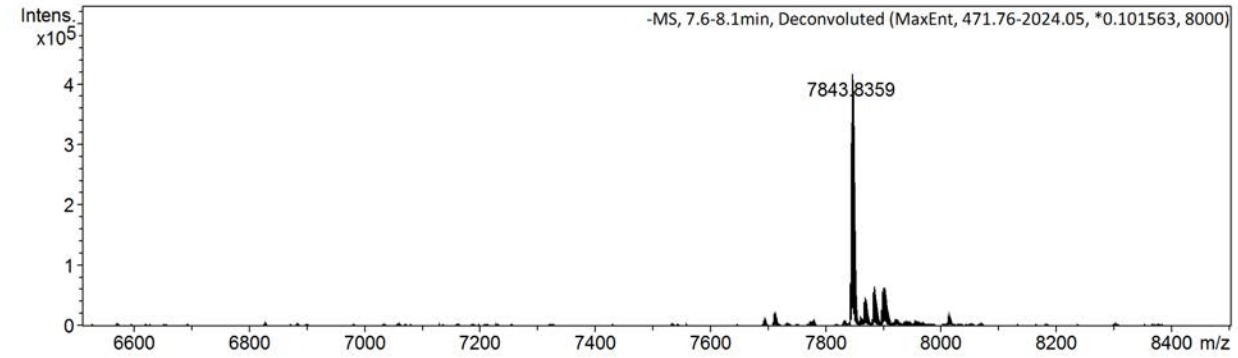

Am-HE$_3$-Am-HE$_3$-Am-ET

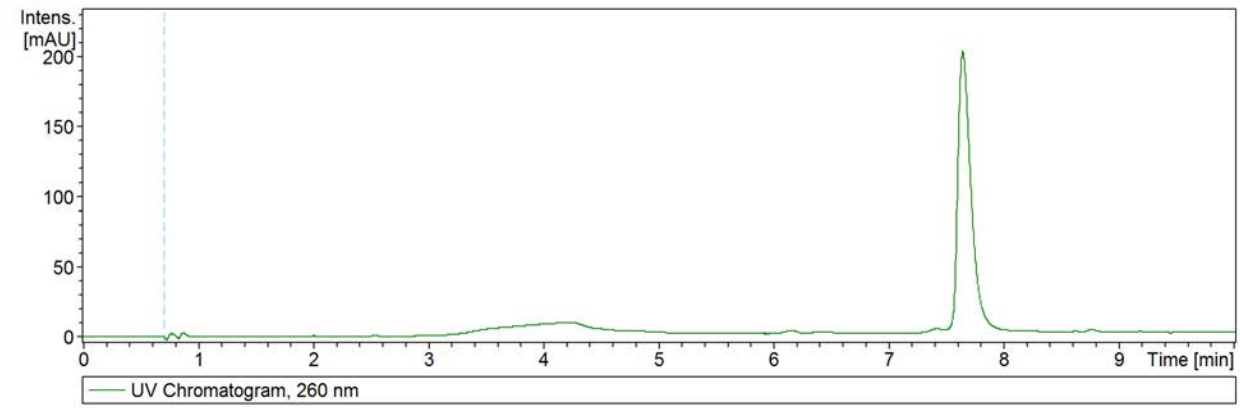

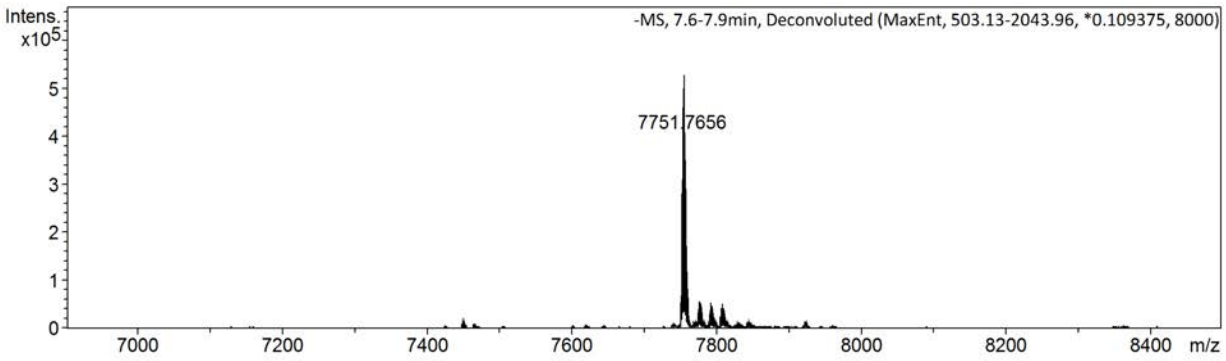

Am-HE$_3$-Am-HE$_3$-Am-HT

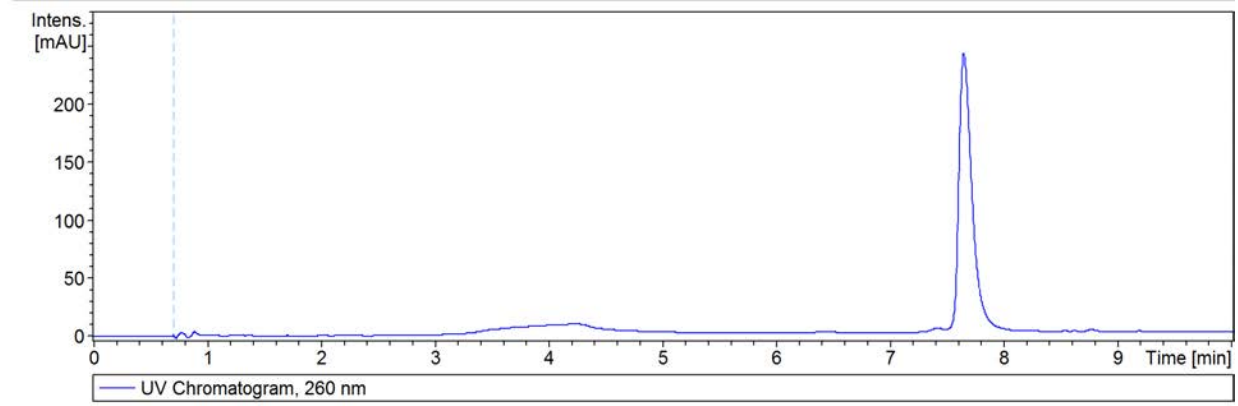

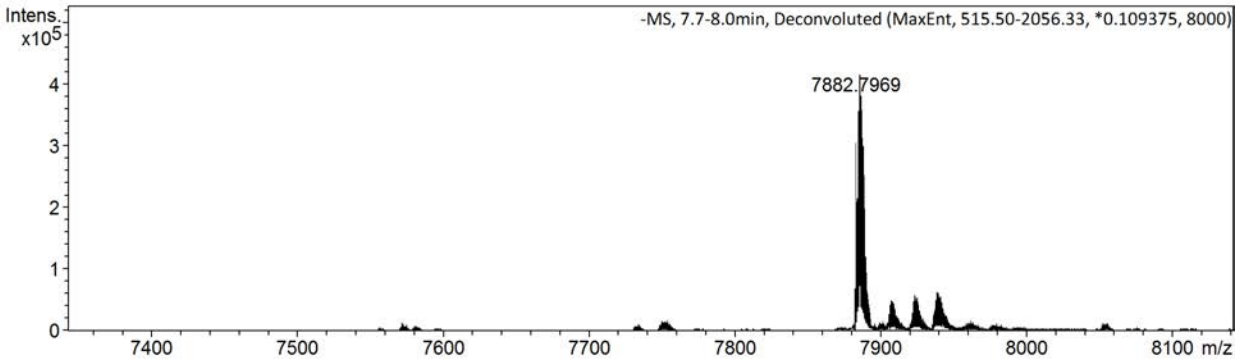

Am-HE$_3$-Am-HE$_3$-Am-IT

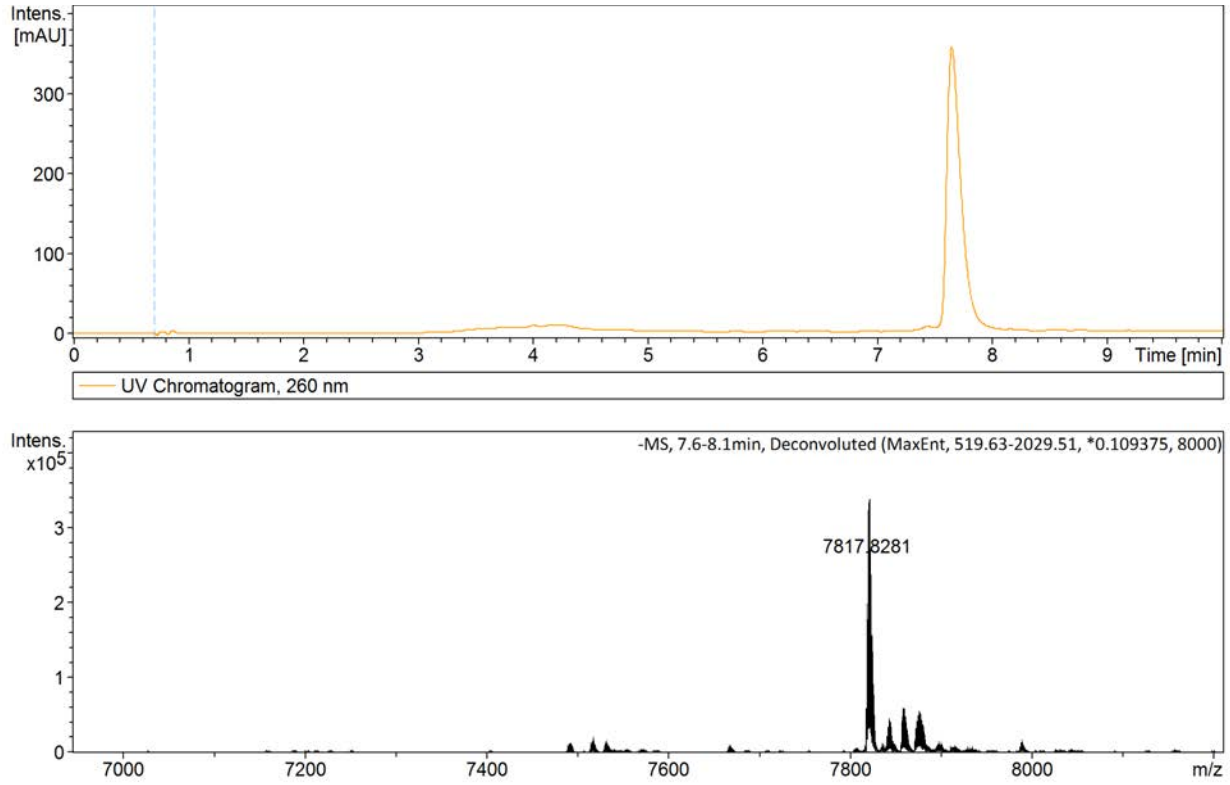

4.5.6. Cage design and assembly

To assemble a cage, the equimolar amounts (1.25 pmole) of all required DNA clips were mixed in 1xTAMg buffer (10 µL) to obtain final cage concentration of 125 nM. The sample was heated at 95ºC for 5 minutes, at 80ºC for 3 minutes, cooled to 60ºC (2 min/ºC), and slowly cooled to 4 ºC (3 mins/ºC).

Summary of the combination of DNA clips for the construction of different cages used in this study:

Cb (correct): 1AB+2CD+3AE+4IH
Cb (wrong): 1BA+ 2EC + 3AD +4IH
TP3: 1AA + 2AA + TP-3AA
Cb to make **6x (1)**: 1AB + 2EC + 3AD + 4HI
Cb-1: 1AB+2AA+3AA + 4AA

Cb-2: 1AA + 2CD+ 3AA + 4AA

Cb-3: 1AB + 2CD + 3AA + 4AA

Cb-4: 1AB + 2CD + 3AE + 4AA

Cb-5: 1AB + 2CD +3AA + 4IH

Set of DNA clips used in "control number of DNA strands" experiment:

Divalent system: 1AB + 2AA + 3AD + 4AA

Trivalent system: 1AB + 2AC + 3AD + 4AA

Tetravalent system: 1AB + 2AC + 3AD + 4AE

Pentavalent system: 1AA + 2CD + 3AE + 4IH

An assembly of the cage was followed by 6% non-denaturing PAGE. The mixture of 10 μL of sample and 2 μL of glycerol mix (7:1 glycerol/H2O) was loaded on 6% native PAGE with 1xTAMg as the running buffer. The gel was run at 250 V for 2.5 hours and stained with GelRed. Cage was formed in near-quantitative yields only in the presence of all required DNA clips. **(**Figure **4.16,** lane **4).** Lane **1**: 1AB, lane **2:** 1AB+2CD, lane **3:** 1AB+2CD+3AE, lane **4:** 1AB+2CD+3AE+4 IH.

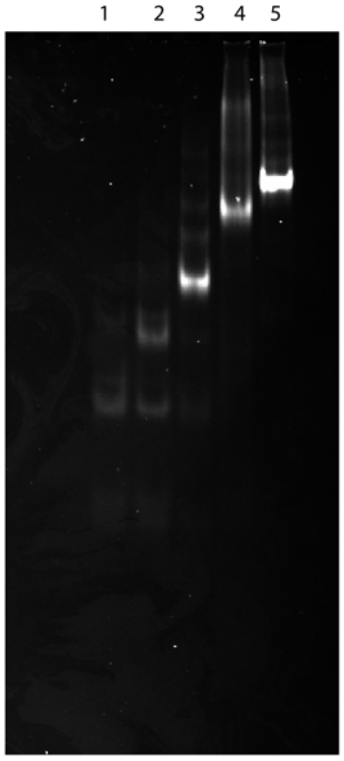

Figure 4.16 | 6% non-denaturing PAGE analysis of step-wise assembly of cube scaffold **(Cb)**. **Lane 1**: 1AB, **lane 2**: 1AB + 2CD, **lane 3**: 1AB + 2CD + 3AE, **lane 4**: 1AB + 2CD + 3AE + 4IH.

4.5.7. Cage assembly with DNA amphiphiles before crosslinking

All required DNA clips and DNA-polymer conjugates in appropriate ratios (1 stoichiometric equivalent per binding site) were mixed in 1x TAMg to obtain final cage concentration of 500 nM. The sample was subjected to the same annealing protocol from 95°C to 4°C in 4 hours, mixed with 2μL glycerol mix and then analyzed on 6% native PAGE with 1xTAMg as the running buffer (250 V for 2.5 hours). The assembly of cube scaffold was then checked by 6% native PAGE (250V, 2h30 mins) before being crosslinked as shown in Figure **1** in the manuscript.

4.5.8. Crosslinking inside DNA cages and purification of printed particle procedure.

After assembly of appropriate DNA amphiphiles to DNA cage scaffold (500nM final concentration), 10mM of sebacic acid bis (*N*-hydroxysuccinimide) (C10-bi) was dissolved in THF and added to the solution of DNA-cube micelle at 1:10 ratio in volume to make final concentration

of 1mM. The reaction mixture was stirred at room temperature overnight (~16 hours). Then, the reaction mixture was concentrated under vacuum at 60°C using Speedvac machine followed by adding 8M urea and running through 12% denaturing PAGE. The gel was then run at 250V for 30 mins and 500V for 2 hours 10 mins with 1xTBE as the running buffer. The desired gel band was excised and recovered using electroelution.

4.5.9. **Comment on crosslinking yield**

We observed from the analysis of band intensity that the yield of printed particle **6x** was 30% in yield. In order to totally connect 6 DNA-amphiphiles strands together, we need at least 5 crosslink molecules (C10-bi) (indicated in red color), which is equivalent to at least 10 reaction points of the amino group (on DNA amphiphles) with the NHS ester functional group (on crosslinker) (see Figure **4.17**). Therefore, the yield of each individual reaction is nearly 90% indicating that the chemistry we used is highly efficient.

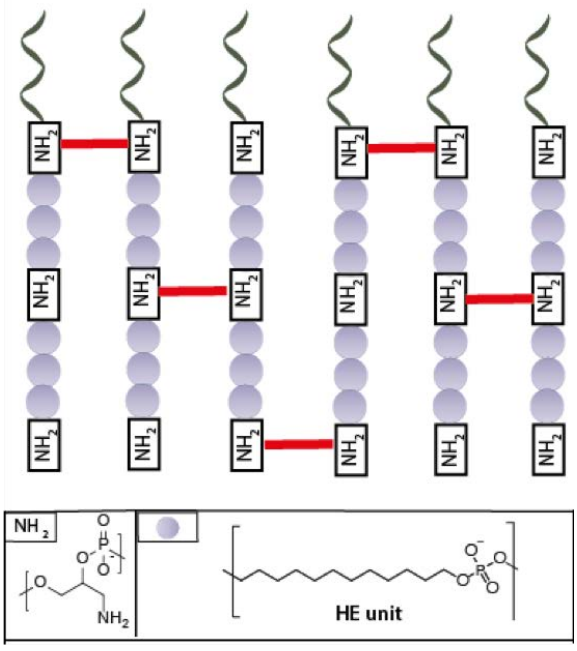

Figure 4.17 | One possible crosslinking between DNA amphiphiles

4.5.10. Stability of 6x and rebinding experiment of 6x after being exposed to heat

- A solution of **6x** in water was incubated in Eppendorf Mastercycler® 96 well thermocycler at 95^{o}C for 2 hours. Then, the solution of heated **6x** was added 8M urea (1:1 volume ratio) and analyzed by 12% denaturing PAGE (1x TBE as running buffer). The gel was run at 250 V for 30 mins and 500 V for 50 mins and stained with Gel Red before imaging. The gel analysis showed that the structure remains intact after being exposed to heat and no smaller fragments was shown up on the gel **(**Figure **4.18 A).**

- Furthermore, the solution of heated **6x** was incubated in excess with pre-formed correct cube scaffold matching sequences and geometries at 250 nM at room temperature for 16 hours. All samples were added 2.0 uL glycerol before loading into 6% non-denaturing PAGE. The gel was run at 250 V for 3 hours in 1x TAMg buffer. The gel showed that **6x** still rebound to the cube scaffold with high binding efficiency, suggesting that **6x** still retains all information inherited from DNA scaffold even after heating (Figure **4.18 B**).

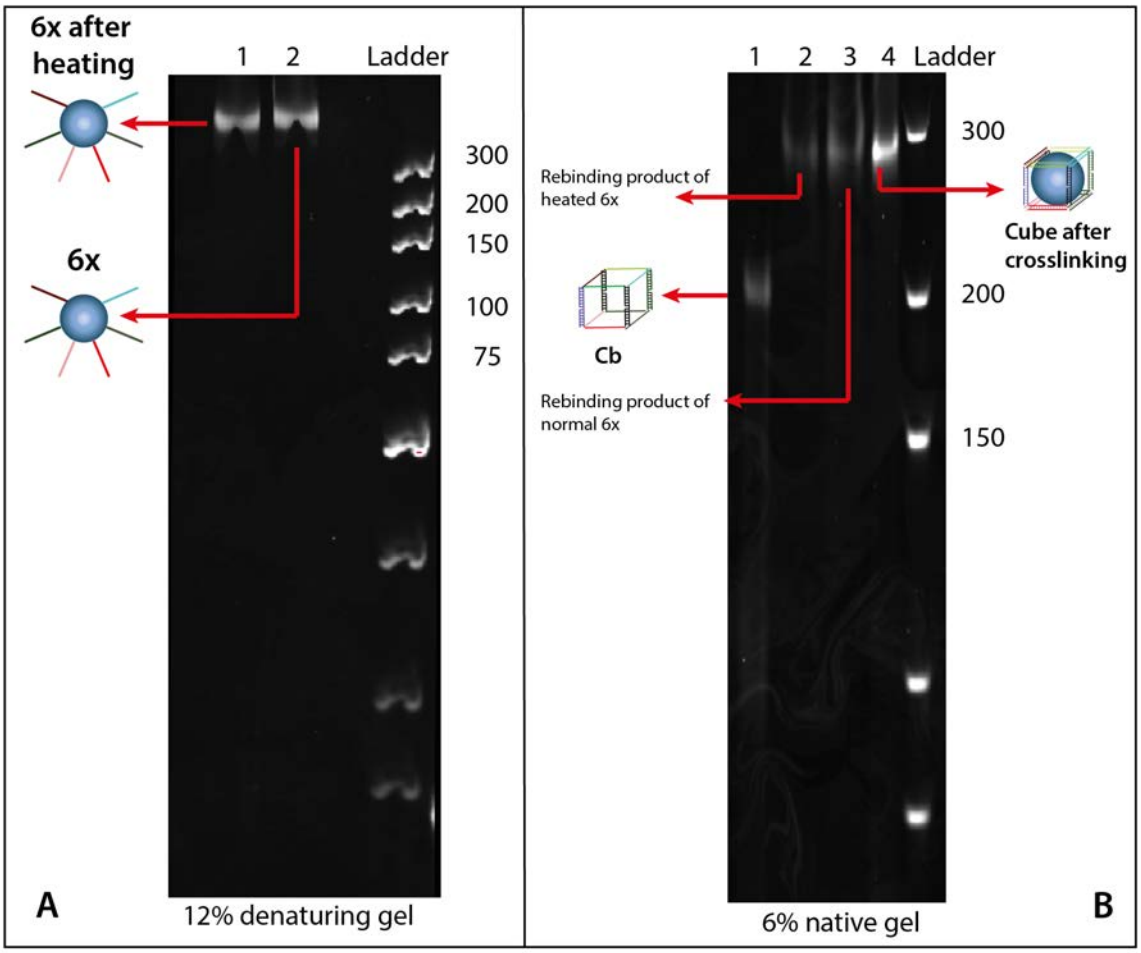

Figure 4.18 | A) 12% denaturing PAGE analysis of **6x** after exposure to heat. **Lane 1:** 6x after incubating at 95°C for 2 hours, **lane 2:** control 6x without heating. B) Rebinding experiment of **6x** after incubating at 95°C analyzed by 6% native PAGE. **Lane 1**: Cube scaffold (Cb), **lane 2:** rebinding product of heated **6x** to correct cube scaffold, **lane 3**: rebinding product of **6x** to correct cube scaffold (control), **lane 4**: cube after crosslinking (control).

4.5.11. Rebinding experiment at higher temperature to correct scaffold

Solution of **6x** in water was incubated with pre-formed cube scaffold at 250nM for 16 hours at different temperatures (30°C, 35°C, 40°C and 45°C). We chose 45°C as the upper limit temperature regarding to the stability of the cube scaffold. Then, rebound product mixtures were mixed with 2uL of glycerol mix before loading to 6% native PAGE. The gel was run at 250 V for 3 hours and stained with Gel Red before imaging. The gel demonstrated that the relative positioning of DNA

strands on the printed particle **6x** is still maintained at higher temperature (Figure **4.19).**

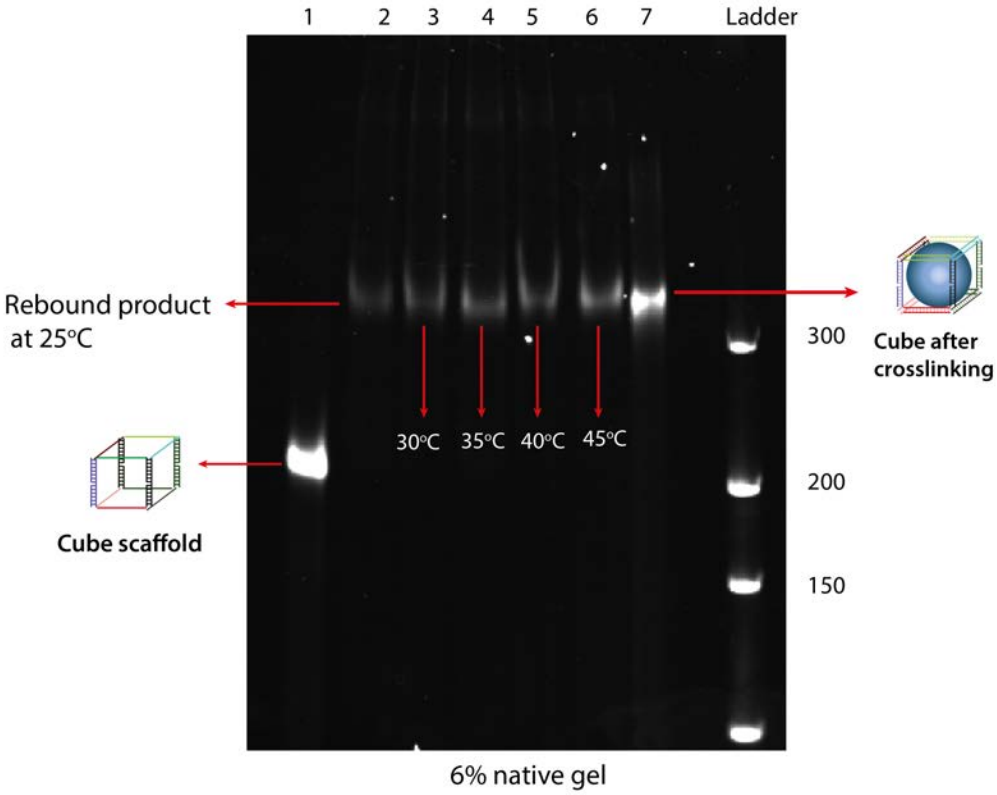

Figure 4.19 | 6% non-denaturing PAGE analysis of rebinding product of 6x to correct scaffold at different temperature. **Lane 1**: Correct cube scaffold (Cb), **lane 2**: rebinding product at 25°C, **lane 3**: rebinding product at 30°C, **lane 4**: rebinding product at 35°C, **lane 5**: rebinding product at 40°C, **lane 6**: rebinding product at 45°C, **lane 7**: cube after crosslinking (control).

4.5.12. Remove 6x from the rebinding product to correct scaffold

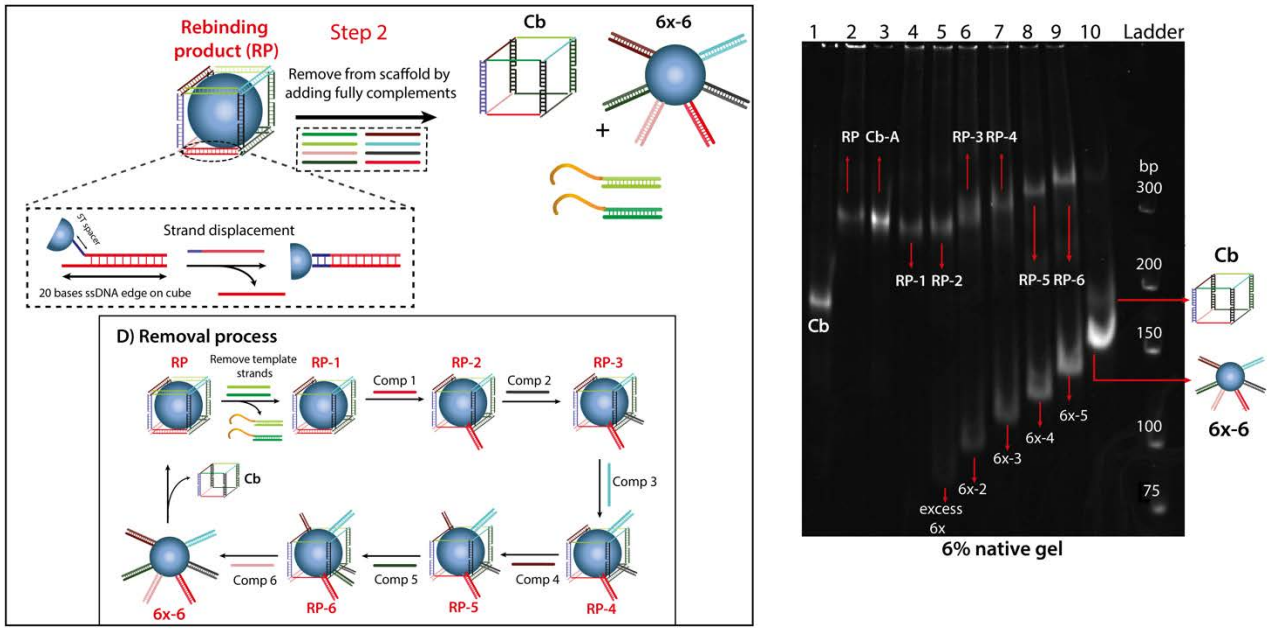

Figure 4.20 | Scheme outlining the removal of **6x** from **Cb** using strands that are fully complementary to **6x (Step 2).** 6% non-denaturing PAGE analysis of the removal experiment **(Step 2)**: **lane 1**: Cb, **lane 2**: rebinding product **(RP), lane 3**: **Cb** with amphiphiles after crosslinking (control), **lane 4**: RP + non-reacting filler strand complements (**comp-temp**) which remove the two non-reacting filler strands, **lanes 5-10: RP** + comp-temp + sequential addition of the complementary strands to **6x** and outlined in D. *Note that since **6x** was used in excess, the unbound **6x** can also hybridize to complementary strands when added to form **6x-2, 6x-3, 6x-4, 6x-5** at the bottom of the gel (Figure **4.8**).*

4.5.13. Compaction of the scaffold when 6x rebound

In order to verify that the binding of **6x** indeed caused the compaction of the scaffold, we designed a control experiment in which **6x** was incubated with scaffolds that have different numbers of binding regions for **6x**, yet retained the relative position of each region with respect to **Cb (Cb-1** to **Cb-6)** (Figure **4.21A**). Interestingly, the rebinding products increase in gel mobility

as the number of complementary sites to **6x** increases, consistent with scaffold compaction (lane **2, 4, 6, 8, 10** and **12**, Figure **4.21B**).

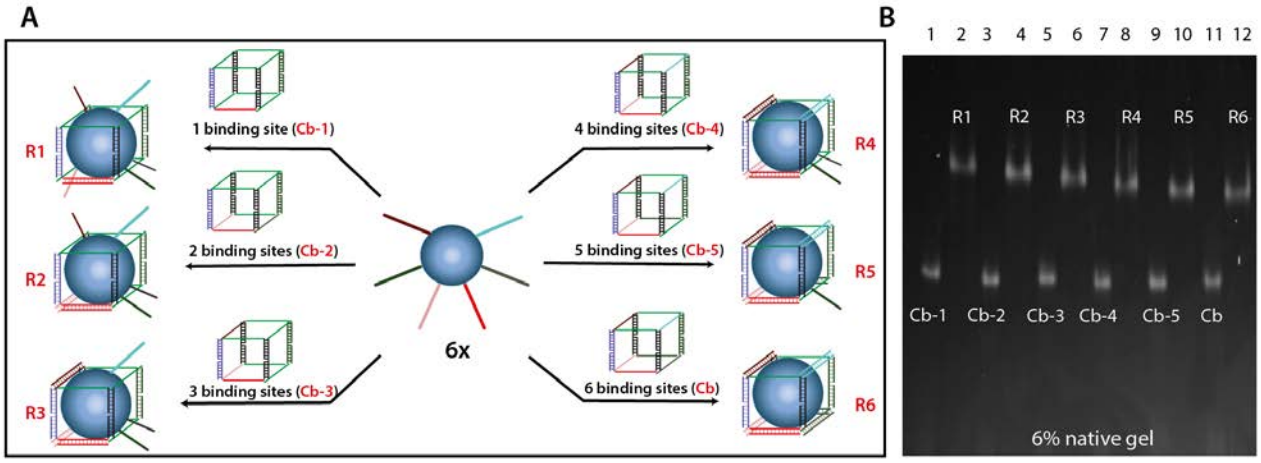

Figure 4.21 | A) Control experiment showing the rebinding of **6x** to scaffolds with different number of binding sites (**Cb, Cb-1, Cb-2, Cb-3, Cb-4** and **Cb-5**). **6x** was incubated with these scaffolds at room temperature for 16 hours. **R1** to **R6** correspond to binding products of **6x** with these different scaffolds. **B)** 6% native PAGE (TAMg 1x as running buffer, 250V for 4 hours) for comparing the gel mobility of each rebinding product (**R1-6**). We observed an increase in the gel mobility of the rebinding products as the number of binding regions for **6x** increases, suggesting that more compact structures were formed: Lane 1: **Cb-1**, lane 2**: 6x + Cb-1,** lane 3**: Cb-2,** lane 4**: 6x + Cb-2,** lane 5**: Cb-3,** lane 6**: 6x + Cb-3,** lane 7**: Cb-4,** lane 8**: 6x + Cb-4,** lane 9**: Cb-5,** lane 10**: 6x + Cb-5,** lane 11**: Cb-6,** lane 12**: 6x + Cb-6.**

4.5.14. Characterization of dimer formation from rebinding experiment to wrong scaffold

A. Remove 6x from the wrong scaffold:

Cb-wrong was designed to keep 3 binding regions (region **1-3** highlighted in Figure **4.22A**) with the same positioning as **Cb** but it has the 3 other binding sites scrambled. We hypothesized that if **6x** embeds all the information transferred from **Cb**, it should not be able to completely bind to **Cb-wrong**. The 6% native PAGE shows that the rebinding product incubated with **Cb-wrong** (lane **2,** Figure **4.22B)** moves slower on the gel than the ones incubated with the correct **Cb** scaffold (lane **4, Figure 4.22B**).

We were interested in a strand displacement experiment of "printed" particles **6x** from the wrong scaffold by adding fully complementary strands with **6x** to rebound product as demonstrated earlier and monitored the process by native PAGE. Interestingly, after **6x** was hybridized with 3 specific complementary strands sequentially (**comp 2,4** and **6**) at the region **1,2** and **3**, there was a noticeable increase in mobility shift of the structure **RW-4** in lane **7** compared to **RW-3** in lane **6** on PAGE along with the formation of a smaller structure at the bottom (lane **7** in Figure **4.22D**). The wrong cube scaffold **(Cb-wrong)** can be fully reformed after adding remaining complementary strands (comp **1,3** and **5**). Surprisingly, when we reversed the order of addition of complementary strands (adding comp **1,3** and **5** then followed by comp **2,4** and **6**), we obtained the same gel pattern as in Figure **4.22D**). Based on the obtained gels, we hypothesized that the rebinding product to wrong scaffold **(RW)** would be 2 "printed" particles rebound to the wrong scaffold. Our hypothesis was: after **6x** and 2 non-reacting filler strands recognized the wrong scaffold at highlighted regions **1** to **5** (**1-3** for **6x** and **4,5** for non-reacting filler strands), another **6x** could come in and rebind to other single-stranded regions of **Cb-wrong**. It suggests that the first **6x** could not bind completely to the wrong scaffold due to different spatial arrangement, thus left behind free single-stranded binding regions on the scaffold for the binding of the second "printed" particle. Our hypothesis was further validated by DLS measurements and several control experiments (see below).

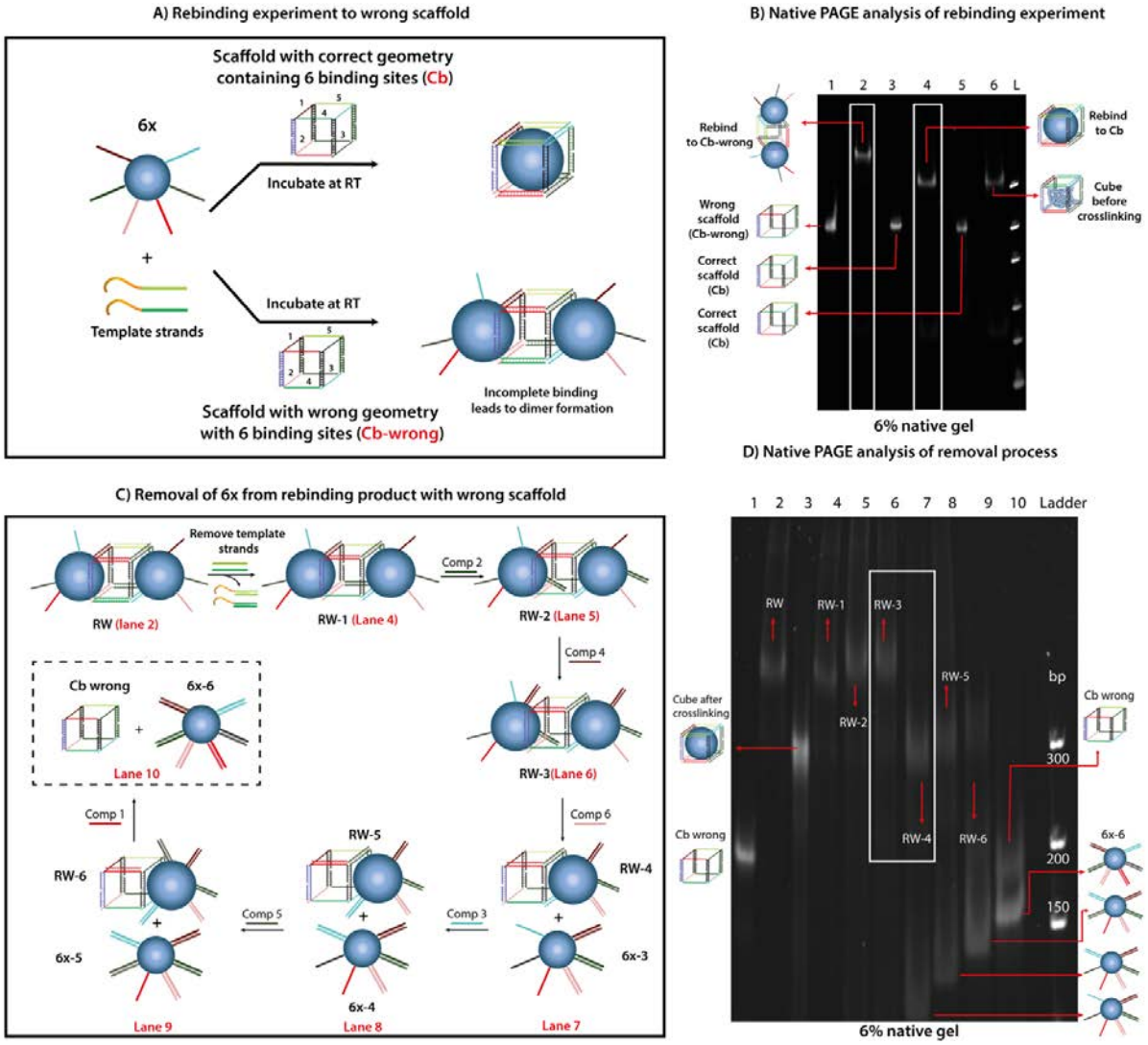

Figure 4.22 | A) Rebinding experiment of **6x** with 2 different scaffolds. The correct scaffold (**Cb**) has 6 complementary binding regions in the same arrangement as **6x**. On the other hand, the wrong scaffold **(Cb-wrong)** also has 6 complementary binding regions but they are designed to have a different arrangement on **Cb. B)** 6% native PAGE analysis of the experiment. Lane 2 reveals the proposed dimer product of **6x** with **Cb-wrong** when compared to lanes 4 (correct binding of **6x** with **Cb**) and 6 (control assembly with amphiphiles before crosslinking): Lane **1**: Cb-wrong, lane **2**: 6x + Cb-wrong (dimer formation), lane **3**: Cb, lane **4**: **6x** + Cb, lane **5**: Cb, lane **6**: cube with 8 HE_6-DNA before crosslinking (control) **C)** Removal experiment of **6x** from a wrong scaffold (**Cb-wrong**) **D)** 6% native PAGE gel mirroring the process in Figure **4.22 c: lane 1**: **Cb-wrong**, **lane 2**: rebinding of **6x** to **Cb-wrong (RW)**, **lane 3**: rebinding product of **6x** to **Cb** (correct) (**RP**), **lane 4**: RW + comp-temps, **lane 5**: RW + comp-temps + comp 2, **lane 6**: RW + comp-temps + comp 2 and 4, **lane 7:** RW + comp-temps + comp 2, 4 and 6, **lane 8**: RW + comp-temps

+ comp 2, 4, 6 and 1, **lane 9:** RW + comp-temps + comp 2, 4, 6, 1 and 3, **lane 10:** RW + comp-temps + comp 2, 4, 6, 1, 3 and 5

B. Control experiment 1:

We performed a control experiment in which we compared the electrophoretic mobility of:

1) **RW** (rebinding product of **6x** to **Cb-wrong**) which is obtained from the incubation of **6x** to **Cb-wrong** to which **comp-temps** (complementary to non-reacting filler strands), comp **2**, **4** and **6** are then added (to remove **6x** from region **1,2** and **3**). The outcome of this process will be **RW-4 (**Figure **4.22 C**).

2) **6x** which is hybridized to comp **2**, **4** and **6** to form **6x-3** and then incubated with **Cb-wrong**.

The process was summarized in the Figure **4.23** below.

After that, 2 samples were added 2.0 uL of glycerol and loaded on a 6% native PAGE. The gel was then run at 250V for 3 hours, followed by staining with Gel Red before imaging (Figure **4.23)**.

Outcome: We found that 2 these samples led to the same mobility shifts on the 6% native PAGE, suggesting they are likely to be the same structures with one **6x** particle bound to the wrong scaffold.

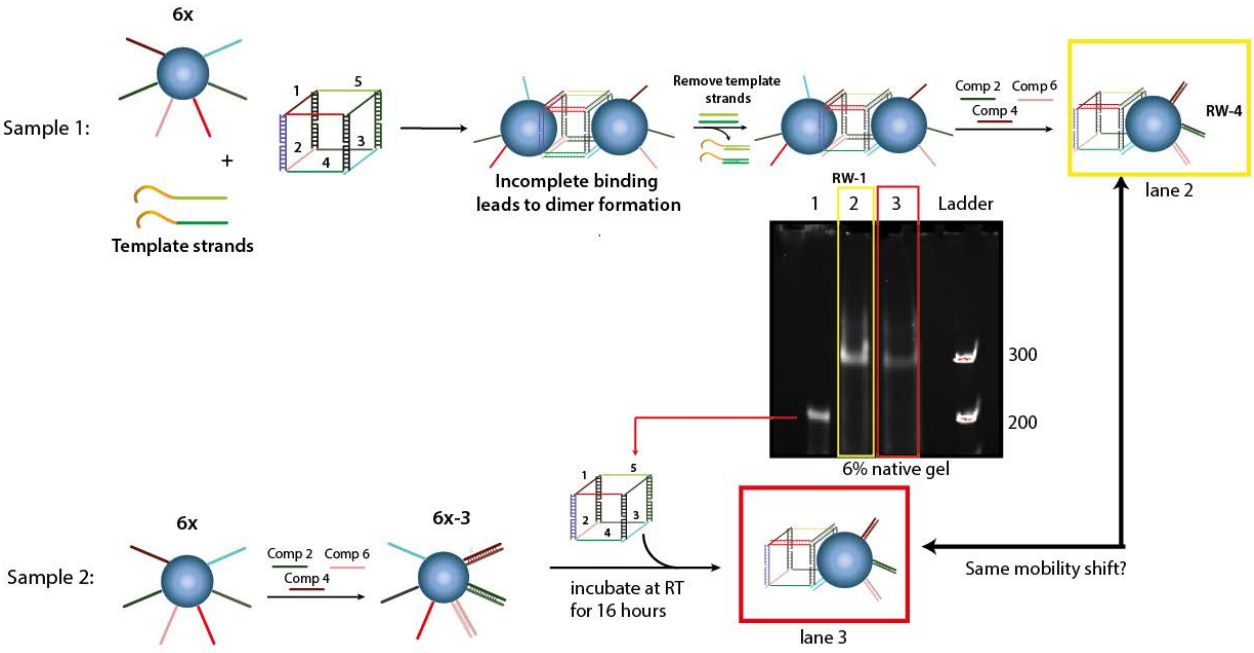

Figure 4.23 | Outline of the control experiment 1. 6% native gel analysis of the outcome of the experiment. **Lane 1**: Wrong cube scaffold (Cb-wrong), **lane 2:** structure resulted from process 1, **lane 3:** structure resulted from process 2.

C. Control experiment 2:

The mobility shifts of the proposed dimer and **R1-R6 (**Figure **4.24)** were then compared. Rebinding products (**R1** to **R6**) were formed as described earlier in Figure **4.21**. In principle, the **RW** (2 printed particles **6x** and 1 cube) should move slower than all rebinding products **(R1** to **R6)** on 6% native PAGE if it contains two **6x** particle bound to one cube scaffold. The gel was run at 250V for 4 hours. As expected, we observed that the band corresponding to the rebinding product to wrong scaffold **RW** moved slower than that of all rebinding products **(R1-R6),** which is in agreement with our prediction (Figure **4.24**). Moreover, the progressive increase in the mobility shifts as the number of complementary regions increases in Figure **4.21** implies that each rebinding product contains one **6x** binding to one cube scaffold, ruling out the possibility of more than 1 printed particle bound to 1 cube.

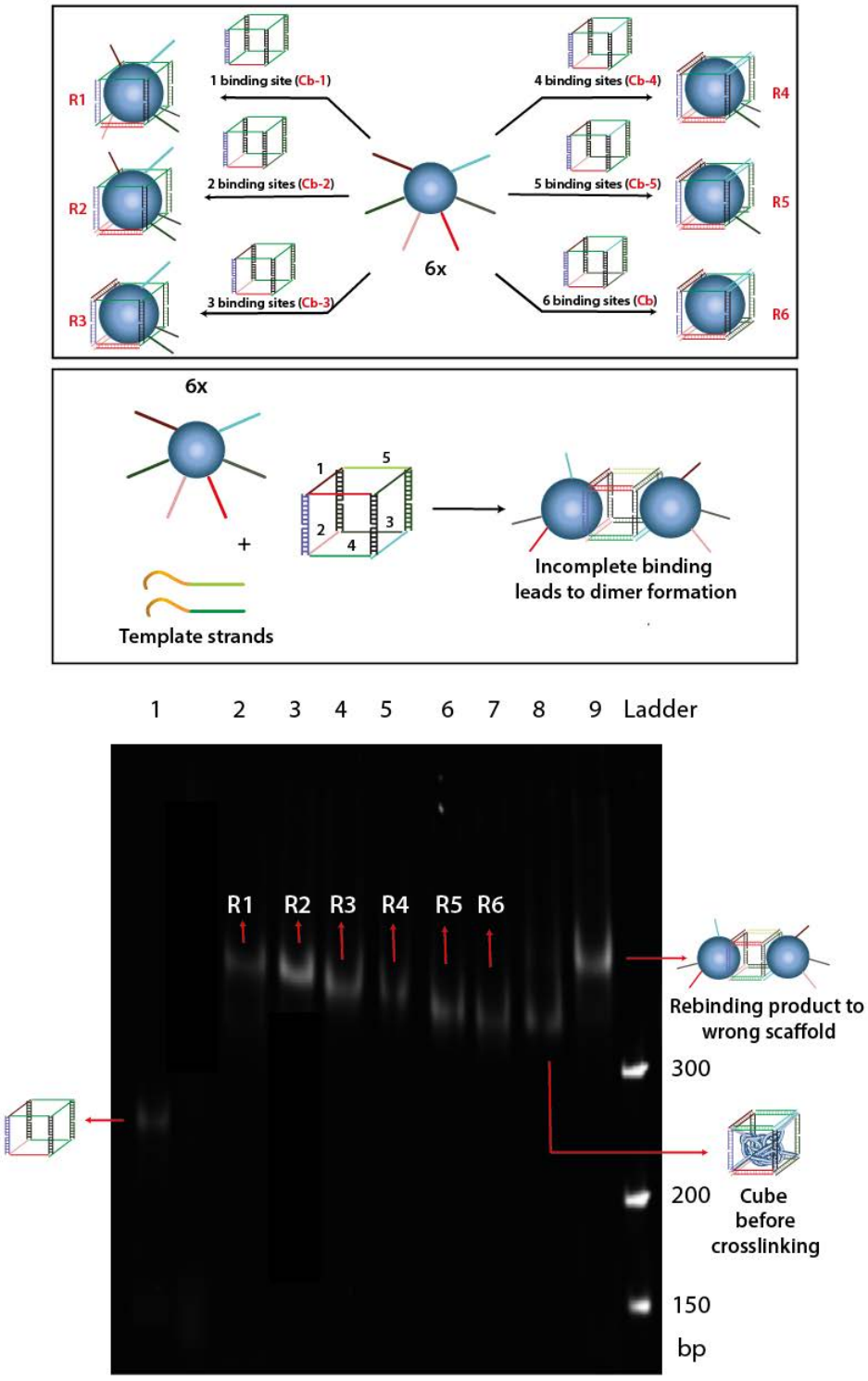

Figure 4.24 | Outline of the control experiment 2. 6% native PAGE analysis of the outcome of the experiment. Lane 1: Wrong cube scaffold (Cb-wrong), lane 2-7: R1-R6 (structure shown above), lane 8: Cube before crosslinking, lane 9: Dimer formed from 6x rebound to wrong scaffold.

4.5.15. Remove 6x from rebinding product to wrong scaffold (reverse order)

First, pre-formed printed particle **6x** (in excess) was incubated with pre-formed wrong cube scaffold (Cb-wrong) (250 nM) at room temperature for 16 hours. Then, **comp-temps** (complementary to non-reacting filler strands) was added followed by adding comp **1, 3, 5, 2, 4** and **6** sequentially. We notice that after adding comp **1, 3** and **5**, there was a significant increase in mobility shift of structure **RW-4** compared to **RW-3** in lane **6** and **7 (**Figure **4.25)**. This gel trend was observed with the sequence of adding presented Experimental Section **4.5.14.** It supported our hypothesis about dimer formation when printed particle 6x rebound to wrong cube scaffold.

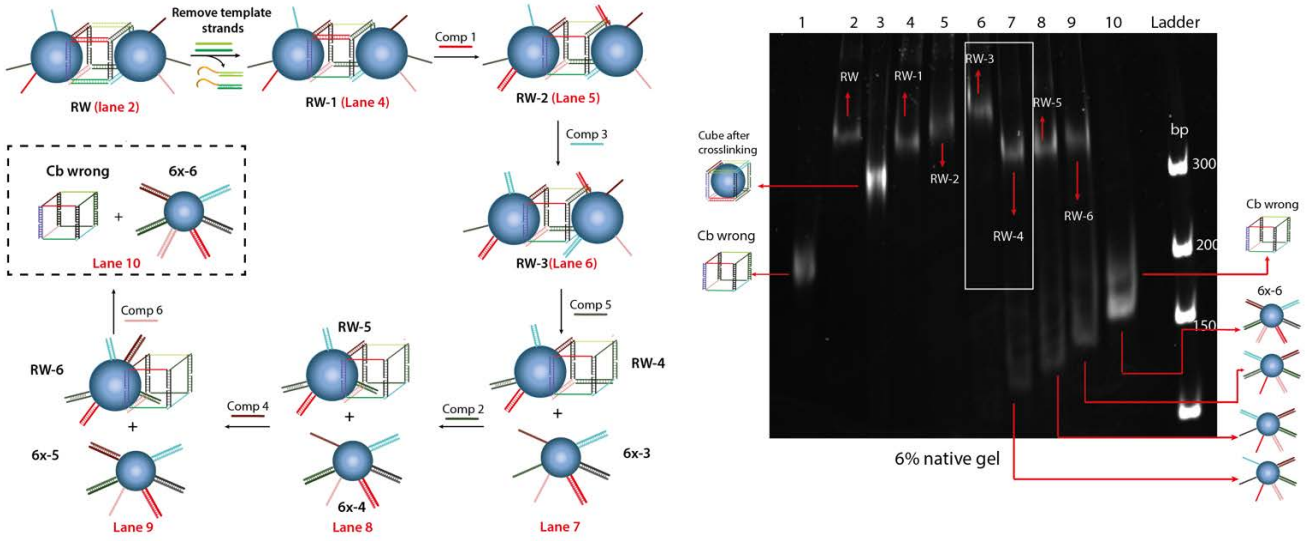

Figure 4.25 | Reverse order of adding complementary sequences to DNA strands on the printed particle. This experiment aims to remove **6x** from the rebinding product to the wrong scaffold. 6% native PAGE analysis of the process. Lane 1: wrong cube scaffold (Cb-wrong), lane 2: Rebinding product of 6x to wrong scaffold (RW), lane 3: Cube after crosslinking (control), **lane 4**: RW + comp-temps, **lane 5**: RW + comp-temps + comp 1, **lane 6**: RW + comp-temps + comp 1 and 3, **lane 7:** RW + comp-temps + comp 1, 3 and 5, **lane 8**: RW + comp-temps + comp 1, 3, 5 and 2, **lane 9:** RW + comp-temps + comp 1, 3, 5, 2 and 4, **lane 10:** RW + comp-temps + comp 1, 3, 5, 2, 4 and 6.

4.5.16. DLS characterization

Our hypothesis of dimer formation when 6x rebound to the wrong scaffold was further validated using DLS measurements to determine the relative size of proposed dimer **(RW)** compared to **6x** and the wrong scaffold **(Cb-wrong)**. The size of the **RW** was 48.5±7.5 nm in diameter, which is close to combination of the size of two **6x** and one cube, given the hydrodynamic size of 14.6±2.4 nm with **Cb-wrong**, 15.7±1.9 nm with **6x** in TAMg. Also, another control **R3** (**6x** rebind to 3-binding region scaffold) was also measured with the size of 28.0±4.9 nm in diameter. The sizes were measured by Zetasizer from Malvern, processed by Zetasizer software and summarized in the table as below.

Structure	Size (d.nm)	Structure	Size (d.nm)
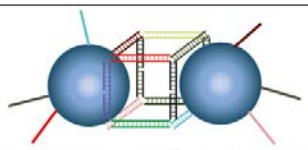	48.5 ± 7.5	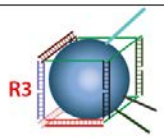	28.0 ± 4.9
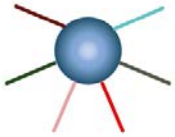	30.6 ± 5.7	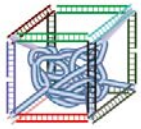	14.0 ± 2.1
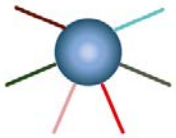	15.7 ± 1.9		14.7 ± 2.5

Figure 4.26 | Summary of DLS measurements. The sizes were listed in nm in diameter.

A. Printed particles (6x) in water:

Size = 30.6±5.7 nm in diameter

-

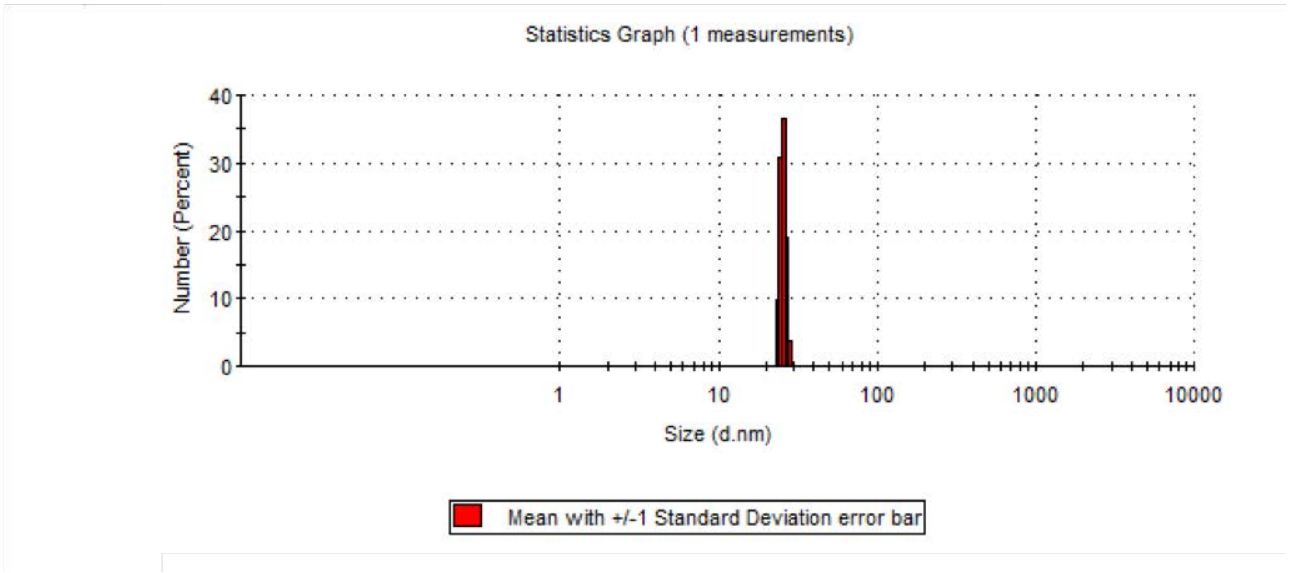
Statistics Graph (1 measurements)
Number (Percent)
40
30
20
10
0
1
10
100
1000
10000
Size (d.nm)
Mean with +/-1 Standard Deviation error bar

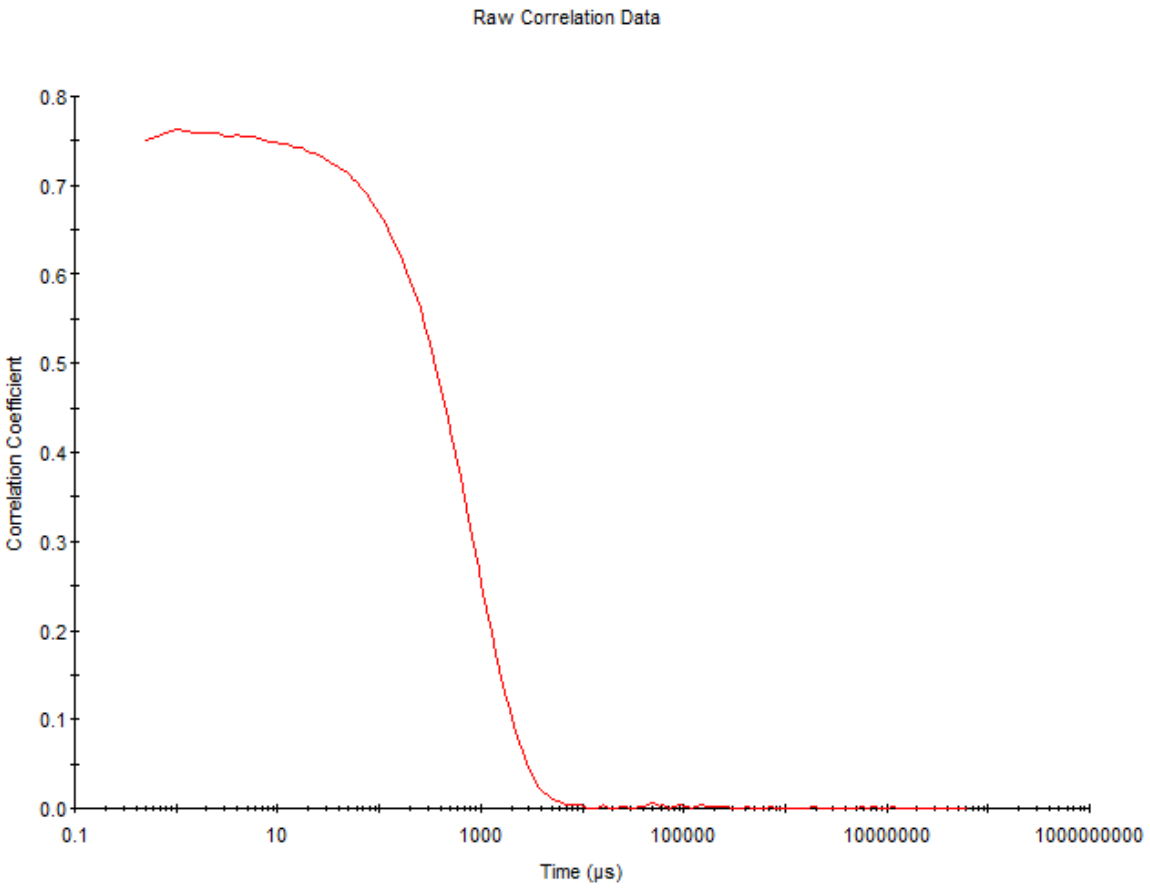
Raw Correlation Data
Correlation Coefficient
0.8
0.7
0.6
0.5
0.4
0.3
0.2
0.1
0.0
0.1
10
1000
100000
10000000
1000000000
Time (µs)

B. 6x in 1x TAMg:

Size = 15.7±1.9 nm in diameter

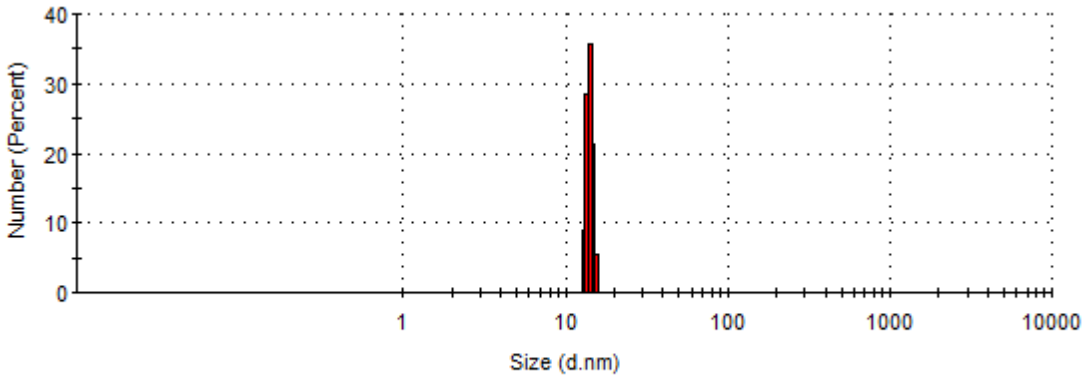

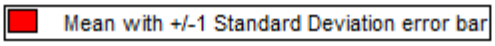

Raw Correlation Data

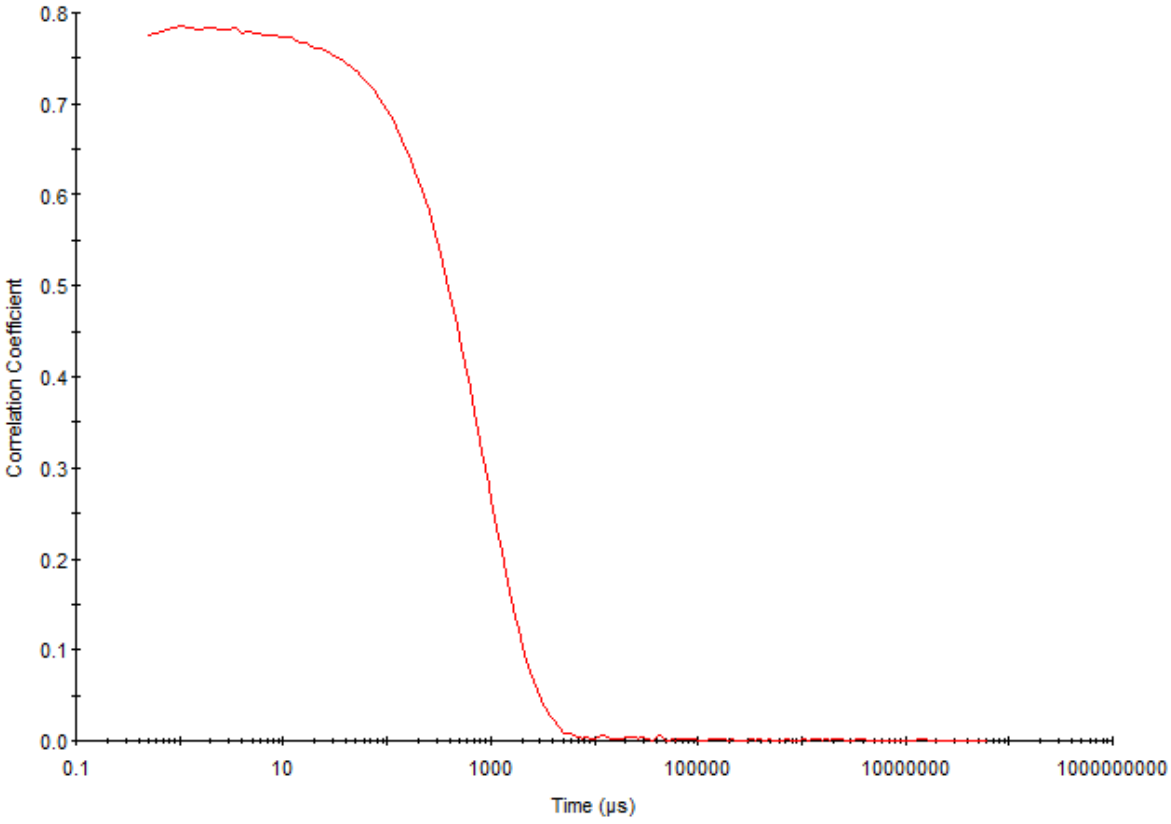

C. Cube decorated with 8 amphiphiles:

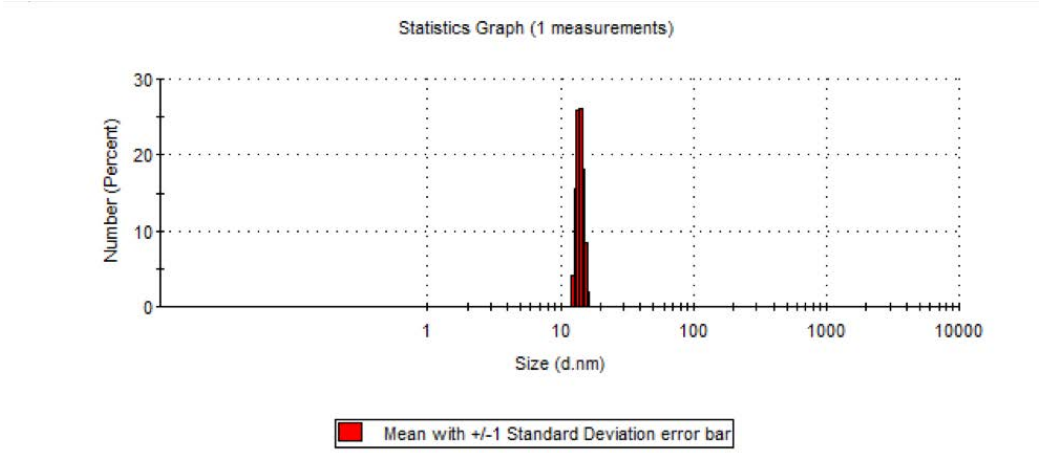

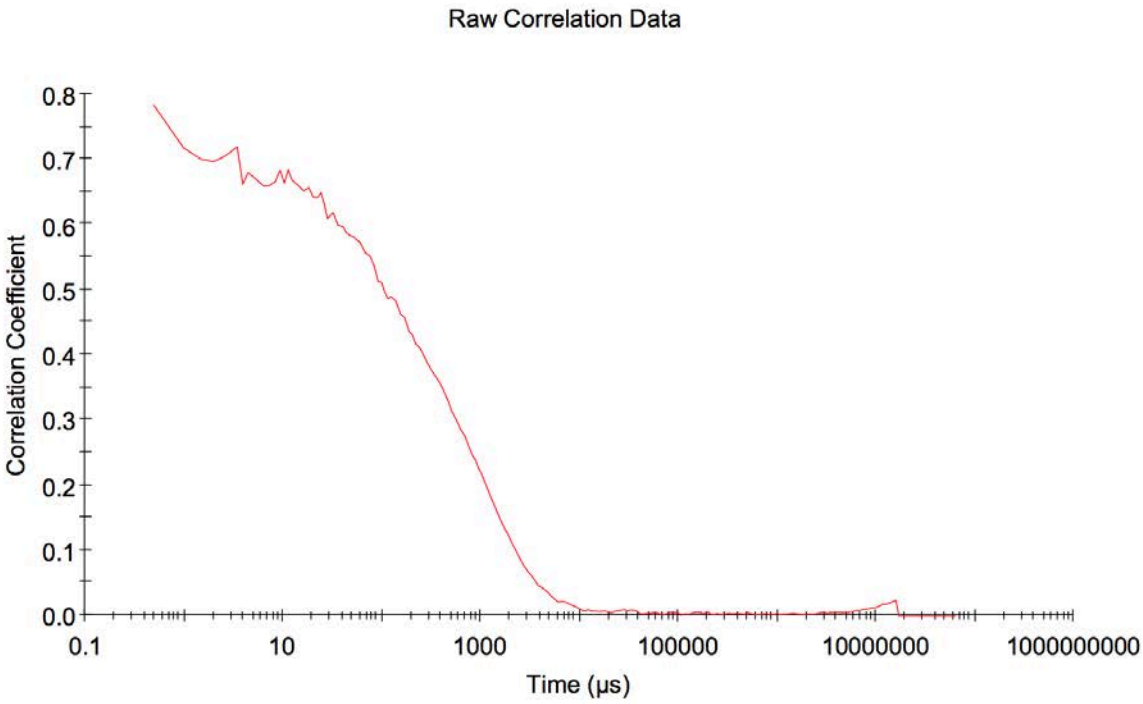

D. 6x rebinds to wrong scaffold:

Size = 48.5±7.5 nm in diameter

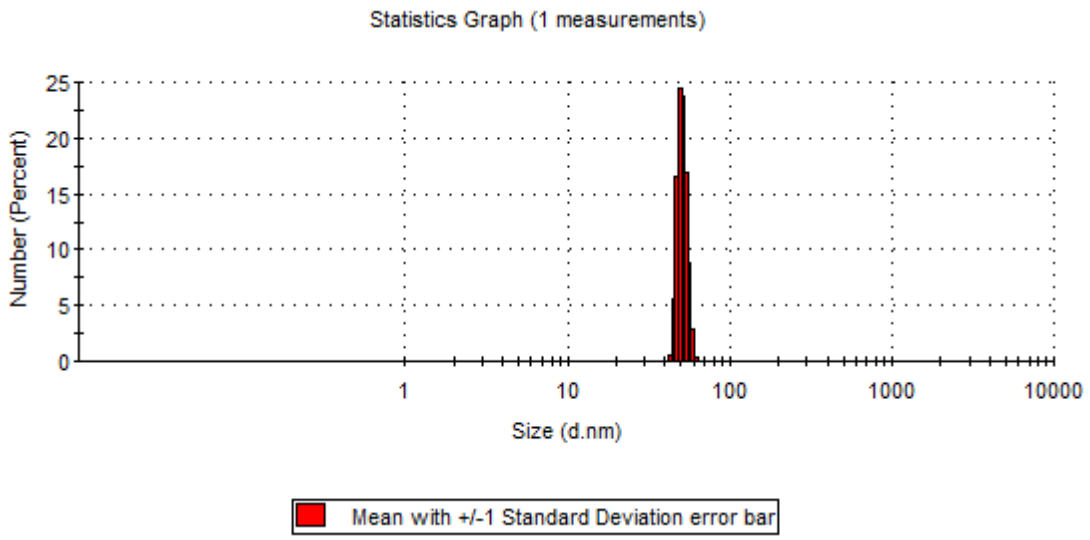

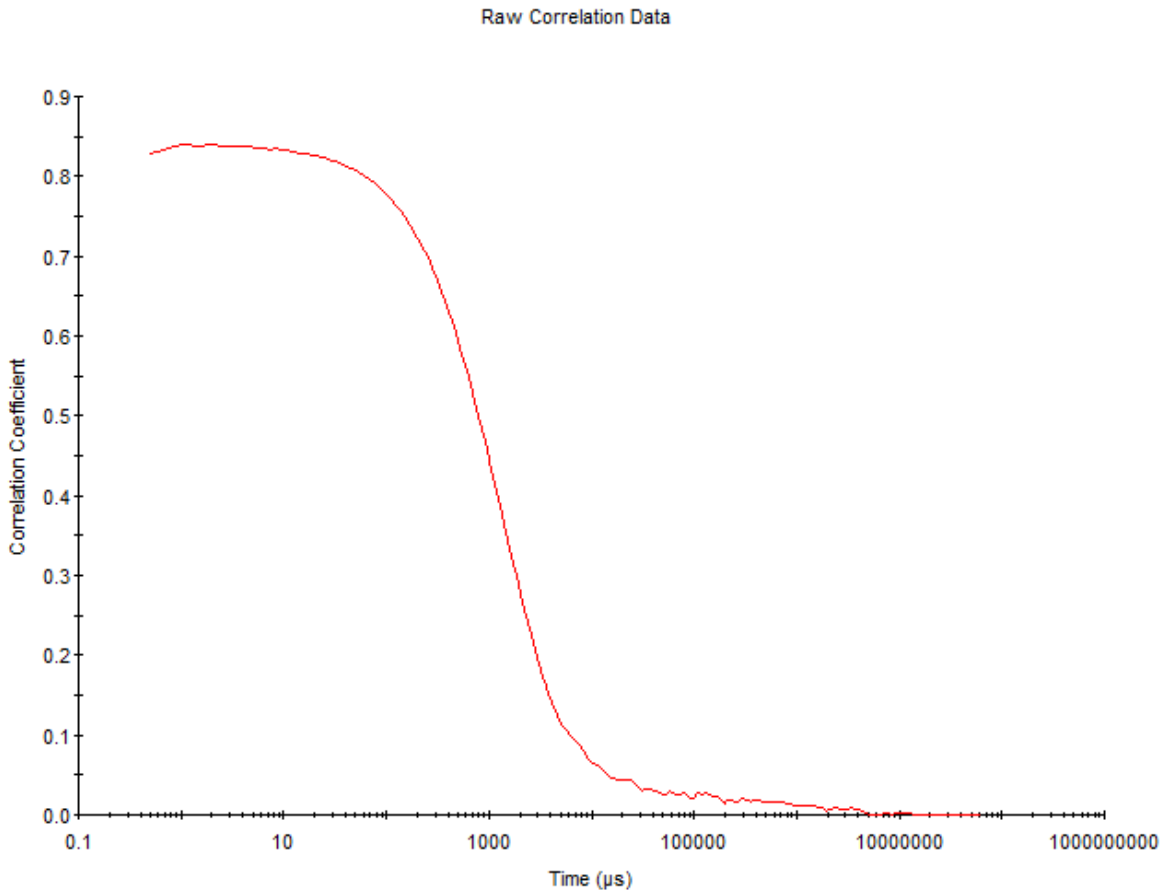

E. 6x rebinds 3-complementary region cube scaffold:

Size = 28.0±4.9 nm in diameter

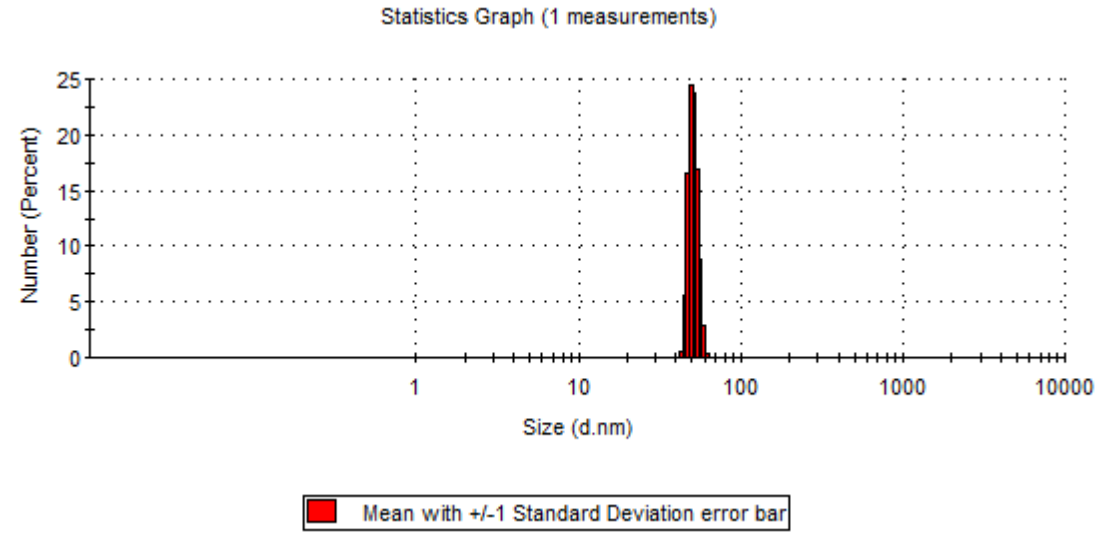

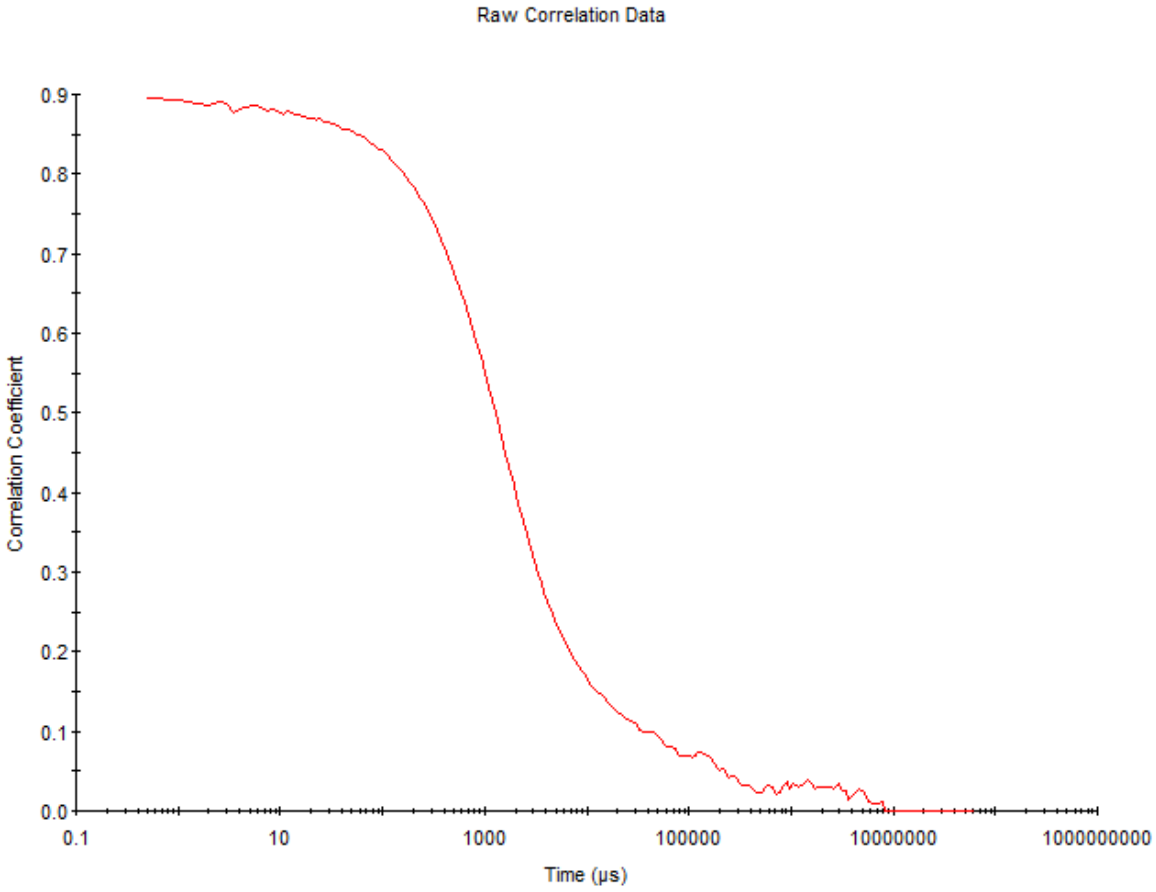

4.5.17. Gel characterization of tetravalent (4x) and pentavalent (5x) printed particles

The tetravalent (**4x**) and pentavalent (**5x**) were extracted from gel and recovered by electroelution as described in the manuscript. The **4x** and **5x** were then sequentially hybridized with fully complementary strands to each DNA strand on them. The resulting structures were analyzed by 6% native PAGE (**250V, 4 hours in 1x TAMg buffer**). The progressive increase in mobility shifts after each hybridization event confirms the number of valency of each type of particle (Figure **4.27**).

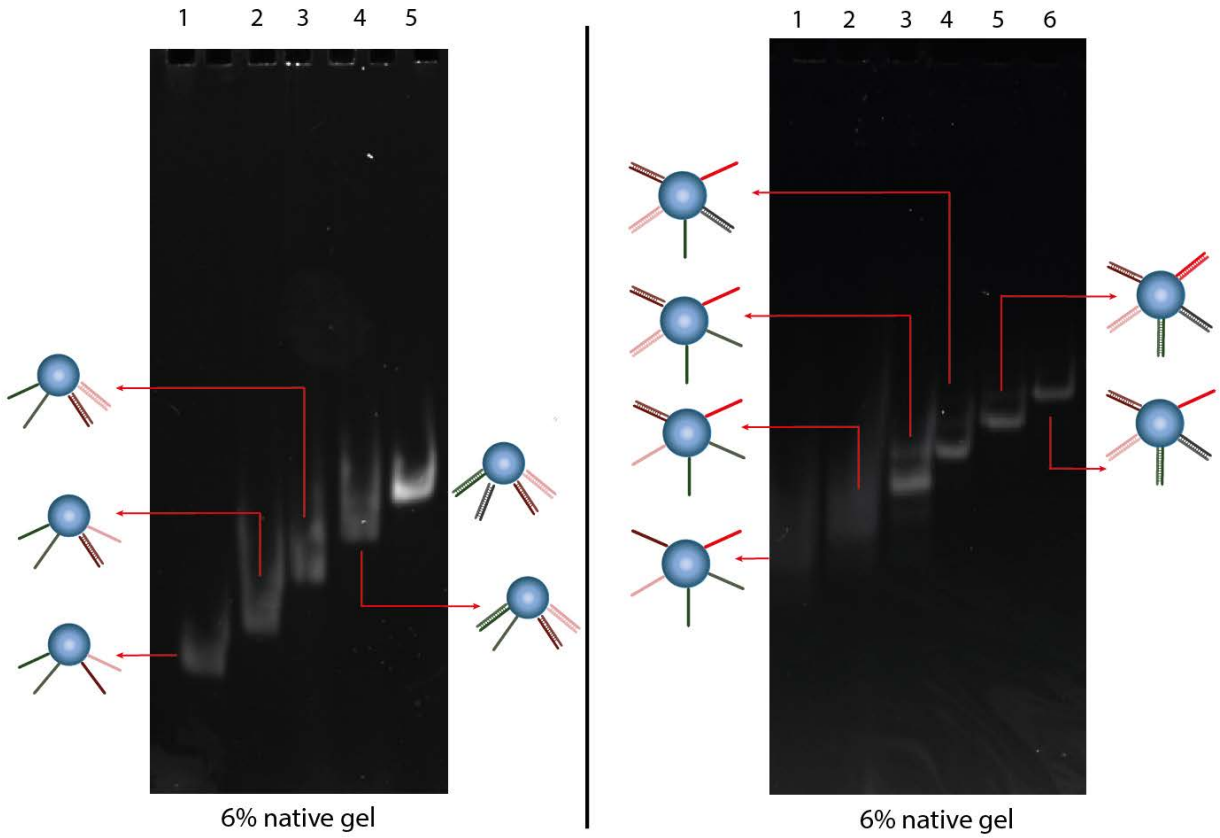

Figure 4.27 | Characterization of **4x** and **5x** printed particle

4.5.18. Gel electrophoresis and AFM characterization of dimer and trimer of printed particles

A. AFM characterization

The sample was diluted with filtered 1x TAMg 5 times to get 5 uL of final sample. 5 µL of sample was deposited on freshly cleaved mica for 10 seconds and washed 4 times with 50 µL of filtered water each time. Excess liquid was blown off by the stream of argon for 30-40 seconds. The sample was then dried under vacuum for at least 20 minutes prior to imaging. Measurement was acquired in Tapping mode under dry condition using OTESPA-R3 probe (tip radius = 7 nm, k = 26 N/m, fo = 300 kHz; Bruker, Camarillo, CA) on MM3 AFM machine from Bruker.
Images were processed by NanoScope Analysis 1.40 Software. The data was treated with flattening to correct tilt, bow and scanner drift. Average particle sizes, distance and numbers of particles (N) were obtained manually from ImageJ software.

a. Dimer formation of printed particle

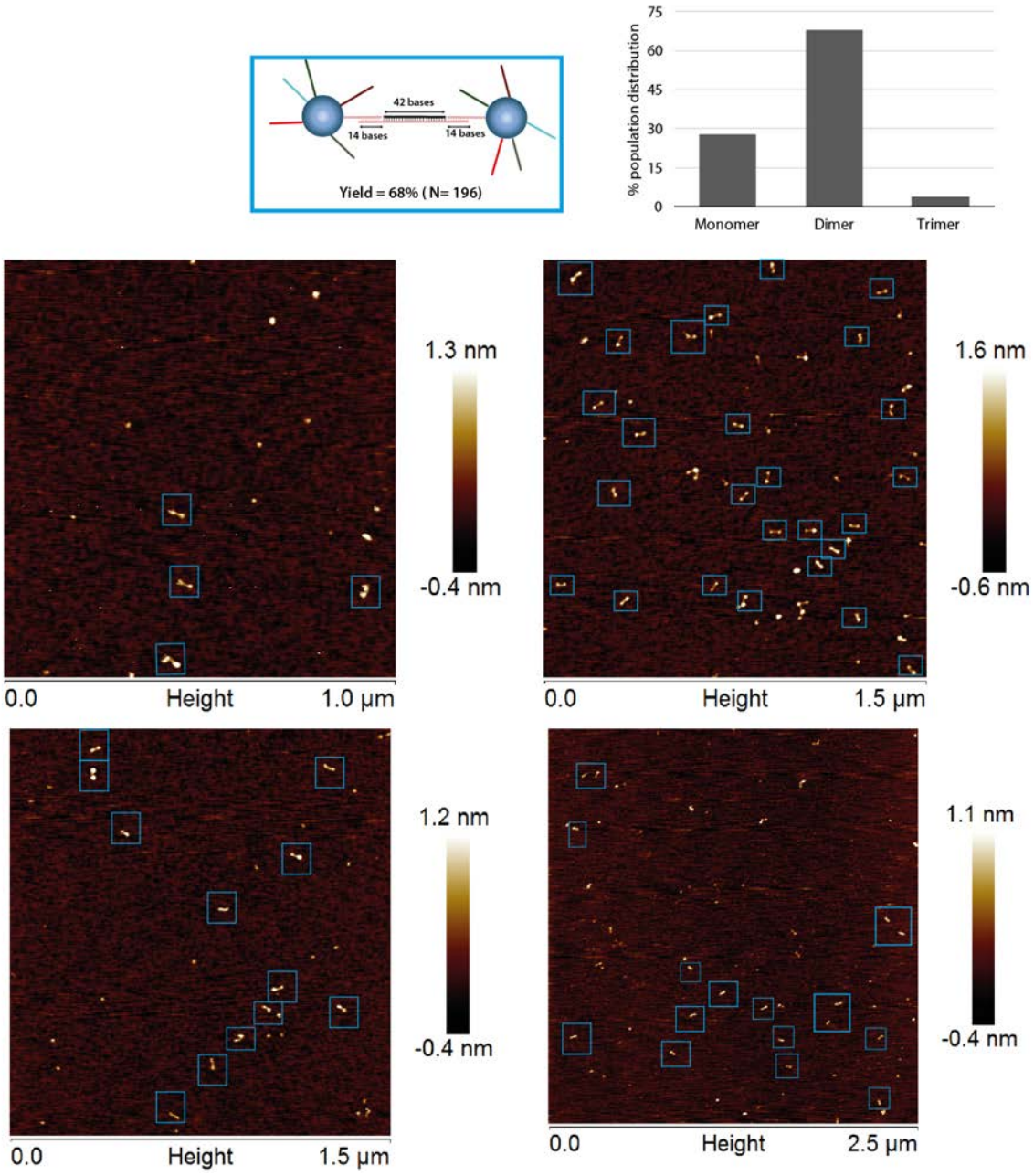

Figure 4.28 | AFM characterization and distribution analysis of the dimer formation of printed particle **6x.**

b. Trimer formation of printed particles (<u>central particle connecting to 2 other particles via adjacent arms</u>)

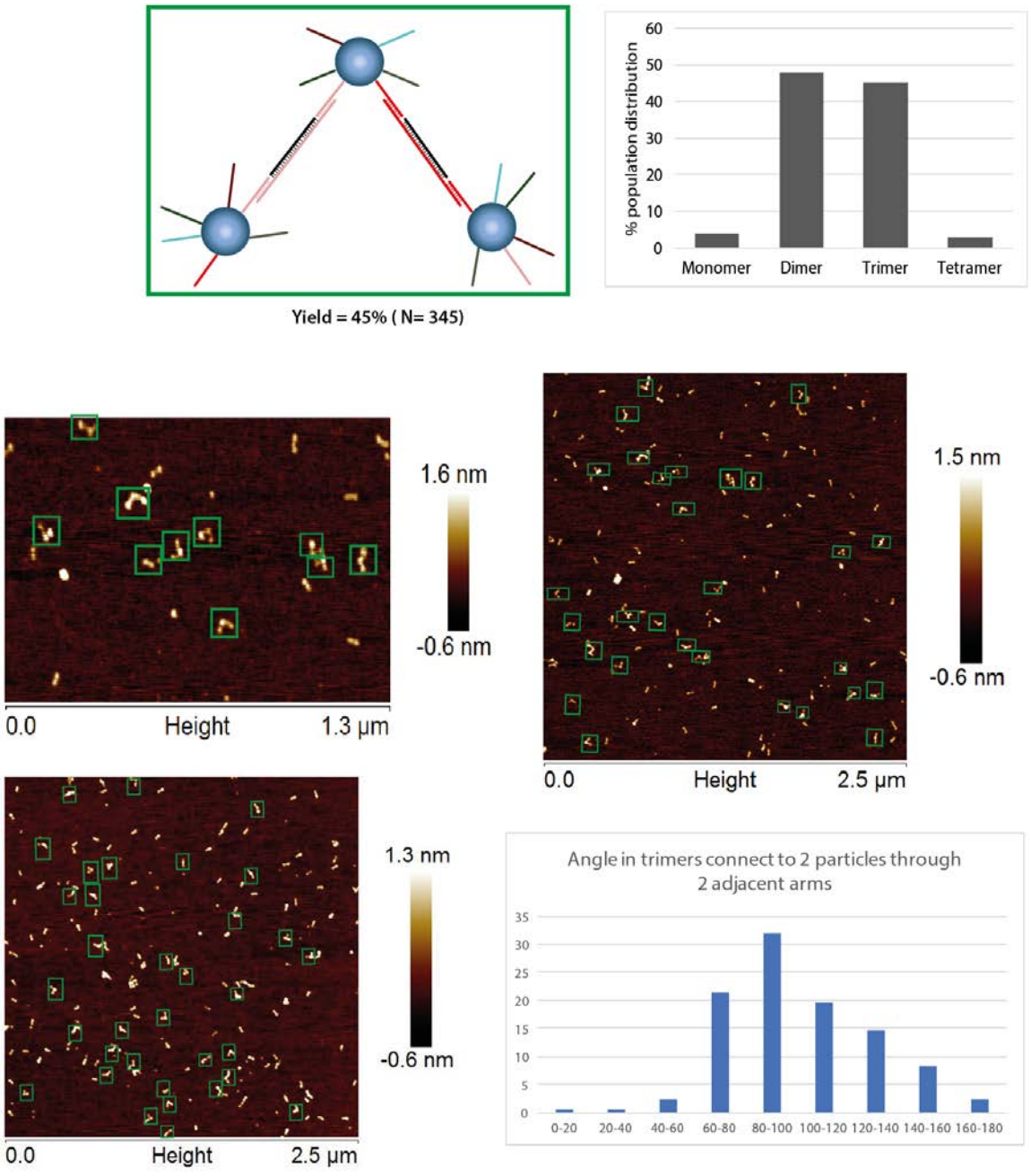

Figure 4.29 | AFM characterization, distribution and angle analysis of the trimer formation of printed particle **6x** (N=130) (central particle connecting to 2 other particles via **adjacent** arms). Measured angle in

trimer **DIPs** = 101±25 degree.

B. Gel electrophoresis characterization

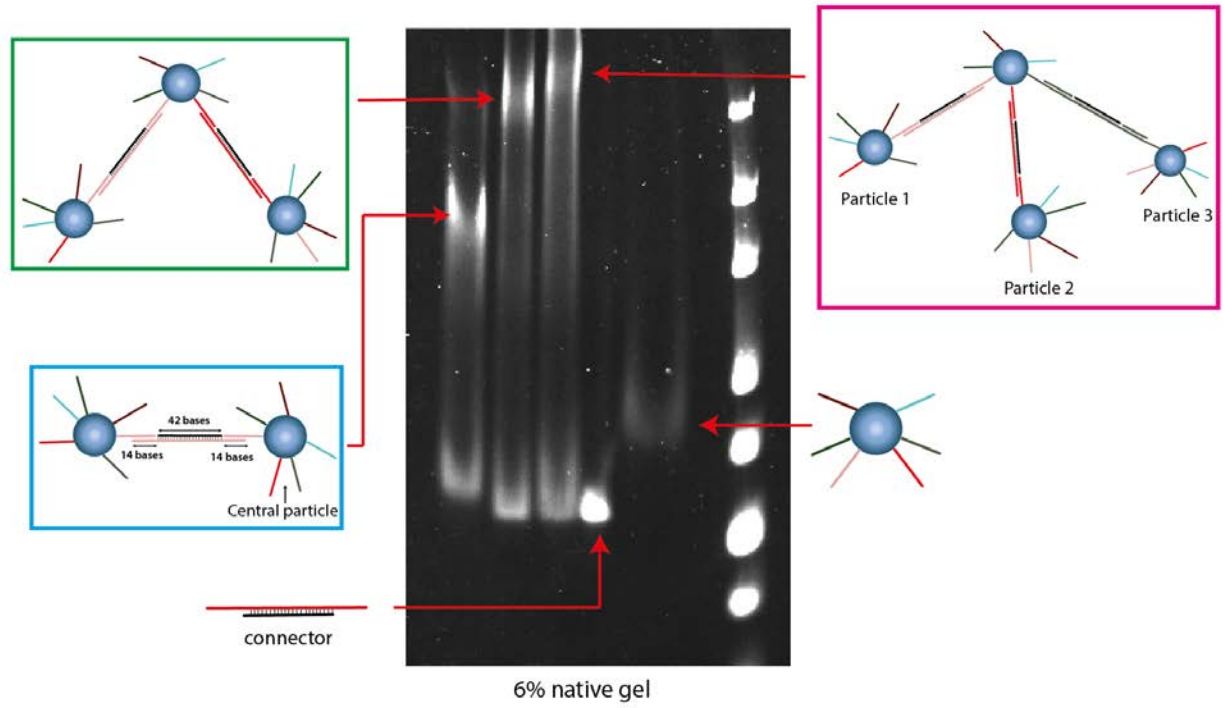

Figure 4.30 | 6% native PAGE analysis of the formation of self-assembled dimer, trimer and tetramer of printed particle **6x**.

4.5.19. AFM characterization and angle analysis of trimer having central particle connecting to 2 other particles at "opposite" position

To investigate the relative placement of our printed particles, we assembled trimer of printed particles using two different arms of the center of the trimer (shown below). The central **6x (1)** particle was made from a different scaffold (see Experimental Section **4.5.6** for sequences). As expected, the trimers formed in this case generally have wider angle (see below for the angle analysis) compared to the case shown previously in Figure **4.29**, suggesting that the printed particle preserves its relative geometry (See below for positioning).

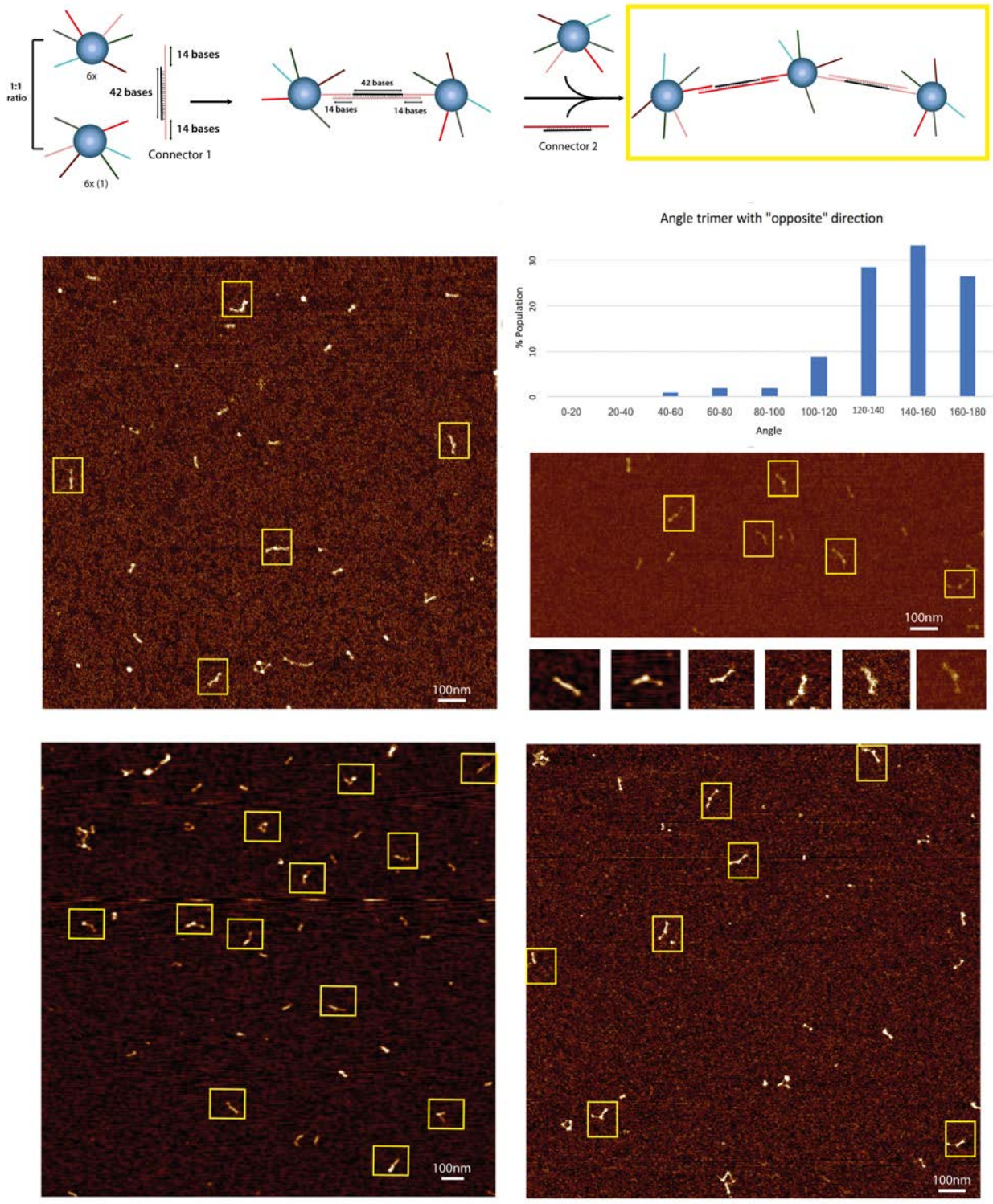

Figure 4.31 | AFM images and angle analysis of trimer with "opposite" direction. Measured angle in trimer "opposite" **DIPs** = 146±22 degree.

4.5.20. AFM characterization of self-assembled tetramer DIPs.

In tetramers, the central particle is connected to other 3 particles through 3 arms (**arm #1, arm #2** and **arm #3** – positioning of each arm on the DNA cube scaffold is presented below).
As can be seen from the AFM images of tetramers and angular distributions analysis using ImageJ, wider angle between particle **1** and **3** in tetramer (**arm #1** and **#3** are **<u>opposite</u>** to each other) compared to angle between particle **1** and **2** (**arm #1** and **#2** are **<u>adjacent</u>**) or between particle **2** and **3** (**arm #2** and **#3** are also **<u>adjacent</u>**) are observed.

Moreover, the angle between particle **1** and **2** is statistically similar to the angle between particle **2** and **3** based on the analysis, in accordance to the relative placements of **arm #1, arm # 2** and **arm #3** on the cube scaffold (**arm #2** is between **arm #1** and **#3**) (see angular analysis below). It again confirms the result of trimer formation experiments above and the relative orientation of printed particles.

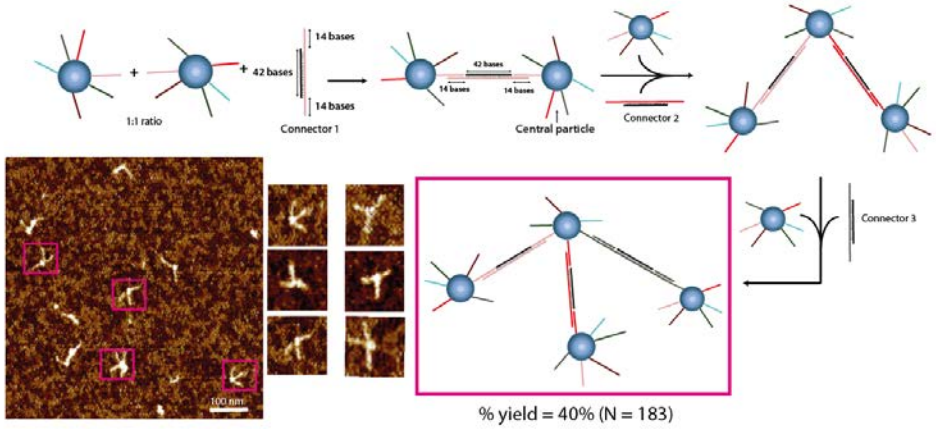

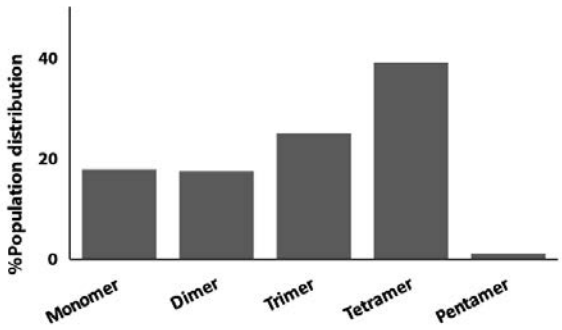

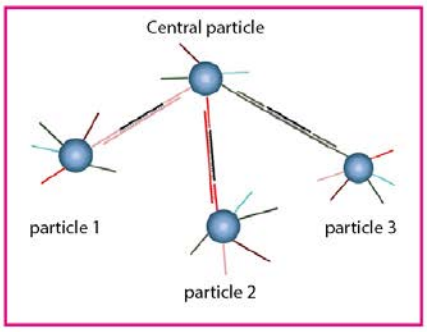
Central particle
particle 1
particle 2
particle 3

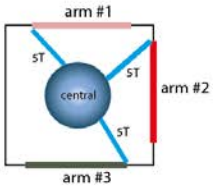
arm #1
5T
5T
central
arm #2
5T
arm #3

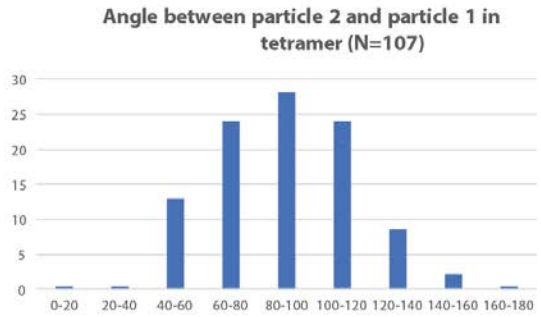
Angle between particle 2 and particle 1 in tetramer (N=107)
30
25
20
15
10
5
0
0-20
20-40
40-60
60-80
80-100
100-120
120-140
140-160
160-180

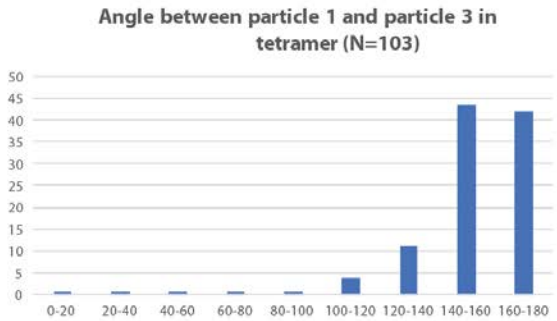
Angle between particle 1 and particle 3 in tetramer (N=103)
50
45
40
35
30
25
20
15
10
5
0
0-20
20-40
40-60
60-80
80-100
100-120
120-140
140-160
160-180

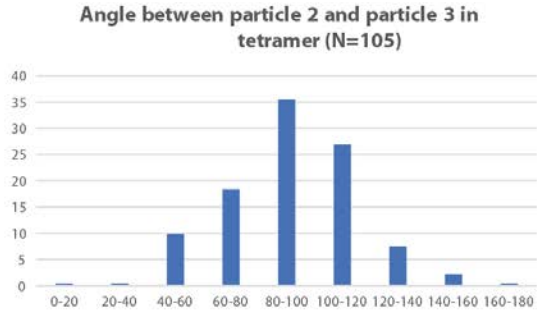
Angle between particle 2 and particle 3 in tetramer (N=105)
40
35
30
25
20
15
10
5
0
0-20
20-40
40-60
60-80
80-100
100-120
120-140
140-160
160-180

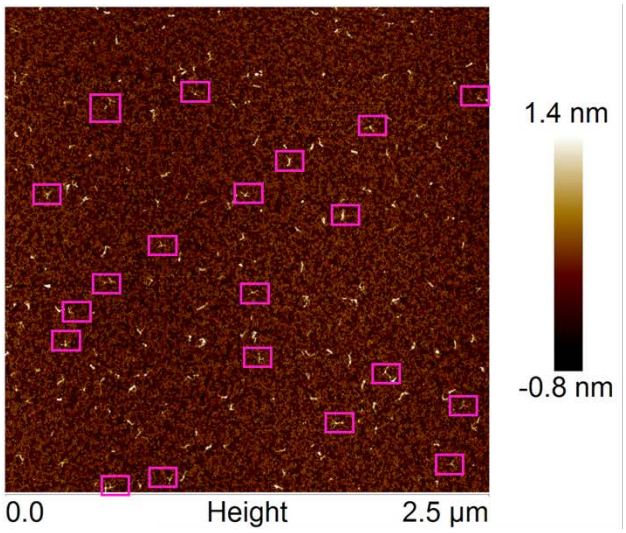
1.4 nm
-0.8 nm
0.0
Height
2.5 µm

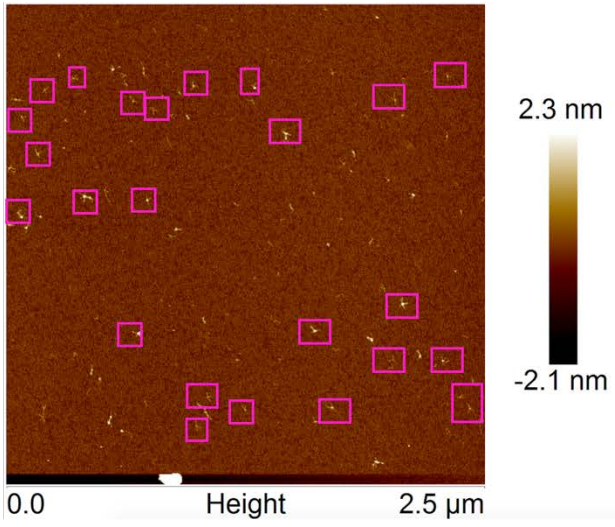
2.3 nm
-2.1 nm
0.0
Height
2.5 µm

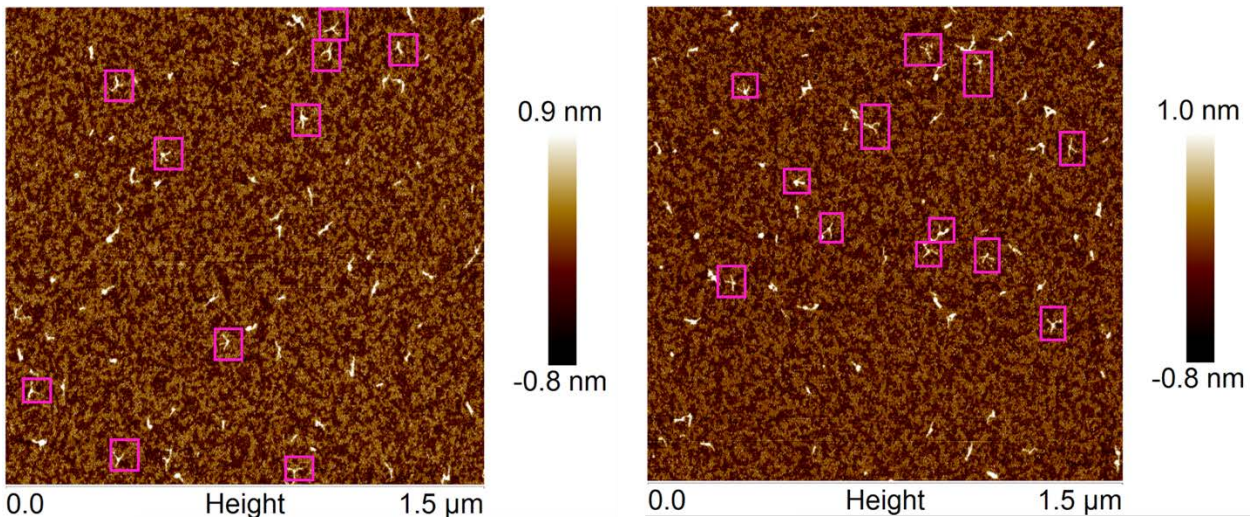

Figure 4.32 | AFM images and angle analysis of self-assembled tetramers **DIPs**.

4.5.21. Modelling cube/DNA amphiphiles (performed by Chenyi Liao and Jianing Li)

Model Preparation. All the models were constructed using the program Maestro (Schrödinger, Inc.). To build the cube scaffold (**Cb**) model, twelve segments of double-stranded DNA were generated based on the sequence design. With all the strands carefully positioned as edges of the cube, we linked them by the hexaethylene glycol linker (**HEG** linker) as the corners and added pre-constructed hydrophobic portions (**HE** chains). Note that only one of the two enantiomers of **Cb** were modeled (as shown in the figure below). To understand the molecular mechanism of the self-assembly, two extreme Cb/DNA amphiphiles models were constructed: one with folded polymers present in **Cb**, while the other one with unfolded polymers pre-assembled in **Cb**. Every model was solvated in a periodic simulation box of ~157×157×157 $Å^3$ with SPC water molecules, counter ions, and $MgCl_2$ to mimic the experimental condition. In addition, we also studied the self-assembly of the HE chains in the absence of **Cb**.

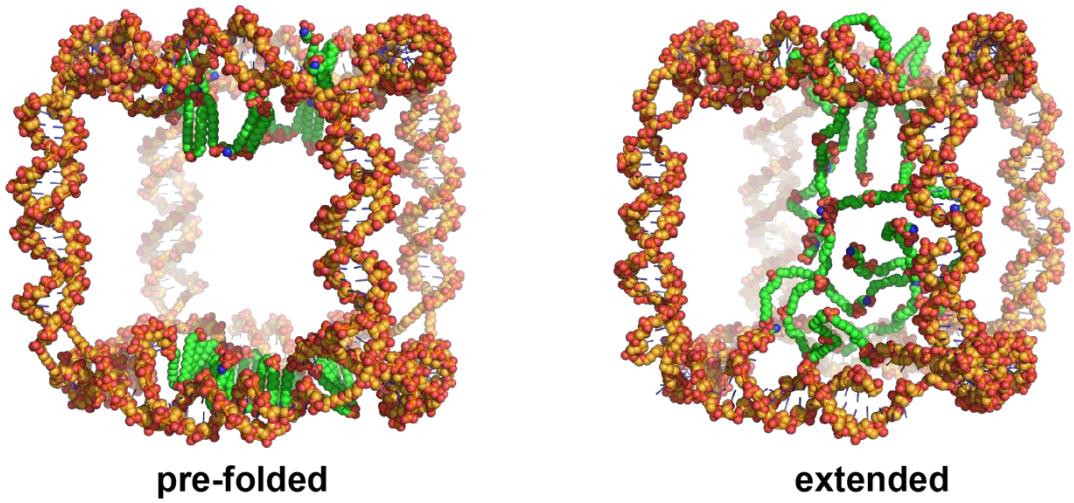

Figure 4.33 | Two molecular models. DNA strands are in orange color; non-reacting and reacting strands are in green color.

Simulation Setup. Each construct was simulated at 313K, 1 atm with two replicas of 20 ns, using the OPLS-AA force field. All the simulations were performed in the Maestro-Desmond program (Schrödinger, Inc.) with a time step of 2 fs. In particular, the particle mesh Ewald technique was used for the electrostatic calculations. The Van der Waals and short-range electrostatics were cut off at 12.0 Å with switch at 9.0 Å. Hydrogen atoms were constrained using the SHAKE algorithm.

Visualization and Analysis. Using our local Tcl and Python tools, we calculated the distance of the nitrogen atoms pair between every two AG strands and draw the average distance map from our four replica simulations. The dimension distortion of the DNA cube was calculated by the root-mean-square deviation (RMSD) of cube edges length with the initial length as the reference. The snapshots were generated by Pymol (Schrödinger, Inc.) and movie was made by VMD 1.9.2 (J. Molec. Graphics 1996, 14.1, 33-38).

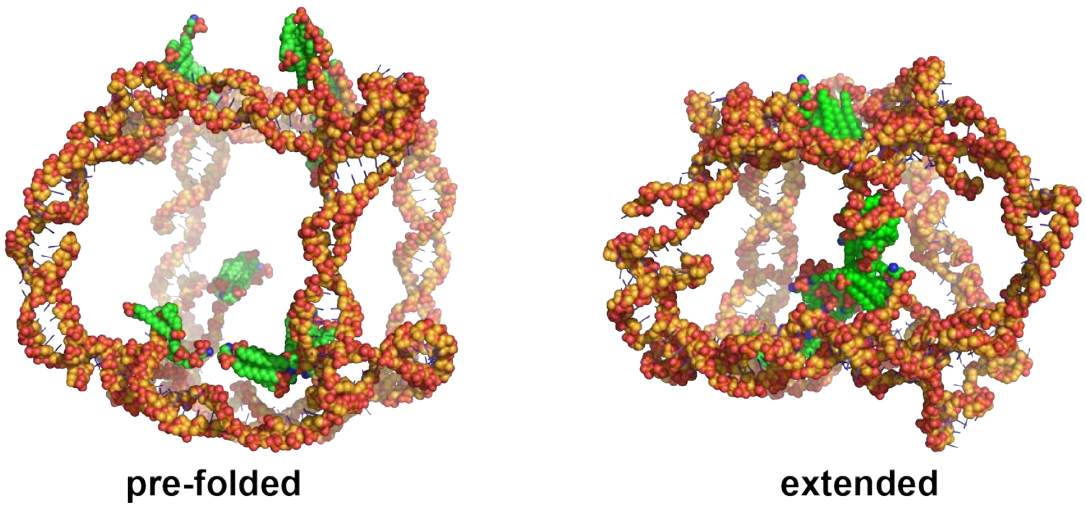

Figure 4.34 | Final snapshots of two molecular models. DNA strands are in orange color; non-reacting and reacting strands are in green color.

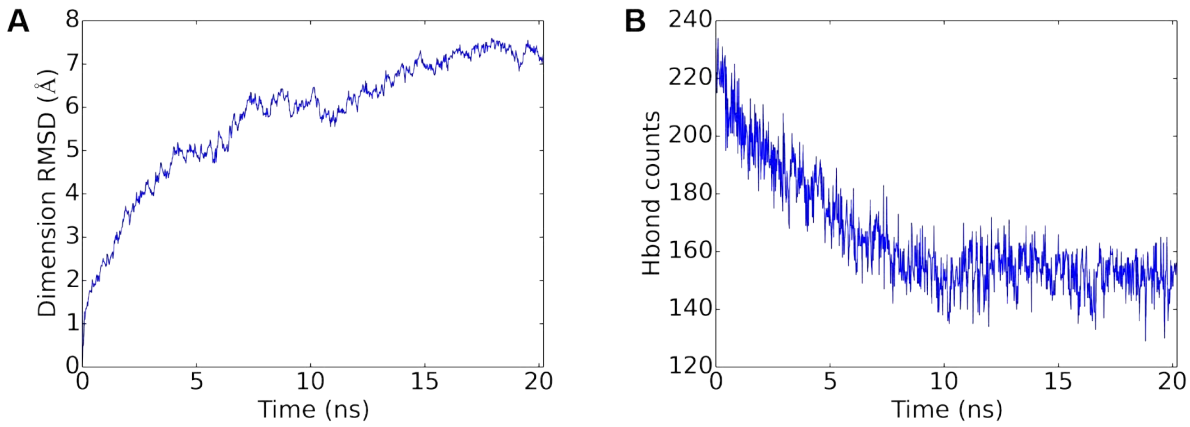

Figure 4.35 | Time evolutions of **(A)** DNA cube dimension distortion and **(B)** DNA cube inter-chain backbone hydrogen bond (Hbond) numbers from one trajectory.

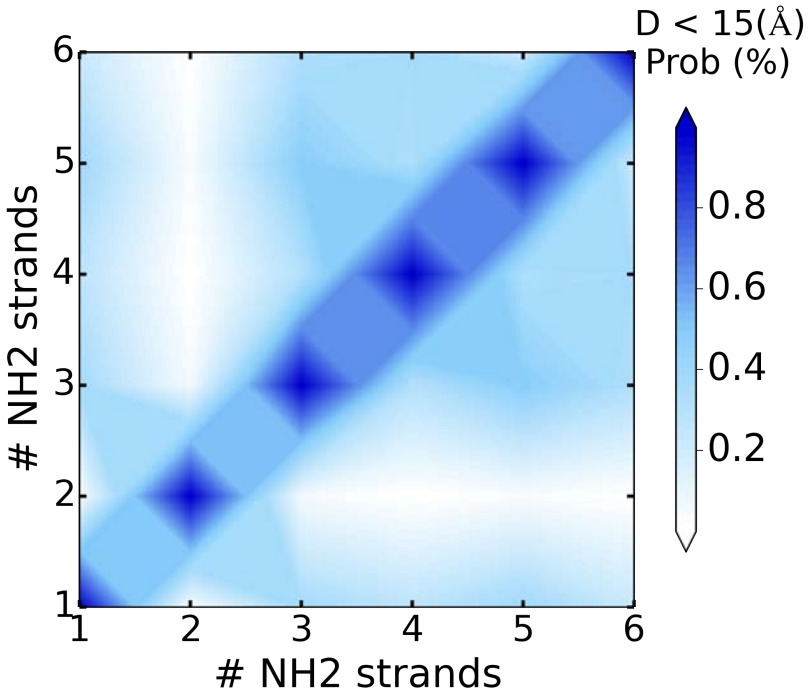

Figure 4.36 | Probability map of nitrogen pair between two strands with **Am** groups within 15 Å.

4.5.22. Octavalent particle formation (8x)

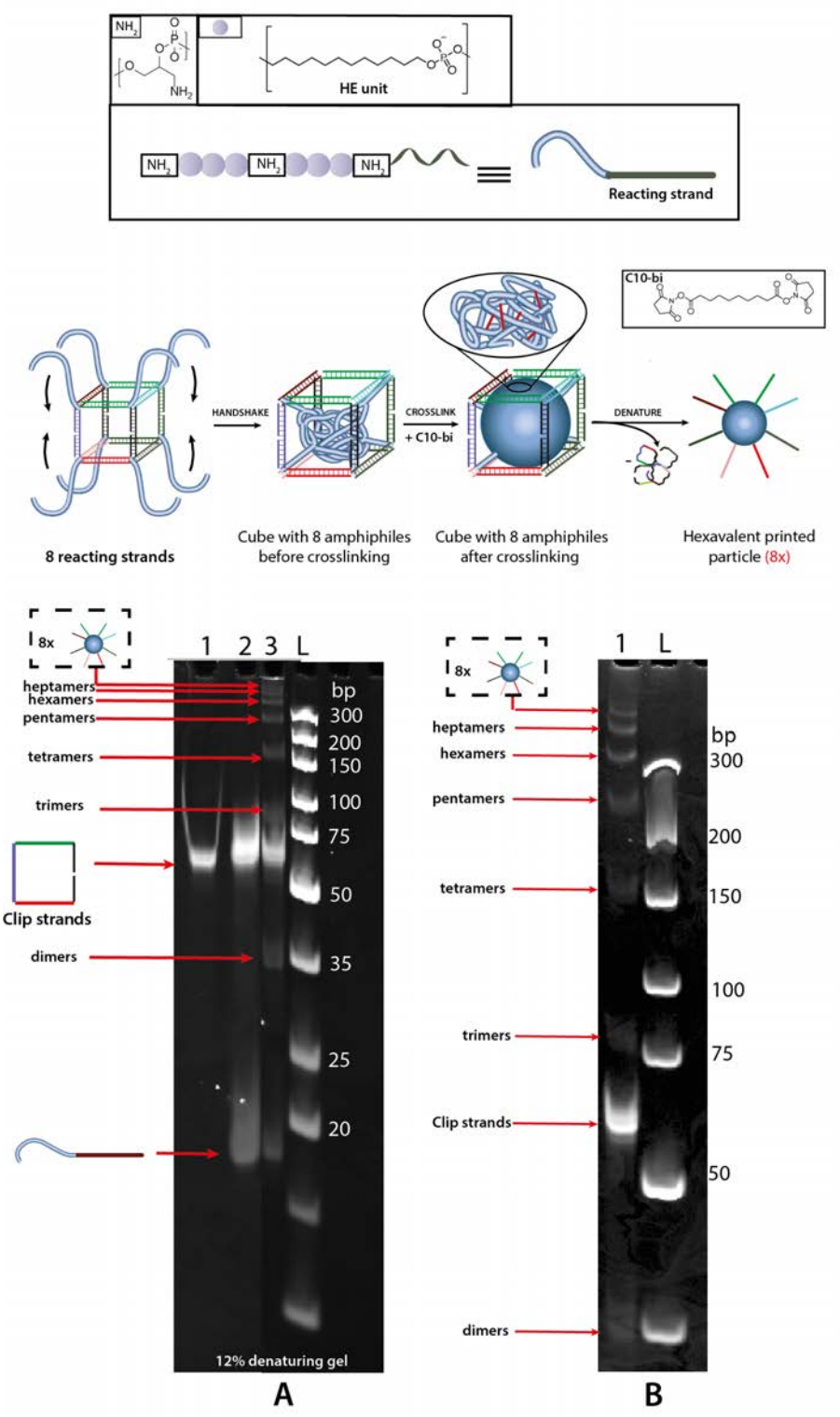

Figure 4.37 | Synthesis of octavalent printed particle.

4.6. References

1. Seeman, N. C., DNA in a material world. *Nature* **2003,** *421* (6921), 427-431.

2. Aldaye, F. A.; Palmer, A. L.; Sleiman, H. F., Assembling Materials with DNA as the Guide. *Science* **2008,** *321* (5897), 1795-1799.

3. Seeman, N. C., DNA engineering and its application to nanotechnology. *Trends Biotechnol.* **1999,** *17* (11), 437-443.

4. Rothemund, P. W. K., Folding DNA to create nanoscale shapes and patterns. *Nature* **2006,** *440* (7082), 297-302.

5. Aldaye, F. A.; Sleiman, H. F., Modular Access to Structurally Switchable 3D Discrete DNA Assemblies. *J. Am. Chem. Soc.* **2007,** *129* (44), 13376-13377.

6. He, Y.; Ye, T.; Su, M.; Zhang, C.; Ribbe, A. E.; Jiang, W.; Mao, C., Hierarchical self-assembly of DNA into symmetric supramolecular polyhedra. *Nature* **2008,** *452* (7184), 198-201.

7. Ke, Y.; Ong, L. L.; Shih, W. M.; Yin, P., Three-Dimensional Structures Self-Assembled from DNA Bricks. *Science* **2012,** *338* (6111), 1177-1183.

8. Winfree, E.; Liu, F.; Wenzler, L. A.; Seeman, N. C., Design and self-assembly of two-dimensional DNA crystals. *Nature* **1998,** *394* (6693), 539-544.

9. Benson, E.; Mohammed, A.; Gardell, J.; Masich, S.; Czeizler, E.; Orponen, P.; Hogberg, B., DNA rendering of polyhedral meshes at the nanoscale. *Nature* **2015,** *523* (7561), 441-444.

10. Douglas, S. M.; Dietz, H.; Liedl, T.; Hogberg, B.; Graf, F.; Shih, W. M., Self-assembly of DNA into nanoscale three-dimensional shapes. *Nature* **2009,** *459* (7245), 414-418.

11. Ke, Y.; Sharma, J.; Liu, M.; Jahn, K.; Liu, Y.; Yan, H., Scaffolded DNA Origami of a DNA Tetrahedron Molecular Container. *Nano Lett.* **2009,** *9* (6), 2445-2447.

12. Kwak, M.; Herrmann, A., Nucleic Acid/Organic Polymer Hybrid Materials: Synthesis, Superstructures, and Applications. *Angew. Chem. Int. Ed.* **2010,** *49* (46), 8574-8587.

13. Alemdaroglu, F. E.; Herrmann, A., DNA meets synthetic polymers-highly versatile hybrid materials. *Org. Biomol. Chem.* **2007,** *5* (9), 1311-1320.

14. Yang, C. J.; Pinto, M.; Schanze, K.; Tan, W., Direct Synthesis of an Oligonucleotide–Poly(phenylene ethynylene) Conjugate with a Precise One-to-One Molecular Ratio. *Angew. Chem.* **2005,** *117* (17), 2628-2632.

15. Jeong, J. H.; Park, T. G., Novel Polymer−DNA Hybrid Polymeric Micelles Composed of Hydrophobic Poly(d,l-lactic-co-glycolic Acid) and Hydrophilic Oligonucleotides. *Bioconjugate Chem.* **2001,** *12* (6), 917-923.

16. Tan, X.; Li, B. B.; Lu, X.; Jia, F.; Santori, C.; Menon, P.; Li, H.; Zhang, B.; Zhao, J. J.; Zhang, K., Light-Triggered, Self-Immolative Nucleic Acid-Drug Nanostructures. *J. Am. Chem. Soc.* **2015,** *137* (19), 6112-6115.

17. Kwak, M.; Herrmann, A., Nucleic acid amphiphiles: synthesis and self-assembled nanostructures. *Chem. Soc. Rev.* **2011,** *40* (12), 5745-5755.

18. Edwardson, T. G. W.; Carneiro, K. M. M.; Serpell, C. J.; Sleiman, H. F., An Efficient and Modular Route to Sequence-Defined Polymers Appended to DNA. *Angew. Chem. Int. Ed.* **2014,** *53* (18), 4567-4571.

19. Albert, S. K.; Thelu, H. V. P.; Golla, M.; Krishnan, N.; Chaudhary, S.; Varghese, R., Self-Assembly of DNA–Oligo(p-phenylene-ethynylene) Hybrid Amphiphiles into Surface-Engineered Vesicles with Enhanced Emission. *Angew. Chem. Int. Ed.* **2014,** *53* (32), 8352-8357.

20. Jiang, S.; Chen, Q.; Tripathy, M.; Luijten, E.; Schweizer, K. S.; Granick, S., Janus Particle Synthesis and Assembly. *Adv. Mat.*
2010, *22* (10), 1060-1071.

21. Wurm, F.; Kilbinger, A. F. M., Polymeric Janus Particles. *Angew. Chem. Int. Ed.* **2009,** *48* (45), 8412-8421.

22. Roh, K.-H.; Martin, D. C.; Lahann, J., Biphasic Janus particles with nanoscale anisotropy. *Nat. Mater.* **2005,** *4* (10), 759-763.

23. Badi, N.; Lutz, J.-F., Sequence control in polymer synthesis. *Chem. Soc.Rev.* **2009,** *38* (12), 3383-3390.

24. Lutz, J.-F.; Ouchi, M.; Liu, D. R.; Sawamoto, M., Sequence-Controlled Polymers. *Science* **2013,** *341* (6146).

25. Qiu, H.; Gao, Y.; Boott, C. E.; Gould, O. E. C.; Harniman, R. L.; Miles, M. J.; Webb, S. E. D.; Winnik, M. A.; Manners, I., Uniform patchy and hollow rectangular platelet micelles from crystallizable polymer blends. *Science* **2016,** *352* (6286), 697-701.

26. Walther, A.; Müller, A. H. E., Janus Particles: Synthesis, Self-Assembly, Physical Properties, and Applications. *Chemical Reviews* **2013,** *113* (7), 5194-5261.

27. Suzuki, K.; Hosokawa, K.; Maeda, M., Controlling the Number and Positions of Oligonucleotides on Gold Nanoparticle Surfaces. *J. Am. Chem. Soc.* **2009,** *131* (22), 7518-7519.

28. Kim, J.-W.; Kim, J.-H.; Deaton, R., DNA-Linked Nanoparticle Building Blocks for Programmable Matter. *Angew. Chem. Int. Ed.* **2011,** *50* (39), 9185-9190.

29. Zanchet, D.; Micheel, C. M.; Parak, W. J.; Gerion, D.; Alivisatos, A. P., Electrophoretic Isolation of Discrete Au Nanocrystal/DNA Conjugates. *Nano Lett.* **2001,** *1* (1), 32-35.

30. Zhao, Z.; Jacovetty, E. L.; Liu, Y.; Yan, H., Encapsulation of Gold Nanoparticles in a DNA Origami Cage. *Angew. Chem. Int. Ed.* **2011,** *50* (9), 2041-2044.

31. Li, Y.; Liu, Z.; Yu, G.; Jiang, W.; Mao, C., Self-Assembly of Molecule-like Nanoparticle Clusters Directed by DNA Nanocages. *J. Am. Chem. Soc.* **2015,** *137* (13), 4320-4323.

32. Wang, Y.; Wang, Y.; Breed, D. R.; Manoharan, V. N.; Feng, L.; Hollingsworth, A. D.; Weck, M.; Pine, D. J., Colloids with valence and specific directional bonding. *Nature* **2012,** *491* (7422), 51-55.

33. Xu, X.; Rosi, N. L.; Wang, Y.; Huo, F.; Mirkin, C. A., Asymmetric Functionalization of Gold Nanoparticles with Oligonucleotides. *J. Am. Chem. Soc.* **2006,** *128* (29), 9286-9287.

34. Li, Z.; Cheng, E.; Huang, W.; Zhang, T.; Yang, Z.; Liu, D.; Tang, Z., Improving the Yield of Mono-DNA-Functionalized Gold Nanoparticles through Dual Steric Hindrance. *J. Am. Chem. Soc.* **2011,** *133* (39), 15284-15287.

35. Pei, H.; Li, F.; Wan, Y.; Wei, M.; Liu, H.; Su, Y.; Chen, N.; Huang, Q.; Fan, C., Designed Diblock Oligonucleotide for the Synthesis of Spatially Isolated and Highly Hybridizable Functionalization of DNA–Gold Nanoparticle Nanoconjugates. *J. Am. Chem. Soc.* **2012,** *134* (29), 11876-11879.

36. Tan, S. J.; Campolongo, M. J.; Luo, D.; Cheng, W., Building plasmonic nanostructures with DNA. *Nat. Nanotech.* **2011,** *6* (5), 268-276.

37. Maye, M. M.; Nykypanchuk, D.; Cuisinier, M.; van der Lelie, D.; Gang, O., Stepwise surface encoding for high-throughput assembly of nanoclusters. *Nat. Mater.* **2009,** *8* (5), 388-391.

38. Tan, L. H.; Xing, H.; Chen, H.; Lu, Y., Facile and Efficient Preparation of Anisotropic DNA-Functionalized Gold Nanoparticles and Their Regioselective Assembly. *J. Am. Chem. Soc.* **2013,** *135* (47), 17675-17678.

39. Tian, Y.; Wang, T.; Liu, W.; Xin, H. L.; Li, H.; Ke, Y.; Shih, W. M.; Gang, O., Prescribed nanoparticle cluster architectures and low-dimensional arrays built using octahedral DNA origami frames. *Nat. Nanotech.* **2015,** *10* (7), 637-644.

40. Schreiber, R.; Santiago, I.; Ardavan, A.; Turberfield, A. J., Ordering Gold Nanoparticles with DNA Origami Nanoflowers. *ACS Nano* **2016,** *10* (8), 7303-7306.

41. Liu, W.; Halverson, J.; Tian, Y.; Tkachenko, A. V.; Gang, O., Self-organized architectures from assorted DNA-framed nanoparticles. *Nat. Chem.* **2016,** *8* (9), 867-873.

42. Edwardson, T. G. W.; Lau, K. L.; Bousmail, D.; Serpell, C. J.; Sleiman, H. F., Transfer of molecular recognition information from DNA nanostructures to gold nanoparticles. *Nat. Chem.* **2016,** *8* (2), 162-170.

43. Zhang, Y.; Chao, J.; Liu, H.; Wang, F.; Su, S.; Liu, B.; Zhang, L.; Shi, J.; Wang, L.; Huang, W.; Wang, L.; Fan, C., Transfer of Two-Dimensional Oligonucleotide Patterns onto Stereocontrolled Plasmonic Nanostructures through DNA-Origami-Based Nanoimprinting Lithography. *Angew. Chem. Int. Ed.* **2016,** *55* (28), 8036-8040.

44. Edwardson, T. G. W.; Carneiro, K. M. M.; McLaughlin, C. K.; Serpell, C. J.; Sleiman, H. F., Site-specific positioning of dendritic alkyl chains on DNA cages enables their geometry-dependent self-assembly. *Nat. Chem.* **2013,** *5* (10), 868-875.

45. Serpell, C. J.; Edwardson, T. G. W.; Chidchob, P.; Carneiro, K. M. M.; Sleiman, H. F., Precision Polymers and 3D DNA Nanostructures: Emergent Assemblies from New Parameter Space. *J. Am. Chem. Soc.* **2014,** *136* (44), 15767-15774.

46. Chidchob, P.; Edwardson, T. G. W.; Serpell, C. J.; Sleiman, H. F., Synergy of Two Assembly Languages in DNA Nanostructures: Self-Assembly of Sequence-Defined Polymers on DNA Cages. *J. Am. Chem. Soc.* **2016,** *138* (13), 4416-4425.

47. Trinh, T.; Chidchob, P.; Bazzi, H. S.; Sleiman, H. F., DNA micelles as nanoreactors: efficient DNA functionalization with hydrophobic organic molecules. *Chem. Comm.* **2016,** *52* (72), 10914-10917.

48. Liao, C.; Esai Selvan, M.; Zhao, J.; Slimovitch, J. L.; Schneebeli, S. T.; Shelley, M.; Shelley, J. C.; Li, J., Melittin Aggregation in Aqueous Solutions: Insight from Molecular Dynamics Simulations. *J. Phys. Chem. B* **2015,** *119* (33), 10390-10398.

49. Macfarlane, R. J.; O'Brien, M. N.; Petrosko, S. H.; Mirkin, C. A., Nucleic Acid-Modified Nanostructures as Programmable Atom Equivalents: Forging a New “Table of Elements”. *Angew. Chem. Int. Ed.* **2013,** *52* (22), 5688-5698.

50. Jones, M. R.; Seeman, N. C.; Mirkin, C. A., Programmable materials and the nature of the DNA bond. *Science* **2015,** *347* (6224).

51. Lee, J. H.; Yigit, M. V.; Mazumdar, D.; Lu, Y., Molecular diagnostic and drug delivery agents based on aptamer-nanomaterial conjugates. *Adv. Drug Delivery Rev.* **2010,** *62* (6), 592-605.

| 5 |

Conclusions and Future Work

5.1. Conclusions and contributions to original knowledge

The work described in this thesis aimed to address several existing challenges in the synthesis of DNA-hybrid materials. Overall, it was found that the use of DNA nanostructures as platforms for chemical transformations, which lies at the foundation of DNA-templated reactions, can significantly simplify the synthesis of DNA-hybrid materials with unprecedented control.

The research presented in chapter 2 addressed the synthetic challenge of DNA-hydrophobic molecules in aqueous environment. It overcame the difficulty in solvent incompatibility between DNA and hydrophobic molecules. The method relies on using highly monodisperse DNA micelles whose components are made by sequence-controlled solid-phase synthesis, as nanoreactors. The DNA micelles can serve as a reaction auxiliary to increase the activity of amino modified DNA. A library of highly hydrophobic molecules was shown to be efficiently conjugated to DNA or DNA amphiphiles using the approach. In the mechanistic work, by deliberately changing the structure of DNA amphiphiles as a function of position of amino group and number of monomers, reactivity trends and some insights into the packing of the DNA micelle nanoreactors could be revealed. The approach opened an opportunity to enable the functionalization of DNA with small molecules or polymers, which can be used in drug delivery, materials science and many other applications.

Chapter 3 extended further the idea in chapter 2 and presented a facile method to functionalize multi-arm small molecules with different DNA strands with control of valency, DNA sequences and directionalities. The strategy utilized a self-assembled multi-arm junction as a template, allowing reactive moieties to be positioned in the middle of the junction, and resulting in an efficient transfer process due to high local concentration in a single step. This approach greatly reduced the number of steps compared to previous synthetic methodologies and avoided tedious and laborious purification process. The resulting DNA-imprinted small molecule could be extended asymmetrically using PCR that was used to study the influence of small molecule core to geometric definition in self-assembly and to precisely organize nanomaterials (i.e. streptavidin) in 2D. Lastly, the DNA-imprinted small molecule was shown to be able to chemically self-replicate to make a daughter generation, which might potentially solve the problem of scalability.

By blending together DNA with synthetic molecules, DNA nanotechnology can acquire new structural motifs and can provide functionality to its typically passive DNA structures.

Lastly, the work in chapter 4 developed from the concept of 2D DNA "printing" in chapter 3 and introduced the concept of 3D DNA "printing" to polymeric materials using minimalist DNA cages as scaffolds. Taking advantage of the confined space with multiple amino functionalities inside the DNA cage, a crosslinking reaction was performed using amide bond formation. The 3D DNA scaffold was shown to create a template which could effectively transfer a specific pattern of DNA strands to the polymeric material. This is the first example of polymeric particles with controllable DNA valency, sequences and directionalities. Different cage geometries could generate particles with different sizes and number of monomers. Normally, block copolymer assembly gives rise to mostly symmetrical morphologies. However, these DNA-imprinted polymeric particles could assemble into asymmetric structures in a highly programmable way using DNA binding, which can potentially be explored to the self-assembly of discrete hybrid nanostructures with arbitrary shapes.

5.2. Suggestions for Future work

The DNA micelles in chapter 2 can be used as a template for controlled polymerization. Instead of placing an amino functionality, DNA can be functionalized with initiator group for living polymerization (e.g. free radical polymerization, atom transfer radical polymerization (ATRP) or reversible addition-fragmentation chain transfer (RAFT)). With defined size and shape of the DNA micelle template, DNA-polymer conjugates with low polydispersity index can potentially be generated inside the micellar core. Moreover, the incorporation of a small molecule unit into DNA can drastically change the self-assembled morphology. Hence, another interesting avenue of research is to study the self-assembly behavior of DNA-hydrophobic small molecule conjugates made by this method. Applications of these DNA-lipid molecule conjugates in delivery and gene silencing can be also of great interest.

Chapter 3 opened an opportunity to generate a library of DNA-imprinted small molecules. One possible direction is to study the structural definition dictated by these molecules, and this area is

currently being explored in the laboratory using PCR elongation. The studies will aid future designs of higher order self-assembled structures based on the angle of each building block, similar to the field of supramolecular chemistry. For molecules having more than 4 arms, the question of DNA positioning and stereochemistry after the "printing" process remains unanswered and this would be an important avenue to pursue. It can be done by using more rigid small molecules for the transfer process that can restrict their free rotation in solution. Then, each arm can be extended simultaneously to different lengths followed by visualization on AFM. Another possibility is to use DNA-imprinted small molecules as junctions in self-assembly of DNA hybrid nanostructures and then study the behavior of these self-assembled structures in drug delivery as organic vertices can have tremendous impact on stability of the structures. Although DNA patterns can be potentially transferred to variety of small molecules core using this method, scalability is still a great challenge. One way to address this challenge is to find a way to exponentially replicate the mother structure, as presented briefly at the end of chapter 3. This chemical copying concept can be used to transfer DNA patterns from one small molecule to another. Also, it is of note that the method is not limited to only small molecules. Different type of materials can be applied to this method such as inorganic particles (e.g. silica), polymeric particles and supramolecular cages that are currently under investigation in the lab. In a relatively new research area, the DNA junction is anticipated to serve as a template to organize biomacromolecule (e.g. peptides) in specific patterns, resulting in a unique DNA-scaffolded peptide structure that can be potentially used for cellular delivery.

The work in chapter 4 presented an interesting method to imprint DNA strands onto polymeric materials in a controllable manner. However, the polymer presented in this chapter is a polyethylene-like polymer having multiple phosphate groups in the middle, which does not have any intrinsic function. Expanding the library of polymers on which DNAs can be imprinted is one of the most important research directions to follow this work. This can potentially bring new functionalities and supramolecular interactions to the particles. Some fundamental studies can be studied with the use of more functional polymer such as energy transfer process between different polymeric particles. 3D DNA strand patterns "printing" to other materials such as gold nanoparticles can be pursued. The use of asymmetric "printed" polymer particles in the creation of discrete higher order nanostructures will also an important next step. Furthermore, these DNA-

imprinted particles can conceivably act as unique delivery vehicles, providing both stability due to crosslinked structure and a possibility of different targeting/therapeutic moieties (e.g. siRNA or aptamer) being incorporated in the same structure. Lastly, scalability is also an important problem that needs to be solved with this approach. This can potentially be addressed by recovering the DNA scaffold or having higher yielding crosslinking chemistry such as copper-catalyzed alkyne-azide ("click" chemistry) and photo-crosslinking reactions (e.g. anthracene dimerization).

5.3. List of Publications

1. Tuan Trinh, Daniel Saliba, Chenyi Liao, Donatien de Rochambeau, Alexander L. Prinzen, Jianing Li, Hanadi F. Sleiman "Printing DNA Strand Patterns on Small Molecules with Control of Valency, Directionality, and Sequence", *Angewandte Chemie International Edition*, **2019**, 57

2. Janane F. Rahbani, Empar Vengut-Climent, Pongphak Chidchob, Yasser Gidi, Tuan Trinh, Gonzalo Cosa, Hanadi F. Sleiman "DNA Nanotubes with Hydrophobic Environments: Toward New Platforms for Guest Encapsulation and Cellular Delivery", *Advanced Healthcare Mater.*, **2018**, 7, 1701049

3. Tuan Trinh, Chenyi Liao, Violeta Toader, Marciej Barlog, Hassan S. Bazzi, Jianing Li, Hanadi F. Sleiman "DNA-imprinted polymer nanoparticles with monodispersity and prescribed DNA-strand patterns", *Nature Chemistry*, **2018**, 10, 184-192

4. Tuan Trinh, Pongphak Chidchob, Hassan S. Bazzi, Hanadi F. Sleiman "DNA micelles as nanoreactors: Efficient DNA functionalization with hydrophobic organic molecules", *Chemical Communications*, **2016**, 52, 10914-10917

5. Johans J. Fakhoury, Thomas W. Edwardson, Justin W. Conway, Tuan Trinh, Farhad Khan, Maciej Barlog, Hassan S. Bazzi, Hanadi F. Sleiman "Antisense precision polymer micelles

require less poly(ethylenimine) for efficient gene knockdown", *Nanoscale*, **2015**, 7, 20625-20634

6. Hanadi Sleiman, Katherine Bujold, Janane Rahbani, Johans Fakhoury, Tuan Trinh, John Hsu "DNA cages and nanotubes for drug and oligonucleotide delivery", *report of invention,* **2015**

Manuscript in preparation:

7. Tuan Trinh, Daniel Saliba, Christophe LaChance Brais, Hanadi F. Sleiman "Templating nanomaterials on DNA tiles in 2D with control of number and location using a minimalist approach", *manuscript in preparation*

8. Michael D. Dore, Tuan Trinh, Donatien de Rochambeau, Pengfei Xu, Hanadi F. Sleiman "Fiber growth of branched sequence-controlled DNA amphiphiles", *manuscript in preparation*